



CONSTRUCTED FACILITIES CENTER



PB99-142820

PERFORMANCE OF FLEXIBLE PAVEMENTS REINFORCED WITH GEOGRIDS

Project: WVDOH #98 / CFC 98-259

Bora Kutuk, Graduate Research Assistant
Hema J. Siriwardane, Professor


Constructed Facilities Center
Department of Civil and Environmental Engineering
College of Engineering and Mineral Resources
West Virginia University
Morgantown, WV 26506-6101

March 1998

*College of Engineering and
Mineral Resources
West Virginia University*

REPRODUCED BY:
U.S. Department of Commerce
National Technical Information Service
Springfield, Virginia 22161

NTIS

1. Report No.	2. Government Accession No.	3. Recipient's Catalog No.	
4. Title and Subtitle Performance of Flexible Pavements Reinforced with Geogrids  PB99-142820		5. Report Date March 1998	
		6. Performing Organization Code	
7. Author(s) Bora Kutuk and Hema J. Siriwardane		8. Performing Organization Report No. CFC 98-259	
9. Performing Organization Name and Address Department of Civil and Environmental Engineering Constructed Facilities Center West Virginia University P.O. Box 6103 Morgantown, WV 26506-6103		10. Work Unit No. (TRAIS)	
		11. Contract or Grant No. WVDOH RP#98	
12. Sponsoring Agency Name and Address West Virginia Department of Transportation Division of Highways 1900 Kanawha Boulevard, East - Building Five Charleston, WV 25305-0430		13. Type of Report and Period Covered Final Report 8/16/94-12/31/97	
		14. Sponsoring Agency Code	
15. Supplementary Notes			
16. Abstract <p>This report presents the results of an investigation on the effectiveness of glass fiber grids as a reinforcement of the asphalt layer in a flexible pavement. The study involved both laboratory experimental work and computer analysis of pavement sections. As part of the experimental work, twenty flexible pavement sections (with and without glass fiber grids) were constructed and tested in the laboratory. The laboratory-scale pavement sections were instrumented with pressure cells, displacement gages, and strain gages. Test sections were subjected to 1,000,000 load applications at a frequency of 1.2 Hz. Static loading tests were conducted at intervals of 100,000 load applications. In thirteen experiments, the glass fiber grid was used in the asphalt layer. Measurement of strain in the reinforcement layer (glass grid) was attempted in five experiments.</p> <p>A series of computer analyses was performed to analyze flexible pavement sections using the KENLAYER [Huang (1993)] computer program and the Finite Element Method (FEM). The laboratory data were compared with results from the computer analysis.</p> <p>The results show that the glass fiber grid used in this study improved the pavement performance. It was also observed that the inclusion of glass fiber grid in the HMA layer provided resistance to crack propagation. Overall, the flexible pavement sections reinforced with glass fiber geogrids showed better performance under laboratory test conditions.</p>			
17. Key Words Flexible Pavement, Glass Fiber Grids, Geogrids, Reinforced Asphalt Layer, Laboratory Test Sections		18. Distribution Statement	
19. Security Classif. (of this report) Unclassified	20. Security Classif. (of this page) Unclassified	21. No. Of Pages 300	22. Price

EXECUTIVE SUMMARY

WVDOH RP 98 / CFC 98-259

PERFORMANCE OF FLEXIBLE PAVEMENTS REINFORCED WITH GEOGRIDS

by

Bora Kutuk
Hema J. Siriwardane

West Virginia University
Constructed Facilities Center
Department of Civil and Environmental Engineering
College of Engineering and Mineral Resources
Morgantown, West Virginia 26506

West Virginia Department of Transportation
Division of Highways

PROTECTED UNDER INTERNATIONAL COPYRIGHT
ALL RIGHTS RESERVED.
NATIONAL TECHNICAL INFORMATION SERVICE
U.S. DEPARTMENT OF COMMERCE

August 1998

EXECUTIVE SUMMARY

PERFORMANCE OF FLEXIBLE PAVEMENTS REINFORCED WITH GEOGRIDS

By

Bora Kutuk and Hema J. Siriwardane

**Department of Civil and Environmental Engineering
West Virginia University**

INTRODUCTION

The main objective of this research work was to evaluate the effectiveness of the use of geogrids as a reinforcement material for flexible pavement systems. This report presents the results of an investigation on the effectiveness of glass fiber grids as a reinforcement of the asphalt base layer in flexible pavements. The study involved both laboratory experimental work and computer analysis of pavement sections. As part of the experimental work, twenty flexible pavement sections with and without glass fiber grids were constructed and tested in the laboratory. The experimental pavement sections were built in a rectangular container with dimensions of 4 feet x 6 feet x 2.5 feet (1.2 m x 1.8 m x 0.8 m). Two containers were constructed of steel for testing flexible pavement sections. Five analog dial gages [1-inch (25 mm)] were placed on top of the asphalt surface to measure permanent vertical displacements. Two earth pressure cells were located at the top of the subgrade soil in each soil container (test box). The depth of the buried pressure cells was 8.5 inches (215.9 mm) below the asphalt/gravel base interface. For the test sections, the maximum applied load on the asphalt surface was 9 kips (40 kN) over a 12-inch (305 mm) diameter loading plate, simulating a tire pressure of 80 psi (551 kN/m²). Test sections were subjected to 1,000,000 load applications at a frequency of 1.2 Hz. Static loading tests were conducted at intervals of 100,000 load applications. Factors such as permanent (cumulative) displacement of the asphalt surface, change in pavement stiffness with number of load cycles, resistance to cracking, strain in the glass fiber grid,

and variation of subgrade stress in reinforced pavement sections were evaluated and compared with results from non-reinforced pavement sections.

EXPERIMENTAL PROGRAM

In two soil containers, A-4 type subgrade material was placed in 3 lifts. The bottom layer was 4 inches (102 mm) in thickness while the remaining layers were placed in 3 inch (76 mm) lifts in each box. Each layer was compacted using a Whacker compacter with a 6 inches (152 mm) square tamper plate. After compacting the soil, two pressure cells were placed on top of the subgrade material. Then, a geotextile fabric was placed on the surface of the subgrade at the interface between the subgrade soil and the gravel base.

After placing the geotextile fabric, the gravel base was placed in two lifts. The first lift was 4.5 inches (114.3 mm) in thickness and the second was 4 inches (102 mm) in thickness. After compacting the gravel base, hot mix asphalt was placed. Asphalt Base II was used as the hot mix asphalt (HMA) in the experimental program. Hot mix asphalt was placed in two lifts. For the first ten experiments, the total thickness of the asphalt layer was 6 inches (152 mm), and was compacted in two 3-inch (76 mm) lifts. The remaining 9 of 10 experiments, the total thickness of the asphalt layer was reduced to 3 inches (76 mm), and was compacted in two 1.5-inch (38.1 mm) lifts. For one experiment, the thickness of the asphalt layer was reduced to 2.5 inches (63.5 mm), and was compacted in 1.5-inch (38.1 mm) and 1-inch (25 mm) lifts. In thirteen experiments, the glass fiber grid was used in the asphalt layer. In three experiments out of thirteen, the glass fiber grid was placed between the gravel base and the hot mix asphalt in addition to the one inside the asphalt base. In five experiments, with and without reinforcement, a crack was simulated in the hot mix asphalt having a thickness of 3-inch (76 mm).

COMPUTER ANALYSES

A series of computer analyses was performed to analyze flexible pavement sections using the KENLAYER [Huang (1993)] computer program and the Finite Element Method (FEM). Throughout the KENLAYER analyses, the asphalt base layer (HMA) and the glass grid layer were considered as linear visco-elastic layers, while the remaining layers (gravel base, subgrade, and geotextile) were considered as linear elastic materials. Also, in some cases the glass grid layer was considered as a linear elastic material since glass grid has very low (or none) creep characteristics. Linear elastic analysis was also performed by using the finite element method (FEM). The laboratory data were compared with results from the computer analysis.

RESULTS AND CONCLUSIONS

In four experiments, failure of the pavement section was observed. Of the two reinforced pavement sections with a simulated crack, neither resulted in failure. Of the three non-reinforced pavement sections with a simulated crack, two resulted in failure. The remaining experiments showed satisfactory performance of the pavement section.

Measurement of strain in the reinforcement layer (glass grid) was attempted in five experiments. During the glass grid installation inside the hot mix asphalt, difficulties were encountered due to the hostile environment conditions for the strain gages such as compaction, dynamic loading, and high temperature. Strain measurements on glass fiber grid were considered as not successful due to the difficulties encountered during compaction and the dynamic loading process.

Observations on doubly reinforced cases indicate that the vertical stresses in the subgrade is lower in pavement sections with stronger glass grids. Observations on the vertical subgrade stress indicate that a reinforced thinner section [thickness of HMA = 3 inches (76 mm)] behaves similar

to that of a non-reinforced thicker pavement section [thickness of HMA = 6 inches (152 mm)].

In terms of cumulative displacement, results indicate that a 6-inch (152 mm) thick non-reinforced hot-mix asphalt base layer does not improve the performance of the pavement system in comparison to a 3-inch (76 mm) thick reinforced asphalt section. However, the results show that the reinforced pavement sections resulted in smaller cumulative displacements in comparison to a non-reinforced test section. This decrease in cumulative displacement shows that an improvement could be gained by reinforcing the structural asphalt base in pavement sections. Test results indicate that the cumulative displacements increase for reductions in grid weight in thick pavement sections where the thickness of asphalt is 6 inches (152 mm).

Observations on thinner pavement sections indicate that the increase in vertical subgrade stress caused by a simulated crack is offset by the decrease in vertical subgrade stress due to the reinforcement of the pavement section. Test results show that the negative influence of the simulated crack seems to have a slightly more impact on cumulative displacements than the positive influence of the glass grid reinforcement. Observations indicate that a similar stiffness may be obtained by reinforcing a thin asphalt section [thickness of Hot Mix Asphalt = 3 inches (76 mm)] in comparison to a non-reinforced thick asphalt section. The results show that the glass fiber grid used in this study improved the pavement performance. It was also observed that the inclusion of glass fiber grid in the HMA layer provided resistance to crack propagation.

Overall, the flexible pavement sections reinforced with glass fiber geogrids showed better performance under laboratory test conditions.

DISCLAIMER

“The contents of this report reflect the views of the authors who are responsible for the facts and accuracy of the data presented herein. The contents of this report do not reflect the official views or policies of the West Virginia Department of Transportation”

ABSTRACT

**PERFORMANCE OF FLEXIBLE PAVEMENTS REINFORCED
WITH GEOGRIDS**

This report presents the results of an investigation on the effectiveness of glass fiber grids as a reinforcement of the asphalt base layer in a flexible pavement. The study involved both laboratory experimental work and computer analysis of pavement sections. As part of the experimental work, twenty flexible pavement sections (with and without glass fiber grids) were constructed and tested in the laboratory. The laboratory-scale pavement sections were instrumented with pressure cells, displacement gages, and strain gages. Test sections were subjected to 1,000,000 load applications at a frequency of 1.2 Hz. Static loading tests were conducted at intervals of 100,000 load applications. In four experiments, failure of the pavement section was observed. In thirteen experiments, the glass fiber grid was used in the asphalt base layer. In five experiments, with and without reinforcement, a crack was simulated in the hot mix asphalt [thickness of 3-inch (76 mm)] base layer. Of the two reinforced pavement sections with a simulated crack, neither resulted in failure. Of the three non-reinforced pavement sections with a simulated crack, two resulted in failure.

A series of computer analyses was performed to analyze flexible pavement sections using the KENLAYER [Huang (1993)] computer program and the Finite Element Method (FEM). Throughout the KENLAYER analyses, the asphalt base layer (HMA) and the glass grid layer were considered as linear visco-elastic layers, while the remaining layers (gravel base, subgrade, and geotextile) were considered as linear elastic materials. Also, in some cases the glass grid layer was considered as a linear elastic material since glass grid has very low (or none) creep characteristics. Linear elastic analysis was also performed by using the finite element method (FEM). The laboratory data were

compared with results from the computer analysis.

Observations on doubly reinforced cases indicate that the vertical stresses in the subgrade is lower in pavement sections with stronger glass grids. In terms of cumulative displacement, results indicate that a 6-inch (152 mm) thick non-reinforced hot-mix asphalt base layer does not improve the performance of the pavement system in comparison to a 3-inch (76 mm) thick reinforced asphalt section. Observations on thinner pavement sections indicate that the increase in vertical subgrade stress caused by a simulated crack is offset by the decrease in vertical subgrade stress due to the reinforcement of the pavement section. Test results show that the negative influence of the simulated crack seems to have a slightly more impact on cumulative displacements than the positive influence of the glass grid reinforcement. With the inclusion of the glass grid inside the HMA, there is a tendency for the displacement (under static loading) to increase, thereby causing a slight decrease in stiffness of the HMA. Observations indicate that a similar stiffness may be obtained by reinforcing a thin asphalt section [thickness of HMA = 3 inches (76 mm)] in comparison to a non-reinforced thick asphalt section. The results show that the glass fiber grid used in this study improved the pavement performance. It was also observed that the inclusion of glass fiber grid in the HMA layer provided resistance to crack propagation. Overall, the flexible pavement sections reinforced with glass fiber geogrids (in the asphalt base layer) showed better performance under laboratory test conditions.

ACKNOWLEDGMENT

The authors would like to acknowledge the financial support provided by the West Virginia Department of Transportation, Division of Highways for this project. The authors especially thank the project monitors, Ms. Melissa Stacy and Mr. Brian Fouch, for their assistance and valuable comments.

TABLE OF CONTENTS

ABSTRACT	i
ACKNOWLEDGEMENT	iii
TABLE OF CONTENTS	iv
LIST OF FIGURES	xii
LIST OF TABLES	xxi
CHAPTER 1	1
INTRODUCTION	1
1.1 INTRODUCTION	1
1.2 OBJECTIVES	7
1.3 SCOPE OF RESEARCH	8
1.4 REPORT OUTLINE	8
CHAPTER 2	9
LITERATURE REVIEW	9
2.1 FABRIC AND GRID INTERLAYERS IN PAVEMENT SYSTEMS	9
2.1.1 Geogrids	9
2.1.2 Geotextiles	14
2.2 FUNCTIONS OF GEOGRIDS AND GEOTEXTILES INFLUENCING PAVEMENT PERFORMANCE	16
2.2.1 Separation	16
2.2.2 Filtration	20

2.2.3	Reinforcement	21
2.3	PROPERTIES OF GEOSYNTHETICS	22
2.4	PHYSICAL PROPERTIES	22
2.5	MECHANICAL PROPERTIES	23
2.5.1	Tensile Strength	23
2.5.2	Stiffness	23
2.5.3	Anchorage Strength	24
2.6	INTERLOCK AND ADHESION (BOND) MECHANISM OF GEOGRID REINFORCEMENT	25
2.7	CREEP RESISTANCE	27
2.8	PAVEMENT PERFORMANCE	27
2.8.1	Pavement Distress	28
2.8.2	Rutting	30
2.8.3	Alligator (Fatigue) And Block Crackings	30
2.8.4	Reflection Cracking	31
2.8.5	Longitudinal And Transverse Cracking	32
2.9	REVIEW OF EXISTING GEOGRID REINFORCEMENT METHODS	35
2.10	SUMMARY	43
CHAPTER 3		45
EXPERIMENTAL PROGRAM		45
3.1	TEST FACILITY	45
3.2	INSTRUMENTATION	47

3.2.1	Dial Gages	47
3.2.2	Pressure Cells	47
3.2.3	Strain Gages	49
3.3	LOADING PROGRAM	49
3.3.1	Load Configuration	51
3.4	TEST SECTION MATERIALS	55
3.4.1	Hot Mix Asphalt (HMA)	55
3.4.2	Gravel Base	56
3.4.3	Subgrade	60
3.4.5	Woven Geotextile	67
3.4.4	Glass Fiber Grid	67
3.5	CONSTRUCTION OF TEST SECTIONS AND OUTLINE OF EXPERIMENTAL PROGRAM	73
CHAPTER 4	79
LABORATORY TEST RESULTS	79
4.1	VERTICAL SUBGRADE STRESS	80
4.1.1	Influence Of Different Glass Grids On Vertical Subgrade Stress	82
4.1.2	Influence Of Glass Grids On Vertical Subgrade Stress On Doubly Reinforced Section	85
4.1.3	Influence Of Reinforcement On Vertical Subgrade Stress [Thickness Of HMA = 6 Inches (152 mm)]	88
4.1.4	Influence Of Reinforcement On Vertical Subgrade Stress [Thickness Of	

	HMA = 2.5 Inches (63.5 mm) And 3 Inches (76 mm)]	92
4.1.5	Comparison Of Non-Reinforced 6-Inch (152 mm) Thick Asphalt Section With Thinner Reinforced Asphalt Sections	96
4.1.6	Influence Of Asphalt Thickness On Vertical Subgrade Stress	99
4.1.7	Influence Of A Simulated Crack On Vertical Subgrade Stress In A Non-Reinforced Pavement Section	104
4.1.8	Influence Of Reinforcement On Vertical Subgrade Stress In A Pavement Section With A Simulated Crack	107
4.1.9	Comparison Of A Non-Reinforced 6 Inches (152 mm) Thick Asphalt Section With A Reinforced Thinner Asphalt Section With A Simulated Crack	110
4.1.10	Influence Of A Simulated Crack And Reinforcement On Vertical Subgrade Stress	114
4.1.11	Summary Of Laboratory Results On Vertical Subgrade Stress	118
4.2	CUMULATIVE DISPLACEMENTS	122
4.2.1	Influence Of Different Glass Grids On Cumulative Displacement	122
4.2.2	Influence Of Glass Grids On Cumulative Displacement On Doubly- Reinforced Section	125
4.2.3	Influence Of Reinforcement On Cumulative Displacement [Thickness Of HMA = 6 Inches (152 mm)]	127
4.2.4	Influence Of Reinforcement On Cumulative Displacement [Thickness Of HMA = 2.5 Inches (63.5 mm) And 3 Inches (76 mm)]	129

4.2.5	Comparison Of Non-Reinforced 6-Inch (152 mm) Thick Asphalt Section With Thinner Reinforced Asphalt Sections	131
4.2.6	Influence Of Asphalt Thickness On Cumulative Displacement	131
4.2.7	Influence Of Reinforcement On Cumulative Displacement In A Pavement Section With A Simulated Crack	136
4.2.8	Comparison Of A Non-Reinforced 6-Inch (152 mm) Thick Asphalt Section With A Reinforced Thinner Asphalt Section With A Simulated Crack .	136
4.2.9	Influence Of Simulated Crack And Reinforcement On Cumulative Displacement	139
4.2.10	Summary Of Laboratory Results On Cumulative Displacements	141
4.3	DISPLACEMENT UNDER STATIC LOADING: PAVEMENT STIFFNESS	144
4.3.1	Influence Of Different Glass Grids On Pavement Stiffness	144
4.3.2	Influence Of Glass Grids On Pavement Stiffness Of A Doubly Reinforced Section	147
4.3.3	Influence Of Reinforcement On Pavement Stiffness [Thickness Of HMA = 6 Inches (152 mm)]	149
4.3.4	Influence Of Reinforcement On Pavement Stiffness [Thickness Of HMA = 3 Inches (76 mm)]	149
4.3.5	Comparison Of Non-Reinforced 6-Inch (152 mm) Thick Asphalt Section With Thinner Reinforced Asphalt Sections	152
4.3.6	Influence Of Asphalt Thickness On Pavement Stiffness	154

4.3.7	Influence Of A Simulated Crack On Stiffness Of A Non-Reinforced Pavement Section	157
4.3.8	Influence Of Reinforcement On Stiffness Of A Pavement Section With A Simulated Crack	159
4.3.9	Comparison Of A Non-Reinforced 6-Inch (152 mm) Thick Asphalt Section With A Reinforced Thinner Asphalt Section With A Simulated Crack .	161
4.3.10	Influence Of A Simulated Crack And Reinforcement On Pavement Stiffness	161
4.3.11	Summary Of Laboratory Results On Displacements Under Static Loading	164
4.4	STRAIN MEASUREMENTS ON GLASS GRID REINFORCEMENT LAYER	169
CHAPTER 5		178
RESULTS OF COMPUTER ANALYSES		178
5.1	DESCRIPTION OF KENLAYER COMPUTER PROGRAM	178
5.1.1	Moving Load Analysis	180
5.1.2	Creep Compliance Analysis	182
5.1.3	Damage Analysis	183
5.2	COMPUTER ANALYSIS OF TEST SECTIONS	184
5.3	COMPUTER ANALYSES OF VERTICAL STRESS	187
5.3.1	Predicted Vertical Stress Variation With Depth	187
5.3.2	Comparison Of Measured And Predicted Vertical Subgrade Stresses	

	In A 6-Inch (152 mm) Thick Asphalt Section	193
5.3.3	Comparison Of Measured And Predicted Vertical Subgrade Stresses In A 3-Inch (76 mm) Thick Asphalt Section	199
5.3.4	Summary Of Results On Computed Vertical Stresses	205
5.4	INFLUENCE OF GEOSYNTHETIC ON PAVEMENT PERFORMANCE ..	206
5.4.1	Influence Of Glass Fiber Grid On Subgrade Stress [Glass Grid Layer As A Visco-Elastic Material]	206
5.4.2	Influence Of Glass Fiber Grid On Subgrade Stress [Glass Grid Layer As An Elastic Material]	210
5.4.3	Summary Of Results On Influence Of Geosynthetic On Pavement Performance	213
5.5	COMPUTER ANALYSES OF SURFACE DISPLACEMENTS	214
5.5.1	Comparison Of Computed Displacements With Measurements Corresponding To A 3-Inch (76 mm) Thick HMA Layer	218
5.5.2	Comparison Of Computed Displacements With Measurements Corresponding To A 6-Inch (152 mm) Thick HMA Layer	222
5.6	COMPUTER ANALYSES OF STRAINS	229
5.6.1	Variation Of Computed Strain With Depth In A Thick Pavement Section	233
5.6.2	Variation Of Computed Strain With Depth In A Thin Pavement Section	236
5.6.3	Computed Strain In The Reinforcement Layer In A 6-Inch (152 mm)	

Thick HMA Layer	240
5.6.4 Computed Strain In The Reinforcement Layer In A 3-Inch (76 mm)	
Thick HMA Layer	243
5.6.5 Influence Of HMA Thickness On Computed Strains in the Reinforcement	
Layer	244
5.6.6 Comparison Of Computed Strains With Measurements	247
5.6.7 Summary Of Results On Computed Strain Analyses	250
5.7 FINITE ELEMENT ANALYSIS (FEA)	252
5.7.1 Results Of The Finite Element Analyses Of Laboratory Test Section ..	253
5.7.2 Results Of The Finite Element Analyses Of A Hypothetical Field	
Section	268
5.7.3 Summary Of Results On Finite Element Analyses	282
CHAPTER 6	284
SUMMARY, CONCLUSIONS, AND RECOMMENDATIONS	284
6.1 SUMMARY	284
6.2 CONCLUSIONS	285
6.2.1 Laboratory Test Results	285
6.2.2 Results Of Computer Analyses	290
6.3 RECOMMENDATIONS FOR FUTURE RESEARCH	294
REFERENCES	296

LIST OF FIGURES

Figure 1-1:	Typical Cross Section of a Conventional Flexible Pavement	2
Figure 1-2:	A Schematic Figure of a Reinforced Pavement Section	6
Figure 2-1:	Separation Function of a Geotextile	17
Figure 2-2:	Schematic Diagram of Burst Resistance in Geosynthetic Fabric	19
Figure 2-3:	Schematic Diagram of Tensile Strength in Geosynthetic Fabric	19
Figure 2-4:	Typical Geogrid Sections	26
Figure 3-1:	Instrumentation for the Laboratory Study	46
Figure 3-2:	Photo Showing the Pressure Cells (EPC-6) on Top of the Subgrade	48
Figure 3-3:	Photo Showing the Strain Gages Installed on Top of the Glass Grid	50
Figure 3-4:	Photo Showing the Material Testing System (MTS) Loading Machine	50
Figure 3-5:	Load Configuration for a Pavement System	53
Figure 3-6:	Particle Size Distribution for the Subgrade Soil	61
Figure 3-7:	California Bearing Ratio (CBR) Value of the A-4 Type Subgrade Soil	63
Figure 3-8:	Standard Compaction Curve of the A-4 Type Subgrade Soil Used in Test Sections	64
Figure 3-9:	Photo Showing the Compaction of the Subgrade Soil	66
Figure 3-10:	Photo Showing Three Different Glass Fiber Grid Types Used in the Experimental Program	69
Figure 3-11:	Experimental Outline for Pavement Section with a 6-Inch (152 mm) Thick Asphalt Layer	75
Figure 3-12:	Experimental Outline for Pavement Section for Reduced Thicknesses	76

Figure 3-13:	Experimental Outline for Pavement Section with a Simulated Crack	77
Figure 4-1:	Influence of Different Glass Grids on Vertical Subgrade Stress	83
Figure 4-2:	Variation of Vertical Subgrade Stress with Number of Load Cycles for Doubly Reinforced Test Sections	86
Figure 4-3:	Influence of Reinforcement on Vertical Subgrade Stress [Thickness of HMA = 6 in. (152 mm)]	89
Figure 4-4:	Influence of Reinforcement on Vertical Subgrade Stress [Thickness of HMA = 2.5 in. (63.5 mm) and 3 in. (76 mm)]	93
Figure 4-5:	Comparison of Non-Reinforced 6-inch (152 mm) Thick Asphalt Section with Thinner Reinforced Asphalt Sections with Respect to Vertical Subgrade Stress	97
Figure 4-6:	Influence of Asphalt Thickness on Vertical Subgrade Stress in Reinforced Test Sections	100
Figure 4-7:	Influence of Asphalt Thickness on Vertical Subgrade Stress in Non-Reinforced Test Sections	102
Figure 4-8:	Influence of Simulated Crack on Vertical Subgrade Stress in a Pavement Section without Reinforcement	105
Figure 4-9:	Influence of Reinforcement on Vertical Subgrade Stress in a Pavement Section with a Simulated Crack	108
Figure 4-10:	Comparison of a Non-Reinforced 6-inch (152 mm) Thick Asphalt Section with a Reinforced Thinner Asphalt Section with a Simulated Crack	111

Figure 4-11:	Comparison of a Non-Reinforced 3-inch (76 mm) Thick Asphalt Section with a Reinforced Asphalt Section with a Simulated Crack	115
Figure 4-12:	Comparison of Experimental Parameters of the HMA Layer for Vertical Subgrade Stress	121
Figure 4-13:	Influence of Different Glass Grids on Cumulative Displacements	124
Figure 4-14:	Influence of Different Glass Grids on Cumulative Displacements for Doubly Reinforced Test Sections	126
Figure 4-15:	Influence of Reinforcement on Cumulative Displacement [Thickness of HMA = 6 in. (152 mm)]	128
Figure 4-16:	Influence of Reinforcement on Cumulative Displacement [Thickness of HMA = 2.5 in. (63.5 mm) and 3 in. (76 mm)]	130
Figure 4-17:	Comparison of Non-Reinforced 6-inch (152 mm) Thick Asphalt Section with Thinner Reinforced Asphalt Sections with Respect to Cumulative Displacements	132
Figure 4-18:	Influence of Asphalt Thickness on Cumulative Displacement in Reinforced Test Sections	133
Figure 4-19:	Influence of Asphalt Thickness on Cumulative Displacement in Non-Reinforced Test Sections	134
Figure 4-20:	Influence of Reinforcement on Cumulative Displacement in a Pavement Section with a Simulated Crack	137
Figure 4-21:	Comparison of a Non-Reinforced 6-inch (152 mm) Thick Asphalt Section with a Reinforced Thinner Asphalt Section with a Simulated Crack	138

Figure 4-22:	Influence of the Simulated Crack and Reinforcement on Cumulative Displacement	140
Figure 4-23:	Influence of Different Glass Grids on Pavement Stiffness	146
Figure 4-24:	A Comparison of Performance of Non-Reinforced and Doubly Reinforced 6-inch (152 mm) Thick Asphalt Sections	148
Figure 4-25:	Influence of Reinforcement on Pavement Stiffness [Thickness of HMA = 6 in. (152 mm)]	150
Figure 4-26:	Influence of Reinforcement on Pavement Stiffness [Thickness of HMA = 3 in. (76 mm)]	151
Figure 4-27:	Comparison of Non-Reinforced 6-inch (152 mm) Thick Asphalt Section with Thinner Reinforced Asphalt Sections with Respect to Displacement Under Static Loading	153
Figure 4-28:	Influence of Asphalt Thickness on Pavement Stiffness of Non-Reinforced Test Sections	155
Figure 4-29:	Influence of Asphalt Thickness on Pavement Stiffness of Reinforced Test Sections	156
Figure 4-30:	Influence of a Simulated Crack on Pavement Stiffness (Under Static Loading) in a Pavement Section without Reinforcement	158
Figure 4-31:	Influence of Reinforcement on Pavement Stiffness in a Pavement Section with a Simulated Crack	160
Figure 4-32:	Comparison of a Non-Reinforced 6-inch (152 mm) Thick Asphalt Section with a Reinforced Thinner Asphalt Section with a Simulated Crack on the Basis	

	of Displacement	162
Figure 4-33:	Comparison of a Non-Reinforced 3-inch (76 mm) Thick Asphalt Section with a Reinforced Asphalt Section with a Simulated Crack on the Basis of Displacement	163
Figure 4-34:	Comparison of Experimental Parameters of the HMA Layer for Displacement Under Static Loading	167
Figure 4-35:	Variation of Strain with Number of Load Cycles for Doubly Reinforced Test Sections	171
Figure 4-36:	Variation of Strain with Number of Load Cycles for Singly Reinforced Test Sections with a Simulated Crack	173
Figure 4-37:	Variation of Strain with Number of Load Cycles for Experiment #20	175
Figure 4-38:	Variation of Strain with Applied Load for Experiment #9	176
Figure 5-1:	A Multilayer System in Cylindrical Coordinates	181
Figure 5-2:	Moving Load as a Function of Time	181
Figure 5-3:	Variation of Predicted Vertical Stress with Depth for a Thin Asphalt Section with Reinforcement	189
Figure 5-4:	Variation of Predicted Vertical Stress Beneath the Center of the Loading Area in a Reinforced Pavement Section	191
Figure 5-5:	Measured and Predicted Upper and Lower Bound Vertical Stresses in a 6-inch (152 mm) Thick Asphalt Section with Reinforcement	194
Figure 5-6:	Measured and Predicted Vertical Stresses in a 6-inch (152 mm) Thick Asphalt Section with Reinforcement	197

Figure 5-7:	Measured and Predicted Vertical Stresses for a 6-inch (152 mm) Thick Asphalt Section with No Reinforcement	198
Figure 5-8:	Measured and Predicted Upper and Lower Bound Vertical Stresses for Thin Asphalt Sections with Reinforcement	200
Figure 5-9:	Measured and Predicted Vertical Stresses for Thin Asphalt Sections with Reinforcement	203
Figure 5-10:	Measured and Predicted Vertical Stresses for Thin Asphalt Sections with No Reinforcement	204
Figure 5-11:	Influence of Geosynthetics on Subgrade Stress in a Thin Asphalt Section [Glass Grid as a Visco-Elastic Material]	208
Figure 5-12:	Influence of Geosynthetics on Subgrade Stress in a Thick Asphalt Section [Glass Grid as a Visco-Elastic Material]	209
Figure 5-13:	Influence of Geosynthetics on Subgrade Stress in a Thin Asphalt Section [Glass Grid as an Elastic Material]	211
Figure 5-14:	Computed Elastic Surface Displacements in a Thin HMA Section with Reinforcement	215
Figure 5-15:	Computed Elastic Surface Displacements in a Thick HMA Section with Reinforcement	216
Figure 5-16:	Measured Displacement versus Predicted Elastic Surface Displacement for a Thin HMA Section with Reinforcement	220
Figure 5-17:	Measured Displacement versus Predicted Elastic Surface Displacement for a Thin HMA Section with No Reinforcement	224

Figure 5-18:	Measured Displacement versus Predicted Elastic Surface Displacement for a Thick HMA Section with Reinforcement	225
Figure 5-19:	Measured Displacement versus Predicted Elastic Surface Displacement for a Thick HMA Section with No Reinforcement	227
Figure 5-20:	Locations of Computed Strains	231
Figure 5-21:	Location and Direction of Strains in Computer Analysis	232
Figure 5-22:	Variation of Computed Strain with Depth in a Thick Pavement Section	234
Figure 5-23:	Variation of Computed Strain with Depth in a Thin Pavement Section	238
Figure 5-24:	Computed Strain in the Reinforcement Layer in a Thick Pavement Section ...	241
Figure 5-25:	Computed Strain in the Reinforcement Layer in a Thin Pavement Section ...	245
Figure 5-26:	Influence of HMA Thickness on Computed Strains	246
Figure 5-27:	Comparison of Measured and Computed Tangential Strains	248
Figure 5-28:	Axisymmetric Approximation	254
Figure 5-29:	Plane Strain Approximation	254
Figure 5-30:	Finite Element Mesh Used for Thin Pavement Section (Axisymmetric Case) ..	256
Figure 5-31:	Schematic Details of a 12-foot (365 mm) Wide Pavement Section	258
Figure 5-32:	Finite Element Mesh Used for Thin Pavement Section (Plane Strain Case) ...	259
Figure 5-33:	Comparison of Vertical Stress Variation Based on Finite Element Analysis (Axisymmetric Case) and KENLAYER Analysis	260
Figure 5-34:	Influence of Glass Grid Reinforcement on Vertical Stress Variation with Depth Based on Finite Element Analysis (Axisymmetric Case)	262
Figure 5-35:	Influence of Subgrade Stiffness on Vertical Stress Variation with Depth Based	

	on Finite Element Analysis (Axisymmetric Case)	263
Figure 5-36:	Comparison of Measured Vertical Subgrade Stresses with the Computed Values Based on Finite Element Analysis (Axisymmetric Case)	264
Figure 5-37:	Influence of Reinforcement Thickness on Vertical Stress Variation Based on Finite Element Analysis (Axisymmetric Case) [Thickness of Reinforcement = 0.5 in. (12.7 mm)]	266
Figure 5-38:	Influence of Reinforcement Thickness on Vertical Stress Variation Based on Finite Element Analysis (Axisymmetric Case) [Thickness of Reinforcement = 1.0 in. (25 mm)]	267
Figure 5-39:	Vertical Stress Variation with Depth Based on Finite Element Analysis	269
Figure 5-40:	Influence of Glass Grid Reinforcement on Vertical Stress Variation with Depth Based on Finite Element Analysis (Plane Strain Case)	270
Figure 5-41:	Influence of Shear Stiffness (G_{int}) for Interface Layer on Vertical Stress Variation with Depth Based on Finite Element Analysis (Plane Strain Case)	271
Figure 5-42:	Influence of Reinforcement (Glass Grid) on Vertical Subgrade Stress on Top of Subgrade Based on Finite Element Analysis (Plane Strain Case)	273
Figure 5-43:	Influence of Reinforcement (Glass Grid) on Vertical Compressive Strain on Top of Subgrade Based on Finite Element Analysis (Plane Strain Case)	275
Figure 5-44:	Influence of Reinforcement on Predicted Horizontal Tensile Strain at the Bottom of HMA Based on Finite Element Analysis (Plane Strain Case)	276
Figure 5-45:	Influence of Shear Stiffness (G_{int}) for Interface Layer on Predicted Vertical Compressive Strain on Top of Subgrade Based on Finite Element Analysis	

	(Plane Strain Case)	277
Figure 5-46:	Influence of Shear Stiffness (G_{int}) for Interface Layer on Predicted Horizontal Tensile Strain at the Bottom of HMA Based on Finite Element Analysis (Plane Strain Case)	279
Figure 5-47:	Influence of Reinforcement on Surface Displacement Based on Finite Element Analysis (Plane Strain Case)	280

LIST OF TABLES

Table 2-1:	Properties Of Fibers And Conventional Bulk Materials	11
Table 2-2:	Characteristics of Reinforcement Materials For Asphalt Pavements	12
Table 2-3:	Distresses In Asphalt Pavements	29
Table 2-4:	Methods Tried For Reducing Or Delaying Reflection Cracking Of AC Pavement Overlays	33
Table 3-1:	Typical Properties of Asphalt Base II Material	57
Table 3-2:	Sieve Analysis of Gravel used in the Asphalt Mix	57
Table 3-3:	Measured Unit Weight of Hot Mix Asphalt Used in the Test Sections	58
Table 3-4:	Grain Size Distribution of Gravel Base	59
Table 3-5:	Measured Unit Weight of Gravel Base	59
Table 3-6:	Atterberg Limits for Different Soil Mixtures	62
Table 3-7:	Measured Unit Weight of Subgrade Soil Used in Test Sections	65
Table 3-8:	Properties of Woven Geotextile Amoco 2002	68
Table 3-9:	Properties of Glass Fiber Grids	70
Table 3-10:	The Outline of the Experimental Program	71
Table 4-1:	Range of Vertical Subgrade Stresses for Pressure Cell #1 and Pressure Cell #2 at 9 kips (40 kN) of Static Loading	81
Table 4-2:	Measured Vertical Subgrade Stress at Cells #1 and #2 for Experiments #2, #3, and #7	87
Table 4-3:	Measured Vertical Subgrade Stress at Cells #1 and #2 for Experiments #8 and #9	87

Table 4-4:	Measured Vertical Subgrade Stress at Cells #1 and #2 for Experiments #4, #5, and #8	90
Table 4-5:	Measured Vertical Subgrade Stress at Cells #1 and #2 for Experiments #11, #12, #14, and #20	94
Table 4-6:	Measured Vertical Subgrade Stress at Cells #1 and #2 for Experiments #4, #17, and #20	101
Table 4-7:	Measured Vertical Subgrade Stress at Cells #1 and #2 for Experiments #3 and #17	101
Table 4-8:	Measured Vertical Subgrade Stress at Cells #1 and #2 for Experiments #4, #12, and #18	103
Table 4-9:	Measured Vertical Subgrade Stress at Cells #1 and #2 for Experiments #18 and #19	106
Table 4-10:	Measured Vertical Subgrade Stress at Cells #1 and #2 for Experiments #13, #14, and #16	109
Table 4-11:	Measured Vertical Subgrade Stress at Cells #1 and #2 for Experiments #4, #14, and #15	112
Table 4-12:	Measured Vertical Subgrade Stress at Cells #1 and #2 for Experiments #12, #14, #15, and #18	117
Table 4-13:	Cumulative Displacements at the Edge of the Loading Plate Corresponding to 500,000 and 1,000,000 Load Cycles	123
Table 4-14:	Range of Displacement Under Static Loading at the Edge of the Loading Plate (Displacement #3)	145

Table 5-1:	Creep Compliance Values for HMA	186
Table 5-2:	Assumed Material Properties Used in the Computer Analyses	186
Table 5-3:	Computed Vertical Stresses for Thin Pavement Section [Thickness of HMA = 3 inches (76 mm)] with Reinforcement	190
Table 5-4:	Computed Vertical Stresses beneath the Center of the Loading Plate for Thick Pavement Section [Thickness of HMA = 6 inches (152 mm)] with Reinforcement	192
Table 5-5:	Computed Vertical Stresses Beneath the Center of the Loading Plate (Stress #1) Corresponding to Case 2 for Two Different HMA Layer Thicknesses	192
Table 5-6:	Measured and Computed Vertical Subgrade Stresses at Cells #1 and #2 for 6-inch (152 mm) Thick Pavement Sections	195
Table 5-7:	Measured and Computed Vertical Subgrade Stresses at Cells #1 and #2 for the Thin Pavement Sections [Thickness of HMA = 3 inches (76 mm)]	202
Table 5-8:	Computed Vertical Stresses at Cell #1 for a Thin Pavement Section Corresponding to Different Elastic Moduli of Geosynthetic Layers for Case 2	212
Table 5-9:	Computed Elastic Surface Displacement for a Thin Pavement Section with Reinforcement Under 9 kips (40 kN) of Loading	217
Table 5-10:	Computed Elastic Surface Displacement for a Thick Pavement Section with Reinforcement Under 9 kips (40 kN) of Loading	217

Table 5-11:	Computed Elastic Displacement in a Thin Pavement Section with Reinforcement for Case 2 of Material Properties	219
Table 5-12:	Computed Elastic Displacement in a Thick Pavement Section with Reinforcement for Case 2 of Material Properties	219
Table 5-13:	Computed Elastic Surface Displacement versus Measured Displacement in a Thin HMA Section with Reinforcement	221
Table 5-14:	Computed Elastic Surface Displacement versus Measured Displacement in a Thin HMA Section with No Reinforcement	226
Table 5-15:	Computed Elastic Surface Displacement versus Measured Displacement in a Thick HMA Section with Reinforcement	226
Table 5-16:	Computed Elastic Surface Displacement versus Measured Displacement in a Thick HMA Section with No Reinforcement	228
Table 5-17:	Effect of Depth on Computed Radial and Vertical Strains in Thick and Thin Pavement Sections	235
Table 5-18:	Effect of Depth on Computed Tangential Strains in Thick and Thin Pavement Sections	237
Table 5-19:	Computed Radial and Tangential Strains on the Reinforcement Layer in Thick and Thin Pavement Sections	242
Table 5-20:	Assumed Material Properties Used in the Finite Element Analysis	257
Table 5-21:	Maximum Surface Displacements Under the Inner Edge of the Each Wheel . .	281

CHAPTER 1

INTRODUCTION

1.1 INTRODUCTION

In the United States, a high percentage of primary and secondary roads are constructed using flexible pavements, and many have been treated with an asphalt overlay on the existing pavement [Asphalt Institute (1989)]. According to the literature [Abdelhalim (1983) and Barksdale (1991)], many existing flexible pavements have either reached the end of their design life or have already deteriorated due to excessive traffic loads. As a result of economic constraints and the need to extend pavement service life, a significant portion of the pavement construction and rehabilitation efforts in many states have focused on improving pavement performance and design life. In support of this long-term objective, development of pavement reinforcement materials has become one research area receiving increased attention [Abdelhalim et al. (1982), Barksdale (1991), Brown et al. (1984), and Button and Lytton (1987)].

Asphalt is defined by the Asphalt Institute (1989) as "a dark brown to black cementitious material in which the predominating constituents are bitumens which occur in nature or are obtained in petroleum processing" [Asphalt Institute (1989)]. As a part of a flexible pavement system, asphalt was first used in the United States in Newark, New Jersey in 1870 [Asphalt Institute (1989) and Huang (1993)]. Since then, flexible pavements have gained favorable attention. The Asphalt Institute (1989) and Huang (1993) reported that by 1989, 94% of the roads in the United States were surfaced with asphalt. A typical cross section of a flexible pavement for a roadway application is illustrated in Figure 1-1.

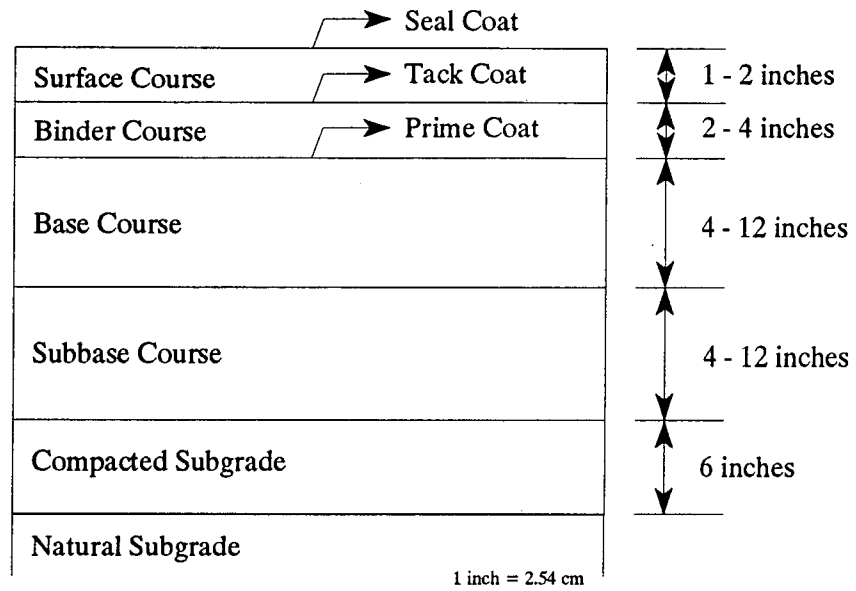


Figure 1-1: Typical Cross Section of a Conventional Flexible Pavement [Huang (1993)]

Engineers started exploring new methods to improve pavement performance in order to reduce highway repair costs. One example of a cost-saving resurface treatment for deteriorating pavements is the use of an asphalt concrete overlay on the existing concrete pavement. During the last decade, many miles of old concrete pavement highways have been repaired or resurfaced using asphalt overlays. The Asphalt Institute (1989) defines asphalt overlay as "one or more courses of asphalt construction on an existing pavement." Placing an asphalt overlay on the existing pavement is one of the most common treatments to correct the surface problems associated with old pavements [Asphalt Institute (1989) and Huang (1993)]. Rehabilitated pavements using asphalt (overlay) offer structural strength and provide riding comfort to return the roadways to safe conditions. Important considerations which are factored into the decision making process on whether to use asphalt overlays include [Barksdale (1991)]:

- structural strength of existing pavements
- traffic volume
- environmental (climate) factors such as rainfall and temperature
- design life of the new treatment
- pavement condition (smoothness and distress)

A major problem encountered with asphalt resurfacing is the phenomenon termed reflection cracking (or reflective cracking). Reflection cracks in pavement overlays are one of the most significant factors in pavement deterioration [Barksdale (1991) and Jackson (1980)]. Reflection cracks are caused by shear and tensile stresses in the asphalt layer induced by traffic loads, change in temperature, expansive subgrade soils, existing cracks, and joint and crack movements in the underlying pavement. In many pavement systems, reflection cracking is not the only problem leading

to roadway deterioration. Some of the roads are built on weak subgrade unable to carry the expected traffic load [Smith et al. (1995)].

Smith et al. (1995) reported that most of the strength of flexible pavements depends on the Hot Mix Asphalt (HMA) and gravel base layers. Problems in these layers leading to rutting (permanent deformation) in the pavement system include poor compaction of the HMA and gravel base, plastic movements of the HMA in hot weather conditions, lateral movements of the material due to traffic load, or consolidation of weak subgrade [Huang (1993)]. In addition to weak subgrade, migration of fine particles into the base course and migration of aggregates into the soft (weak) subgrade cause movements and eventually loss of strength in the pavement system. This process leads to surface roughness, rutting and eventual cracking [Smith et al. (1995)]. Stabilizing the subgrade and/or gravel base layer and increasing the thickness of the HMA and/or gravel base layer are measures which could be taken to obtain structurally adequate roads [Smith et al. (1995)]. However, these are costly processes and may not be viable in many engineering instances.

To improve pavement performance economically, fabric materials have been used since the 1920's as reinforcements and continue to gain acceptance in pavement resurfacing applications [Huang (1993), Koerner (1994), and Smith et al. (1995)]. Researchers have different opinions about the use of fabric reinforcement, but the majority have concluded that fabric reinforcement reduces surface failures (rutting and cracking) [Barksdale (1991) and Smith et al. (1995)]. The application of geosynthetics in roadway work has become more popular in recent years due to their high strength, good chemical resistance, and low cost [Barksdale (1991), Koerner (1994), and Smith et al. (1995)]. In pavement applications, they function to relieve stress by reinforcing the pavement and reducing water infiltration to underlying layers [Barksdale (1991)]. With these advantages, however, there

were initial concerns over the possibility that the high temperature of asphalt might cause some shrinkage in the synthetic fabrics used as reinforcement. Similarly, the development of shear stresses caused by traffic loads could cause slippage cracks in overlay materials [Barksdale (1991)]. In terms of reinforcement, Barksdale (1991) indicated that studies to date have shown that geosynthetics have performed better under load-related fatigue distress than in thermal-related failures. Various types of geosynthetics have been used to improve pavement performance. These include geotextiles and plastic grids. Some researchers have shown that geotextiles were not very effective in preventing and/or reducing reflection cracking [Barksdale (1991), Button and Lytton (1987), and Lytton (1989)]. However, some success was reported under favorable conditions [Abdelhalim (1983) and Barksdale (1991)]. Reducing water infiltration into the pavement structure and providing separation in underlying layers have provided substantial benefits in terms of performance. According to Lytton (1989), reinforcing the HMA inside the pavement system requires that the elastic modulus of the fabric be greater than that of the surrounding material (HMA). Glass fiber grids meet these requirements in terms of stiffness, and they provide better resistance against lateral movements than that provided by geotextiles [Barksdale (1991) and Lytton (1989)].

In the past, most research work on flexible pavements has focused on geotextile and polymer-based grid reinforcement, which do provide some reinforcement benefits. There is limited published information on glass fiber grid reinforcement inside the HMA in a pavement system [Button and Lytton (1987)]. This growing research area is the focus of the research presented in this report. A schematic figure of a reinforced pavement section is shown in Figure 1-2. Designing a flexible pavement reinforced with glass fiber grid and establishing the performance of a reinforced pavement system is a complex problem requiring considerable research and study. The fundamental

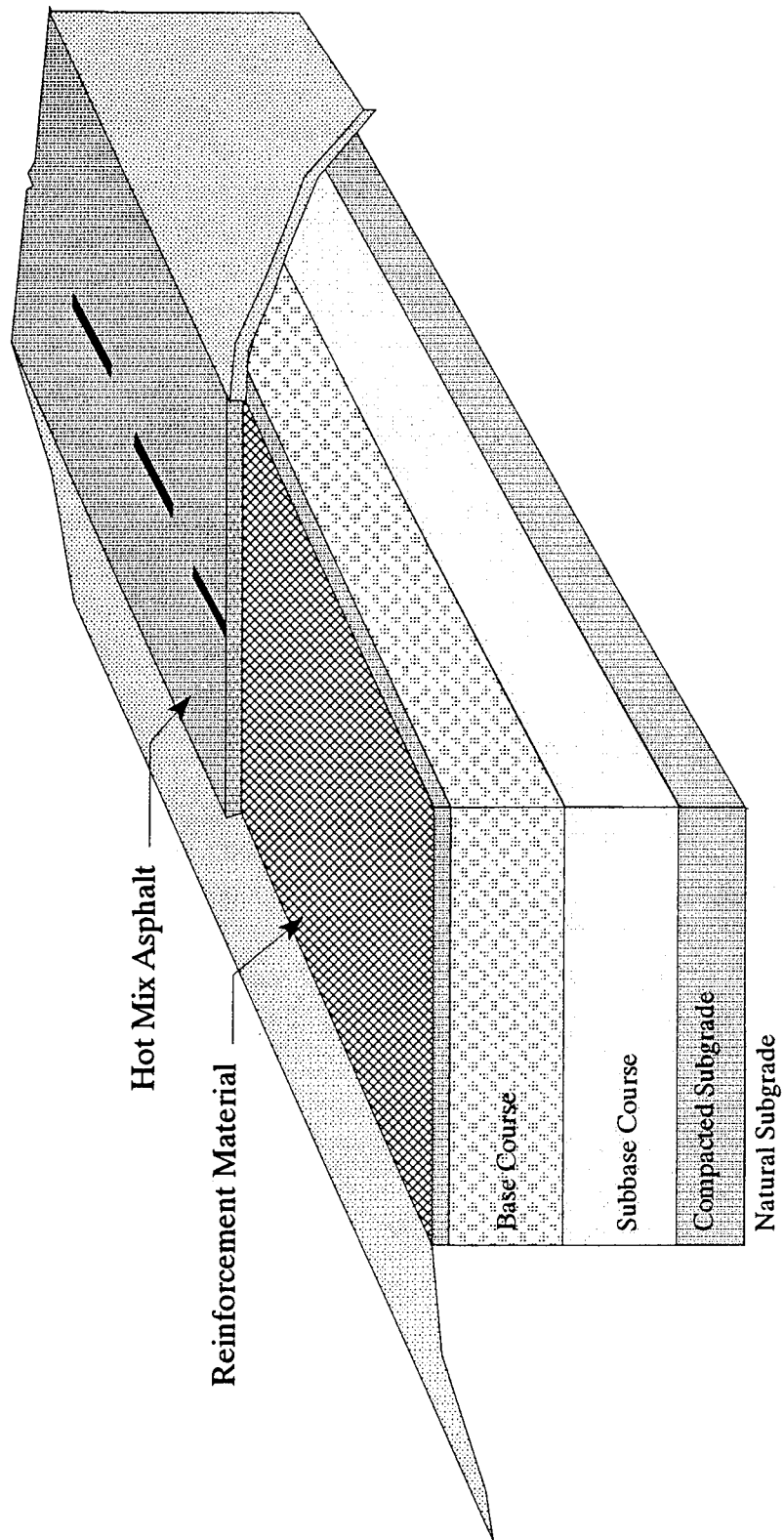


Figure 1-2: A Schematic Figure of a Reinforced Pavement Section

mechanisms related to glass fiber grid performance must be identified and analyzed for a better understanding of the reinforcement function of the grid in the pavement section.

1.2 OBJECTIVES

The full-depth asphalt pavements have been successfully used in the past and such pavements can potentially be used in the State of West Virginia. The major objective of this research project was to determine the influence of glass fiber grids used within the asphalt base course on the performance of pavement sections. The following items highlight the specific objectives of this research work:

- Influence of the glass grid reinforcement on 6-inch (152 mm) thick asphalt sections
- Influence of the glass grid reinforcement on 3-inch (76 mm) thick asphalt sections
- Influence of the glass grid reinforcement on a 2.5-inch (63.5 mm) thick asphalt section
- Influence of three different types of glass grids on 6-inch (152 mm) thick asphalt sections
- Influence of a simulated crack on 3-inch (76 mm) thick asphalt sections
- Computer analyses of flexible pavement sections
- Comparison of the results from computer analyses with the laboratory measurements

To achieve these objectives, twenty flexible pavement sections, with and without glass fiber grids, were constructed and tested in the laboratory. At the recommendation of the sponsoring agency, West Virginia Department of Transportation, Asphalt Base II was used as the hot mix asphalt in the experimental program.

1.3 SCOPE OF RESEARCH

- The scope of this study was limited to the laboratory and computer analyses of a flexible pavement system.
- The scope was limited to the reinforcement of the asphalt base course only.
- In the laboratory study, wheel load simulation was done by a circular loading plate.
- Computer analyses were limited to linear visco-elastic analyses and two dimensional finite element analyses.

1.4 REPORT OUTLINE

A literature review on previous studies related to the reinforcement of flexible pavements (laboratory and numerical) is included in Chapter 2. Chapter 3 contains the details of the construction of test section and experimental program. Chapter 4 contains the laboratory test results with data reduction and performance evaluation. The details of the computer analyses and its results are presented in Chapter 5. Summary, conclusions, and recommendations are given in Chapter 6.

CHAPTER 2

LITERATURE REVIEW

2.1 FABRIC AND GRID INTERLAYERS IN PAVEMENT SYSTEMS

The main objective of this research work was to evaluate the effectiveness of the use of geogrids as a reinforcement material for flexible pavement systems. Various types of fabrics and grids have been used in flexible pavements in both laboratory studies and field experiments [Abdelhalim et al. (1982), Abdelhalim (1983), Barksdale (1991), Brown et al. (1984), Brown et al. (1985), Brownridge (1964), Button and Lytton (1987), Carroll et al. (1987), Giroud et al. (1984), Giroud and Noiray (1981), Haas (1984), Hozayen et al. (1993), Jackson (1980), Jewel et al. (1984), Kennepohl et al. (1985), Lytton (1989), Smith and Gartner (1959), Smith et al. (1995), Siriwardane and Kutuk (1997) and Webster (1992)]. The main functions of these materials are stress relief, pavement reinforcement, water infiltration reduction, and separation [Barksdale (1991) and Koerner (1994)]. Geogrids and geotextiles are the only geosynthetic materials studied in this research and their material properties are introduced in this chapter. Detailed properties of available fabrics and manufacturers can be found elsewhere [Geotechnical Fabrics Association International (1995)].

2.1.1 Geogrids

Geogrids are usually stiff materials formed into a grid like structure with large apertures [Koerner (1994)]. Geogrids are made of different fiber reinforced composite materials such as glass fibers and/or polymeric fibers. Agarwal and Broutman (1990) define fibrous composite materials as having two or more chemically distinct structures with a distinct interface separating them. Due to the small cross-sectional areas, using fibers alone in engineering applications is not suitable. Therefore, the fibers are embedded in matrix materials to form fibrous composites. The purpose of

a matrix is to serve as a binder and to transfer loads to the fibers, as well as to protect the fibers against hostile environmental conditions such as chemical substances. Table 2-1 shows the properties of fibers and conventional bulk materials prior to forming as a composite material. Table 2-2, conversely, shows the properties of various reinforcement materials in composite form. The discrepancy in the properties of the reinforcement materials (Table 2-1 versus Table 2-2) may be explained by the volume fractions of the composite materials. The relative proportions of the matrix and reinforcing material can be defined as the volume fractions or the weight fractions. A mathematical model to define the longitudinal properties (tensile strength and modulus of elasticity) of a unidirectional composite material can be found in detail in the literature [Agarwal and Broutman (1990)]. Based on this mathematical model, average elastic modulus of the composite material can be simply written as:

$$E_c = E_f V_f + E_m V_m \quad (2.1)$$

where

E_c = Elastic modulus of the composite

E_f = Elastic modulus of the fiber

E_m = Elastic modulus of the matrix

V_f = Volume fraction of the fiber

V_m = Volume fraction of the matrix

From this equation, it can be said that the average composite properties are proportional to their volume fractions. By bonding the fibers with the matrix, the elastic modulus of the composite gets smaller in comparison to the modulus of the fiber itself. Furthermore, the measured strengths of most

Table 2-1: Properties Of Fibers And Conventional Bulk Materials [Agarwal and Broutman (1990)]

Material		Tensile Modulus (E) (GPa)	Tensile Strength (σ_u) (GPa)	Density (ρ) (g/cm ³)	Specific Modulus (E/ ρ)	Specific Strength (σ_u/ρ)
Fibers	E-Glass	72.4	3.5 ^a	2.54	28.5	1.38
	S-Glass	85.5	4.6 ^a	2.48	34.5	1.85
	Silica	72.4	5.8	2.19	33	2.65
	Beryllium	240	1.3	1.83	131	0.71
	Kevlar 49 (aramid polymer)	130	2.8	1.5	87	1.87
Conventional Materials	Steel	210	0.34 - 2.1	7.8	26.9	0.043 - 0.27
	Aluminum Alloys	70	0.14 - 0.62	2.7	25.9	0.052 - 0.23

^a Virgin strength values. Actual strength values prior to incorporation into composite are approximately 2.1 GPa.

Table 2-2: Characteristics of Reinforcement Materials For Asphalt Pavements [Kennepohl and Kamel (1984)]

Property	Steel Mesh	Glass Fiber	Polypropylene
Tensile Strength (psi) [kN/m ²]	6,525 [44,957]	72,500 [499,525]	5,510 [37,964]
Elastic Modulus (psi) [kN/m ²]	3,770,000 [25,975,300]	4,205,000 [28,972,450]	217,500 [1,498,575]

materials are found to be much smaller in comparison to their theoretical strengths due to the presence of imperfection flaws in the material [Agarwal and Broutman (1990)].

Geogrids are primarily stretched in one or two directions. One type of geogrid, the uniaxial grid, is designed for applications where the major principal stress direction is known. For application where the geogrid stresses are random, biaxial geogrids were developed. To function as a reinforcing material, geogrids must have high elastic modulus and tensile strength relative to their surrounding materials [Koerner (1994)]. Thermal stability, biodegradability, ease of installation, and cost effectiveness are additional desirable criteria in determining the desirable geogrid material. A number of factors affect the choice of glass fiber grid from among the potential grids made of materials such as steel, polypropylene, kevlar, and carbon fibers. The properties of several types of fibers with conventional materials are shown in Tables 2-1 and 2-2 [Agarwal and Broutman (1990) and Kennepohl and Kamel (1984)]. Based on previous studies [Brownridge (1964), Smith and Gartner (1959) and Tons and Korokosky (1960)], steel wire mesh was the first material to be ruled out due to construction (installation difficulties) and performance (corrosion or rusting) problems. Even though carbon and kevlar fibers had unique properties such as high tensile strength, high modulus, and low fiber elongation for reinforcement, the cost is the major drawback for these fiber materials [Agarwal and Broutman (1990) and GlassGrid Manufacturer's Literature (1995)]. Kevlar fibers also showed very poor compression characteristics, such as compressive strength of one-eighth of its tensile strength.

In addition to the aforementioned mechanical properties (high tensile strength, high modulus, and low elongation) which meet the requirements for reinforcement, the glass fiber's relative low cost in comparison to the cost of carbon and kevlar fibers is an advantage [Agarwal and Broutman

(1990)]. The biaxial structure, low elongation at break, absence of creep, and interlock mechanism of glass fiber grid offer additional advantages over other grid types and geotextiles. As shown in Table 2-2, glass fiber's tensile strength is over ten times higher than the steel mesh's tensile strength. Furthermore, glass fiber's elastic modulus is clearly the highest in comparison to the reinforcing materials such as steel mesh and polypropylene. These advantages clearly show that the glass grid has good characteristics for reinforcement. While glass fiber grids have some disadvantages such as poor resistance against organic chemical attacks, the fibers are protected against such chemical attacks by encapsulated bundles. The small cross-sectional diameter of glass fibers helps its structure by allowing for less surface area contact to the chemical substance attack, and providing the flexibility for the glass fiber grids to bend without breaking. Large diameter fibers are extremely brittle [Barksdale (1991), Agarwal and Broutman (1990) and GlassGrid Manufacturer's Literature (1995)]. Usually glass fibers are made with fibers of very small diameters (9 or 13 mm) [Agarwal and Broutman (1990)]. The glass fiber grid used in this research was coated with modified polymer and adhesive backing. There is some question about the effectiveness of the interlock mechanism of the glass fiber grid inside the asphalt layer since it is laid out on a flat surface after the first lift of Hot Mix Asphalt (HMA). Based on the observations made during the construction of test sections in this study, it can be stated that asphalt compacted on top of the glass grid may provide good interaction between the asphalt material and the grid apertures.

2.1.2 Geotextiles

Koerner (1994) defines geotextiles as "permeable textile-like materials (usually synthetic) used with soil, rock, or any other geotechnical engineering-related material to enhance the performance or cost of human-made product, structure, or system." These materials are commonly used for

separation of different soil materials, reinforcement of low strength soils and other materials, and filtration and drainage applications. Major uses of these materials can be found in the literature [Koerner (1994)]. The application of geotextiles in pavement systems has focused on separation to prevent migration of fines into the gravel base, drainage or filtration to remove water from the pavement system, and prevention and reduction of reflective cracking [Abdelhalim (1983), Barksdale (1991) and Koerner (1994)].

As demonstrated in the literature [Abdelhalim (1983)], these applications are designed for supporting the pavement system rather than for reinforcing internal strength, though they add some strength to the pavement system. In order to reinforce the pavement system, the geotextile layer must have high elastic modulus, tensile strength, low elongation, and good creep characteristics. Some textile fabrics on the market have the properties and potential to be used in an asphalt layer. However, they possess high elongation, which is not a desirable feature for reinforcement in comparison to glass fiber grids.

Koerner (1994) explained that, for unpaved roads, the geotextiles used in soils with a California Bearing Ratio (CBR) higher than 6.0 would have a very low reinforcement function and their primary function would be for separation. The reinforcement function would have more effect in the system for soils having a CBR value lower than 3.0. The reason for this is that placing an asphalt surface over an excessively yielding soil (deformable soil) would have instability problems such as cracking [Koerner (1994)]. For many state transportation agencies, the acceptable lower limit of CBR values range between 10 and 13. The geotextile used between the soil subgrade and gravel base course in this research project is only for separation purposes.

2.2 FUNCTIONS OF GEOGRIDS AND GEOTEXTILES INFLUENCING PAVEMENT PERFORMANCE

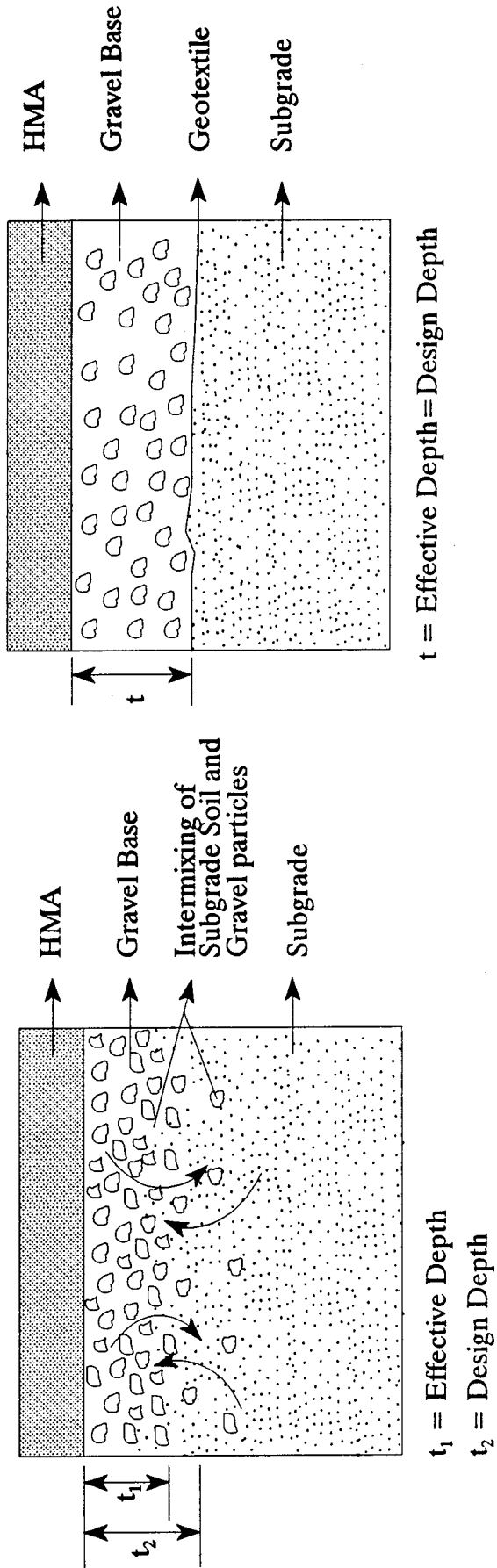
The main functions of geogrids and geotextiles to improve flexible pavement performance are:

1. Separation
2. Filtration
3. Reinforcement

Separation and filtration are the functions applicable to a geotextile. However, a geotextile may provide some support for the reinforcement mechanism of the pavement system, and reinforcement is a function applicable to the grid used in this research project.

2.2.1 Separation

The purpose of separation is to prevent mixing of the two different materials (soil and gravel). This action maintains the integrity of the soil structure by preventing the subgrade soils from migrating into the gravel base and mixing. Reduction of the effective base thickness due to intermixing of the two different layers causes a decrease in the load-carrying capacity of the pavement system [Figure 2-1] [Koerner (1994), Smith et al. (1995) and Amoco Manufacturer's Literature (1994)]. Intrusion of the subgrade soil into the gravel base further decreases the drainage capability of the gravel base. Intermixing of the two different materials leads to the pavement deterioration. For these reasons, it is important to place a geotextile fabric between the gravel base and the weak subgrade for the purpose of separation. To fulfill the separation function, geotextiles must satisfy several important engineering parameters, including burst resistance, tensile strength, puncture (tear) resistance, and impact resistance [Koerner (1994)]. These parameters are discussed in more detail in the following sections.



a) Without Geotextile

b) With Geotextile

Figure 2-1 : Separation Function of a Geotextile [Amoco Manufacturer's Literature (1994)]

Burst Resistance: Under a traffic load, the stresses in the subgrade soil will try to push the geotextile fabric into the voids of the gravel base [Figure 2-2]. Geotextile must withstand this resistance for successful operation. The required geotextile strength can be calculated as [Koerner (1994)]:

$$T_{req} = \frac{1}{2} p' d_v [f(\epsilon)] \quad (2.2)$$

where

- T_{req} = the required geotextile strength,
- $f(\epsilon)$ = the strain function of the deformed geotextile,
- p' = the stress at the geotextile's surface (equal or less than the tire inflation pressure " p "),
- d_v = the maximum void diameter $\approx 0.33 d_a$,
- d_a = the average aggregate diameter.

Detailed explanations can be found in the reference [Koerner (1994)].

Tensile Strength Requirement: During the separation and reinforcement processes, the geotextile must accommodate the lateral forces applied by aggregates that lie against the fabric. A tensile stress in the fabric should be mobilized to prevent an upper piece of gravel (aggregate) from forcing itself between the two lower pieces that lie against the fabric, as shown in Figure 2-3. The mobilized tensile force can be calculated as [Koerner (1994)]:

$$T = p' (d_v)^2 [f(\epsilon)] \quad (2.3)$$

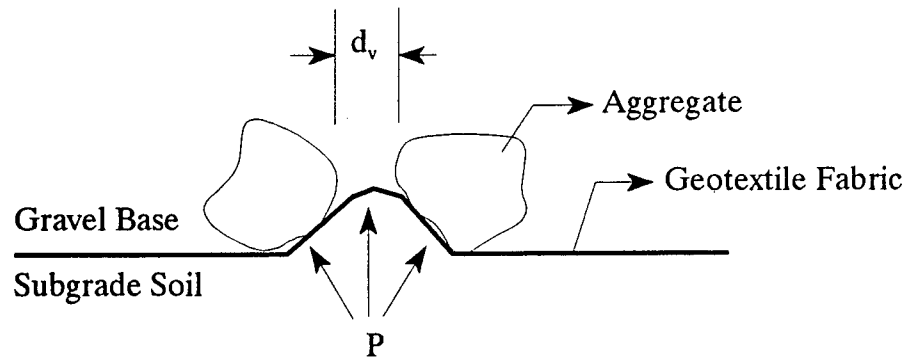


Figure 2-2: Schematic Diagram of Burst Resistance in Geosynthetic Fabric [Koerner (1994)]

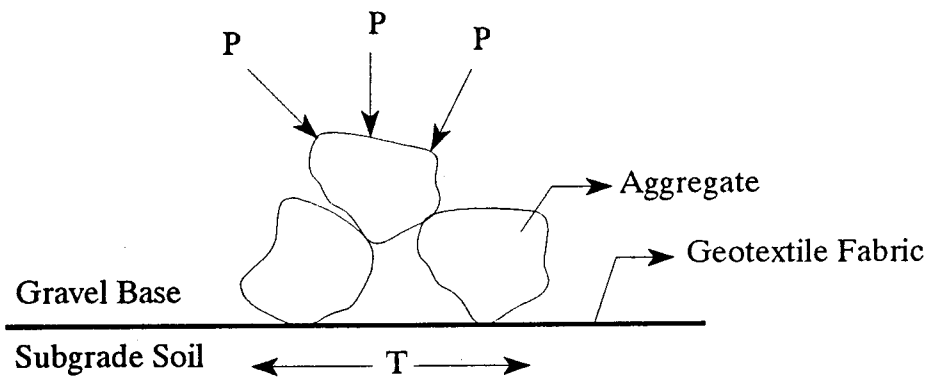


Figure 2-3: Schematic Diagram of Tensile Strength in Geosynthetic Fabric [Koerner (1994)]

where

- T = the mobilized tensile force,
- $f(\epsilon)$ = the strain function of the deformed geotextile,
- p' = the applied pressure,
- d_v = the maximum void diameter $\approx 0.33 d_a$,
- d_a = the average aggregate diameter.

In addition to the tensile strength requirement of the fabric, puncture resistance and impact resistance are the two other features that should be considered. Sharp objects such as angular stones which lie against the geotextile may puncture the fabric either during the installation process or under the applied traffic loads. The geotextile must resist this puncturing process. In addition, the geotextile must demonstrate resistance to falling material during installation. For example, rocks and construction equipment can damage the geotextile. Detailed explanations of these subjects can be found in the reference [Koerner (1994)].

2.2.2 Filtration

Filtration is a major geotextile function. Geogrids, unlike geotextile fabrics, are not suitable for this purpose since they are not intentionally designed to prevent the migration of fine particles. The purpose of geotextile filtration is to provide adequate permeability while retaining the soil without clogging (fine particle intrusion). To accomplish this function, geotextiles must have adequate open fabric structure for water flow, and a tight enough fabric structure for soil retention [Koerner (1994) and Smith et al. (1995)].

2.2.3 Reinforcement

The subgrade and the gravel base are designed to withstand compressive forces; however, they lack the ability to withstand tensile forces. It is important for pavement layers to have enough tensile strength to resist tensile forces in the pavement system. Inclusion of a geotextile inside the pavement system may increase the tensile strength, thereby providing better performance for the pavement system [Koerner (1994), Smith et al. (1995) and Amoco Manufacturer's Literature (1994)]. Therefore, the most important factor for the reinforcement function is how the pavement system performs in tension (tensile stresses and strains). To satisfy the reinforcement function, a fabric must [Abdelhalim (1983)]:

- a) carry and spread most of the tensile stresses induced by traffic loading,
- b) retard or prevent the reflective cracking.

Even though geotextiles have most of the desired mechanical properties for a reinforcement material, their poor physical and endurance properties such as stiffness and creep, respectively, in comparison to geogrids make them more suitable for application to lower layers of a pavement system (such as the subgrade or gravel base). Since the most important feature of the reinforcement material is its high tensile strength, geotextiles do not fulfill this requirement. However, three functions of geotextiles (separation, stabilization, and filtration) can increase the strength of the pavement system. It is apparent that the installation of a geotextile at the gravel base-subgrade interface would reduce particle migration and increase water drainage, important functions in preventing pavement deterioration.

Geogrids with large openings provide good lateral confinement (restraint reinforcement) within the load-bearing stone structure of the pavement system due to an interlock mechanism

[GlassGrid Manufacturer's Literature (1995), Carroll et al. (1987) and Smith et al. (1995)]. Their high tensile strength, modulus, and low creep under applied load can provide good reinforcement to the hot mix asphalt (HMA). Barksdale (1991) concluded that only the stiffest grids have potential as reinforcement material in an asphalt concrete overlay. Therefore, geogrids used in the hot mix asphalt (HMA) seem more feasible and promising than geotextile fabrics [Abdelhalim (1983), Barksdale (1991) and Koerner (1994)].

2.3 PROPERTIES OF GEOSYNTHETICS

Physical and mechanical properties play an important role in the process of selecting the best geosynthetic material for reinforcement in a flexible pavement system. It is important to define and discuss some of the critical properties with respect to HMA reinforcement. Tensile strength and stiffness are the main properties for a reinforcement material [Abdelhalim (1983 and Barksdale (1991)]. In addition to physical and mechanical properties, endurance properties like creep resistance and environmental properties like temperature, chemical and biological resistance must be considered [Abdelhalim (1983) and Koerner (1994)]. Since the properties of products on the market vary widely, it is up to the design engineer to evaluate the properties and choose the best candidate for the application.

2.4 PHYSICAL PROPERTIES

Physical properties include the type of structure, type of geogrid, aperture size, thickness, weight, and width. These physical properties play an important role in the selection process since they are related to economic considerations and convenience of handling [Abdelhalim (1983) and Koerner

(1994)]. The physical properties of chosen glass fiber grid and geotextile are discussed in Chapter 3.

2.5 MECHANICAL PROPERTIES

Some of the important mechanical properties of a geogrid with respect to the reinforcement mechanism of a flexible pavement system are tensile strength, stiffness, and anchorage strength. These properties are discussed in more detail in the following paragraphs.

2.5.1 Tensile Strength

To increase the performance of a flexible pavement, the geogrid must provide high tensile strength to the pavement system for use as a reinforcement material. The test procedure to measure the tensile strength of a geogrid calls for placing the fabric within a set of clamps and stretching it from the ribs until failure occurs [Koerner (1994)]. During this stretching process, both load and deformation are measured and a plot of the stress-strain relationship is graphed. From this process, valuable informations such as fabric strength (maximum tensile stress), maximum elongation (strain at failure), toughness, and elastic modulus are obtained. There are two types of manufactured geogrids: uniaxial and biaxial. Some geogrids are uniaxial, which means that the tensile strength of the fabric is in its manufactured machine direction. For biaxial products, the tensile strength is developed in both machine and cross-machine directions. Biaxial geogrids are for applications where the stresses are random under applied loads [Koerner (1994)].

2.5.2 Stiffness

A geogrid's stiffness when used as a reinforcement material is equal to its elastic modulus times its thickness [Barksdale (1991)]. One of the studies has shown that low stiffness fabrics were not successful in reinforcing a gravel base layer which was subjected to low deformation [Barksdale

(1991)]. Since flexible pavements are subjected to low deformation conditions, glass fiber grids with high stiffness inside the hot mix asphalt (HMA) are more capable of reinforcing a pavement system. To be effective in a reinforcement mechanism, a reinforcing material must be as stiff as its surrounding material [Barksdale (1991)]. Barksdale (1991) states that to reinforce an asphalt concrete layer, a fabric stiffness must be at least 4000 lbs/in before reinforcement begins, but having a high elastic modulus alone does not mean that reinforcement will take place. In the same study, it was also shown that a geogrid with a large aperture size in unstabilized gravel base would provide the same reinforcement as a woven geotextile which was 2 to 2.5 times stiffer than the geogrid [Barksdale (1991)]. In conclusion, the geogrid should be stiff enough to withstand vertical stresses, and flexible enough to distribute the stresses uniformly and reduce the intensity to underlying layers [Abdelhalim (1983)].

2.5.3 Anchorage Strength

In the literature [Smith et al. (1995)], anchorage strength is defined as the horizontal tensile force required to pull out the geogrid confined by surrounding material. The geogrid must be gripped from within the surrounding material to find out the frictional (pull out) resistance between the surrounding material and the geogrid. If it is gripped from outside the surrounding material, unknown additional stresses could be imposed on the front portion of the geogrid. Three separate mechanisms would affect this anchorage strength [Koerner (1994)]:

1. Shear strength of the longitudinal ribs,
2. Shear strength of the transverse ribs,
3. Passive resistance of the soil against the front of the transverse ribs.

The frictional resistance of the transverse ribs must be transferred to the longitudinal ribs by the nodes

of a geogrid (Figure 2-4). Therefore, it is important to evaluate the node strength of the geogrid. Anchorage strength developed by the interlock mechanism in the aggregate base course improves the performance of paved roads [Abdelhalim (1983) and Koerner (1994)].

2.6 INTERLOCK AND ADHESION (BOND) MECHANISM OF GEOGRID REINFORCEMENT

This is one of the most important mechanisms for geogrids used as reinforcement. It not only increases the tensile strength but also provides good lateral confinement for the reinforcement mechanism. The use of geogrids within the gravel base in a pavement system would provide a good interlock advantage due to their large aperture sizes. In the literature [Abdelhalim (1983)], it is explained that the tensile stresses caused by traffic loads are transferred through the aggregate to the geogrid's longitudinal and transverse ribs. Due to very high modulus of geogrids, some compressive stresses are assumed to occur in the asphalt aggregate mix, leading to less tensile stress in the asphalt layer. Additionally, high friction caused by the interlock mechanism between the geogrid and the hot mix asphalt would increase the anchorage strength and improve the performance of the pavement system. Proper bonding between the grid and the asphalt mix would increase the tensile strength of the hot mix asphalt (HMA) [Abdelhalim (1983)]. The ability to increase the tensile strength is a good feature for preventing or limiting fatigue cracking and rutting if the geogrid is placed in the tension zone of the asphalt layer of the pavement system [Kennepohl et al. (1985)]. Good adhesion (bond) between the geogrid and the hot mix asphalt (HMA) is essential in preventing shearing and delamination between the materials. It is believed that this feature with the help of interlock mechanism increases the performance of the glass fiber grid in the hot mix asphalt (HMA) even

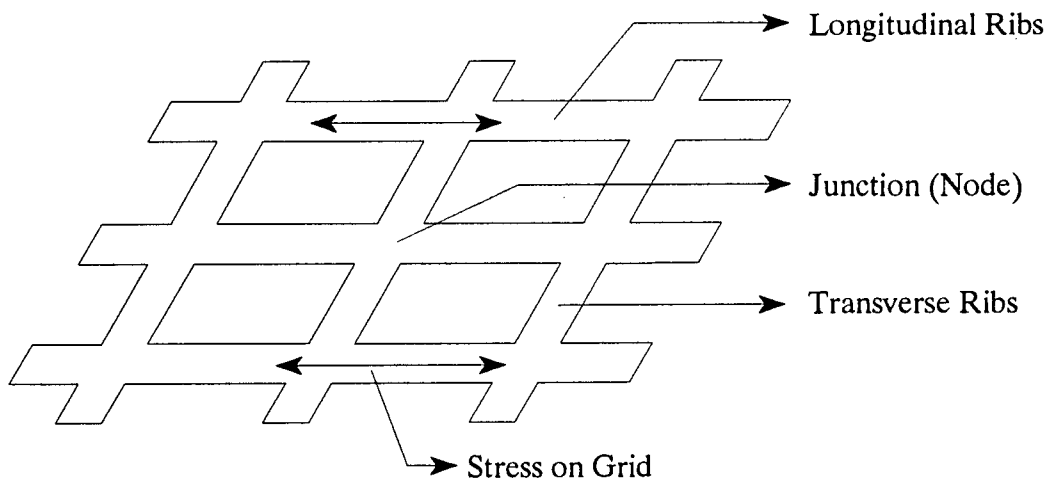


Figure 2-4: Typical Geogrid Sections [Koerner (1994)]

further.

2.7 CREEP RESISTANCE

Initially many reinforcement materials seem to be stable, but over a long term they exhibit load-deformation or “creep” under constant loading [Koerner (1994)]. The load is usually determined as a percentage of the fabric’s strength. Creep rates are calculated from the percent strain versus log time graph. If fabrics exhibit very low or no creep deformation, the fabric lasts longer and eventually increases the pavement’s performance [GlassGrid Manufacturer’s Literature (1995)]. Glass fiber grids have low creep characteristics compared with polymeric materials. Therefore, glass grids have a better potential for use as a reinforcing material in asphaltic pavements.

2.8 PAVEMENT PERFORMANCE

Flexible pavements are a complex engineering structure. Some of the factors and parameters which affect pavement performance identified in the literature [Abdelhalim (1983), Barksdale (1991) and Huang (1993)] include:

- pavement distress,
- structural strength,
- materials,
- traffic volume,
- serviceability,
- climate.

Several of these items, such as serviceability, were not applicable to laboratory testing conditions, and

therefore are not discussed here. The important parameters as identified in the literature [Abdelhalim (1983) and Barksdale (1991)] include:

- elastic properties of the flexible pavement layers such as elastic modulus and poisson's ratio of HMA, gravel base, subgrade, and reinforcement material,
- thickness of the layers such as hot mix asphalt (HMA),
- load magnitude and load duration (volume of traffic),
- failure criteria with respect to rutting and cracking,
- environmental factors such as climate and aging.

2.8.1 Pavement Distress

Knowledge of pavement distress is an important part of the evaluation of the pavement performance, and requires special consideration. Two types of failure can occur in flexible pavements. These are classified as either (1) structural or (2) functional failures [Huang (1993) and Yoder and Witczak (1975)]. Structural and functional failures are either load related or non-load related [Huang (1993)]. A good classification of distress types, and whether they are structural or functional failures (and load or non-load related distresses), is identified by Huang (1993) (Table 2-3). Structural failure of the pavement is defined as the breakdown of components or the inability of one or more of the layers to carry the applied load. Functional failure is defined as the pavement's inability to function properly. For example, poor ride quality due to roughness of the surface course is considered as a functional failure. Functional failure may or may not be the result of structural failure [Huang (1993) and Yoder and Witczak (1975)].

Table 2-3: Distresses In Asphalt Pavements [Huang (1993)]

Types of Distress	Structural	Functional	Load Associated	Non-Load Associated
Alligator or Fatigue Cracking	✓		✓	
Bleeding		✓		✓
Block Cracking	✓			✓
Corrugation		✓		✓
Depression		✓		✓
Joint Reflection Cracking	✓			✓
Lane/Shoulder Dropoff or Heave		✓		✓
Lane/Shoulder Separation		✓		✓
Longitudinal and Transverse Cracking	✓			✓
Patch Deterioration	✓	✓	✓	
Polished Aggregate		✓	✓	
Potholes	✓	✓	✓	
Pumping and Water Bleeding	✓	✓	✓	✓
Raveling and Weathering		✓		✓
Rutting		✓	✓	
Slippage Cracking	✓		✓	
Swell	✓	✓		✓

2.8.2 Rutting

In flexible pavements, rutting is identified as one of the most commonly encountered deterioration problems, and usually appears during the first few years of pavement design life. Rutting, defined as the depression of the asphalt surface along the wheel paths, is classified as a functional failure, and might lead to major structural failures. Some of the reasons which lead to rutting are [Huang (1993) and Yoder and Witczak (1975)]:

- 1) the consolidation of the subgrade,
- 2) the consolidation of the gravel base (to a lesser extent),
- 3) lateral movements of the pavement materials due to heavy traffic loads,
- 4) under-design of thickness,
- 5) plastic movements of hot mix asphalt due to hot weather,
- 6) inadequate compaction of the layers.

2.8.3 Alligator (Fatigue) And Block Crackings

Alligator cracking resembles the skin of an alligator. It is caused by fatigue of the asphalt surface and/or excessive movement of the pavement layers under repeated traffic loads. One of the causes to this failure is weak or poorly compacted base layers or subgrades. Additionally, subgrade softening due to the freeze-thaw cycles is another cause of this type of failure. Alligator cracking, classified as major structural failure, is load-related [Huang (1993) and Yoder and Witczak (1975)].

Block cracking, on the other hand, is classified as structural failure but is not load-related. The primary cause is the shrinkage of hot mix asphalt due to temperature cycling, which causes cyclic stresses and strains in the asphalt layer [Huang (1993)].

2.8.4 Reflection Cracking

The propagation of existing cracks from the old or existing (rigid) pavement layer into the new overlay is called reflection cracking [Jayawickrama and Lytton (1987) and Lytton (1989)]. This type of cracking usually appears in the surface (overlay) at the location of transverse or longitudinal joints of old concrete slabs, although some non-joint cracks are possible. Tensile and shear stresses caused by the underlying pavement across cracks and joints due to traffic loading (movements), moisture changes, thermal movements (expansion and contraction), or curling and warping of rigid slabs cause the cracks to propagate into the overlay. The traffic, crack spacing, subgrade stiffness, presence of voids beneath the pavement surface, overlay thickness, and fabric position affect the rate of crack propagation [Lytton (1989)]. The crack propagation theory is based on the empirical fracture mechanics law and can be expressed as [Paris and Erdogan (1963)]:

$$\frac{dc}{dN} = AK^n \quad (2.4)$$

where,

- c = Crack length,
- N = Number of load cycles to failure,
- K = Stress intensity factor at crack tip,
- A, n = Fracture properties of the material.

If the stress intensity factor at the crack tip decreases, crack propagation decreases. This would be theoretically possible with the inclusion of a reinforcement layer, which reduces the tensile stress at the crack tip [Barksdale (1991), Brownridge (1964), Paris and Erdogan (1963) and Smith (1983)].

Treatments and techniques tried over the years to reduce or prevent reflective cracking

include [Barksdale (1991) and Jackson (1980)]:

- Placement of fabrics under the AC overlay,
- Reinforcement of AC overlay (steel wire mesh, fabrics such as polymer grids),
- Increased thickness of asphalt overlay,
- Stress relieving interlayers,
- Asphalt mix additives,
- Bond breakers at joints of PCC pavements.

In summary, methods for reducing or delaying reflective cracking are listed in Table 2-4 [Barksdale (1991)] with further explanations found in the literature [Lytton (1989)].

2.8.5 Longitudinal And Transverse Cracking

Asphalt hardening due to cold temperature, frost action (volume change in the subgrade soil), cracks from the old pavement, or lack of internal friction in the gravel base or/and subgrade soil are some of the causes of longitudinal and transverse cracking [Huang (1993) and Yoder and Witczak (1995)]. Longitudinal cracks usually appear on longitudinal widening joints and are also referred to as joint reflection cracks [Huang (1993)]. Joint reflection cracking is mainly caused by the movement of rigid slabs beneath the asphalt surface. Usually these cracks are not associated with load. However, traffic loading may cause the failure to progress even further. Rutting and cracking are the major distresses which can occur in flexible pavements. These two types of distress are addressed in Chapter 4. There are also other types of distresses such as frost heave, swelling on the pavement surface, consolidation of subgrades, slippage cracking, and so on. These types of distress are addressed in detail in the literature [Huang (1993) and Yoder and Witczak (1995)] and are summarized in Table 2-3.

Table 2-4: Methods Tried For Reducing Or Delaying Reflection Cracking Of AC Pavement Overlays [Barksdale (1991)]

Interlayers	Stress Absorbing Interlayer	Asphalt or rubber layer with stone chips (SAMI)
		Paving fabric saturated with asphalt
		Softer asphalt layer
	Cushion Interlayer	Open graded asphalt concrete mix
		Unstabilized granular layer
		Asphalt stabilized soil aggregate
	Bond Breakers at Joints of PCC Pavements	Sandcushions, aluminum foil lamina, wax paper, sisal paper, tar paper, polyethylene, polypropylene fabric, galvanized sheet metal
Modify Asphalt Concrete Overlay	Increase Asphalt Concrete Thickness	-
	Modify the Asphalt Cement	Soft asphalt cement
		Rubber asphalt (latex and neoprene rubber)
		Carbon black with soft asphalt cement
		Fiber asphalt cement (asbestos, polyester, polypropylene)
		Polymer, sulfur, modified asphalt cement
		Dry lime
	Saw-Cut AC Overlay and Seal Joints	-
Reinforcement Of AC Overlay	Steel Wire Mesh	-
	Expanded Metal	-
	Polymer Grids	-
	Glass Grids	-

Table 2-4 (continued): Methods Tried For Reducing Or Delaying Reflection Cracking Of AC Pavement Overlays [Barksdale (1991)]

Modify/ Rehabilitate Old Pavement	Flexible Pavement	Maintenance--seal joints, repair raveling, replace structurally failed areas; patches, leveling/scratch courses	
		Seal coat	
		Heat scarifier	
		Hot/cold recycling	
	PCC Pavement	Rehabilitate--underseal, seal joints, replace joints and deteriorated areas, grind surface, install load transfer devices	
		Reduce joint spacing	Crack and seat
			Saw new joints
			Rubblize

2.9 REVIEW OF EXISTING GEOGRID REINFORCEMENT METHODS

A significant portion of the pavement construction and rehabilitation effort in the United States has focused on improving pavement performance. To overcome problems like reflection cracking and rutting, stress-relieving interlayers have been used for delaying reflective cracking or reducing rutting. The idea of providing reinforcement is not a new concept and dates back to the 1920's [Asphalt Institute (1989)]. In late 1950's and early 1960's wire mesh was experimented with in the United States and Canada [Brown et al. (1985), Brownridge (1964) and Smith and Gartner (1959)]. Many applications of welded wire mesh reinforcement in pavements demonstrated unreliability to prevent or reduce reflection cracking due to installation difficulties such as buckling. On the other hand, correct installation of wire mesh has shown some additional resistance to reflection cracking, and limited success with this kind of reinforcement was observed in Southern Ontario under normal temperature conditions [Smith and Gartner (1959)]. When a pavement section was subjected to low temperature conditions in Northern Ontario, the welded wire mesh reinforcement was not effective in controlling transverse cracking [Huang (1993)].

During the last two decades, advances have been made in the development of materials such as geogrids and geotextiles as reinforcing materials in flexible pavements [Barksdale (1991) and Koerner (1994)]. As reinforcement materials, geosynthetics are not only a cost-effective alternative for increasing the strength of a subgrade soil, but also their high strength and chemical resistance are good features for reinforcement of flexible pavements. Several studies have incorporated the use of polymer-based geosynthetics in pavement sections [Abdelhalim et al. (1982), Abdelhalim (1983), Barksdale (1991), Brown et al. (1984), Brown et al. (1985), Button and Lytton (1987), Carroll et al. (1987), Giroud et al. (1984), Giroud and Noiray (1981), Haas (1984), Hozayen et al. (1993),

Jewel et al. (1984), Kennepohl et al. (1985), Lytton (1989), Smith and Gartner (1959), Smith et al. (1995), Jackson (1980) and Webster (1992)]. The results of these studies have been variable in terms of design considerations, but a majority of the past research work has concluded that geosynthetic reinforcement showed additional improvements in performance of flexible pavements. However, no general guidelines are available for the design of such interlayers (reinforcements).

Several studies to investigate the influence of polymer grid reinforcement on the development of permanent deformation and crack propagation in an asphalt overlay have been performed and are reported in the literature [Abdelhalim et al (1982), Brown et al. (1985) and Haas (1984)]. These studies have shown that certain reductions in rut depth and increase in crack propagation time in asphalt layer were possible. Brown et al. (1985) reported that a 20 to 58 percent reduction in rut depth was possible with the use of polymer grids. However, compaction of the hot mix asphalt (HMA) in two lifts with the grid between the interface showed lower reinforcement than the HMA compacted in one lift. This might be better explained by the study performed by Jewel et al. (1984) on the mechanics of soil particles and grid aperture interaction. Jewel et al. (1984) showed that the size of the soil particles and grid apertures affected the sliding resistance. When the coarse particles interlocked well with a grid aperture, the sliding resistance increased. Two sets of experiments on beams with polymer grid reinforcement were conducted to determine the influence of a grid on crack growth in an asphalt overlay over a defined crack in the layer below [Brown et al. (1985)]. The results showed that when the grid was placed at the bottom of the layer, an increase in life expectancy by a factor of three was possible. Besides crack propagation, the fatigue life of asphalt layers may be increased by a factor of ten for the above situation. However, when the grid was placed at a three-quarters depth and up, this factor was reduced to two. Brown et al. (1985) concluded that using a

grid over a cracked surface and placing an asphalt overlay on top of the geogrid may eliminate reflective cracking entirely.

Similar research was done to evaluate a polymer geogrid in terms of behavior and its effectiveness in paved road structures [Abdelhalim et al. (1982), Abdelhalim (1983) and Haas (1984)]. In their first experimental program, Abdelhalim et al. (1982) focused on geogrid reinforcement of the full depth asphalt pavement with respect to dynamic strains, permanent deformation, and load applications to failure. The experimental study was performed in a 13.1 ft. x 7.9 ft. x 6.6 ft. (4 m. x 2.4 m. x 2 m.) deep concrete pit. Variables in the experiments included different thicknesses of full depth asphalt, reinforced versus unreinforced test sections, and different subgrade strengths. A loading of 9 kips (40 kN) of peak dynamic loading with a frequency of 10 Hz was applied through a 12-inch (300 mm.) diameter circular plate. At predetermined cycle intervals, a single static load of the same intensity was applied. The geogrid material used was a polypropylene plastic (biaxially oriented) having holes 0.2-inch (0.5 cm.) by 0.2-inch (0.5 cm.). They found that for the same thicknesses, reinforced sections required more than double the number of load applications to failure in comparison to the non-reinforced sections. Also, the magnitude of the elastic tensile strain at the bottom of the asphalt layer was reduced by approximately 30% with the help of reinforcement. It was found that under the reinforced sections the vertical stresses on the subgrade were 30-40% lower than that in the non-reinforced test sections. The reason for this difference (percentage) was explained by the inclusion of the geogrid mesh reinforcement in the pavement system. In terms of cracking, non-reinforced sections failed early and cracks progressed to severe cracks, while reinforced sections resulted in a few hairline cracks at the end of the loading cycles. This test showed that if reinforcement was placed at the bottom of the asphalt layer, two of the critical

strains within the pavement structure (horizontal tensile strain at the bottom of the asphalt layer and vertical compressive strain at the top of the subgrade) reduced substantially.

In summary, the behavior and performance of the reinforced section compared with a non-reinforced section of the same thickness [6-inch (15 cm.)] under different subgrade conditions (weak and strong) were compared. Results of the experiments have shown that asphalt thickness savings ranged from 2 inches (5 cm.) to 4 inches (10 cm.) when the flexible pavements were reinforced with the polymer geogrid. In addition, vertical stresses on the strong subgrade for reinforced and non-reinforced asphalt sections of the same thickness [4.5-inch. (11.5 cm.)] were compared [Abdelhalim et al. (1982) and Haas (1984)]. More details of the research conducted at Royal Military College (RMC) and University of Waterloo experimental facilities can be found in the literature [Abdelhalim (1983) and Haas (1984)].

An additional test program using a polypropylene grid for reinforcement, following the work done at the Royal Military College, was performed at the University of Waterloo, Canada [Carroll et al. (1987) and Kennepohl et al. (1985)]. The loading program followed was identical, with the exception of a loading frequency of 8 Hz. rather than 10 Hz. Smith et al. (1995) mentioned in the literature that a frequency of this type (8 Hz.) did not model actual (typical) type of traffic conditions. In this series of experiments, a granular base layer was introduced, and the geogrid reinforcement was placed within the granular base layer. The results showed that reinforcement of the granular base layer substantially improves the pavement performance (in terms of pavement deformation). Moreover, the best reinforcement location was found to be within the lower half of the granular layer. In this study, the thickness effect of reinforced granular bases was also examined. The thin reinforced sections with thick non-reinforced sections under the same conditions were compared, and the reinforced pavement

sections have performed better than the non-reinforced pavement sections.

Full-scale field experiments were designed and constructed following the laboratory experiments. The results from field experiments showed that the best results for reinforcement were achieved when the grid was covered with a chip seal or a slurry seal prior to the application of the hot mix [Kennepohl et al. (1985)]. The idea of using these seals was to protect the grid against damages from drag and motion of the paving equipment and the heat of the paving mix. Since the grid was not self-adhesive, the possibility of some slippage of the grid at high stress levels was high. The use of a slurry seal or a chip to affix the geogrid to the paving surface was not very practical. In the laboratory studies, Carroll et al. (1987) concluded that some slippage of the reinforcement grid at high stress levels was caused by the lack of anchorage. In this study, pavement sections were examined for a very weak subgrade (CBR of 1%) (very fine grained beach sand-99 percent passing the No.40, 32 percent passing the No.100, and 4 percent passing the No. 200). Even though this fine grained beach sand was not commonly found in pavement subgrades, the study was noteworthy in terms of performance of pavements over a very weak subgrade condition. The results indicated that the improvement of the service life of the pavement structure was threefold with a reinforcement. Since the pavement section was underdesigned, the rutting was more than 0.79 inches (2 cm) in less than 3000 cycles.

Another concern for using polypropylene grids for reinforcement was a reduced range of laying temperature where the adequate compaction was difficult to achieve during cold winter conditions [Brown et al. (1984)]. The geogrid material used inside the asphalt mix had a tendency to distort above 320 °F (160 °C). This distortion occurred when the hot mix asphalt inside the truck was around or above 320 °F (160 °C) during the placement process.

In another study [Webster (1992)], it was concluded that polymer geogrids were better than geotextiles for reinforcement purposes in the granular base layer due to their interlocking capabilities. In this study [Webster (1992)], a series of field tests was performed to examine the influence of a geogrid base reinforcement for flexible pavements subjected to light aircraft loads of 30 kips (133.5 kN). Four traffic lanes with different geometric cross-sections were designed for this test. For a subgrade CBR value of 8%, the thicknesses of the granular base layers (crushed limestone) were 6 inches (152 mm.) and 10 inches (254 mm). For a subgrade CBR value of 3%, the thicknesses of the granular base layers were 12 inches (305 mm), 14 inches (356 mm), and 18 inches (457 mm). All of these test sections were tested with and without geogrid reinforcement. Moreover, the influence of channelized traffic on the wheel path was studied on the 14 inches (356 mm) thick (granular base) sections. From this test program, the thickness design criteria was developed to determine the equivalent thickness of the unreinforced test section corresponding to the thickness of the reinforced test section. For example, a 14.5-inch (368.3 mm) thick base unreinforced section would correspond to a 12-inch (305 mm) thick reinforced section to give the same performance. The best placement of the geogrid was found to be at the bottom of the granular base layer.

The use of geotextiles in asphalt concrete overlays for reinforcement and strain relief was explained in detail in the literature [Button and Lytton (1987) and Lytton (1989)]. This work concluded that in a strain-relieving mode, geotextiles with an elastic stiffness lower than that of the asphalt concrete only retarded the crack propagation (reflective cracking). On the other hand, reinforcing materials like polypropylene grids had a chance to redirect the crack when it reached the reinforcing material and propagated horizontally [Button and Lytton (1987) and Lytton (1989)]. In another study [Coetzee and Monismith (1979)], the effects of a rubber-asphalt stress-absorbing-

membrane-interlayer (SAMI) between a Portland Cement Concrete (PCC) pavement system and an Asphalt Concrete (AC) overlay were investigated by using a finite element computer program. In this theoretical study, Coetzee and Monismith (1979) showed that a significant reduction of the stress at the crack tip and a reduction of the rate of crack propagation was possible.

A study [Giroud and Noiray (1981)] involving geotextile reinforcement in unpaved roads has shown that the reduction of the required aggregate thickness by using a geotextile generally ranged between 20% to 60%. They developed specific charts to determine the thickness of the aggregate layer for an unpaved road reinforced with a geotextile layer. These charts were applicable only to cohesive subgrade soils and roads subjected to light to medium traffic [Giroud and Noiray (1981)]. Further studies by Giroud et al. (1984) describe the behavior of unreinforced and geogrid reinforced unpaved roadways in detail, and the mechanisms (improvement in load distribution of the granular base layer and confinement of the subgrade soil) involved in their relationship. These studies have also shown that the required thickness of the aggregate layer could be lowered with the use of geogrid and geotextile reinforcement.

Several computer analyses to study the performance of flexible pavement systems with and without reinforcement are described in the literature [Wathugala et al. (1996) and Zaghoul and White (1993)]. As reported in the literature [Zaghoul and White (1993)], a three-dimensional dynamic finite element program, ABAQUS, and a multi-layer elastic analysis program, BISAR, were used to analyze the flexible pavement sections. No reinforcement was considered in this research. The dimensions of the modeled section were 36 feet (11 m) wide and 50 feet (15 m) long. The layers of the pavement cross-section included an asphalt concrete layer with a thickness of 4 inches (102 mm), and a granular base course layer with a thickness of 10 inches (254 mm) on a sandy subgrade. In the multi-layer

elastic analysis, all of the material properties were assumed to be linear elastic, whereas in the finite element analysis the asphalt layer was assumed to be a viscoelastic material. The base course and subgrade were modeled by using the Drucker-Prager constitutive model, which predicts the elastic-plastic response of the subgrade and the base course. Material properties used in the cited study [Zaghloul and White (1993)] are comparable to those used in the analysis presented later in Chapter 5. As described in the literature, the results from computer analyses were compared with measured findings from other studies. The results from both analyses (finite element and multi-layer elastic) were found to be correlative by assuming static loads with linear elastic materials. It was found that the higher loads generated higher stresses in the subgrade than the subgrade's yield stress, which caused significant rutting in the pavement system. Another approach focused on the effect of the loading frequency [Zaghloul and White (1993)]. It was concluded that the deflection at a lower speed [1.75 mph (2.82 kmh)] was much higher than the deflection at a higher speed [10 mph (16 kmh)]. This indicates that the lower speed vehicles or static loading are more damaging to the pavement than the higher speed vehicles or dynamic loading.

In another study [Wathugala et al. (1996)], geosynthetic reinforced flexible pavements were investigated by using the numerical finite element program ABAQUS. Linear elastic and elasto-plastic models were presented and compared. Flexible pavement systems were considered with and without geosynthetic reinforcement. Different elastic moduli values were assigned for the geosynthetic layer. In this study, the geosynthetic layer was placed at the bottom of the granular base layer (crushed lime stone). In the pavement section analyzed, the thickness of the HMA was 3.5 inches (89 mm.), the thickness of the base layer was 5.5 inches (140 mm.), and the thickness of the reinforcement layer was 0.1 inches (2.5 mm). The results showed that the vertical stresses under the applied load for all the

cases were somewhat similar to each other and very little difference was observed from the values predicted from Boussinesq's equation. The reduction in computed settlements from the linear elastic analyses was very small when geosynthetics were included. In contrast, a large reduction in computed settlements from the elasto-plastic analyses was observed, especially with stiffer geosynthetics. In terms of pavement performance, linear elastic analyses with reinforcement showed little improvement while the elasto-plastic analyses showed large improvements when the reinforcement was included.

2.10 SUMMARY

The limitations of previous studies and new approaches of this study can be summarized as follows:

- Several studies presented in the past suggest that geosynthetic reinforcement showed additional improvements in the performance of flexible pavements. Most of these studies investigated the influence of polymer-based geosynthetics in pavement sections.
- No studies are available to determine the influence of glass grid reinforcement inside the asphalt base in a large-scale experiment. Some of the available studies on glass grid were based on a small-scale asphaltic beam. Because of its good characteristics such as high elastic modulus and tensile strength, glass grid reinforcement inside the asphalt base was studied in a large-scale experiment in the present study.
- Most of the geosynthetic reinforcement was done at the granular base level of the flexible pavement system. Limited applications (studies) on geogrid reinforcement in the HMA are available, and most of these are limited to small-scale asphaltic beam experiments [Jayawickrama and Lytton (1987) and Lytton (1989)]. Similar to the previous laboratory

studies [Haas (1984) and Smith et al. (1995)], a circular loading plate [diameter = 12 inches (305 mm)] was used in the laboratory experiments to simulate the effects of a wheel load in the study presented herein. This report presents the first research study where a glass fiber grid reinforcement was included in the asphalt base course layer.

- This research study is the first of its kind to simulate a crack inside the hot mix asphalt in a large-scale experiment.
- In the laboratory test sections, the frequency of loading was chosen as 1.2 Hz instead of 10 Hz (as in previous studies) since the damaging effect to the pavement system is greater at slower speeds.
- None of the traditional methods allow inclusion of reinforcements in the analysis of pavement sections. In this research study, the reinforcement element (glass grid) was simulated as a special interface element in the finite element method of analyses.

CHAPTER 3

EXPERIMENTAL PROGRAM

3.1 TEST FACILITY

Experimental work described in this section was conducted in the major units laboratory of the Department of Civil and Environmental Engineering at West Virginia University. Twenty experiments on flexible pavement test sections were conducted in this test facility. The experimental pavement sections were built in a rectangular container with dimensions of 4 feet x 6 feet x 2.5 feet (1.2 m x 1.8 m x 0.8 m). Two containers were constructed of steel for testing flexible pavement sections. Details of a typical asphalt test section are shown in Figure 3-1.

Among the states, traffic on paved roadways varies in terms of the number of vehicles and the magnitude of loadings. Pavements must be designed to serve traffic needs adequately by carrying the traffic loads. Since the widely accepted procedure is to convert each load group into an equivalent 18-kip (80 kN) single axle (ESAL), the 18-kip (80 kN) single axle load was applied over four tires up to 1,000,000 load applications (cycles) to simulate traffic. In this study, a circular loading plate was used to apply the wheel load on the pavement section. The thickness of the loading plate was 1 inch (25 mm), and the diameter of the single circular contact area (loading plate) was found to be 12-inch (305 mm). Detailed explanation of the load plate configuration can be found in Section 3.3.1.

Figure 3-1: Instrumentation for the Laboratory Study

a) Cross Section

b) Plan View

3.2 INSTRUMENTATION

The instrumentation used in this study includes dial gages, pressure cells, and strain gages. Details on the instrumentation are given below.

3.2.1 Dial Gages

As shown in Figure 3-1, five analog dial gages [1-inch (25 mm)] were placed on the top of the asphalt surface to measure permanent vertical displacements with the number of load cycles. This arrangement provided the necessary measurements on the maximum surface displacement (rutting) under the applied load as a function of the number of load applications. Two of the dial gages were located on each side, 6-inch (152 mm) apart from the center of the loading plate. Two other dial gages were located 6-inch (152 mm) apart from the edge of the loading plate on each side. The fifth dial gage was placed between the two dial gages (the dial gage 6-inch apart from the center of the loading area and the dial gage 12-inch apart from the center of the loading area on the same side) which was 2.5-inch (63.5 mm) away from the one edge of the loading plate [Figure 3-1].

3.2.2 Pressure Cells

Two earth pressure cells (EPC-6) were used in each soil container (test box) and were located at the top of the soil subgrade [Figures 3-1 and 3-2]. These pressure cells were precalibrated by the manufacturer. The depth of the buried pressure cells was 8.5-inch (215.9 mm) below the asphalt/gravel base interface as shown in Figure 3-1. One of the pressure cells was buried directly below the centerline of the loading area. The center of the other pressure cell was 6-inch (152 mm) apart from the center of the first pressure cell. The subgrade material placed around the pressure cell was hand compacted to the same level as the surrounding soil [Figure 3-2]. The stresses induced by the loading plate on top of the subgrade were observed by using these two pressure cells and

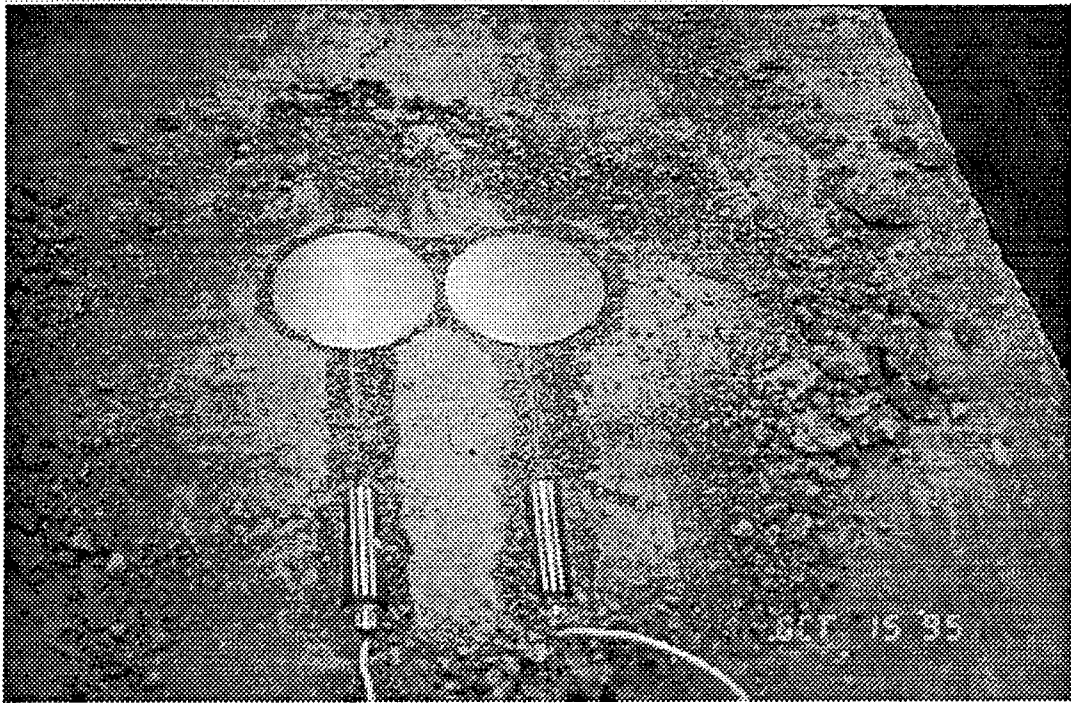


Figure 3-2: Photo Showing the Pressure Cells (EPC-6) on Top of the Subgrade

recorded by using a multi-channel P-350A strain indicator.

3.2.3 Strain Gages

Six strain gages (Micro Measurements' foil type 350 ohm) were bonded to top of the glass fiber grid. One strain gage (SG #1) was placed directly below the loading plate and others (Strain Gages #2, #3, #4, and #5) were placed at intervals of 6 inches (152 mm) as shown in Figure 3-1. Strain Gage #6 was placed very close to Strain Gage #1. Strain Gages (SG) #4, #5, and #6 were installed as back up gages in case any one of the primary strain gages (Strain Gages #1, #2, and #3) failed. The strain gages were used in five experiments. Figure 3-3 shows a view of strain gages installed in a typical reinforced test section. The strains were recorded during static loading using a P-3500 digital strain indicator. The purpose of using strain gages on the glass grid was to evaluate the behavior of the reinforcement layer.

3.3 LOADING PROGRAM

A Material Testing System (MTS) loading machine with a servo-hydraulic controller was used to perform the static and dynamic loading tests [Figure 3-4]. A circular shape metal loading plate [1 inch (25 mm) thick, 12 inches (305 mm) diameter] was used to simulate a wheel load. The loading plate was attached to the actuator rod in the MTS loading machine. Each test section was subjected to 1,000,000 loading cycles.

In previous studies [Abdelhalim et al. (1982) and Kennepohl et al. (1985)], the frequency of the loading was chosen as 10 Hz to simulate a typical traffic loading. In a study by Carroll et al. (1987), the frequency of a dynamic loading was chosen as 8 Hz. However, Smith et al. (1995) reported that the frequency of 8 Hz did not model typical traffic conditions. These frequencies were

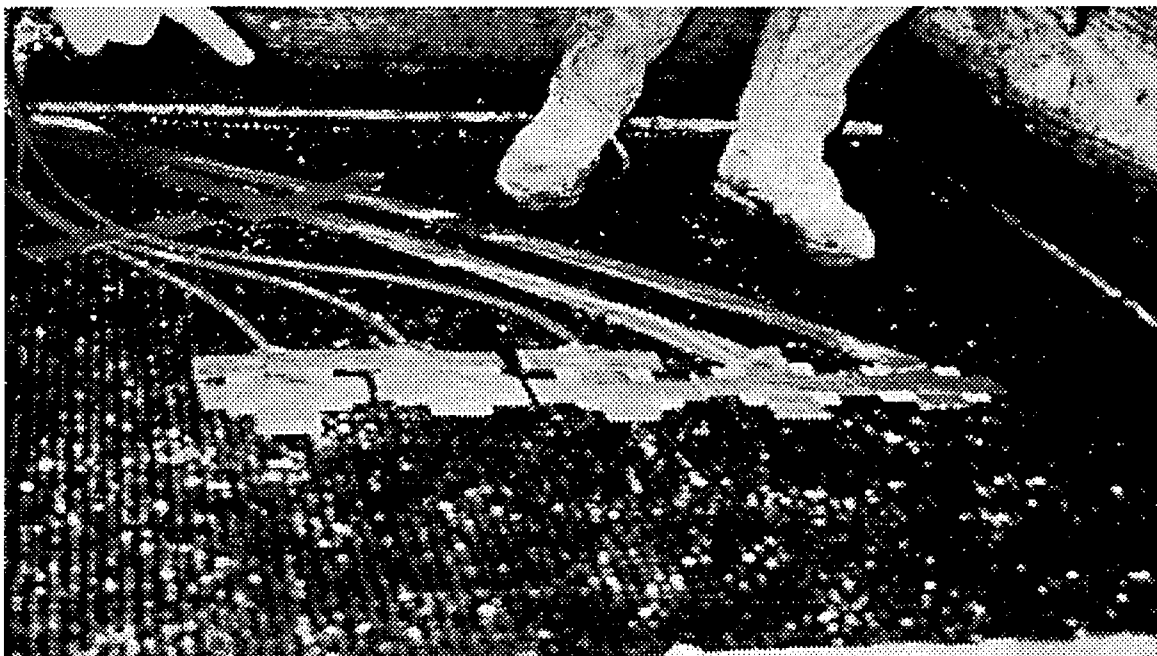


Figure 3-3: Photo Showing the Strain Gages Installed on Top of the Glass Grid

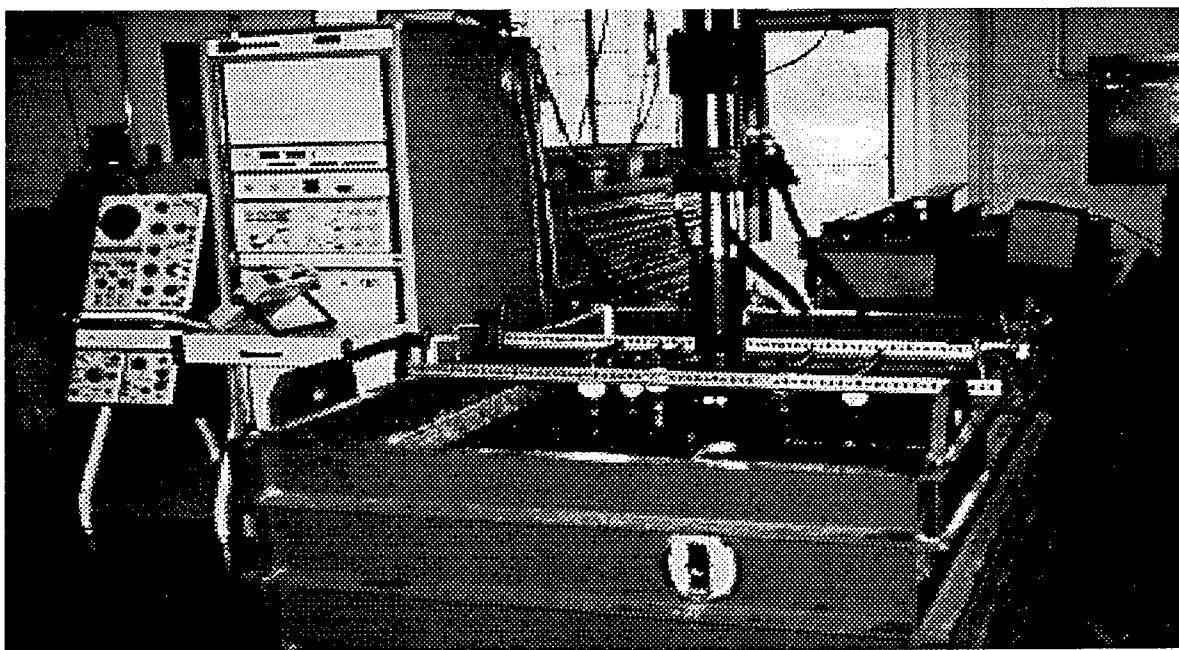


Figure 3-4: Photo Showing the Material Testing System (MTS) Loading Machine

based on the passage of a front and a rear wheel of a typical truck. As explained in the literature [Huang (1993), Yoder and Witczak (1973) and Zaghoul and White (1993)], the greater the speed, the smaller the strains in the pavement system, and vice versa. It was explained in the literature that the average time interval between one vehicle and the following vehicle is $1\frac{1}{2}$ seconds [Merritt (1983)]. This translates to a frequency of 0.7 Hz. This time interval of $1\frac{1}{2}$ seconds is equivalent to a spacing of 132 feet (40 m) at a speed of 60 miles per hour. If the time interval was kept constant at $1\frac{1}{2}$ seconds, the distance between vehicles for different vehicle speeds would be different.

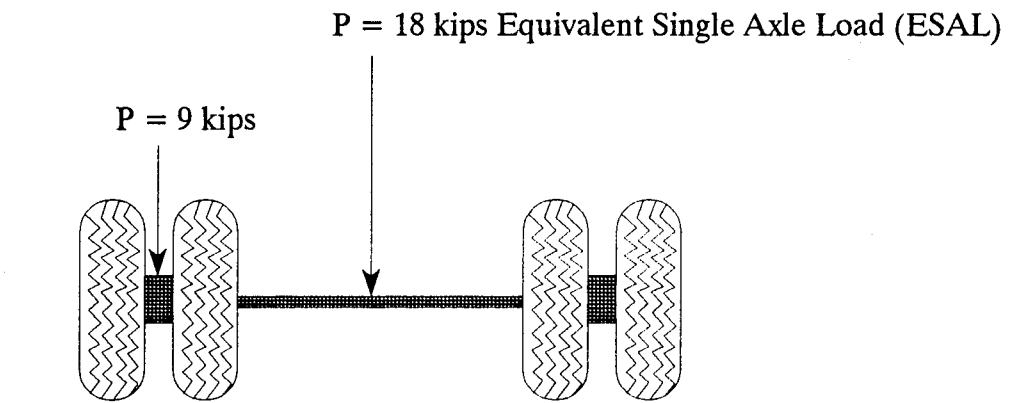
In the laboratory test sections, the frequency of loading was chosen as 1.2 Hz to shorten the time of the experiment duration. This chosen frequency (1.2 Hz) was also justifiable in comparison to 10 Hz since the damage to the pavement system was greater with slower vehicle speeds. The span of the sinusoidal load was checked and verified using an oscilloscope [Figure 3-4]. The maximum applied load on the asphalt surface was 9 kips (40 kN) generating a pressure of 80 psi (551 kN/m²) through the 12-inch (305 mm) diameter loading plate. Static loading tests were conducted after every 100,000 load cycles. During the static loading, the maximum applied load was 18 kips (80 kN).

3.3.1 Load Configuration

Among the states, traffic on paved roadways varies in terms of the number of vehicles and the magnitude of loadings. In the structural design of a flexible pavement system, pavements must be designed to serve traffic needs adequately and efficiently by carrying the traffic loads. During the design stage, one of the primary concerns is to estimate the number and weights of axle load applications correctly. Studies has shown that a widely accepted procedure to overcome this concern is to convert an axle load of any mass into Equivalent Single Axle Load (ESAL) applications [Asphalt Institute (1981), Asphalt Institute (1989), AASHTO (1993), Huang (1993) and Yoder and Witczak

(1975)]. According to AASHTO (1993) design guideline "The results of the AASHTO Road Test have shown that the damaging effect of the passage of an axle of any mass (commonly called load) can be represented by a number of 18-kip single axle loads or ESAL's." The reason for making this conversion is to prevent the unsafe and/or over design conditions of the pavement. In the design of flexible pavements, only one side of an axle load needs to be considered [Huang (1993)]. Generally, the pavement design practice is based on the load configuration of a heavier axle load on dual wheels. As mentioned in the literature [Huang (1993)], heavier axle loads are always applied on dual tires. Since the widely accepted procedure is to convert each load group into an equivalent 18-kip (80 kN) single axle, the 18-kip (80 kN) single axle load is applied over four tires to design the loading plate for the laboratory conditions [Figure 3-5].

It is important to know the contact area of the tire on a pavement surface to simulate the load. As explained in the literature [Huang (1993)], the layered theory used for flexible pavement design is based on the assumption that the tire contact area is axisymmetric. This can only be accomplished by assuming the tire contact area to be a circle. To simplify the analysis of flexible pavement design, use of a single circle with the same contact area as the dual wheels is a common procedure instead of using two circular areas [Huang (1993)] [Figure 3-5]. In this research study, it was assumed that the 18-kip (80 kN) single axle load is applied over four tires. Since the contact area is closely related to the tire pressure, the tire pressure must be determined to find the tire contact area. The following equations were used to determine the diameter of the circular loading plate used in the laboratory experiments to simulate the effects of a wheel load [Yoder and Witczak (1975)]:



Geometry of Tire Imprints

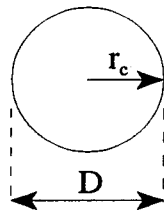


Figure 3-5: Load Configuration for a Pavement System

$$r_c = \sqrt{\frac{P}{p_c \pi}} \quad (3.1)$$

$$D = 2r_c \quad (3.2)$$

here

r_c = radius of contact,
 P = total load on the tire,
 p_c = tire inflation pressure,
 D = diameter of contact.

Heavier axle loads generally have heavier tire pressures than the tire contact pressure. Therefore, the contact pressure is usually assumed to be equal to the tire pressure to be on the safe side. The contact pressure is defined as the pressure acting against the tire. To be consistent with previous research [Abdelhalim (1983), Smith et al. (1995), and Haas (1984)], the tire pressure was chosen as 80 psi (551 kN/m²) in this research program. By using these established values in Equations 3.1 and 3.2, the contact area for a dual tire imprint with a single axle load of 18 kips (80 kN) was found to determine the size of the loading plate. The thickness of the loading plate was 1 inch (25 mm). The diameter of the single circular contact area (loading plate) was found to be 12-inch (305 mm). These dimensions were used for the loading plate to simulate the dual wheel load in the laboratory experiments. The size of the loading plate used in this study is consistent with the published literature [Haas (1984), Huang (1993) and Smith et al. (1995)].

While the circular tire imprint is the common procedure to simulate the wheel load for the flexible pavement design, it is also common to use rectangular areas for the analysis of rigid

pavements, the analysis of airfield designs, and/or highway bridges [AASHTO (1993) and Huang (1993)].

3.4 TEST SECTION MATERIALS

As shown in Figure 3-1, a typical test section consisted of hot mix asphalt (HMA), granular base, and subgrade soil. In some experiments, a glass fiber grid was used inside the HMA as a reinforcement. A geotextile layer was used between the gravel base and the subgrade soil in all of the experiments [Figure 3-1]. Details of the materials used in the test sections are given below.

3.4.1 Hot Mix Asphalt (HMA)

The full-depth asphalt pavements have been successfully used in the past [Huang (1993)] and such pavements can potentially be used in the State of West Virginia. The objective of this research project was to determine the influence of glass fiber grids used within the asphalt base course on the performance of pavement sections. At the recommendation of the sponsoring agency, West Virginia Department of Transportation, Asphalt Base II was used as the hot mix asphalt in the experimental program. The type of Base II was AC-20 (Type-Grade). Asphalt cements are graded with respect to viscosity, viscosity after aging, and penetration. Each system has different grades and consistency. A more common system used in the United States is based on viscosity. In the viscosity system, the unit of measurement for absolute viscosity is called the "poise". The higher the number of poises, the more viscous the asphalt becomes. Viscosity grade changes between AC-2.5 to AC-40. AC-2.5 is known as a soft asphalt. The AC-20 is referred as Asphalt Cement with a viscosity of 2000 poises at a temperature of 140 °F (160 °C) [Asphalt Institute (1983)]. The fines-to-asphalt ratio for Base II type of asphalt is 1.0, while the maximum size of the aggregate in the mix is 1 inch (25 mm). Typical

properties of the Asphalt Base II are listed in Tables 3-1 and 3-2. The density measurements were made by a representative of the West Virginia Department of Highways (WVDOH) by using a nuclear (Troxler) densitometer during the construction of test sections. Temperature measurements were also made during the construction. All of the test sections met WVDOH specifications on density and temperature. The results of the measured unit weights for each test section are listed Table 3-3.

3.4.2 Gravel Base

The granular material used for the base layer [Figure 3-1] meets Class 1 (307-1) specifications under section 307 (Crushed Aggregate Base Course), and section 704.6.2 (Gradation, Quality and Crushed Particle Requirements) of standard specifications for West Virginia Department of Highways (WVDOH) [West Virginia Department of Highways (1986)]. This is a common gravel size used by contractors in the state of West Virginia. The standard sizes of Class 1 material are listed in Table 3-4. Unit weight of the granular material was found to be 112.7 pcf. (17.7 kN/m³) by the gravel supplier¹. The density measurements of the gravel base for each test section are listed in Table 3-5.

¹ This information was supplied by Greer Limestone Company, West Virginia

Table 3-1: Typical Properties of Asphalt Base II² Material

Optimum Asphalt Content (%)	4.6
Stability (N)	10,809
Air Voids (%)	4
Flow (0.25 mm)	9.9
Maximum Density (kcm)	2,513
VMA (%)	12.73
Fines to Asphalt Ratio	1

Table 3-2: Sieve Analysis of Gravel used in the Asphalt Mix¹

Nominal Size Square Openings (in.)	Percent Passing (%)
1 (25 mm)	100
3/4 (19 mm)	93
3/8 (9.5 mm)	67
#4 (4.75 mm)	51
#8 (2.36 mm)	38
#30 (600 µm)	20
#50 (300 µm)	10
#200 (75 µm)	5

² This information was supplied by West Virginia Department of Highways (WVDOT)

Table 3-3: Measured Unit Weight of Hot Mix Asphalt Used in the Test Sections

Experiment #	Thick. of HMA (in.)	Lift of Compaction	Measured Unit Weight (pcf)	Experiment #	Thick. of HMA (in.)	Lift of Compaction	Measured Unit Weight (pcf)
1	6	1 st	144.30	11	3	1 st	146.10
		2 nd	147.30			2 nd	144.80
2	6	1 st	143.60	12	3	1 st	144.20
		2 nd	146.00			2 nd	144.60
3	6	1 st	147.10	13	3	1 st	147.50
		2 nd	143.70			2 nd	147.60
4	6	1 st	144.90	14	3	1 st	147.30
		2 nd	144.40			2 nd	147.60
5	6	1 st	145.25	15	3	1 st	147.40
		2 nd	145.00			2 nd	150.40
6	6	1 st	146.50	16	3	1 st	144.90
		2 nd	145.25			2 nd	148.00
7	6	1 st	146.00	17	3	1 st	144.80
		2 nd	148.60			2 nd	145.70
8	6	1 st	146.50	18	3	1 st	148.80
		2 nd	149.50			2 nd	147.80
9	6	1 st	144.10	19	3	1 st	148.70
		2 nd	146.10			2 nd	146.00
10	6	1 st	143.90	20	2.5	1 st	148.10
		2 nd	143.60			2 nd	149.70

Note: 1 pcf = 0.157 kN/m³
1 inch = 25 mm

Table 3-4: Grain Size Distribution of Gravel Base³

Nominal Size Square Openings (in.)	Percent Passing (%)
1½ (37.5 mm)	100
¾ (19 mm)	70
⅜ (9.5 mm)	41
#4 (4.75 mm)	23
#8 (2.36 mm)	16
#16 (1.18 mm)	11
#40 (0.425 mm)	7
#200 (0.075 mm)	4

Table 3-5: Measured Unit Weight of Gravel Base

Experiment #	Measured Unit Weight (pcf)	Experiment #	Measured Unit Weight (pcf)
1	135.09	11	134.75
2	134.83	12	134.00
3	134.83	13	136.25
4	135.10	14	136.00
5	134.75	15	135.33
6	134.45	16	135.67
7	135.00	17	136.00
8	134.77	18	137.00
9	135.50	19	134.70
10	135.33	20	134.20

Note: 1 pcf = 0.157 kN/m³

³ This information was supplied by Greer Limestone Company, Morgantown, West Virginia

3.4.3 Subgrade

The soil subgrade chosen for this study is classified as A-4, according to the AASHTO soil classification system [Holtz and Kovacs (1981)]. The grain size distribution determined in the laboratory is listed in Figure 3-6. The subgrade soil was obtained by mixing approximately 60% Ohio River Sand, 35% Georgia Kaolin and 5% Western Bentonite. This type (A-4) of soil had a Liquid Limit (LL) of 22.75 and a Plasticity Index (PI) of 8.57. To obtain this type of a soil, several experiments were conducted to determine the Atterberg Limits for the different soil mixtures as listed in Table 3-6. A laboratory CBR (California Bearing Ratio) value was found to be 8% as shown in Figure 3-7. Figure 3-8 shows the relationship between the dry unit weight and water content compaction curve determined using a standard proctor test. These standard proctor tests were performed to characterize the subgrade material. The unit weight measurements for the subgrade soil used in test sections are presented in Table 3-7.

In each soil container, A-4 type subgrade material was placed in 3 lifts. The bottom layer was 4 inches (102 mm) in thickness while the remaining layers were placed in 3-inch (76 mm) lifts in each box. Each layer was compacted at an average desired moisture content of 10.5%, and to an average unit weight of 131 pcf (20.6 kN/m³) using a Whacker compacter with a 6 inches (152 mm) square tamper plate [Figure 3-9]. The density measurement for each lift of the subgrade soil is listed in Table 3-7. The subgrade compaction was the same for all twenty experiments. After compacting the soil, two pressure cells were placed on top of the subgrade material. Then a geotextile fabric was placed on the surface of the subgrade at the interface between the subgrade soil and the gravel base.

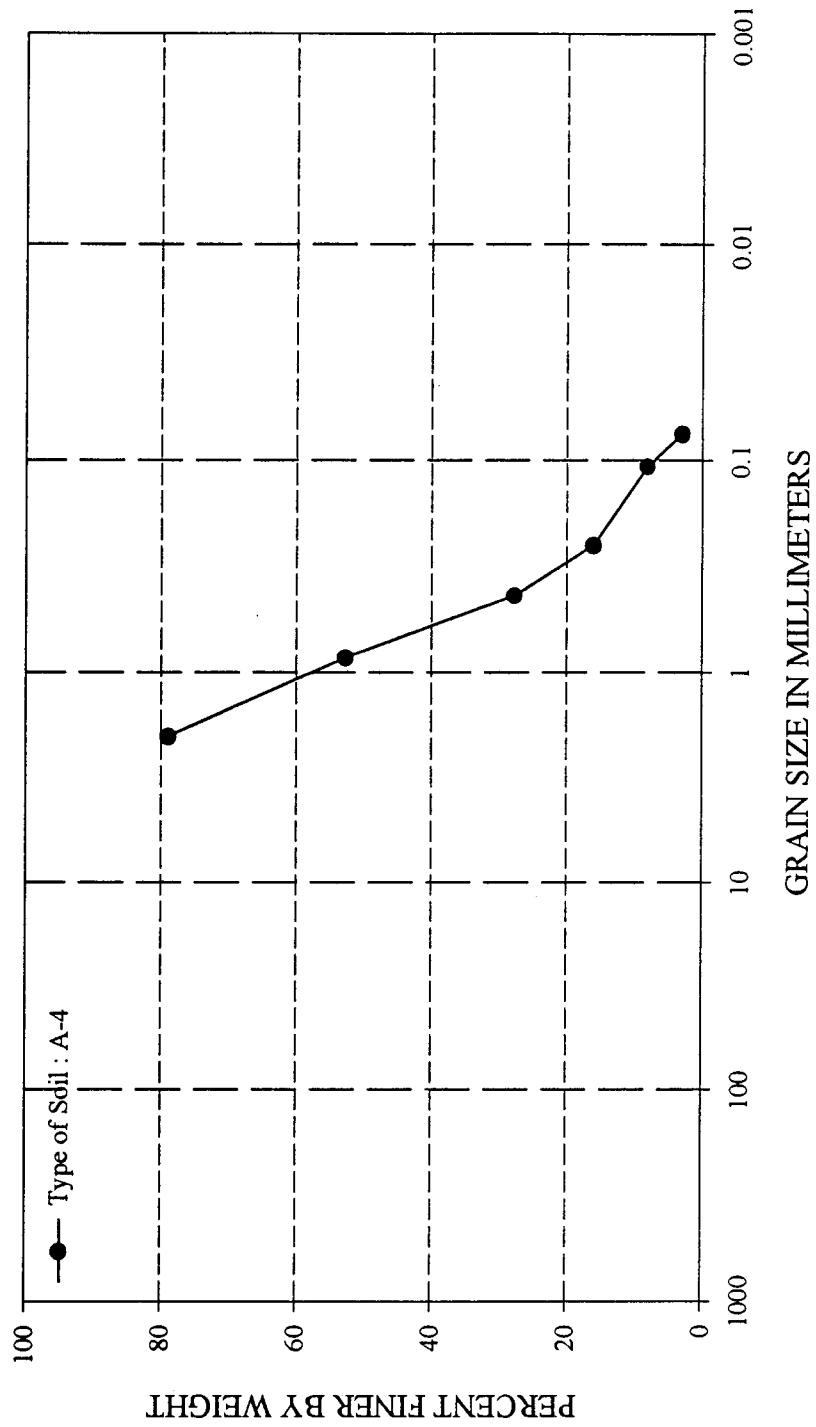


Figure 3-6: Particle Size Distribution for the Subgrade Soil

Table 3-6: Atterberg Limits for Different Soil Mixtures

Soil Description	Atterberg Limits			AASHTO Soil Classification
	Liquid Limit (LL)	Plastic Limit (PL)	Plasticity Index (PI)	
40% Georgia Kaolin + 60% Ohio River Sand	19.60	14.89	4.71	A-4
45% Georgia Kaolin + 55% Ohio River Sand	21.50	15.72	5.78	A-4
50% Georgia Kaolin + 50% Ohio River Sand	24.00	16.56	7.44	A-4
60% Georgia Kaolin + 40% Ohio River Sand	26.50	20.92	5.58	A-4
80% Georgia Kaolin + 20% Ohio River Sand	37.00	28.24	8.76	A-4
10% Bentonite + 90% Ohio River Sand	28.50	20.73	7.77	A-2-4
20% Bentonite + 80% Ohio River Sand	50.55	25.09	25.46	A-2-7
30% Bentonite + 70% Ohio River Sand	83.00	31.05	51.95	A-2-7
50% Bentonite + 50% Ohio River Sand	119.50	45.24	74.26	A-7-5
65% Ohio River Sand + 10% Bentonite + 25% Kaolin	33.00	16.19	16.81	A-6
65% Ohio River Sand + 15% Bentonite + 20% Kaolin	41.00	18.32	22.68	A-7-6
60% Ohio River Sand + 20% Bentonite + 20% Kaolin	55.00	21.65	33.35	A-7
60% Ohio River Sand + 5% Bentonite + 35% Kaolin	24.50	15.62	8.88	A-4
60% Ohio River Sand + 5% Bentonite + 35% Kaolin	22.75	14.18	8.57	A-4
Natural Subgrade Soil (Site Soil from Beechurst, Morgantown)	30.00	24.70	5.30	A-4

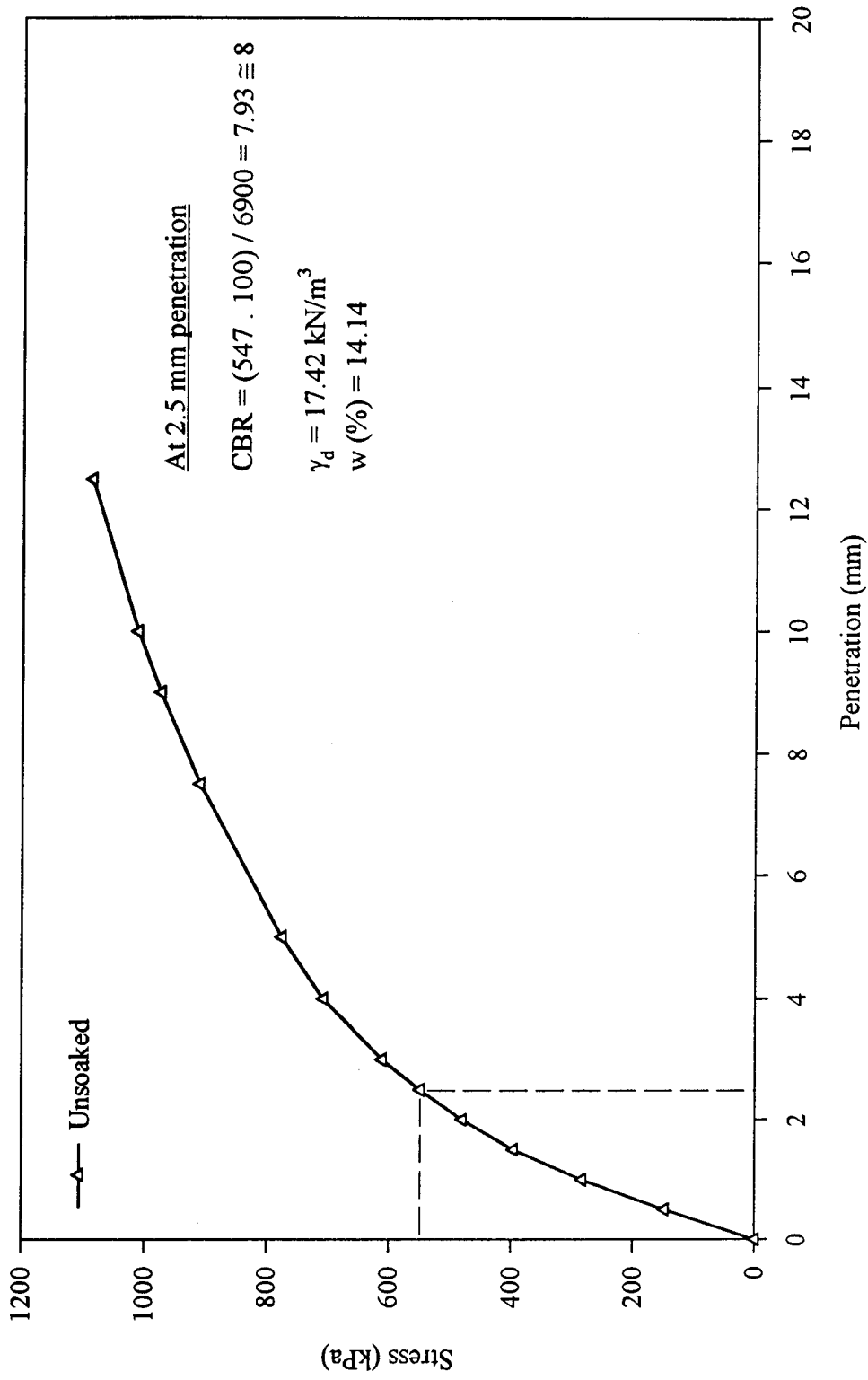


Figure 3-7: California Bearing Ratio (CBR) Value of the A-4 Type Subgrade Soil

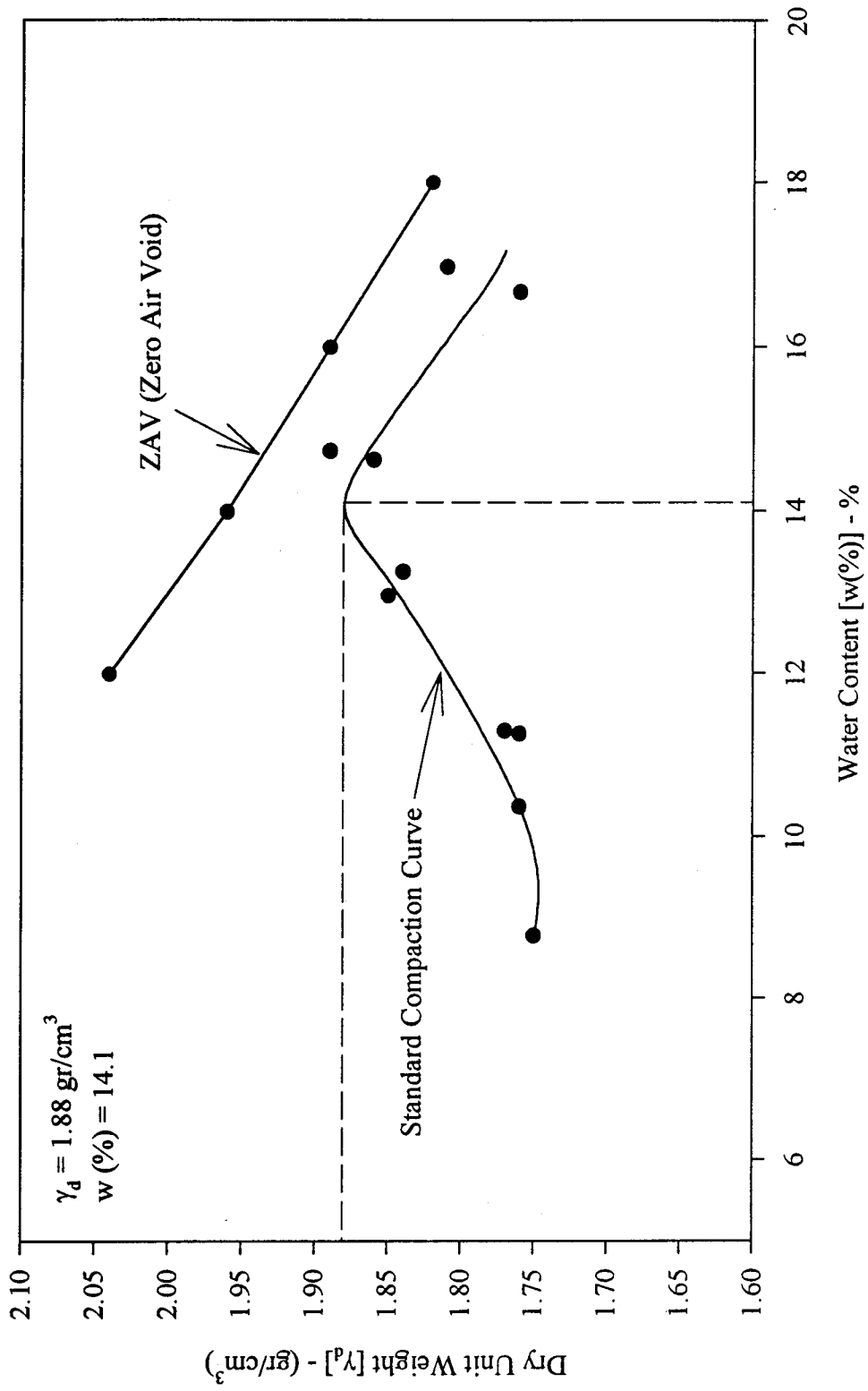


Figure 3-8: Standard Compaction Curve of the A-4 Type Subgrade Soil Used in Test Sections

Table 3-7: Measured Unit Weight of Subgrade Soil Used in Test Sections

Lift of Compaction	Soil Box #1	Soil Box #2
	Measured Unit Weight (pcf) [kN/m ³]	Measured Unit Weight (pcf) [kN/m ³]
1 st	130.80 [20.54]	131.32 [20.62]
2 nd	132.35 [20.78]	130.64 [20.51]
3 rd	130.66 [20.51]	132.84 [20.86]
Average	131.27 [20.61]	131.60 [20.66]

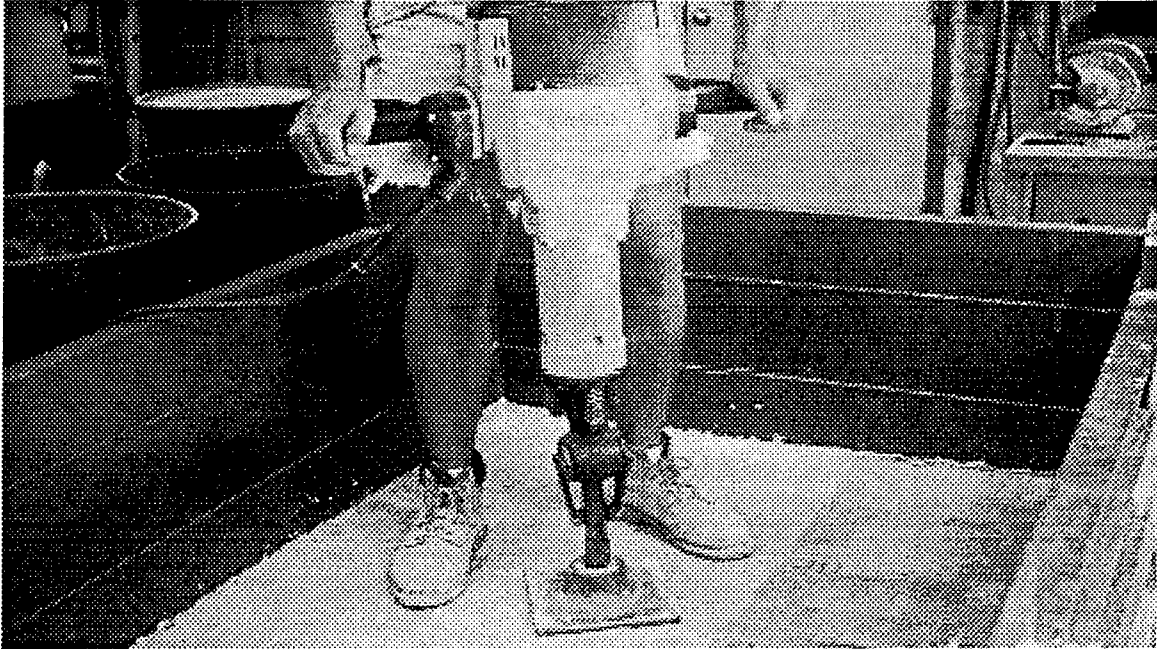


Figure 3-9: Photo Showing the Compaction of the Subgrade Soil

3.4.4 Woven Geotextile

The purpose of the woven geotextile was to separate the gravel base and the subgrade to prevent the migration of fine particles between the layers. One type of geotextile was used in all of the experiments in this research study. The woven polypropylene-based geotextile, Amoco 2002, was chosen to separate the gravel base and the subgrade [Figure 3-1]. This woven geotextile was successfully used in a previous research study [Smith et al. (1995)]. Table 3-8 lists the material properties.

3.4.5 Glass Fiber Grid

Three types of glass fiber grids were used as asphalt reinforcements in this study. These are shown in Figure 3-10. These were considered to have good bonding characteristics with the asphalt due to their self adhesive feature. The characteristics of the glass fiber grids used in the HMA are listed in Table 3-9. The usage of these materials can be seen in Table 3-10.

GlassGrid 8501 (GG 8501) represents the lightest (weakest) glass grid while GlassGrid 8511 (GG 8511) represents the heaviest (strongest) glass grid among the three glass grids used in this research. GlassGrid 8502 (GG 8502) has a weight between those of GG 8501 and GG 8511.

Table 3-8: Properties of Woven Geotextile Amoco 2002 [(Amoco Manufacturer's Literature (1994)]

Property	ASTM Test Method	Amoco 2002 N/A-Not Available
Grab Tensile Strength (lbs.) [kN]	D-4632	200 [0.89]
Grab Tensile Elongation (%)	D-4632	15
Wide Width Tensile (lbs./ft.) [kN/m]	D-4595	N/A
Wide Width Elongation (%)	D-4595	N/A
Mullen Burst (psi) [kPa]	D-3786	400 [2756]
Puncture (lbs.) [kN]	D-4833	90 [0.40]
Trapezoid Tear (lbs.) [kN]	D-4533	75 [0.33]
UV Resistance (%) ⁴	D-4355 ⁵	70
Apparent Opening Size (US Sieve) [mm]	D-4751	50 [0.300]
Permittivity (sec. ⁻¹)	D-4491	0.04
Flow Rate (gal./min./ft. ²) [l/min/m ²]	D-4491	4 [163]

⁴ Percent of minimum grab tensile after conditioning

⁵ Fabric conditioned as per ASTM-D-4355

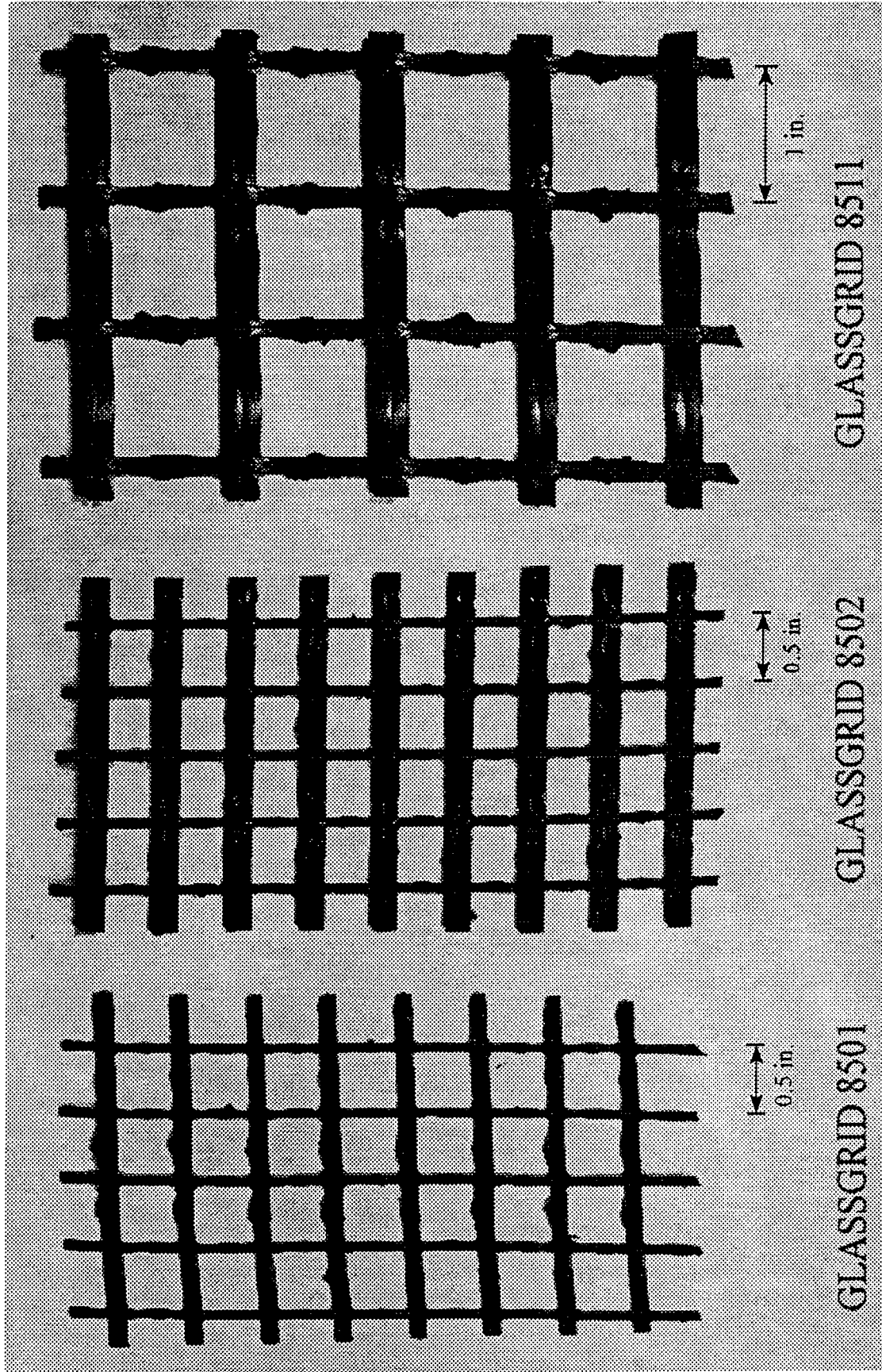


Figure 3-10: Photo Showing Three Different Glass Fiber Grid Types Used in the Experimental Program

Table 3-9: Properties of Glass Fiber Grids [GlassGrid Manufacturer's Literature (1995)]

Grid Type	GlassGrid 8501	GlassGrid 8502
Grid Size	0.5 in. x 0.5 in. (12.5 mm. x 12.5 mm.)	0.5 in. x 0.5 in. (12.5 mm. x 12.5 mm.)
Tensile Strength	560 lb/in. x 560 lb/in. (100 kN/m. x 100 kN/m.) component strand strengths	1120 lb/in. x 560 lb/in. (200 kN/m. x 100 kN/m.) component strand strengths
Area Weight	13 oz/yd ² (450 gr/m ²)	19 oz/yd ² (650 gr/m ²)
Elongation at Break	4% maximum	4% maximum
Melt Point	above 1800 °F (above 1000 °C)	above 1800 °F (above 1000 °C)

Table 3-10: The Outline of the Experimental Program

Test #	Thickness of Asphalt Layer (inches) [mm]	GlassGrid 8501			GlassGrid 8511			GlassGrid 8502		No Grid	Crack
		Inside the HMA	Between the HMA and the Gravel Base	Inside the HMA	Between the HMA and the Gravel Base	Inside the HMA	Between the HMA and the Gravel Base	Inside the HMA	Between the HMA and the Gravel Base		
1	6 [152]									✓	
2						✓					
3		✓									
4										✓	
5		✓									
6				✓							
7				✓							
8				✓	✓		✓				
9		✓			✓		✓				
10				✓	✓		✓				

Table 3-10 (continued): The Outline of the Experimental Program

Test #	Thickness of Asphalt Layer (inches) [mm]	GlassGrid 8501		GlassGrid 8511		GlassGrid 8502		No Grid	Crack
		Inside the HMA	Between the HMA and the Gravel Base	Inside the HMA	Between the HMA and the Gravel Base	Inside the HMA	Between the HMA and the Gravel Base		
11	3 [76]	✓							
12								✓	
13								✓	✓
14		✓							✓
15		✓							✓
16								✓	✓
17		✓							
18								✓	
19								✓	✓
20	2.5 [63.5]	✓							

3.5 CONSTRUCTION OF TEST SECTIONS AND OUTLINE OF EXPERIMENTAL PROGRAM

The main objective of the research work presented herein was to evaluate the effectiveness of the use of geogrids as a reinforcement material for the asphalt base layer in a flexible pavement system. Factors such as permanent deformation of the asphalt surface, change in pavement stiffness with number of load cycles, resistance to reflective cracking, strain measurements of the glass fiber grid and subgrade stress variation of reinforced pavements were evaluated and compared with results from unreinforced pavement sections. To achieve this objective, 20 pavement sections, with and without glass fiber grids, were constructed and tested in the laboratory. The experimental results from this study were compared with the results from a computer analysis of the pavement sections.

In two soil containers, A-4 type subgrade material was placed in 3 lifts. The bottom layer was 4 inches (102 mm) in thickness while the remaining layers were placed in 3 inch (76 mm) lifts in each box. Each layer was compacted at an average desired moisture content of 10.5%, and to an average unit weight of 131 pcf (20.6 kN/m³) using a Whacker compacter with a 6 inches (152 mm) square tamper plate. The density measurement for each lift of the subgrade soil is listed in Table 3-7. The subgrade compaction was the same for all twenty experiments. After compacting the soil, two pressure cells were placed on top of the subgrade material. Then a geotextile fabric was placed on the surface of the subgrade at the interface between the subgrade soil and the gravel base.

After placing the geotextile fabric, the gravel base was placed in two lifts. The first lift was 4.5 inches (114.3 mm) in thickness and the second was 4 inches (102 mm) in thickness. Each lift was compacted to an average unit weight of 135 pcf (21.2 kN/m³). The unit weight measurements for all the experiments are listed in Table 3-5. After compacting the gravel base, hot mix asphalt was placed.

Based on the experience gained from a preliminary experiment, it was decided to separate the asphalt from the side walls of the steel box to prevent the friction caused by the asphalt/box interaction. The reason for the change was a big difference in measured values of vertical subgrade stresses that was observed by preventing the friction. This process was accomplished by placing wooden plates as a liner to the side walls of the steel box before pouring the hot mix asphalt (HMA) for each test section. After accomplishing the HMA compaction, these wooden plates were removed without disturbing the HMA before the test started. Hot mix asphalt was placed in two lifts. For the first ten experiments, the total thickness of the asphalt layer was 6 inches (152 mm), and was compacted in two 3-inch (76 mm) lifts as shown in Figure 3-11. The remaining 9 of 10 experiments, the total thickness of the asphalt layer was reduced to 3 inches (76 mm), and was compacted in two 1.5-inch (38.1 mm) lifts. For the remaining experiment, the thickness of the asphalt layer was reduced to 2.5 inches (63.5 mm), and was compacted in 1.5-inch (38.1 mm) and 1-inch (25 mm) lifts as shown in Figure 3-12. The range for the desired unit weight of the hot mix asphalt was 143.5 pcf (22.5 kN/m³) to 151.2 pcf (23.7 kN/m³). The results of the measured unit weight of asphalt layer for all the experiments are listed in Table 3-3.

In thirteen experiments, the glass fiber grid was used in the asphalt layer. In three experiments out of thirteen, the glass fiber grid was placed between the gravel base and the hot mix asphalt in addition to the one inside the HMA. In five experiments, with and without reinforcement, a steel bar was used to simulate a crack in the hot mix asphalt having a thickness of 3-inch (76 mm) as shown in Figure 3-13. After compacting the HMA, the steel bar was pulled out without disturbing the HMA before the cooling down process occurred. The size of the crack (fracture) for each test section was 0.5-inch (12.7 mm) wide and 1.5-inch (38.1 mm) high. Lengthwise, the crack extended from one end

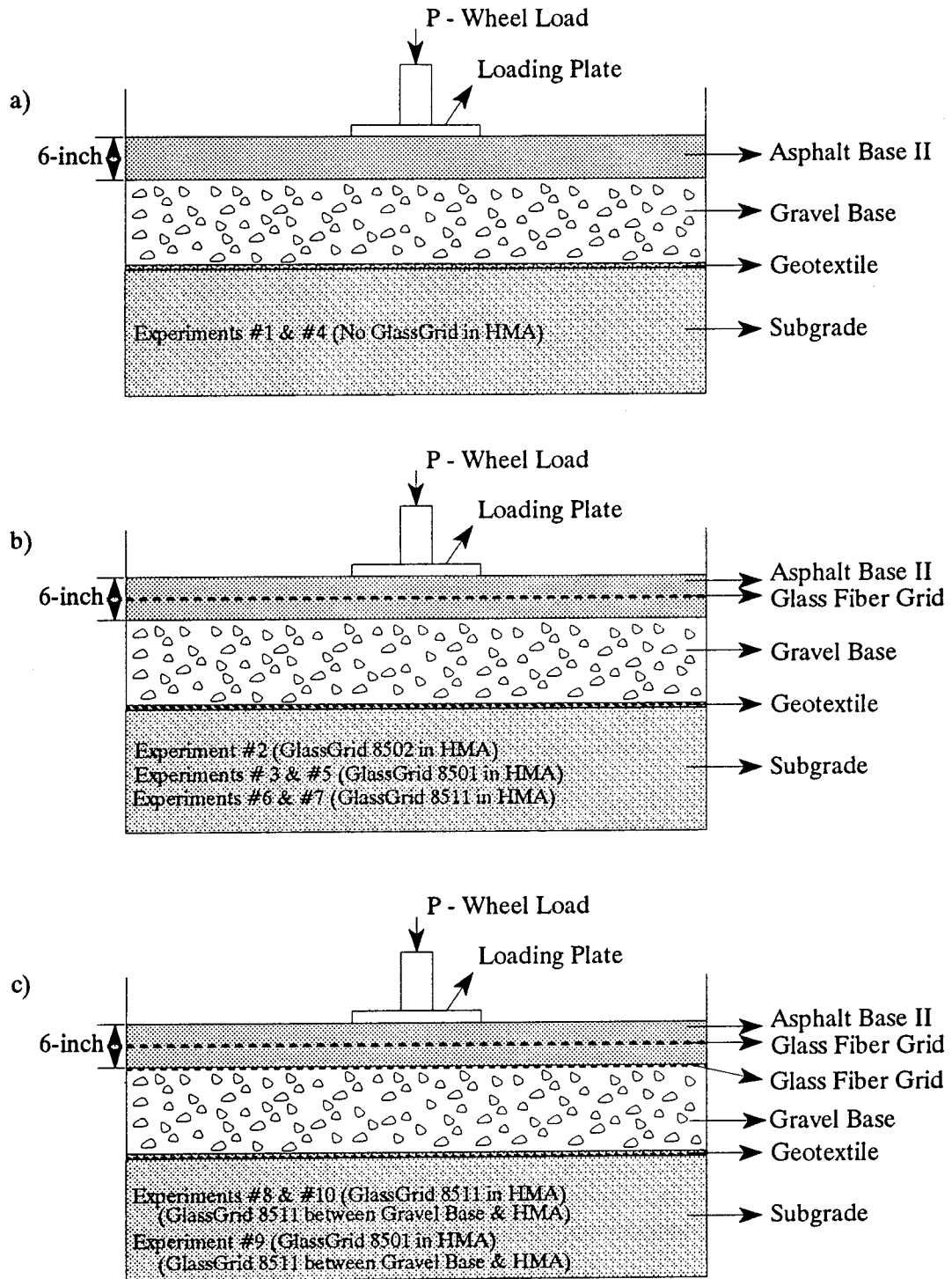


Figure 3-11: Experimental Outline for Pavement Section with a 6-Inch (152 mm) Thick Asphalt Layer

- a) No Reinforcement in Asphalt Layer
- b) Reinforcement in Asphalt Layer
- c) Doubly Reinforced Asphalt Layer

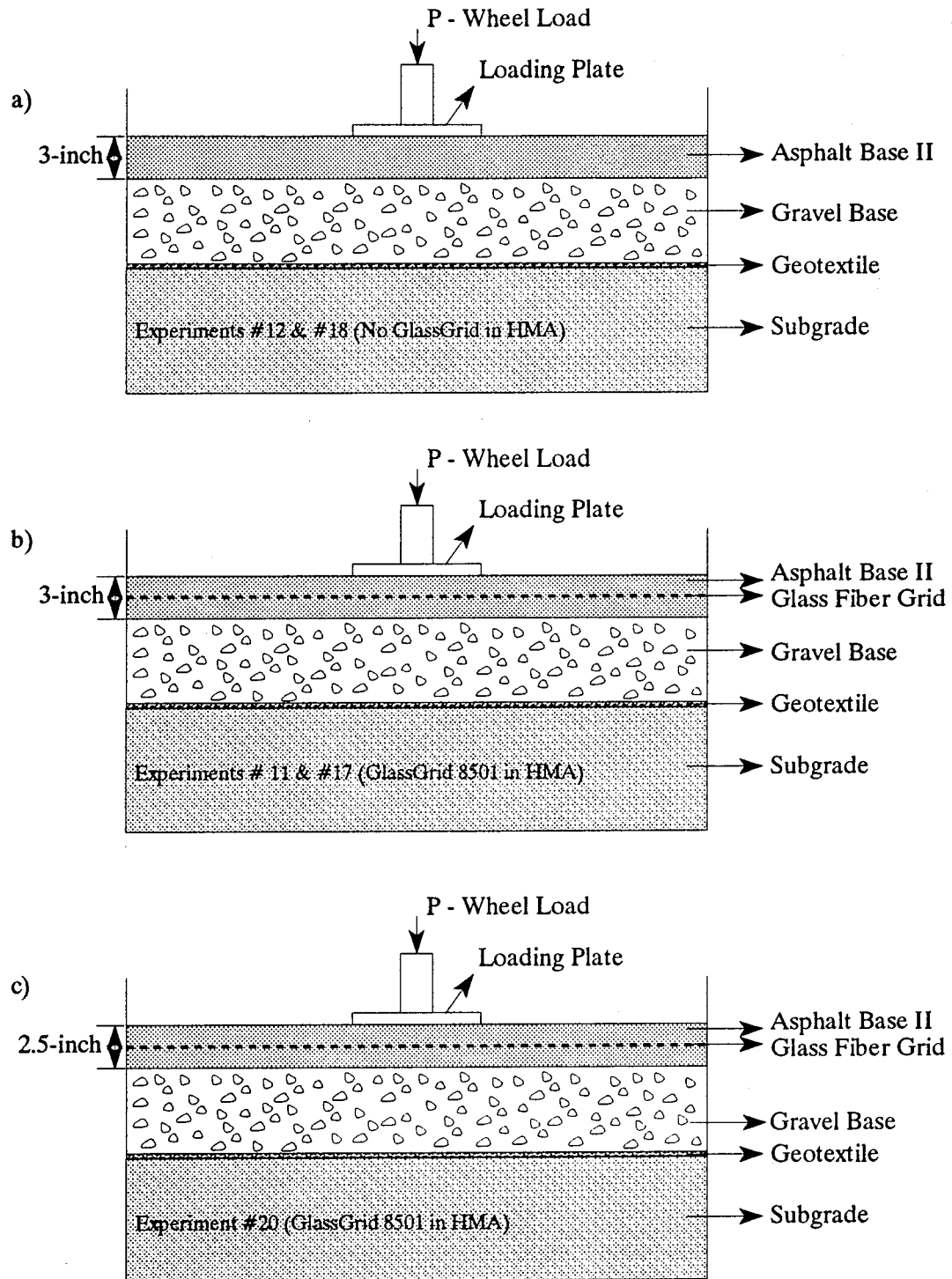


Figure 3-12: Experimental Outline for Pavement Section for Reduced Thicknesses

- a) No Reinforcement in Asphalt Layer
- b) Reinforcement in Asphalt Layer for Thickness of 3-inch
- c) Reinforcement in Asphalt Layer for Thickness of 2.5-inch

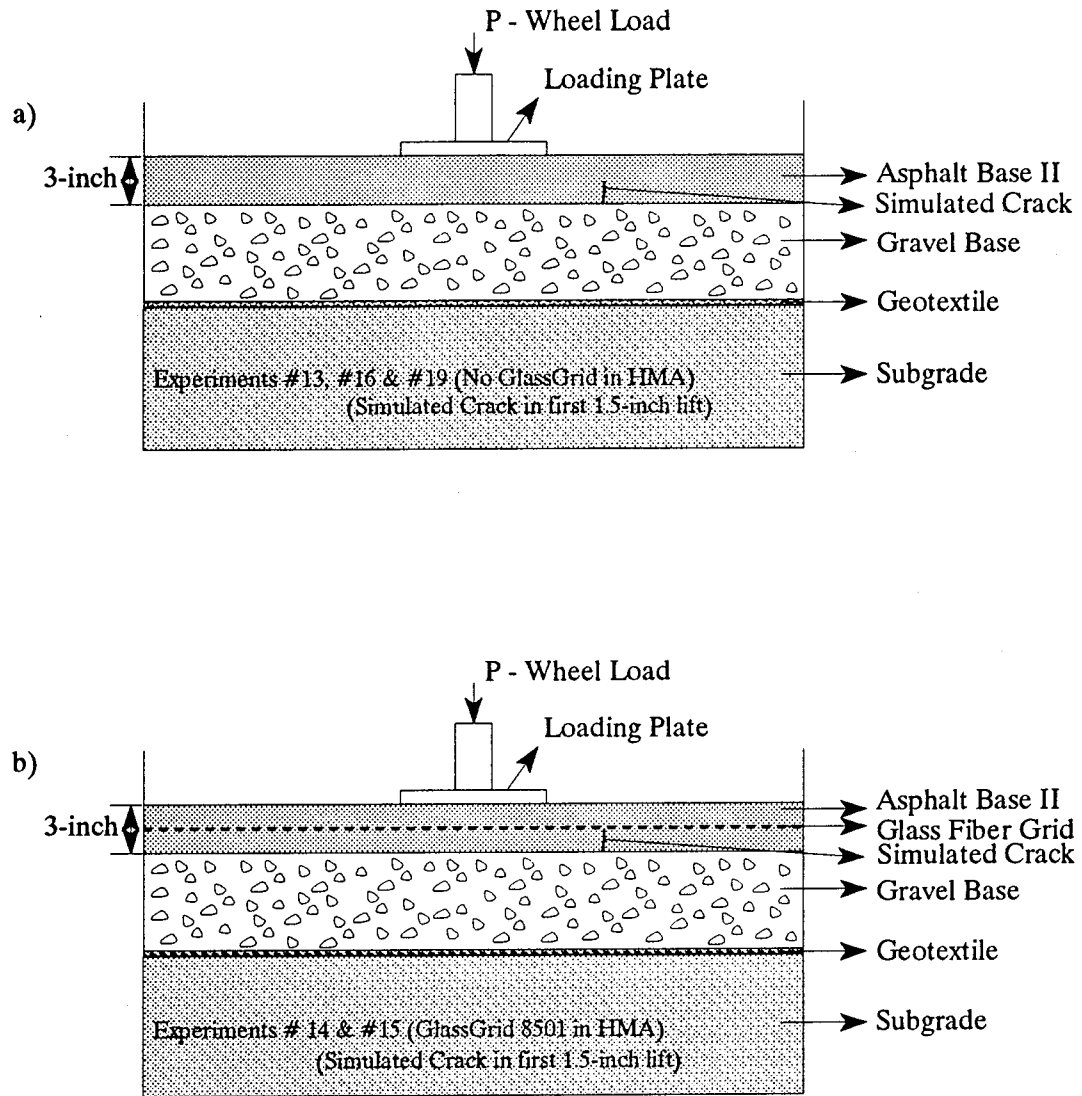


Figure 3-13: Experimental Outline for Pavement Section with a Simulated Crack

a) No Reinforcement in Asphalt Layer

b) Reinforcement in Asphalt Layer

to the other end of the soil bin. Seven sections were tested without any glass fiber reinforcement. The parametric details of all of the experiments are listed in Table 3-10 and Figures 3-11, 3-12, and 3-13. The laboratory test results with data reduction and performance evaluation are given in the next chapter. The details of the computer analyses and its results are presented in Chapter 5.

CHAPTER 4

LABORATORY TEST RESULTS

The major objective of this research was to evaluate the effectiveness of geogrid (glass fiber grid) for reinforcing structural asphalt layers in a flexible pavement section. This study involved both laboratory experimental work and computer analyses of flexible pavement sections. As part of the experimental work, twenty flexible pavement sections (with and without glass fiber grids) were constructed and tested in the laboratory. The laboratory-scale pavement sections were instrumented with pressure cells, displacement gages, and strain gages. Test sections were subjected to 1,000,000 load applications at a frequency of 1.2 Hz. Static loading tests were conducted at intervals of 100,000 load applications (cycles). Twenty experiments were performed, of which the first was a trial iterative section. In four experiments, failure of the pavement section was observed. In the remaining fifteen experiments, failure of the pavement section was not observed. The results of Experiment #1 were considered unreliable and are not presented. In Experiments #4 and #5, the pavement section failed due to severe rutting. The measured cumulative surface displacements for these pavement sections were less than 1 inch (25 mm); however, based on visual observations, the cumulative displacement at the edge on one side of the loading plate (where the dial gages were not installed) was more than 1 inch (25 mm) and was considered to indicate failed. Based on visual observation, bulging occurred during Experiment #13 at the side of the simulated crack. This swelling was in excess of 1 inch (25 mm), and the simulated crack was found to be filled with asphalt. Therefore, this section was also considered to have failed. During Experiment #16, the simulated crack was found to be filled with asphalt and considered to have failed. The remaining experiments showed a satisfactory performance of the pavement section.

In this study, measurement of strain in the reinforcement layer (glass grid) was attempted in five experiments. During the glass grid installation inside the hot mix asphalt, difficulties were encountered due to the hostile environment conditions for the strain gages such as compaction, dynamic loading, and high temperature. Strain measurements on glass fiber grid were considered as not successful due to the difficulties encountered during compaction and the dynamic loading process. Therefore, the uncertainty of the results on strain measurements should be noted.

The experimental data from this study was compared with results from computer analyses of pavement sections. Laboratory results are presented in detail in Chapter 4. Results from the computer analyses are presented in Chapter 5.

4.1 VERTICAL SUBGRADE STRESS

The purpose of measuring vertical stresses at the top of the subgrade was to evaluate the structural performance and compare the differences between the reinforced and non-reinforced flexible pavement sections. The influence of the asphalt layer thickness on the vertical subgrade stress was investigated by evaluating asphalt layer thicknesses of 2.5 inches (63.5 mm), 3 inches (76 mm) and 6 inches (152 mm). The influence of the glass grids on pavement performance was investigated by including the reinforcement in the middle of the hot mix asphalt layer for thirteen experiments. Also, an additional reinforcement layer at the gravel base/hot mix asphalt interface (in addition to the reinforcement in the hot mix asphalt) was included in three experiments.

Figures 4-1 through 4-11 show the variation of vertical subgrade stress with the number of load cycles under the applied static load of 9 kips (40 kN) for different experiments. The ranges of measured vertical subgrade stresses at cells #1 and #2 for each experiment are presented in Table 4-1.

Table 4-1: Range of Vertical Subgrade Stresses for Pressure Cell #1 and Pressure Cell #2 at 9 kips (40 kN) of Static Loading

Experiment #	Range of Vertical Subgrade Stress at Pressure Cell #1 minimum value - maximum value (psi) [kN/m ²]	Range of Vertical Subgrade Stress at Pressure Cell #2 minimum value - maximum value (psi) [kN/m ²]
1	Not Available	
2	3.49 - 5.27 [24.05 - 36.31]	0.86 - 1.13 [5.93 - 7.79]
3	2.10 - 7.50 [14.47 - 51.68]	1.38 - 2.37 [9.51 - 16.33]
4	4.83 - 5.38 [33.28 - 37.07]	1.20 - 2.30 [8.27 - 15.85]
5	2.50 - 7.40 [17.23 - 50.99]	1.38 - 1.98 [9.51 - 13.64]
6	5.77 - 7.31 [39.76 - 50.37]	1.31 - 2.23 [9.03 - 15.36]
7	4.96 - 7.85 [34.17 - 54.09]	1.39 - 1.91 [9.58 - 13.16]
8	2.80 - 7.50 [19.29 - 51.68]	1.58 - 2.18 [10.89 - 15.02]
9	4.96 - 9.29 [34.17 - 64.01]	0.94 - 1.75 [6.48 - 12.06]
10	2.50 - 5.70 [17.23 - 39.27]	1.48 - 1.88 [10.20 - 12.95]
11	4.50 - 8.90 [31.01 - 61.32]	1.78 - 2.47 [12.26 - 17.02]
12	6.85 - 8.46 [47.20 - 58.29]	0.93 - 1.57 [6.41 - 10.82]
13	6.63 - 8.41 [45.68 - 57.94]	1.55 - 2.49 [10.67 - 17.16]
14	3.60 - 8.10 [24.80 - 55.81]	1.68 - 2.08 [11.58 - 14.33]
15	4.20 - 8.60 [28.94 - 59.25]	2.08 - 2.87 [14.33 - 19.77]
16	7.11 - 8.09 [48.99 - 55.74]	1.75 - 2.61 [12.06 - 17.98]
17	5.60 - 9.80 [38.58 - 67.52]	1.78 - 2.47 [12.26 - 17.02]
18	6.75 - 7.56 [46.51 - 52.09]	0.74 - 1.57 [5.10 - 10.82]
19	5.90 - 9.00 [40.65 - 62.01]	3.56 - 7.91 [24.53 - 54.50]
20	4.82 - 6.21 [33.21 - 42.79]	0.38 - 0.96 [2.62 - 6.61]

Figure 3-1 shows the locations of pressure cell #1 and pressure cell #2. The physical properties corresponding to each glass grid type were mentioned earlier (Section 3.4.5) and listed in Table 3-9. GlassGrid 8501 (GG 8501) represents the lightest glass grid while GlassGrid 8511 (GG 8511) represents the heaviest glass grid. GlassGrid 8502 (GG 8502) has a weight between those of GG 8501 and GG 8511.

4.1.1 Influence Of Different Glass Grids On Vertical Subgrade Stress

Figures 4-1 (a) and (b) show the influence of different glass grids on vertical subgrade stress at two different pressure cells. The vertical subgrade stress at cell #1 for Experiment #3 with (GG 8501) indicated some fluctuation throughout the experiment [Figure 4-1 (a)]. The vertical subgrade stress was 2.1 psi (14.47 kN/m²) at the beginning of experiment and increased to 5.50 psi (37.90 kN/m²) at 300,000 load cycles. After 300,000 load cycles, the vertical stress decreased to 5.10 psi (35.14 kN/m²) at 400,000 load cycles and then increased to 5.82 psi (40.10 kN/m²) at 500,000 load cycles. It was 4.90 psi (33.76 kN/m²) at 700,000 load cycles and after this point the vertical stress increased to 7.5 psi (51.68 kN/m²) at 1,000,000 load cycles. This fluctuation shows that such behavior could be caused by some gravel movement in the gravel base during the dynamic loading. The vertical subgrade stress at cell #1 for Experiment #2 (with GG 8502) displayed more consistent behavior in comparison to Experiment #3 [Figure 4-1 (a)]. The initial reading for vertical stress was 3.49 psi (24.05 kN/m²) and increased to 4.34 psi (29.90 kN/m²) at 100,000 load cycles. After this point, the increase was more gradual. The vertical subgrade stress was 5.27 psi (36.31 kN/m²) at 1,000,000 load cycles. The vertical subgrade stress at cell #1 for Experiment #7 displayed consistent behavior between 100,000 and 1,000,000 load cycles. After the initial stress [7.85 psi (54.09 kN/m²)], the vertical stress decreased to 4.96 psi (34.17 kN/m²) at 100,000 load cycles and increased

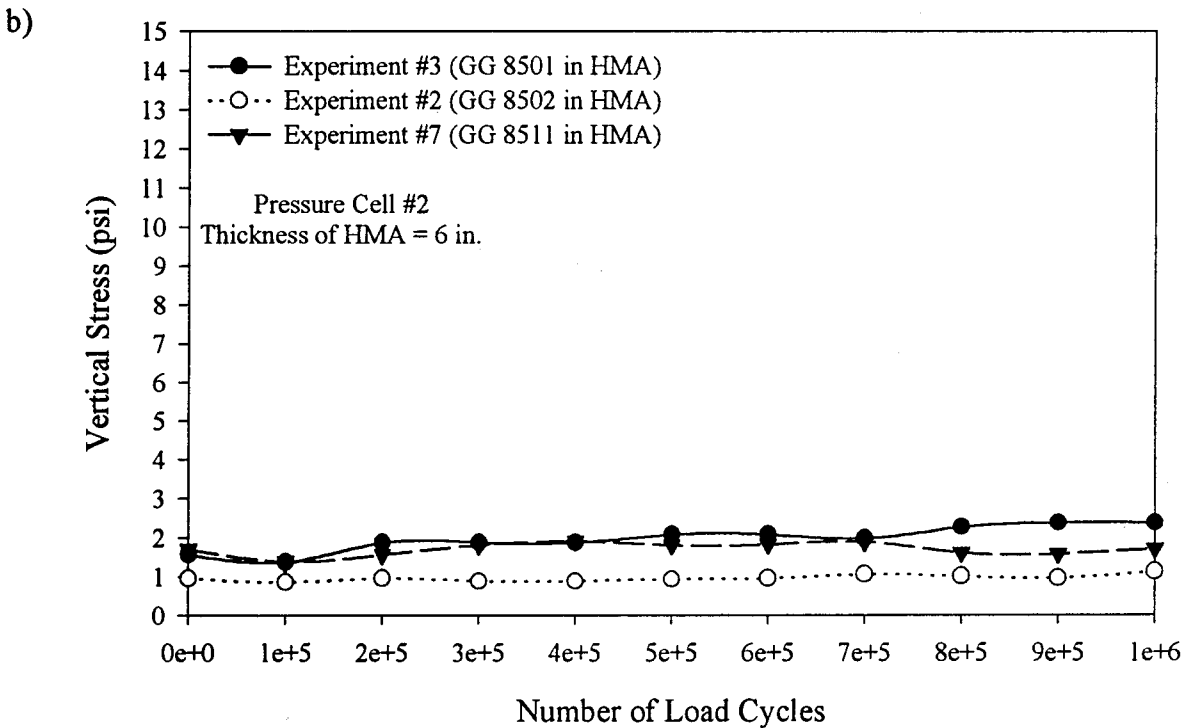
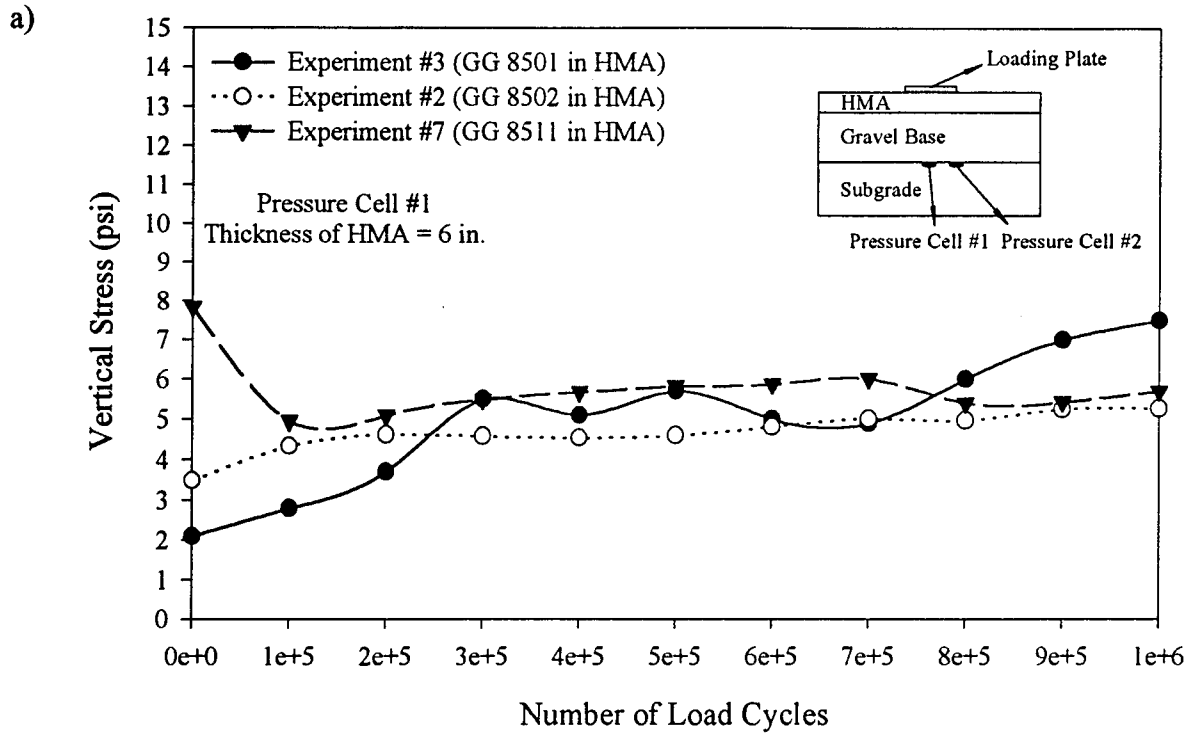


Figure 4-1: Influence of Different Glass Grids on Vertical Subgrade Stress
a) Stress at Cell #1
b) Stress at Cell #2

gradually to 6.01 psi (41.41 kN/m²) at 700,000 load cycles. The vertical subgrade stress was 5.70 psi (39.27 kN/m²) at 1,000,000 load cycles. Based on these results and as shown in Figure 4-1 (a), stress at cell #1 for the test section (Experiment #7) with the heaviest glass grid (GG 8511) was higher than the test sections (Experiments #2 and #3) with lighter glass grids up to 700,000 load cycles. After 700,000 load cycles, stress for the test section (Experiment #7) with the heaviest glass grid (GG 8511) dropped to the same level as the stress for the section (Experiment #2) with the lighter glass grid (GG 8502). Vertical subgrade stress for Experiment #3 fluctuated throughout the experiment and was the highest at 1,000,000 load cycles in comparison to Experiments #2 and #7. These results indicate that the influence of different glass grids reinforcement on vertical subgrade stress is not significant when the thickness of asphalt base is 6 inches (152 mm).

Figure 4-1 (b) shows the vertical subgrade stress distribution at cell #2. The value of vertical stress at cell #2 for each case [Figure 4-1 (b)] was lower than that at cell #1 [Figures 4-1 (a)]. Throughout the experiments, vertical subgrade stresses at cell #2 for the experiments (Experiments #2, #3, and #7) displayed similar behavior with respect to each other. The maximum difference in range for vertical subgrade stress of Experiment #2 was 0.27 psi (1.86 kN/m²). The maximum differences were 0.99 psi (6.89 kN/m²) for Experiment #3 and 0.52 psi (3.58 kN/m²) for Experiment #7 (Table 4-1). As shown in Figure 4-1 (b), the vertical stress at cell #2 for Experiment #2 was slightly smaller than the vertical stress at cell #2 for Experiments #3 and #7. The vertical subgrade stresses for Experiments #3 and #7 behaved similarly up to 700,000 load cycles and then the stress for Experiment #7 decreased slightly [Figure 4-1 (b)].

The vertical subgrade stresses at cells #1 and #2 corresponding to these experiments (Experiments #2, #3, and #7) at 0, 500,000, and 1,000,000 cycles are presented in Table 4-2. These

results also indicate that the influence of different glass grids on vertical subgrade stress is not significant when the thickness of asphalt base is 6 inches (152 mm).

4.1.2 Influence Of Glass Grids On Vertical Subgrade Stress On Doubly Reinforced Section

Figures 4-2 (a) and (b), and Table 4-3 show the influence of glass grids on vertical subgrade stress for doubly reinforced test sections. The vertical subgrade stress at cell #1 for Experiment #8 decreased continuously throughout the experiment. The vertical subgrade stress for the same experiment was 7.5 psi (51.68 kN/m²) initially and decreased to 5.60 psi (38.58 kN/m²) at 500,000 load cycles. After 500,000 load cycles, the vertical subgrade stress continued to decrease to 2.8 psi (19.29 kN/m²) at 1,000,000 load cycles. The vertical subgrade stress at cell #1 for Experiment #9 was 9.29 psi (64.01 kN/m²) initially and the stress decreased to 5.79 psi (39.89 kN/m²) at 100,000 load cycles. Between 100,000 and 500,000 load cycles, the vertical subgrade stress for Experiment #9 was lower than the stress for Experiment #8. At 500,000 load cycles, the vertical subgrade stress was 5.50 psi (37.90 kN/m²), very close to the stress for Experiment #8. After 500,000 load cycles, the stress for Experiment #9 gradually increased to 5.70 psi (39.27 kN/m²) at 1,000,000 load cycles.

Based on the results shown in Figure 4-2 (a), the vertical stress at cell #1 decreased substantially for the doubly reinforced cases. This trend cannot be seen for stresses at cell #2 [Figure 4-2 (b)]. Vertical subgrade stress at cell #1 for Experiment #8 with a heavy glass grid (GG 8511 in the HMA and between the Gravel base and the HMA) decreased significantly in comparison to Experiment #9 with a lighter glass grid (GG 8501 in the HMA and GG 8511 between the Gravel Base and the HMA). At 1,000,000 load cycles, a reduction of approximately 51% in vertical subgrade stress (at cell #1) was observed when a stronger glass grid was used in the doubly reinforced pavement section. Unlike the vertical subgrade stress at cell #1, the vertical subgrade stress at cell #2

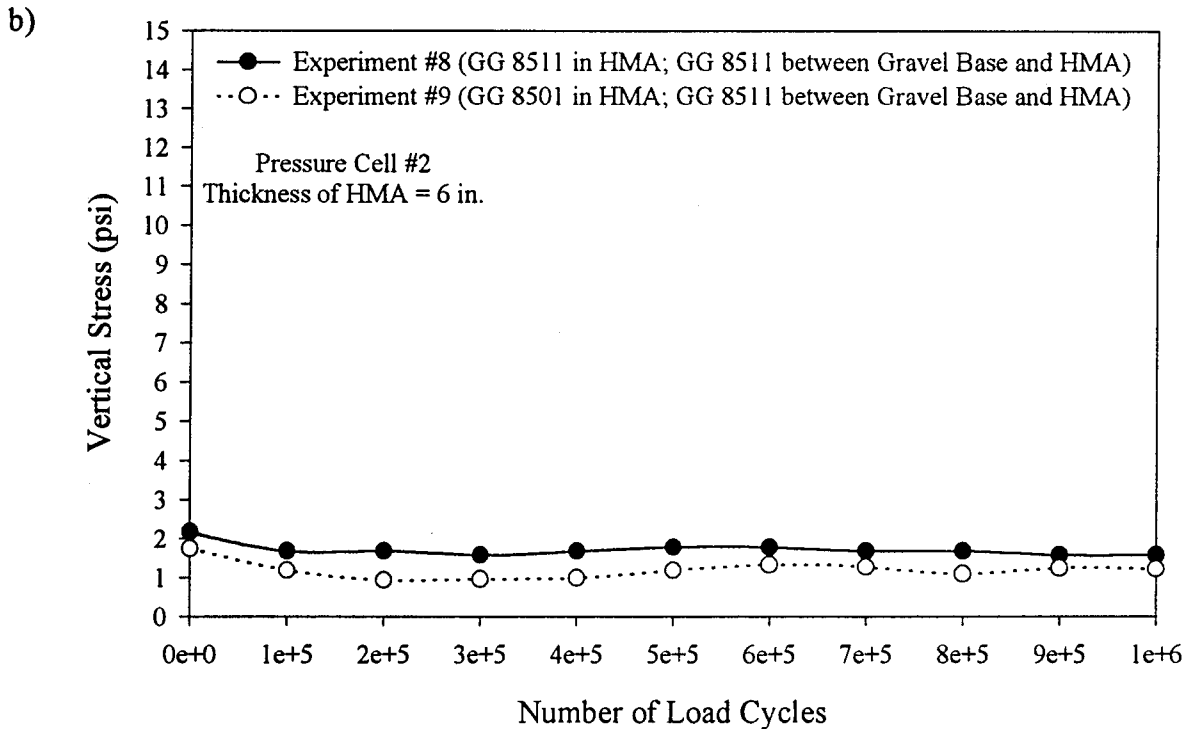
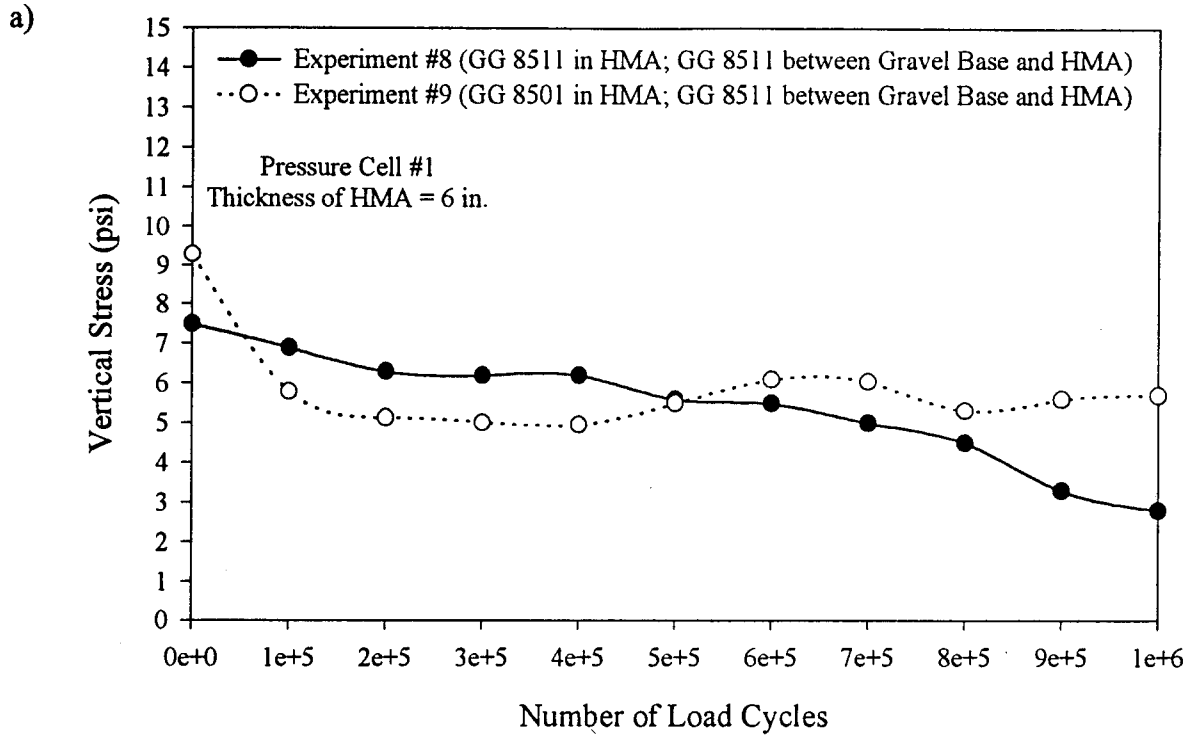


Figure 4-2: Variation of Vertical Subgrade Stress with Number of Load Cycles for Doubly Reinforced Test Sections
a) Stress at Cell #1
b) Stress at Cell #2

Table 4-2: Measured Vertical Subgrade Stress at Cells #1 and #2 for Experiments #2, #3, and #7

	Thick. of HMA (in.) [mm] ↓	Vertical Subgrade Stress (psi) [kN/m ²] Cell #1			Vertical Subgrade Stress (psi) [kN/m ²] Cell #2		
		Number of Load Cycles			Number of Load Cycles		
		0	500,000	1,000,000	0	500,000	1,000,000
Experiment #2 (GG 8502)	6 [152]	3.49 [24.05]	4.60 [31.69]	5.27 [36.31]	0.96 [6.61]	0.94 [6.48]	1.13 [7.79]
Experiment #3 (GG 8501)	6 [152]	2.10 [14.47]	5.70 [39.27]	7.50 [51.68]	1.58 [10.89]	2.08 [14.33]	2.37 [16.33]
Experiment #7 (GG 8511)	6 [152]	7.85 [54.09]	5.82 [40.10]	5.70 [39.27]	1.71 [11.78]	1.81 [12.47]	1.71 [11.78]

Table 4-3: Measured Vertical Subgrade Stress at Cells #1 and #2 for Experiments #8 and #9

	Thick. of HMA (in.) [mm] ↓	Vertical Subgrade Stress (psi) [kN/m ²] Cell #1			Vertical Subgrade Stress (psi) [kN/m ²] Cell #2		
		Number of Load Cycles			Number of Load Cycles		
		0	500,000	1,000,000	0	500,000	1,000,000
Experiment #8 (GG 8511+ GG 8511)	6 [152]	7.50 [51.68]	5.60 [38.58]	2.80 [19.29]	2.18 [15.02]	1.78 [12.26]	1.58 [10.89]
Experiment #9 (GG 8501+ GG 8511)	6 [152]	9.29 [64.01]	5.50 [37.90]	5.70 [39.27]	1.75 [12.06]	1.19 [8.20]	1.22 [8.41]

for Experiment #9 was lower than the stress for Experiment #8 throughout the experiment. Based on these results, it can be stated that the vertical stress in the subgrade is lower in pavement sections with stronger glass grids [Figures 4-1 and 4-2].

4.1.3 Influence Of Reinforcement On Vertical Subgrade Stress [Thickness Of HMA = 6 Inches (152 mm)]

Figures 4-3 (a) and (b) show a comparison of reinforced cases with non-reinforced cases based on vertical subgrade stress for thick asphalt sections. As shown in Figure 4-3 (a), the vertical subgrade stress at cell #1 for Experiment #4 was steady throughout the test. The vertical subgrade stress reached its maximum point [5.38 psi (37.07 kN/m²)] at 600,000 load cycles. The vertical subgrade stress was 5.21 psi (35.90 kN/m²) initially, 4.95 psi (34.11 kN/m²) at 500,000 load cycles, and 5.23 psi (36.03 kN/m²) at 1,000,000 load cycles (Table 4-4). At the beginning of Experiment #8 (doubly-reinforced case), the vertical subgrade stress was 7.50 psi (51.68 kN/m²), which decreased gradually to 5.5 psi (37.90 kN/m²) at 600,000 cycles. Initially, the vertical stress for Experiment #8 was higher than the stresses for Experiments #4 and #5.

The vertical subgrade stress for Experiment #5 was 7.40 psi (50.99 kN/m²) initially and decreased to 3.30 psi (22.74 kN/m²) at 100,000 load cycles. This value further decreased to 2.5 psi (17.23 kN/m²) at 300,000 load cycles. After 300,000 load cycles, the stress started to increase until the failure caused due to rutting. The vertical subgrade stress was 5.20 psi (35.83 kN/m²) at 700,000 load cycles and 6.2 psi (42.72 kN/m²) at 900,000 load cycles. Between 100,000 and 600,000 cycles, the vertical stress for Experiment #5 was lower than the stresses for Experiments #4 and #8. At 700,000 load cycles, all stresses were almost similar for each experiment. The vertical subgrade stresses were 5.00 psi (34.45 kN/m²) for Experiment #8, 5.19 psi (35.76 kN/m²) for Experiment #4,

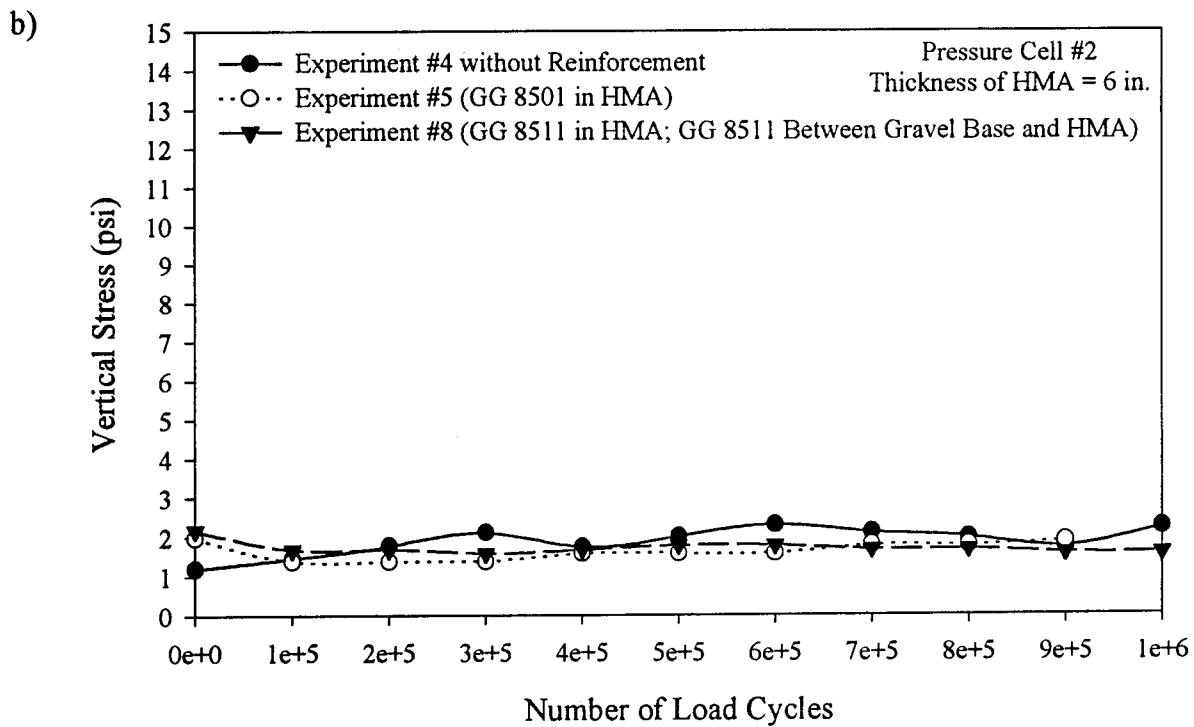
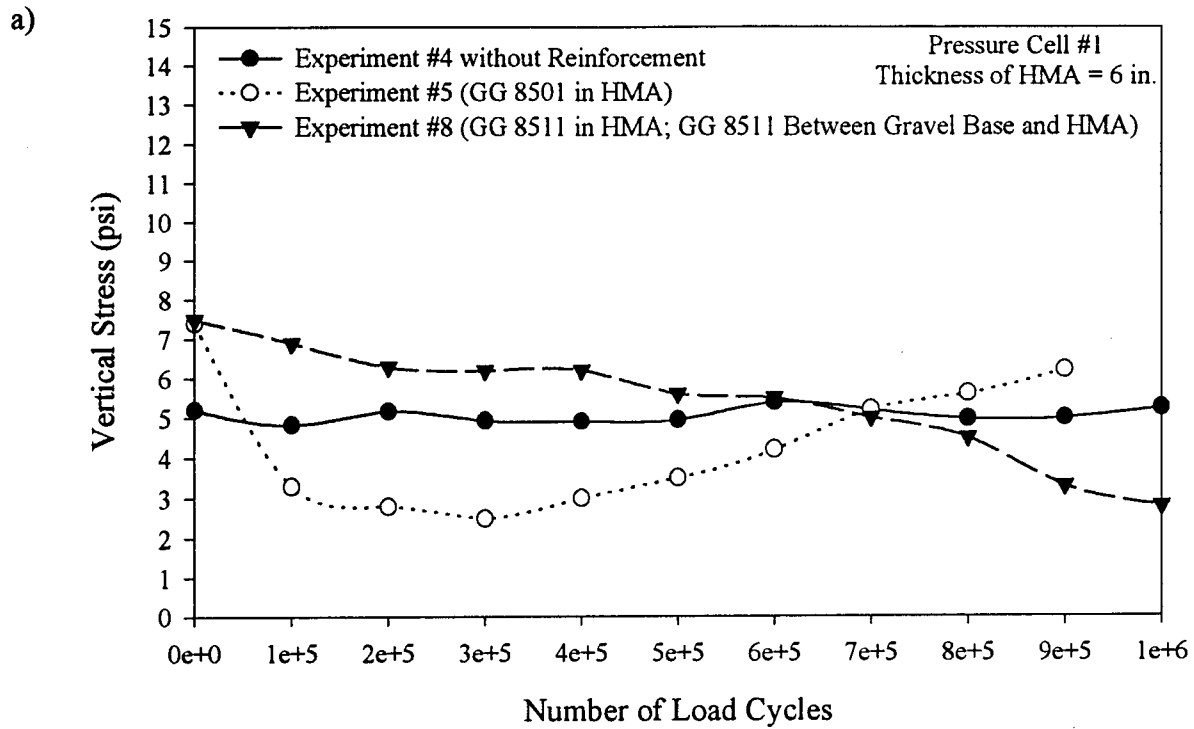


Figure 4-3: Influence of Reinforcement on Vertical Subgrade Stress
[Thickness of HMA = 6 in. (152 mm)]

a) Stress at Cell #1

b) Stress at Cell #2

Table 4-4: Measured Vertical Subgrade Stress at Cells #1 and #2 for Experiments #4, #5, and #8

	Thick. of HMA (in.) [mm] ↓	Vertical Subgrade Stress (psi) [kN/m ²] Cell #1 Note: N/A - Not Available			Vertical Subgrade Stress (psi) [kN/m ²] Cell #2		
		Number of Load Cycles			Number of Load Cycles		
		0	500,000	1,000,000	0	500,000	1,000,000
Experiment #4 (No Reinforcement)	6 [152]	5.21 [35.90]	4.95 [34.11]	5.23 [36.03]	1.20 [8.27]	2.02 [13.92]	2.23 [15.36]
Experiment #5 (GG 8501)	6 [152]	7.40 [50.99]	3.50 [24.12]	N/A	1.98 [13.64]	1.58 [10.89]	N/A
Experiment #8 (GG 8511+ GG 8511)	6 [152]	7.50 [51.68]	5.60 [38.58]	2.80 [19.29]	2.18 [15.02]	1.78 [12.26]	1.58 [10.89]

and 5.20 psi (35.83 kN/m²) for Experiment #5. After 700,000 load cycles, the stress for Experiment #5 continued to increase and was higher than that of Experiments #4 and #8, while the stress for Experiment #8 continued to decrease and was lower than that of Experiments #4 and #5.

Even though the pavement section failed in Experiment #5 (GG 8501), the beneficial influence of reinforcement could be seen up to 700,000 load cycles from Figure 4-3 (a), where the vertical stress for Experiment #5 was lower than the stresses corresponding to the non-reinforced case. The vertical subgrade stress for Experiment #8 (doubly-reinforced case) decreased continuously with the number of load applications throughout the experiment. Eventhough the vertical stress for Experiment #8 (doubly-reinforced case) was slightly higher than the vertical stress for Experiment #4 (non-reinforced case) initially, the stress continued to decrease with the number of load cycles [2.8 psi (19.3 kN/m²) at 1,000,000 load cycles]. At 500,000 load cycles, the vertical subgrade stress for the singly reinforced pavement section (Experiment #5) was approximately 29% lower than the stress for the non-reinforced pavement section (Experiment #4). Even though the vertical subgrade stress for the doubly reinforced pavement section (Experiment #8) was slightly higher than the stress for the non-reinforced pavement section (Experiment #4) initially, the influence of the doubly reinforced pavement section was clearly apparent at 1,000,000 load cycles. At 1,000,000 load cycles, the vertical subgrade stress at cell #1 for doubly reinforced pavement section (Experiment #8) was approximately 46% lower than the stress for the non-reinforced pavement section (Experiment #4).

The effect of reinforcement is also apparent in the reduction of stress at cell #2 for reinforced cases [Figure 4-3 (b)]. The vertical subgrade stress at cell #2 for each experiment was steady throughout the experiment. The vertical subgrade stress for Experiment #5 was 1.88 psi (12.95 kN/m²) at 900,000 load cycles just before failure. The vertical subgrade stresses at 1,000,000 load

cycles were 1.58 psi (10.89 kN/m²) for Experiment #8 and 2.23 psi (15.36 kN/m²) for Experiment #4 (Table 4-4). Figure 4-3 (b) also shows that the vertical stresses for both reinforced cases were lower than the vertical stress for the non-reinforced case. At 500,000 load cycles, the reduction in vertical subgrade stress for the doubly reinforced case (Experiment #8) was approximately 12%. This reduction was even more evident at 1,000,000 load cycles, approximately 29%. Even though the pavement section failed in Experiment #5, the vertical subgrade stress at cell #2 for the single reinforced pavement section (Experiment #5) was approximately 22% at 500,000 load cycles was smaller than that of the non-reinforced pavement section (Experiment #4). The vertical subgrade stresses at cells #1 and #2 corresponding to these experiments (Experiments #4, #5, and #8) at 0, 500,000, and 1,000,000 load cycles are presented in Table 4-4. In conclusion, Figures 4-3 (a) and (b) show that the glass grid reinforcement seems to spread the load over a larger area in the lower layers causing lower subgrade stresses.

4.1.4 Influence Of Reinforcement On Vertical Subgrade Stress [Thickness Of HMA = 2.5 Inches (63.5 mm) And 3 Inches (76 mm)]

A similar comparison was performed for the asphalt sections where the thicknesses of HMA was 2.5 inches (63.5 mm) and 3 inches (76 mm) [Figures 4-4 (a) and (b)] (Table 4-5). The vertical subgrade stress at cell #1 for Experiment #12 was initially 8.46 psi (58.29 kN/m²) and decreased to 6.94 psi (47.82 kN/m²) at 100,000 load cycles. Upon further loading, the stress increased gradually up to 7.6 psi (52.36 kN/m²) at 1,000,000 load cycles. The vertical subgrade stress for Experiment #11 was the highest initially [8.90 psi (61.32 kN/m²)], and decreased substantially to 4.50 psi (31.01 kN/m²) at 100,000 load cycles. The vertical subgrade stress increased up to 7.50 psi (51.68 kN/m²) at 1,000,000 load cycles.

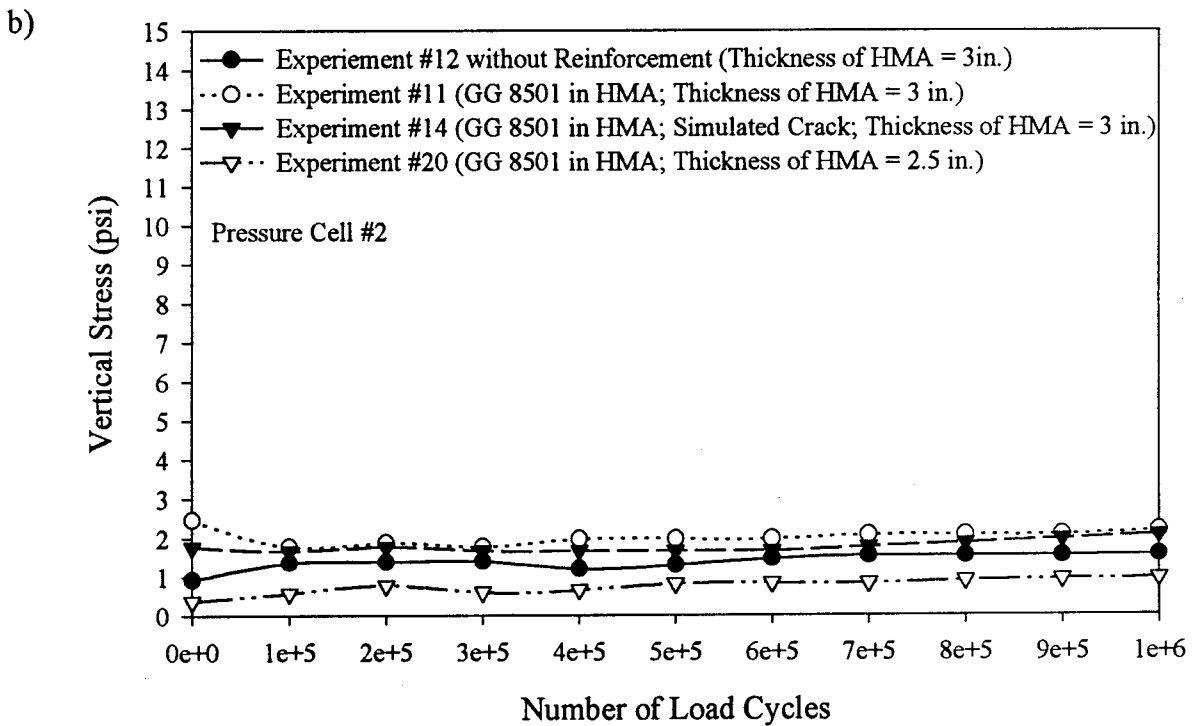
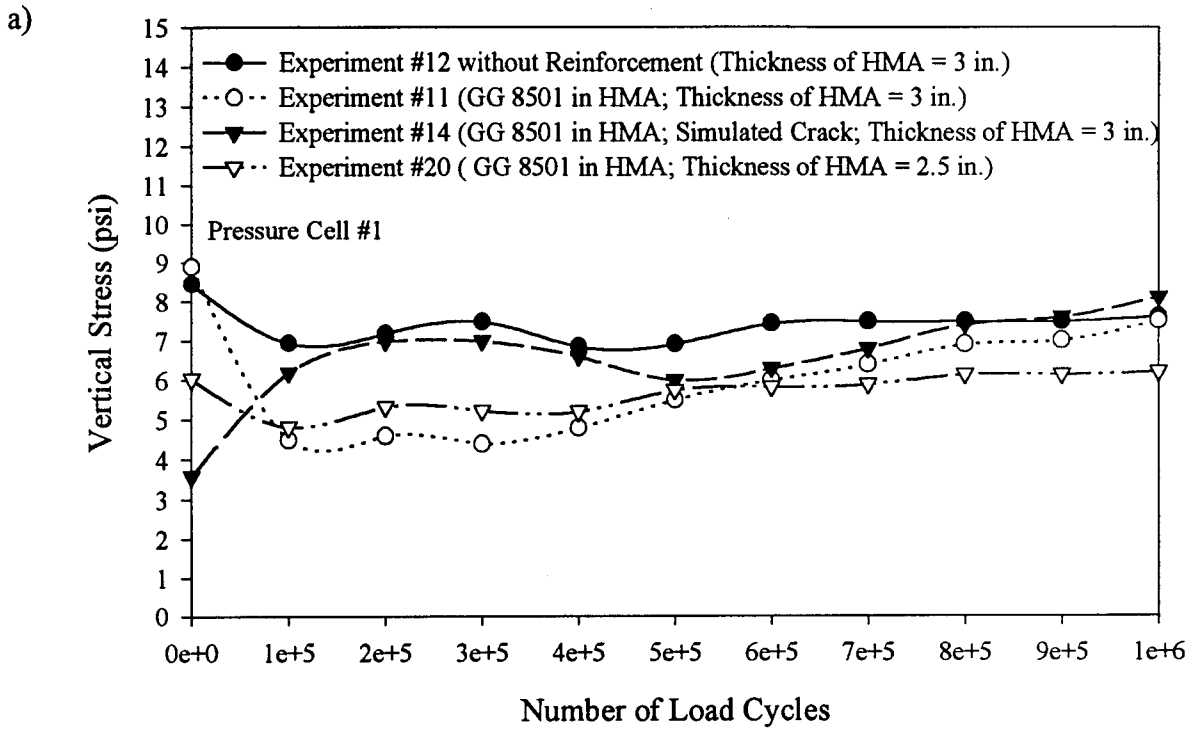


Figure 4-4: Influence of Reinforcement on Vertical Subgrade Stress
 [Thickness of HMA = 2.5 in. (63.5 mm) and 3 in. (76 mm)]
 a) Stress at Cell #1
 b) Stress at Cell #2

Table 4-5: Measured Vertical Subgrade Stress at Cells #1 and #2 for Experiments #11, #12, #14, and #20

	Thick. of HMA (in.) [mm] ↓	Vertical Subgrade Stress (psi) [kN/m ²] Cell #1			Vertical Subgrade Stress (psi) [kN/m ²] Cell #2		
		Number of Load Cycles			Number of Load Cycles		
		0	500,000	1,000,000	0	500,000	1,000,000
Experiment #11 (GG 8501)	3 [76]	8.90 [61.32]	5.50 [37.90]	7.50 [51.68]	2.47 [17.02]	1.98 [13.64]	2.18 [15.02]
Experiment #12 (No Reinforcement)	3 [76]	8.46 [58.29]	6.92 [47.68]	7.60 [52.36]	0.93 [6.41]	1.31 [9.03]	1.57 [10.82]
Experiment #14 (GG 8501) (Simulated Crack)	3 [76]	3.60 [24.80]	6.00 [41.34]	8.10 [55.81]	1.78 [12.26]	1.68 [11.58]	2.08 [14.33]
Experiment #20 (GG 8501)	2.5 [63.5]	6.04 [41.62]	5.75 [39.62]	6.21 [42.79]	0.38 [2.62]	0.82 [5.65]	0.96 [6.61]

At the beginning of the experiment the vertical subgrade stress for Experiment #14 (section with the simulated crack) was 3.60 psi (12.96 kN/m²), which was lower than the stress for Experiments #11, #12, and #20. The stress increased to 7.00 psi (48.23 kN/m²) at 300,000 load cycles and then decreased to 6.00 psi (41.34 kN/m²) at 500,000 load cycles. After this point, the stress consistently increased to 8.10 psi (55.81 kN/m²) at 1,000,000 load cycles and was highest at this point in comparison to Experiments #11, #12, and #20. The vertical subgrade stress for Experiment #20 decreased from 6.04 psi (41.62 kN/m²) initially to 4.82 psi (33.21 kN/m²) at 100,000 load cycles. After 100,000 load cycles, the stress increased gradually to 6.21 psi (42.79 kN/m²) at 1,000,000 load cycles. Between 600,000 and 1,000,000 load cycles, the stress was lower than the stresses corresponding to Experiments #11, #12, and #14.

At 500,000 load cycles, the vertical subgrade stress at cell #1 for the reinforced pavement section with a simulated crack (Experiment #14) was approximately 13% lower than the stress for the non-reinforced pavement section (Experiment #12). For another reinforced pavement section without the simulated crack (Experiment #11), the vertical subgrade stress at the same load application was approximately 21% lower than the stress for the non-reinforced pavement section (Experiment #12). Reduction in vertical subgrade stress for the reinforced pavement section where the thickness of the HMA was 2.5 inches (63.5 mm) (Experiment #20) was approximately 17%. Based on these results, it can be stated that the vertical subgrade stress at cell #1 was smaller for the reinforced cases (Experiments #11, #14 and #20) than the stress for the non-reinforced case (Experiment #12) [Figure 4-4 (a)]. The vertical stress for the reinforced cases without the simulated crack (Experiments #11 and #20) was lower than the vertical stress for the reinforced case with the simulated crack (Experiment #14). This behavior indicates that the vertical stress was influenced by

the presence of a simulated crack. Inclusion of glass grid within the HMA seems to distribute loads over a larger area of the subgrade causing a reduction in vertical subgrade stress. It is worth noting the lower stresses at cell #1 for the reinforced case with the simulated crack (Experiment #14) in comparison to the non-reinforced case without simulated crack (Experiment #12) up to 900,000 load cycles [Figure 4-4 (a)].

Figure 4-4 (b) shows the same comparison for cell #2. The vertical subgrade stresses at cell #2 were consistent throughout the experiments compared herein. As shown in Figure 4-4 (b), all test sections behaved similarly in terms of vertical stress. In addition to the Figures 4-4 (a) and (b), the vertical subgrade stresses for both cells (cells #1 and #2) at 0, 500,000, and 1,000,000 load cycles are presented in Table 4-5. Vertical stresses at cell #2 were very small, ranging between 0.38 psi (2.62 kN/m²) and 2.47 psi (17.02 kN/m²).

4.1.5 Comparison Of Non-Reinforced 6-Inch (152 mm) Thick Asphalt Section With Thinner Reinforced Asphalt Sections

Figures 4-5 (a) and (b) show the comparison of the non-reinforced pavement section (Experiment #4) with reinforced pavement sections (Experiments #17 and #20) for different HMA thicknesses. The behavior of vertical subgrade stress at cell #1 for Experiment #4 was explained previously in Section 4.1.3 in Figure 4-3 (a). The vertical subgrade stress for Experiment # 4 ranged from 4.38 psi (30.18 kN/m²) to 5.38 psi (37.07 kN/m²) (Table 4-1). The vertical subgrade stress at cell #1 for Experiment #20 [thickness of HMA = 2.5 inches (63.5 mm)] decreased from 6.04 psi (41.62 kN/m²) to 4.82 psi (33.21 kN/m²) in first 100,000 load cycles. After 100,000 load cycles, the vertical subgrade stress increased gradually to 6.21 psi (42.79 kN/m²) at 1,000,000 load cycles. The vertical subgrade stress at cell #1 for Experiment #17 [thickness of HMA = 3 inches (76 mm)]

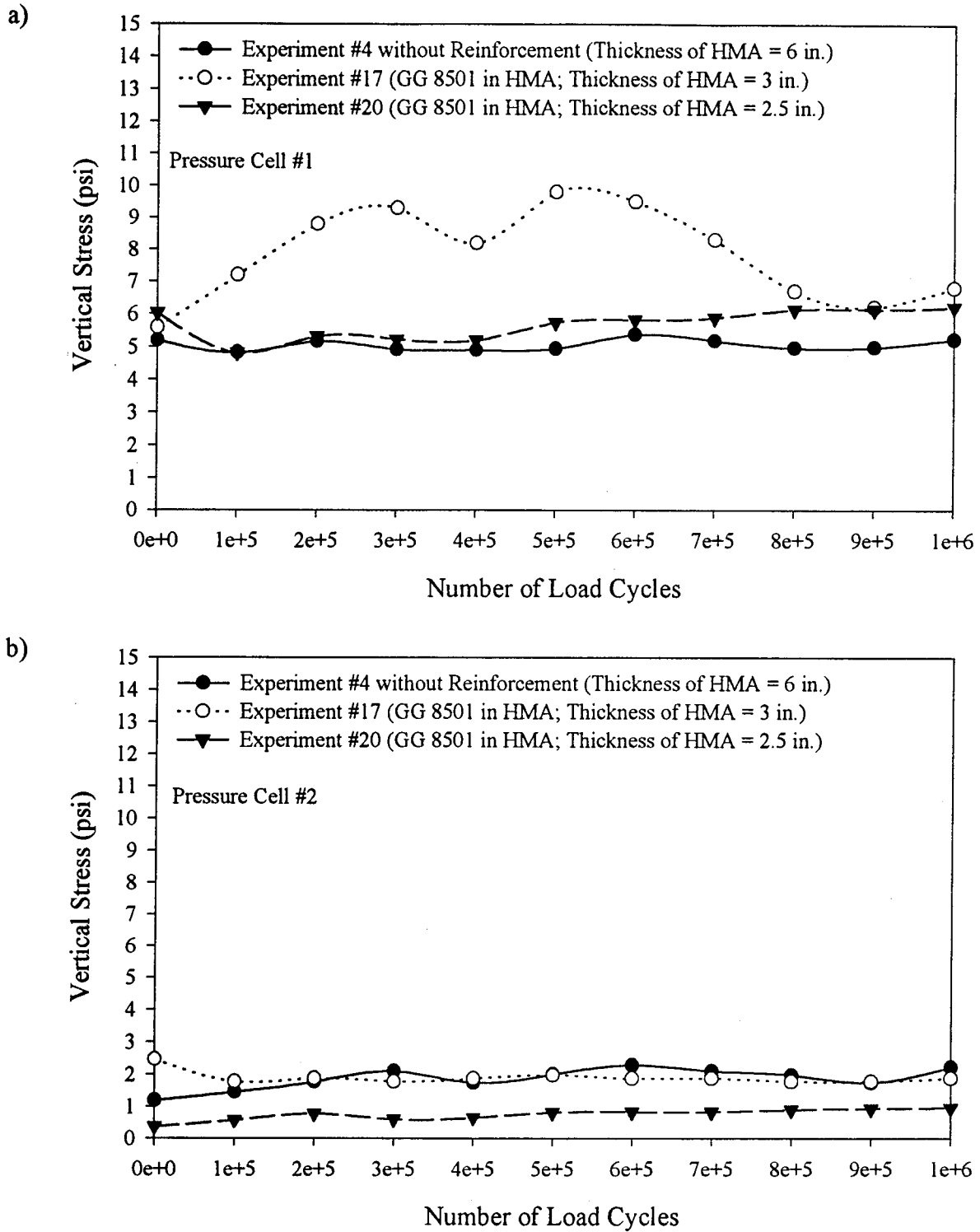


Figure 4-5: Comparison of Non-Reinforced 6-inch (152 mm) Thick Asphalt Section with Thinner Reinforced Asphalt Sections with Respect to Vertical Subgrade Stress

a) Stress at Cell #1

b) Stress at Cell #2

fluctuated noticeably in the range of about 6 - 9 psi (41.34 - 62.01 kN/m²).

This fluctuation indicates some granular movement in the gravel base during the dynamic loading. As shown in Figure 4-5 (a) and Table 4-6, the vertical subgrade stress at cell #1 for Experiment #4 was lower than the stress for Experiments #17 and #20. For example, at 1,000,000 load cycles, the stresses were 5.23 psi (36.03 kN/m²) for Experiment #4, 6.21 psi (42.79 kN/m²) for Experiment #20, and 6.8 psi (46.85 kN/m²) for Experiment #17 (Table 4-6). Based on these results at cell #1 as shown in Figure 4-5 (a) and Table 4-6, it can be stated that a reinforced thinner section behaves similar to that of a non-reinforced thicker pavement section.

The results at cell #2 for the same pavement sections gave different results on the effectiveness of thickness on vertical subgrade stress. For example, at 1,000,000 load cycles the reduction in vertical subgrade stress at cell #2 for Experiment #17 was approximately 16% in comparison to Experiment #4, and the reduction for Experiment #20 was approximately 57% in comparison to Experiment #4. As shown in Figure 4-5 (b), the vertical stresses for reinforced cases of thin asphalt sections [2.5 inches (63.5 mm) and 3 inches (76 mm)] were lower than the vertical stress for the non-reinforced case with a thicker asphalt section [6 inches (152 mm)]. Based on the vertical subgrade stress at cell #2, a hot mix asphalt with a thickness of 6 inches (152 mm) does not necessarily improve the performance of the pavement system in comparison to thin reinforced asphalt sections [Figure 4-5 (b)]. However, the stresses at cell #2 and the differences between the experiments are much lower than those at cell #1. Based on the stresses at cell #1, it can be stated that a 6-inch (152 mm) thick non-reinforced hot mix asphalt layer leads to slightly lower subgrade stresses in comparison to a thinner reinforced pavement section.

4.1.6 Influence Of Asphalt Thickness On Vertical Subgrade Stress

Influence of asphalt thickness on vertical subgrade stress for reinforced cases is also shown in Figures 4-6 (a) and (b), and Table 4-7. In these figures, vertical subgrade stresses corresponding to two thickness of reinforced HMA are shown. The vertical subgrade stress at cell #1 for Experiment #3 started from 2.1 psi (14.47 kN/m²) at the beginning of the experiment and increased to 7.5 psi (51.68 kN/m²) at 1,000,000 load cycles. Reduction in vertical subgrade stress at cell #1 for the thicker reinforced pavement section (Experiment #3) was 42% at 500,000 load cycles in comparison to the thinner reinforced pavement section (Experiment #17). Up to 800,000 cycles, the influence of thickness was clear and this behavior indicated that when the thickness of the asphalt increases, the vertical subgrade stress decreases.

The vertical subgrade stresses at cell #2 for Experiments #3 and #17 were very similar throughout the test. Based on these results, it can be stated that the thicker asphalt layer resulted in a lower vertical subgrade stress at cell #1, while vertical subgrade stresses were almost the same at cell #2 for both thicknesses [Figure 4-6 (b)]. This shows that vertical stresses away from the applied load decrease substantially in comparison to the stresses beneath the center of the loading area [Figures 4-6 (a) and (b), and (Table 4-7)].

Influence of asphalt thickness on subgrade stress for non-reinforced cases is shown in Figures 4-7 (a) and (b). The measured vertical subgrade stresses at cells #1 and #2 for Experiments #4, #12, and #18 at 0, 500,000, and 1,000,000 load cycles are presented in Table 4-8. The effect of thickness on vertical subgrade stress is clear: the higher the thickness of the asphalt layer, the lower the vertical subgrade stresses [Figure 4-7 (a)]. As expected, when the thickness of the HMA was increased from 3 inches (76 mm) to 6 inches (152 mm), the improvement of the vertical stress at cell #1 ranged from

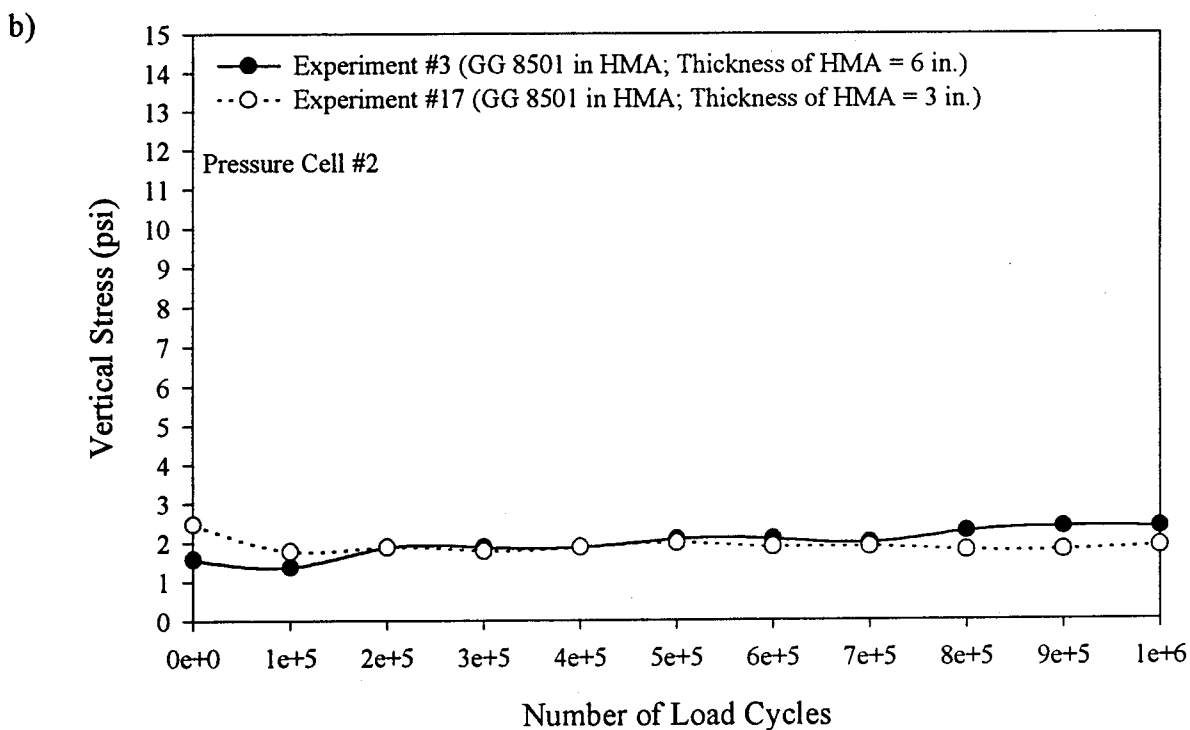
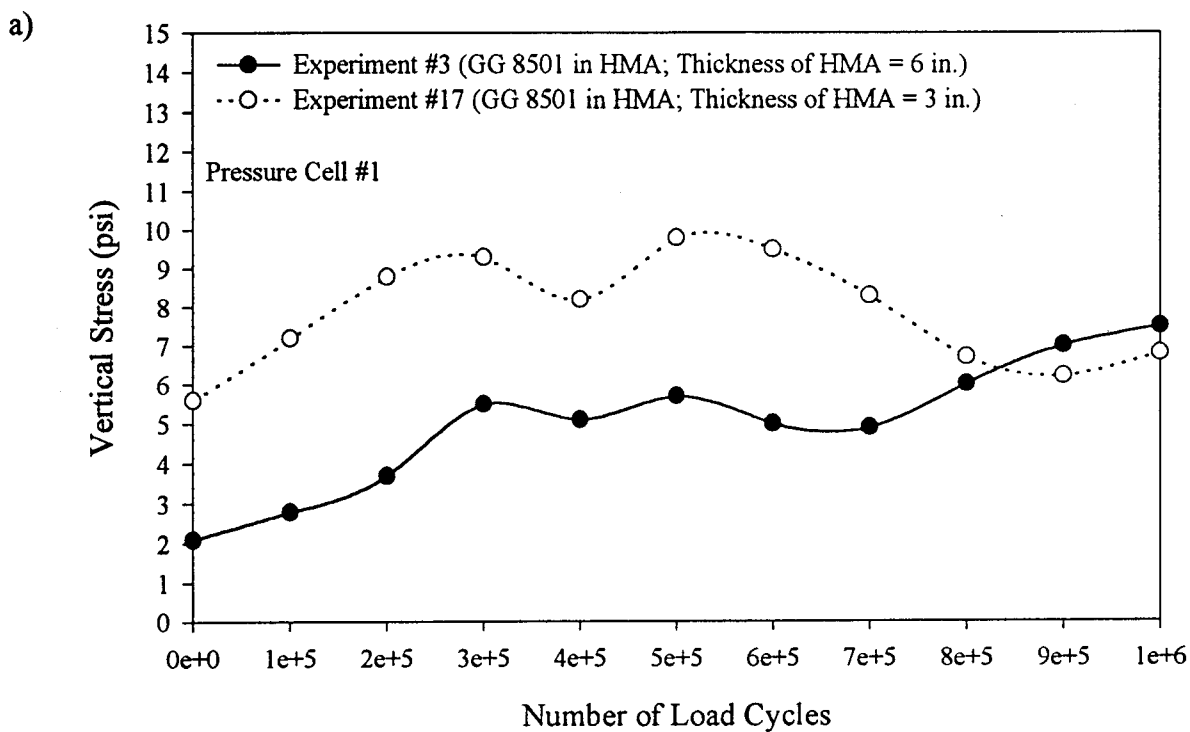


Figure 4-6: Influence of Asphalt Thickness on Vertical Subgrade Stress in Reinforced Test Sections

a) Stress at Cell #1

b) Stress at Cell #2

Table 4-6: Measured Vertical Subgrade Stress at Cells #1 and #2 for Experiments #4, #17, and #20

	Thick. of HMA (in.) [mm] ↓	Vertical Subgrade Stress (psi) [kN/m ²] Cell #1			Vertical Subgrade Stress (psi) [kN/m ²] Cell #2		
		Number of Load Cycles			Number of Load Cycles		
		0	500,000	1,000,000	0	500,000	1,000,000
Experiment #4 (No Reinforcement)	6 [152]	5.21 [35.90]	4.95 [34.11]	5.23 [36.03]	1.20 [8.27]	2.02 [13.92]	2.23 [15.36]
Experiment #17 (GG 8501)	3 [76]	5.60 [38.58]	9.80 [67.52]	6.80 [46.85]	2.47 [17.02]	1.98 [13.64]	1.88 [12.95]
Experiment #20 (GG 8501)	2.5 [63.5]	6.04 [41.62]	5.75 [39.62]	6.21 [42.79]	0.38 [2.62]	0.82 [5.65]	0.96 [6.61]

Table 4-7: Measured Vertical Subgrade Stress at Cells #1 and #2 for Experiments #3 and #17

	Thick. of HMA (in.) [mm] ↓	Vertical Subgrade Stress (psi) [kN/m ²] Cell #1			Vertical Subgrade Stress (psi) [kN/m ²] Cell #2		
		Number of Load Cycles			Number of Load Cycles		
		0	500,000	1,000,000	0	500,000	1,000,000
Experiment #3 (GG 8501)	6 [152]	2.10 [14.47]	5.70 [39.27]	7.50 [51.68]	1.58 [10.89]	2.08 [14.33]	2.37 [16.33]
Experiment #17 (GG 8501)	3 [76]	5.60 [38.58]	9.80 [67.52]	6.80 [46.85]	2.47 [17.02]	1.98 [13.64]	1.88 [12.95]

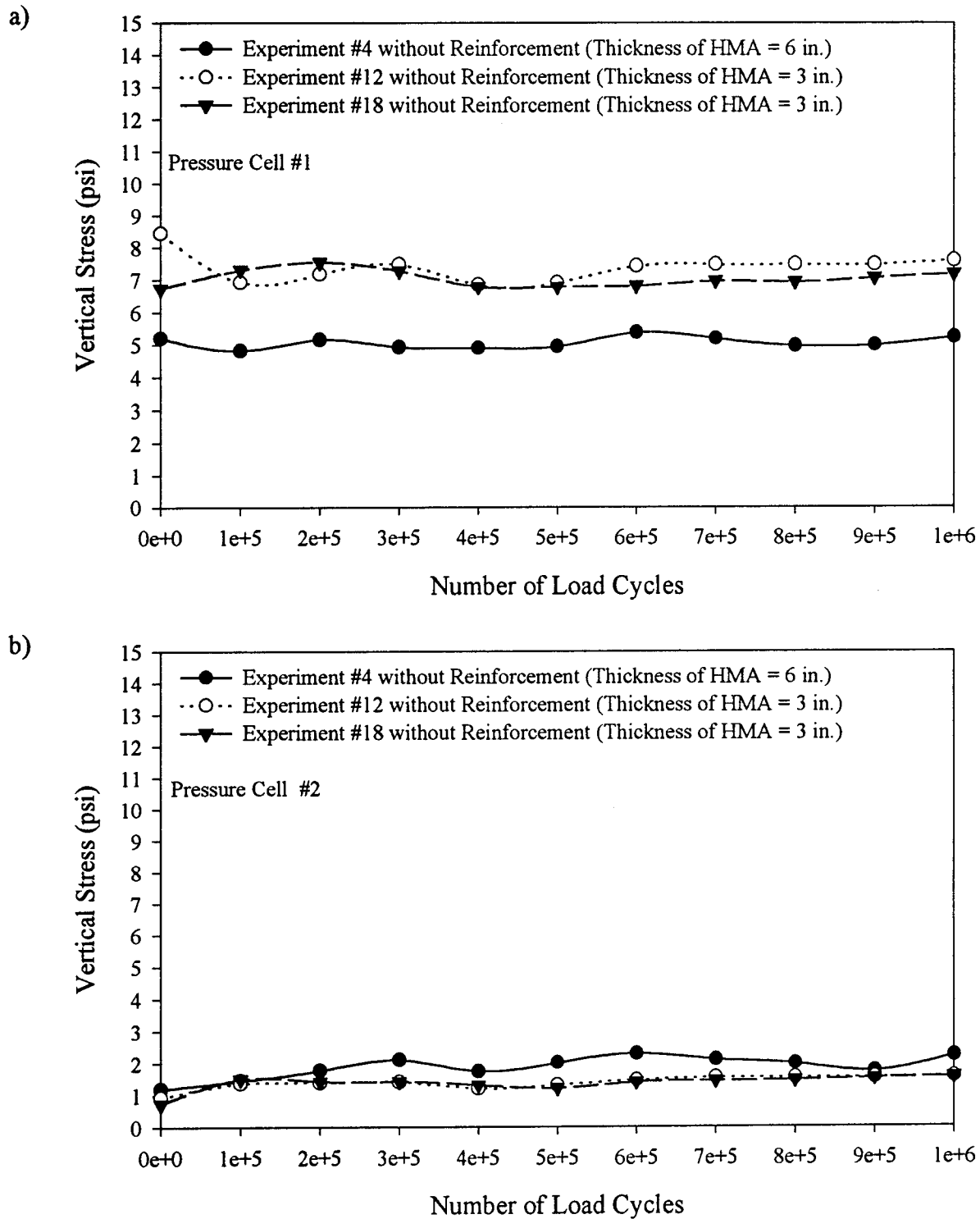


Figure 4-7: Influence of Asphalt Thickness on Vertical Subgrade Stress in Non-Reinforced Test Sections

a) Stress at Cell #1

b) Stress at Cell #2

Table 4-8: Measured Vertical Subgrade Stress at Cells #1 and #2 for Experiments #4, #12, and #18

	Thick. of HMA (in.) [mm] ↓	Vertical Subgrade Stress (psi) [kN/m ²] Cell #1			Vertical Subgrade Stress (psi) [kN/m ²] Cell #2		
		Number of Load Cycles			Number of Load Cycles		
		0	500,000	1,000,000	0	500,000	1,000,000
Experiment #4 (No Reinforcement)	6 [152]	5.21 [35.90]	4.95 [34.11]	5.23 [36.03]	1.20 [8.27]	2.02 [13.92]	2.23 [15.36]
Experiment #12 (No Reinforcement)	3 [76]	8.46 [58.29]	6.92 [47.68]	7.60 [52.36]	0.93 [6.41]	1.31 [9.03]	1.57 [10.82]
Experiment #18 (No Reinforcement)	3 [76]	6.75 [46.51]	6.80 [46.85]	7.19 [49.54]	0.74 [5.10]	1.22 [8.41]	1.57 [10.82]

approximately 27 % to 29% at 500,000 load cycles [Figure 4-7 (a)]. The reduction in vertical subgrade stress was approximately 27% to 31% at 1,000,000 load cycles.

Vertical stress at cell #2 for thicker asphalt section (Experiment #4) was higher than the stress for thin asphalt sections (Experiments #12 and #18) as shown in Figure 4-7 (b). However, the stresses were too low to have any significant impact on the subgrade.

4.1.7 Influence Of A Simulated Crack On Vertical Subgrade Stress In A Non-Reinforced Pavement Section

The influence of the simulated crack on vertical subgrade stress in non-reinforced HMA cases is shown in Figures 4-8 (a) and (b), and Table 4-9. The vertical subgrade stress at cell #1 for Experiment #18 was steady throughout the experiment and the maximum variation (between the maximum and minimum stresses) for vertical subgrade stress of Experiment #18 was 0.81 psi (5.51 kN/m²) (Table 4-1). The vertical subgrade stress for Experiment #18 was 6.75 psi (46.51 kN/m²) at the beginning of the experiment, 6.8 psi (46.85 kN/m²) at 500,000 load cycles and 7.19 psi (49.54 kN/m²) at 1,000,000 load cycles (Table 4-9). Unlike in Experiment #18, there was some fluctuation observed in Experiment #19. Initially, the vertical stress was 9 psi (62.01 kN/m²) and decreased to 5.9 psi (40.65 kN/m²) at 100,000 load cycles. From 100,000 load cycles to 400,000 load cycles, the stress for Experiment #19 was lower than the stress for Experiment #18. At 500,000 load cycles, the stress for Experiment #19 increased to 7.0 psi (48.23 kN/m²) and continued to increase to 9 psi (62.01 kN/m²) at 1,000,000 load cycles. After 500,000 load cycles, the stress for Experiment #19 was higher than the stress for Experiment #18. Reduction in vertical subgrade stress at cell #1 for Experiment #18 was approximately 2.9% at 500,000 load cycles and 20% at 1,000,000 load cycles in comparison to Experiment #19.

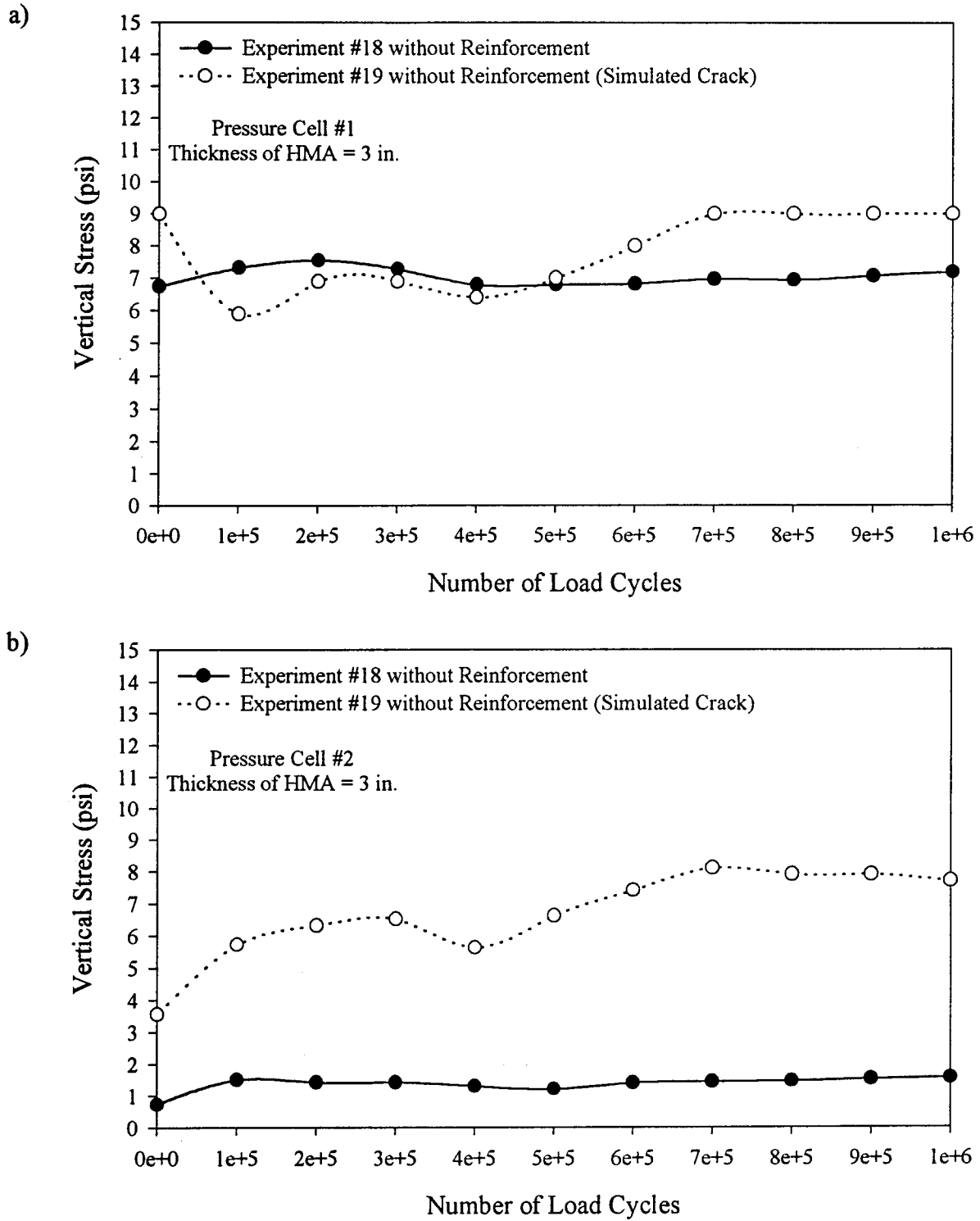


Figure 4-8: Influence of Simulated Crack on Vertical Subgrade Stress in a Pavement Section without Reinforcement
a) Stress at Cell #1
b) Stress at Cell #2

Table 4-9: Measured Vertical Subgrade Stress at Cells #1 and #2 for Experiments #18 and #19

	Thick. of HMA (in.) [mm] ↓	Vertical Subgrade Stress (psi) [kN/m ²] Cell #1			Vertical Subgrade Stress (psi) [kN/m ²] Cell #2		
		Number of Load Cycles			Number of Load Cycles		
		0	500,000	1,000,000	0	500,000	1,000,000
Experiment #18 (No Reinforcement)	3 [76]	6.75 [46.51]	6.80 [46.85]	7.19 [49.54]	0.74 [5.10]	1.22 [8.41]	1.57 [10.82]
Experiment #19 (No Reinforcement) (Simulated Crack)	3 [76]	9.00 [62.01]	7.00 [48.23]	9.00 [62.01]	3.56 [24.53]	6.63 [45.68]	7.71 [53.12]

These reductions were significantly large for the vertical subgrade stresses at cell #2. The reduction was approximately 82% at 500,000 load cycles and 80% at 1,000,000 load cycles. While the vertical subgrade stress at cell #2 for Experiment #18 was steady and ranged from 0.74 psi (5.10 kN/m²) to 1.57 psi (10.82 kN/m²), the vertical stress for Experiment #19 fluctuated and increased substantially from 3.56 psi (25.15 kN/m²) at 0 cycle to 7.71 psi (53.12 kN/m²) at 1,000,000 cycles. Before conducting Experiments #19 and #20, the pressure cells were removed for calibration. It is not certain if removal and reinstallation for calibration is the cause for higher stresses at cell #2 in Experiment #19.

Based on these results, the vertical subgrade stress at cell #1 for the test section with the simulated crack (Experiment #19) fluctuated throughout the experiment and increased as shown in Figure 4-8 (a). For the test section without the simulated crack (Experiment #18), stress at cell #1 was almost constant. This behavior was even more evident at cell #2, where the stress for the test section with the simulated crack (Experiment #19) was much higher than the stress corresponding to the case without simulated crack (Experiment #18) [Figure 4-8 (b)].

4.1.8 Influence Of Reinforcement On Vertical Subgrade Stress In A Pavement Section With A Simulated Crack

Figures 4-9 (a) and (b), and Table 4-10 show the comparison of vertical subgrade stresses corresponding to reinforced (Experiment #14) and non-reinforced thin asphalt sections (Experiments #13 & 16) with simulated cracks. The Experiment #13 is a duplicate of Experiment #16. The vertical subgrade stress at cell #1 for Experiment #14 was 3.6 psi (24.80 kN/m²) initially and increased to 8.10 psi (55.81 kN/m²) at 1,000,000 load cycles. The stress for Experiment #14 was lower than the stress for Experiment #16 until 900,000 load cycles. Also, the vertical stress for Experiment #14 was

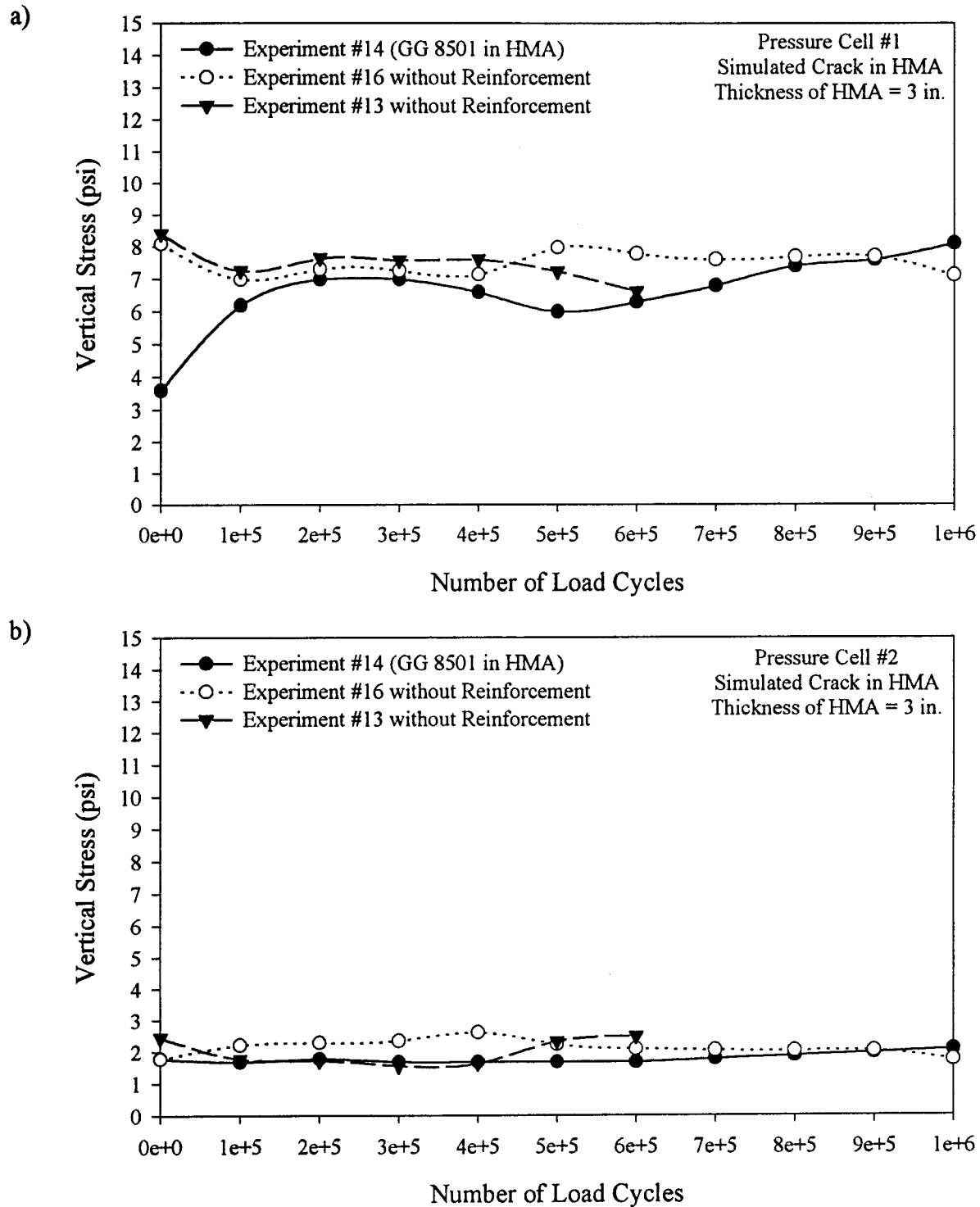


Figure 4-9: Influence of Reinforcement on Vertical Subgrade Stress in a Pavement Section with a Simulated Crack
a) Stress at Cell #1
b) Stress at Cell #2

Table 4-10: Measured Vertical Subgrade Stress at Cells #1 and #2 for Experiments #13, #14, and #16

	Thick. of HMA (in.) [mm] ↓	Vertical Subgrade Stress (psi) [kN/m ²] Cell #1 Note: N/A - Not Available			Vertical Subgrade Stress (psi) [kN/m ²] Cell #2		
		Number of Load Cycles			Number of Load Cycles		
		0	500,000	1,000,000	0	500,000	1,000,000
Experiment #13 (No Reinforcement) Simulated Crack	3 [76]	8.41 [57.94]	7.24 [49.88]	N/A	2.45 [16.88]	2.33 [16.05]	N/A
Experiment #14 (GG 8501) Simulated Crack	3 [76]	3.60 [24.80]	6.00 [41.34]	8.10 [55.81]	1.78 [12.26]	1.68 [11.58]	2.08 [14.33]
Experiment #16 (No Reinforcement) Simulated Crack	3 [76]	8.09 [55.74]	7.97 [54.91]	7.11 [48.99]	1.77 [12.20]	2.23 [15.36]	1.75 [12.06]

lower than the stress for Experiment #13 until 600,000 load cycles. It is important to note that the pavement section failed around 300,000 load cycles in Experiment #13. The vertical stress for Experiment #16 was 8.09 psi (55.74 kN/m²) initially and decreased to 6.99 psi (48.16 kN/m²) at 100,000 load cycles. The stress increased gradually to 7.11 psi (48.99 kN/m²) at 1,000,000 load cycles. At 500,000 load cycles, improvement in vertical subgrade stress at cell #1 for the reinforced thin pavement section with the simulated crack (Experiment #14) ranged from approximately 17% to 25% in comparison to non-reinforced thin pavement sections with a simulated crack (Experiments #13 and #16). This improvement was also evident for the vertical subgrade stress at cell #2. Reduction in vertical subgrade stress under the same conditions ranged from approximately 25% to 28%.

Based on these results, it can be stated that stresses at cell #1 and cell #2 were lower for the reinforced case (Experiment #14) than the stresses for the non-reinforced cases (Experiments #13 and #16). The test section without glass grid reinforcement and with the simulated crack (Experiment #13) failed after 600,000 load cycles [Figures 4-9 (a) and (b)]. Additionally, the pavement section in Experiment #16 can be considered to have failed since it was visually observed that the simulated crack deformed and was filled with HMA.

4.1.9 Comparison Of A Non-Reinforced 6 Inches (152 mm) Thick Asphalt Section With A Reinforced Thinner Asphalt Section With A Simulated Crack

A comparison of the non-reinforced 6-inch (152 mm) thick asphalt section (Experiment #4) with the reinforced thinner asphalt sections [thickness of HMA = 3 inches (76 mm)] with the simulated crack (Experiment #14 and #15) is shown in Figures 4-10 (a) and (b), and Table 4-11. The Experiment #15 is a duplicate of Experiment #14. The vertical subgrade stress at cell #1 for

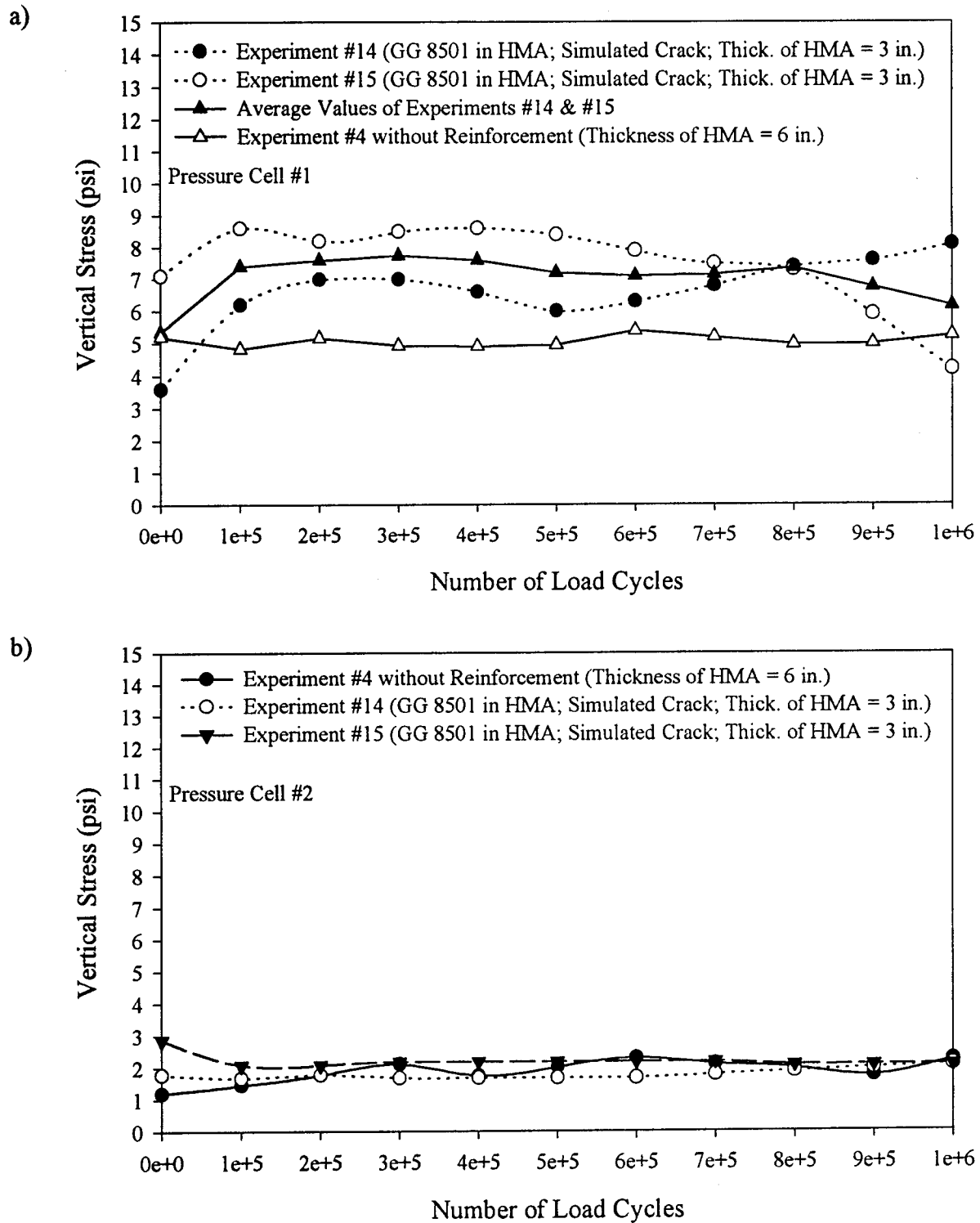


Figure 4-10: Comparison of a Non-Reinforced 6-inch (152 mm) Thick Asphalt Section with a Reinforced Thinner Asphalt Section with a Simulated Crack
a) Stress at Cell #1
b) Stress at Cell #2

Table 4-11: Measured Vertical Subgrade Stress at Cells #1 and #2 for Experiments #4, #14, and #15

	Thick. of HMA (in.) [mm] ↓	Vertical Subgrade Stress (psi) [kN/m ²] Cell #1			Vertical Subgrade Stress (psi) [kN/m ²] Cell #2		
		Number of Load Cycles			Number of Load Cycles		
		0	500,000	1,000,000	0	500,000	1,000,000
Experiment #4 (No Reinforcement)	6 [152]	5.21 [35.90]	4.95 [34.11]	5.23 [36.03]	1.20 [8.27]	2.02 [13.92]	2.23 [15.36]
Experiment #14 (GG 8501) Simulated Crack	3 [76]	3.60 [24.80]	6.00 [41.34]	8.10 [55.81]	1.78 [12.26]	1.68 [11.58]	2.08 [14.33]
Experiment #15 (GG 8501) Simulated Crack	3 [76]	7.10 [48.92]	8.40 [57.88]	4.20 [28.94]	2.87 [19.77]	2.18 [15.02]	2.08 [14.33]

Experiment #4 was steady as previously described in Section 4.1.3. For Experiment #4, the stress was 5.21 psi (35.90 kN/m²) at the beginning, and at the end of the experiment the stress was 5.23 psi (36.03 kN/m²). The vertical subgrade stress for Experiment #14 increased from 3.6 psi (24.80 kN/m²) at the beginning to 8.1 psi (55.81 kN/m²) at 1,000,000 load cycles. For the most part, the stress for Experiment #14 was higher than the stress for Experiment #4 throughout the experiment. The vertical stress for Experiment #15 was 7.1 psi (48.92 kN/m²) at the beginning of the experiment and 7.4 psi (50.99 kN/m²) at 800,000 load cycles. Then, the stress decreased from 7.4 psi (50.99 kN/m²) to 4.2 psi (28.94 kN/m²) at 1,000,000 load cycles.

Based on the results shown in Figure 4-10 (a), at 1,000,000 load cycles approximately 15% reduction in vertical subgrade stress at cell #1 for non-reinforced thick pavement section (Experiment #4) was possible in comparison to the average vertical stress of the reinforced thin pavement sections (Experiments #14 and #15) with a simulated crack. However, it is noteworthy that the non-reinforced 6-inch (152 mm) thick asphalt section (Experiment #4) failed based on displacement as explained in Section 4.2.3. The reinforced pavement sections with the simulated cracks (Experiments #14 and #15) did not result in failure.

The average of the stress for Experiments #14 and #15 is shown in Figure 4-10 (a). It is clear that the average vertical subgrade stress for the case with a simulated crack in a reinforced section is higher than the stress in a 6-inch (152 mm) thick non-reinforced pavement. Earlier in Section 4.1.5, it was shown that a reinforced thinner section behaves similar to that of a non-reinforced thicker section. Therefore, the difference in the behavior can be attributed to the simulated crack.

A similar comparison is shown for the vertical stress at cell #2 in Figure 4-10 (b), where the stresses in each case were comparable and followed the same trend. At 1,000,000 cycles, the vertical

subgrade stresses [2.08 psi (14.33 kN/m²)] for reinforced thin pavement sections with simulated cracks (Experiments #14 and #15) were slightly smaller than the stresses [2.23 psi (15.36 kN/m²)] for the non-reinforced thick pavement section (Experiment #4).

4.1.10 Influence Of A Simulated Crack And Reinforcement On Vertical Subgrade Stress

Figures 4-11 (a) and (b), and Table 4-12 show a comparison of vertical stresses corresponding to a reinforced case with a crack (Experiments #14 and #15) and stresses corresponding to a non-reinforced case (Experiments #12 and #18). The thickness of HMA layer was kept at 3 inches (76 mm). The vertical stresses for Experiments #14 and #15 were explained previously and presented in Section 4.1.9 in Figure 4-10 and Table 4-11. The vertical subgrade stresses for Experiments #12 and #18 were explained previously as well and presented in Section 4.1.6 in Figure 4-7 and Table 4-8. Based on these results, vertical stresses at cell #1 for the non-reinforced cases were steady and behaved in a similar manner [Figure 4-11 (a)]. Vertical subgrade stresses on both reinforced test sections with the simulated cracks (Experiments #14 and #15) behaved in a different manner. The subgrade stress for Experiment #15 [Figure 4-11 (a)] was higher than other sections for up to 600,000 cycles. After 600,000 cycles, the stresses decreased substantially. For Experiment #14, the stress was lowest up to 700,000 cycles and increased slightly [Figure 4-11 (a)]. These two behaviors of vertical subgrade stress for two different pavement sections were promising in terms of glass grid reinforcement of pavement sections.

The average stresses for Experiments #14 and #15 and for Experiments #12 and #18 are shown in Figure 4-11 (b). It is clear that the average vertical subgrade stress for the case with a simulated crack (Experiments #14 and #15) in a reinforced section is similar to that of the non-reinforced case without a simulated crack (Experiments #12 and #18). Therefore, it can be stated that

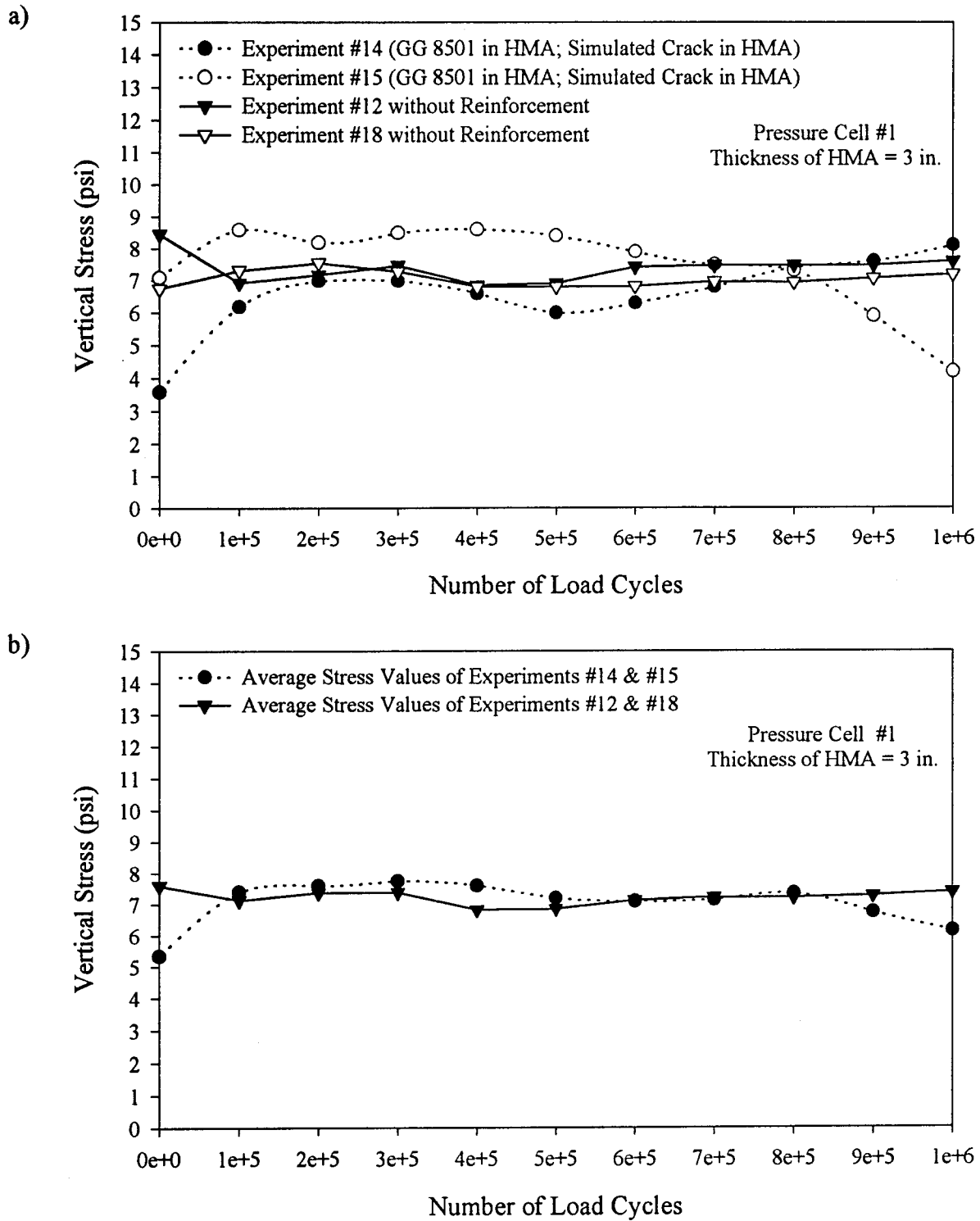


Figure 4-11: Comparison of a Non-Reinforced 3-inch (76 mm) Thick Asphalt Section with a Reinforced Asphalt Section with a Simulated Crack
a) Stress at Cell #1
b) Average Stress at Cell #1

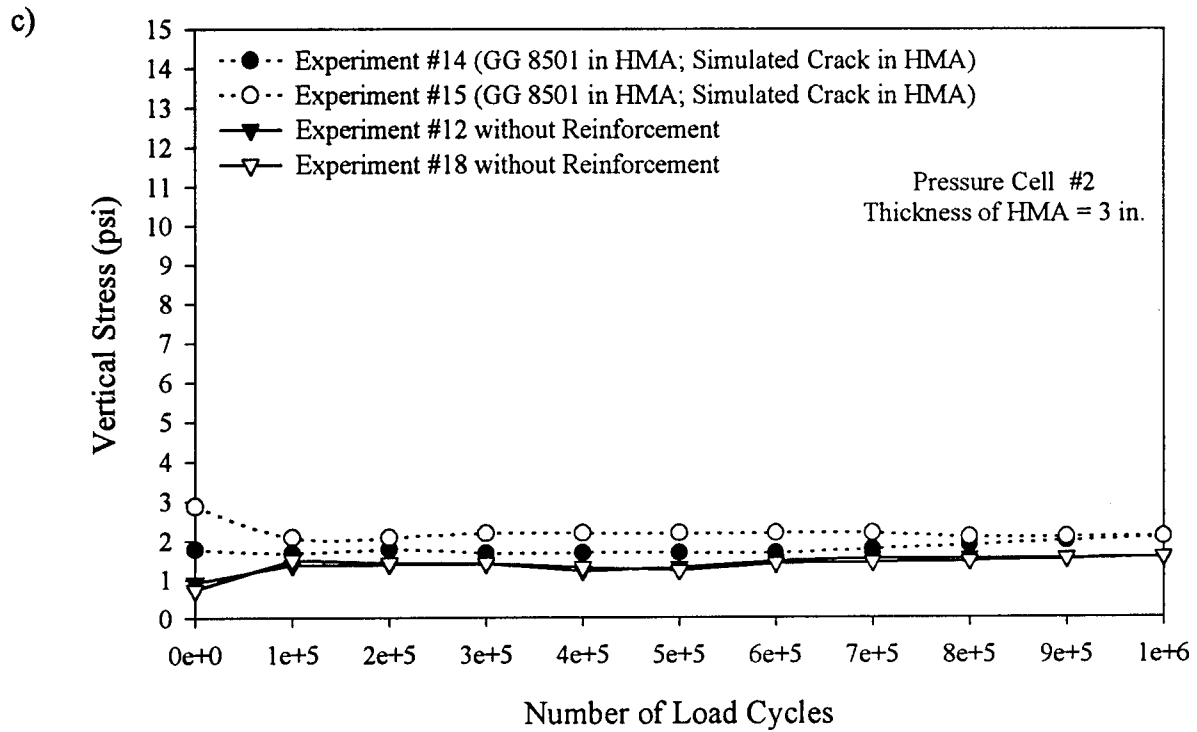


Figure 4-11 (Continued): Comparison of a Non-Reinforced 3-inch (76 mm) Thick Asphalt Section with a Reinforced Asphalt Section with a Simulated Crack
c) Stress at Cell #2

Table 4-12: Measured Vertical Subgrade Stress at Cells #1 and #2 for Experiments #12, #14, #15, and #18

	Thick. of HMA (in.) [mm] ↓	Vertical Subgrade Stress (psi) [kN/m ²] Cell #1			Vertical Subgrade Stress (psi) [kN/m ²] Cell #2		
		Number of Load Cycles			Number of Load Cycles		
		0	500,000	1,000,000	0	500,000	1,000,000
Experiment #12 (No Reinforcement)	3 [76]	8.46 [58.29]	6.92 [47.68]	7.60 [52.36]	0.93 [6.41]	1.31 [9.03]	1.57 [10.82]
Experiment #14 (GG 8501) (Simulated Crack)	3 [76]	3.60 [24.80]	6.00 [41.34]	8.10 [55.81]	1.78 [12.26]	1.68 [11.58]	2.08 [14.33]
Experiment #15 (GG 8501) (Simulated Crack)	3 [76]	7.10 [48.92]	8.40 [57.88]	4.20 [28.94]	2.87 [19.77]	2.18 [15.02]	2.08 [14.33]
Experiment #18 (No Reinforcement)	3 [76]	6.75 [46.51]	6.80 [46.85]	7.19 [49.54]	0.74 [5.10]	1.22 [8.41]	1.57 [10.82]

the increase in vertical subgrade stress caused by a simulated crack is offset by the decrease in vertical subgrade stress due to the reinforcement of the pavement section.

Effects of simulated cracks are also shown in Figure 4-11 (c). Stresses for reinforced cases with simulated cracks were higher than the stresses for non-reinforced test sections without simulated cracks although the stresses were low and the differences insignificant.

4.1.11 Summary Of Laboratory Results On Vertical Subgrade Stress

Based on the results presented above, the following conclusions can be made for the vertical subgrade stress in the pavement section:

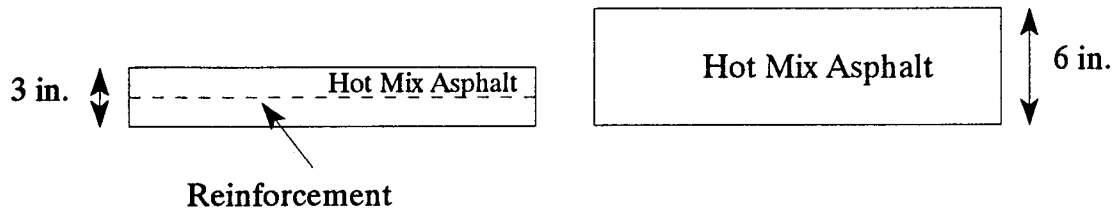
- The influence of different glass grid reinforcements on vertical subgrade stress was not significant when the thickness of asphalt base was 6 inches (152 mm) [See Section 4.1.1].
- Observations on doubly reinforced cases indicated that the vertical stress in the subgrade was lower in pavement sections with stronger glass grids [See Section 4.1.2].
- Observations on 6-inch (152 mm) thick asphalt sections indicated that at 1,000,000 load cycles, the reduction in vertical subgrade stress for the doubly reinforced case (Experiment #8) was approximately 46% in comparison to the non-reinforced pavement section (Experiment #4). The vertical subgrade stress at cell #1 for the singly reinforced case (Experiment #5) was approximately 29% smaller at 500,000 load cycles than that of the non-reinforced pavement section (Experiment #4). These results show that the glass grid reinforcement seems to spread the load over a larger area in the lower layers causing lower subgrade stresses [See Section 4.1.3].
- A 6-inch (152 mm) thick non-reinforced hot mix asphalt layer led to slightly lower subgrade stresses in comparison to a thinner reinforced pavement section. It can be stated that a

reinforced thinner section [thickness of HMA = 3 inches (76 mm)] behaved similar to that of a non-reinforced thicker pavement section [thickness of HMA = 6 inches (152 mm)].

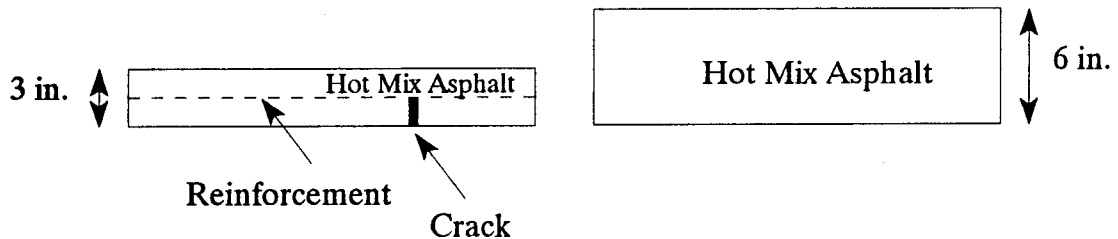
- When the thickness of the HMA was increased from 3 inches (76 mm) to 6 inches (152 mm), the improvement of the vertical stress at cell #1 ranged from approximately 27 % to 29% at 500,000 load cycles. This reduction in vertical subgrade stress was approximately 27% to 31% at 1,000,000 cycles. The influence of thickness on vertical subgrade stress is clear: the higher the thickness of the asphalt layer, the lower the vertical subgrade stress [See Section 4.1.6].
- Influence of reinforcement on vertical subgrade stress in a pavement section with a simulated crack was investigated. At 500,000 cycles, improvement in vertical subgrade stress at cell #1 for the reinforced thin pavement section with the simulated crack (Experiment #14) ranged from approximately 17% to 25% in comparison to non-reinforced thin pavement sections with a simulated crack (Experiments #13 and #16) [See Section 4.1.8].
- Observations on thin asphalt sections [thickness of HMA = 2.5 in. (63.5 mm) and 3 in. (76 mm)] indicated that the vertical stress for the reinforced cases without the simulated crack (Experiments #11 and #20) was lower than the vertical stress for the reinforced case with the simulated crack (Experiment #14). This behavior indicates that the vertical stress was influenced by the presence of a simulated crack [See Section 4.1.4].
- The test section without grid reinforcement and with the simulated crack (Experiment #13) failed after 600,000 cycles. Additionally, Experiment #16 was considered to have failed since the simulated crack was deformed and filled with HMA.
- It was shown that a reinforced thinner section behaves similar to that of a non-reinforced

thicker section. [Figure 4-12 (a)]. It is also clear that the average vertical subgrade stress for the case [thickness of HMA = 3 inches (76 mm)] with a simulated crack in a reinforced section is higher than the stress in a 6-inch (152 mm) thick non-reinforced pavement [Figure 4-12 (b)]. Therefore, the difference in the behavior can be attributed to the simulated crack [See Section 4.1.9].

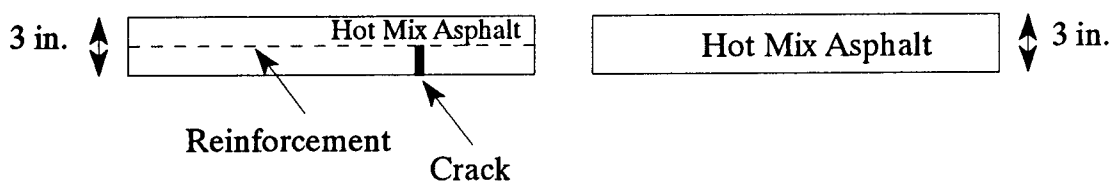
- The average vertical subgrade stress for the case with a simulated crack (Experiments #14 and #15) in a reinforced section is similar to that of the non-reinforced section without a crack (Experiments #12 and #18) where the thickness of the HMA was kept at 3 inches (76 mm). It can be stated that the increase in vertical subgrade stress caused by a simulated crack is offset by the decrease in vertical subgrade stress due to the reinforcement of the pavement section [See Section 4.1.10 and Figure 4-12 (c)].
- Based on vertical subgrade stresses at cells #1 and #2 [Figure 3-1 (a)], the influence of glass grid reinforcement was more apparent at cell #1 than at cell #2.



- a) Reinforced 3 in. (76 mm) thick HMA Layer versus Non-Reinforced 6 in. (152 mm) thick HMA Layer



- b) Reinforced 3 in. (76 mm) thick HMA Layer with a Simulated Crack versus Non-Reinforced 6 in. (152 mm) thick HMA Layer



- c) Reinforced 3 in. (76 mm) thick HMA Layer with a Simulated Crack versus Non-Reinforced 3 in. (76 mm) thick HMA Layer

Figure 4-12: Comparison of Experimental Parameters of the HMA Layer for Vertical Subgrade Stress

4.2 CUMULATIVE DISPLACEMENTS

In every experiment conducted in this study (Table 4-13), cumulative displacements on the HMA surface were measured to evaluate the structural performance and compare the differences between the reinforced and non-reinforced flexible pavement sections. The influence of the asphalt layer thickness was investigated by evaluating thicknesses of 2.5 inches (63.5 mm), 3 inches (76 mm) and 6 inches (152 mm). The influence of the glass grids was investigated by including the reinforcement in the middle of the hot mix asphalt layer for thirteen experiments. In three experiments an additional reinforcement layer at the gravel base/hot mix asphalt interface (in addition to the reinforcement in the hot mix asphalt) was included. Cumulative displacements at the edge of the loading plate corresponding to 1,000,000 load cycles were evaluated and the results at 500,000 and 1,000,000 load cycles are presented in Table 4-13.

4.2.1 Influence Of Different Glass Grids On Cumulative Displacement

As shown in Figure 4-13, the influence of three different glass grids on pavement sections was compared with respect to cumulative displacement. The asphalt thickness of each case was 6 inches (152 mm). It was observed that the lowest cumulative displacement at the edge of the loading area was obtained with the heaviest glass grid (GG 8511), and the cumulative displacements increased with reductions in grid weight [Figure 4-13]. The heaviest glass grid (GG 8511) in the pavement section showed a reduction of approximately 38% in cumulative displacement with respect to the lightest glass grid (GG 8501) in the pavement section. GG 8502 has a weight between those of GG 8501 and GG 8511. Between the two glass grids (GG 8501 and GG 8502), approximately 21% improvement on cumulative displacement was possible at 1,000,000 load cycles when the heavier glass grid (GG 8502) was used. The heaviest glass grid (GG 8511) showed an improvement of about

Table 4-13: Cumulative Displacements at the Edge of the Loading Plate Corresponding to 500,000 and 1,000,000 Load Cycles

Experiment #	Cumulative Displacement at the Edge of the Loading Plate (inches) [mm]	
	500,000 Load Cycles	1,000,000 Load Cycles
1	Not Available	Not Available
2	0.157 [3.988]	0.179 [4.547]
3	0.187 [4.750]	0.227 [5.766]
4	0.282 [7.163]	0.370 [9.398]
5	0.123 [3.124]	0.423 [10.744]
6	0.120 [3.048]	0.140 [3.556]
7	0.108 [2.743]	0.178 [4.521]
8	0.156 [3.962]	0.185 [4.699]
9	0.123 [3.124]	0.148 [3.759]
10	0.115 [2.921]	0.124 [3.150]
11	0.121 [3.073]	0.159 [4.039]
12	0.086 [2.184]	0.107 [2.718]
13	Not Available	Not Available
14	0.110 [2.794]	0.133 [3.378]
15	0.239 [6.071]	0.270 [6.858]
16	Not Available	Not Available
17	0.152 [3.861]	0.168 [4.267]
18	0.109 [2.769]	0.114 [2.896]
19	0.086 [2.184]	0.125 [3.175]
20	0.116 [2.946]	0.136 [3.454]

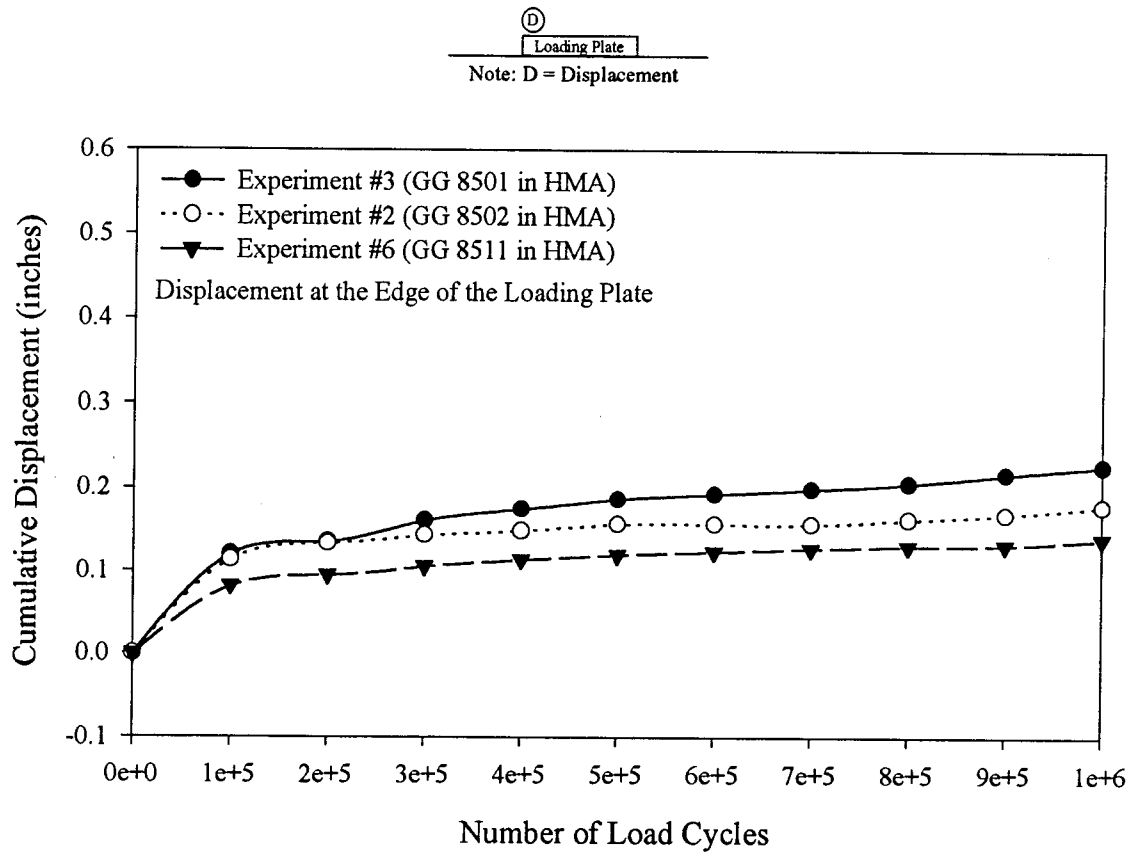


Figure 4-13: Influence of Different Glass Grids on Cumulative Displacements

22% in cumulative displacement with respect to GG 8502 at 1,000,000 load cycles. Based on the above results, it can be stated that a 21% to 38% improvement in cumulative displacement was possible when the weight of glass grid in the pavement section was increased.

4.2.2 Influence Of Glass Grids On Cumulative Displacement On Doubly-Reinforced Section

Similar comparisons were performed for the doubly glass grid reinforced cases [Figures 4-14 (a) and (b)]. For this purpose, the lightest and the heaviest glass grids (GG 8501 and GG 8511) were used in the HMA for doubly reinforced test sections. For three test sections (Experiments #8, #9, and #10), GG 8511 was used at the gravel base/hot mix asphalt interface. For one pavement section (Experiment #9), GG 8501 was used inside the HMA, while for two other pavement sections (Experiments #8 and #10), GG 8511 was used inside the HMA. One of the doubly reinforced test sections (Experiment #8) with heavy glass grids (GG 8511 and GG 8511) resulted in a slightly higher cumulative displacement than the remaining ones (Experiments #9 and #10). At 1,000,000 load cycles, the cumulative displacement in Experiment #10 was approximately 16% lower than that corresponding to Experiment #9 [Figure 4-14 (a)]. This slight improvement could be attributed to either (a) difference in compaction effort or (b) difference in weights of glass grids (GG 8501 and GG 8511).

The average values of cumulative displacements [Figure 4-14 (b)] for two pavement sections (Experiments #8 and #10) produce almost similar displacements when heavier glass grid was used in HMA layer in a doubly-reinforced test sections in place of the lighter grid [Figure 4-14 (b)]. The difference in cumulative displacement in doubly-reinforced test sections (between the average cumulative displacement of Experiments (#8 and #10) and Experiment #9) seems to be insignificant.

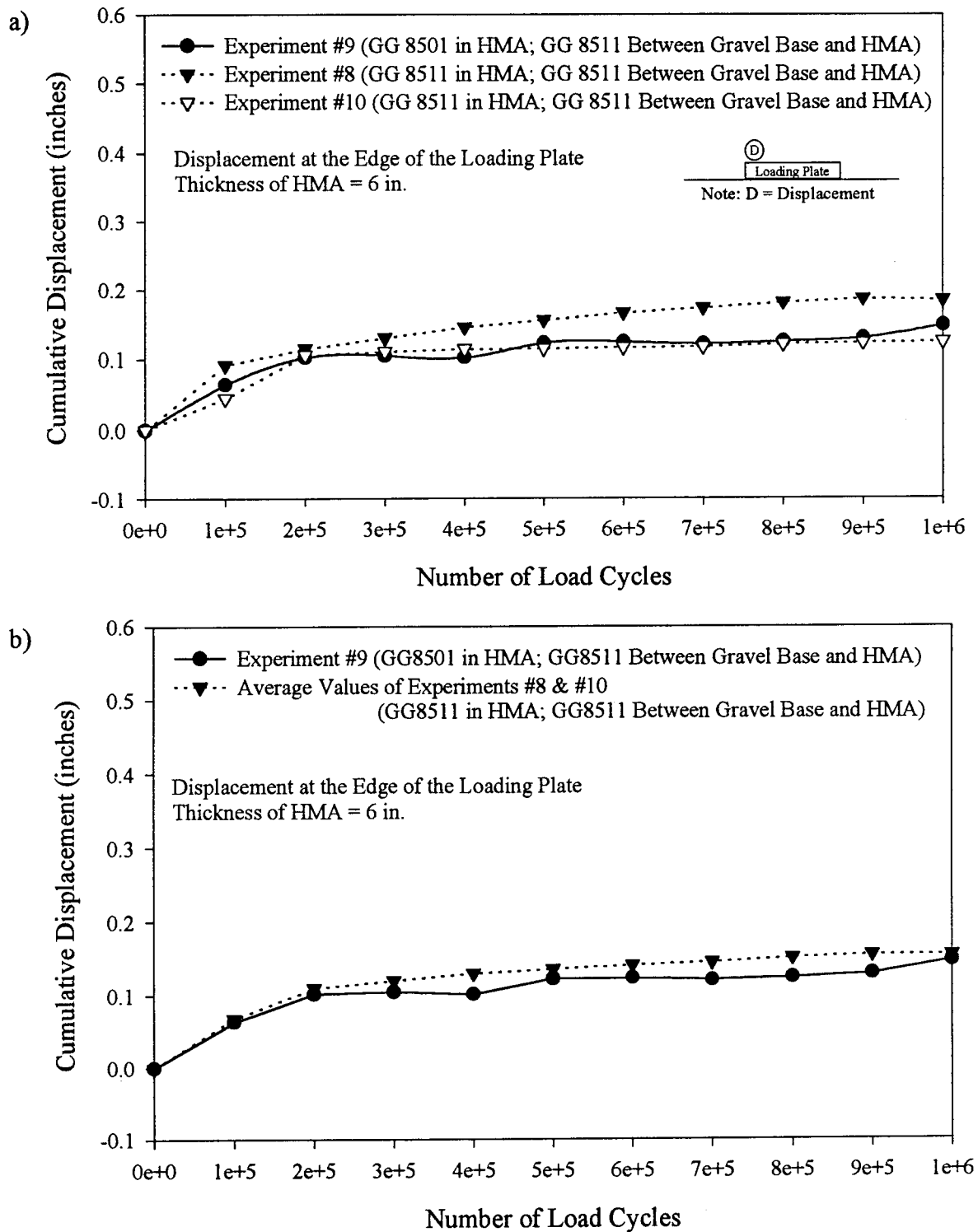


Figure 4-14: Influence of Different Glass Grids on Cumulative Displacements for Doubly Reinforced Test Sections
 a) Individual Displacements for Experiments #8, #9, and #10
 b) Individual Displacement for Experiment #9 and Average Cumulative Displacement of Experiments (#8 and #10)

The results show a general trend of improvement in pavement performance when a heavier glass grid is used as the reinforcement of the HMA layer. However, the improvement in performance in a doubly-reinforced section is not significant as the improvement observed in a singly reinforced case for the same weight of HMA reinforcement.

The difference in improvement (in performance) due to heavier glass grid reinforcement (GG 8511) is not significant in doubly-reinforced section. In other words, when the hot mix asphalt (HMA) thickness is 6 inches (152 mm) in a doubly-reinforced test section, both lighter weight (GG 8501) and heavier weight of reinforcement (GG 8511) in the hot mix asphalt (HMA) layer results in almost similar performance.

4.2.3 Influence Of Reinforcement On Cumulative Displacement [Thickness Of HMA = 6 Inches (152 mm)]

Figure 4-15 shows the comparison of reinforced and non-reinforced pavement sections with a 6-inch (152 mm) thick hot mix asphalt layer. It was found that the cumulative displacements in the reinforced sections were smaller than those of the section without reinforcement. An approximate 39% improvement in cumulative displacement with respect to the non-reinforced pavement section (Experiment #4) was possible when the single reinforcement (GG 8501) was included in the hot mix asphalt. The inclusion of any additional reinforcement layer (doubly reinforced) at the gravel base/hot mix asphalt interface (in addition to the reinforcement in the hot mix asphalt) improved the performance substantially (by approximately 60%) [Figure 4-15]. Additionally, in Experiment #4, the pavement section failed due to severe rutting. The measured cumulative surface displacement for this pavement section was less than 1 inch (25 mm); however, based on visual observations, the cumulative displacement at the edge on one side of the loading plate (where the dial gages were not

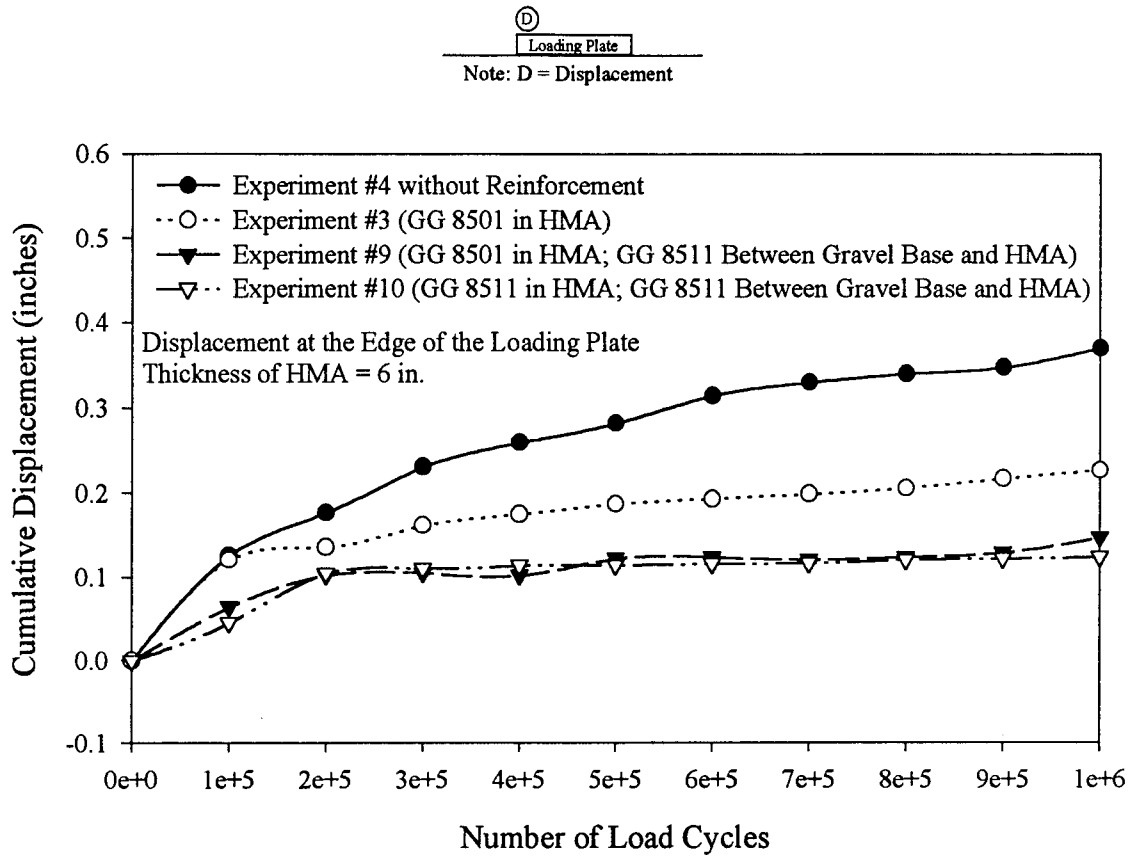


Figure 4-15: Influence of Reinforcement on Cumulative Displacement
[Thickness of HMA = 6 in. (152 mm)]

installed) was more than 1 inch (25 mm) and was considered to indicate failed.

The results show that when the HMA thickness is 6 inches (152 mm) in a test section, the improvement in performance indicated by cumulative displacements of a doubly reinforced section (about 60%) is higher than the improvement (about 40%) observed in the singly reinforced test section in comparison to a non-reinforced test section. This substantial decrease in cumulative displacement shows that an improvement could be gained by reinforcing the structural asphalt base in a pavement section.

4.2.4 Influence Of Reinforcement On Cumulative Displacement [Thickness Of HMA = 2.5 Inches (63.5 mm) And 3 Inches (76 mm)]

Similar comparison was made between the thin asphalt sections where the thicknesses of the HMA were 2.5 inches (63.5 mm) and 3 inches (76 mm) [Figure 4-16]. For thin asphalt sections, the cumulative displacements were very low. Improvements due to reinforced cases (Experiments #14 and #20) could not be seen in comparison to a non-reinforced case (Experiment #18). The differences between the non-reinforced (Experiment #18) and reinforced cases (Experiments #14 and #20) were very minor [approximately 0.02 inches (0.05 mm)] after 1,000,000 cycles. For another reinforced case (Experiment #17), the cumulative displacement was slightly higher than that of the case without the reinforcement (Experiment #18), although the difference was very small [0.054 inches (1.372 mm)]. For each case the incremental rate in cumulative displacement decreased with the number of load cycles. For thinner HMA layers, it appears that the influence of reinforcement is not significant. This could be due to the fact that the compaction effort plays a bigger role than the reinforcement.

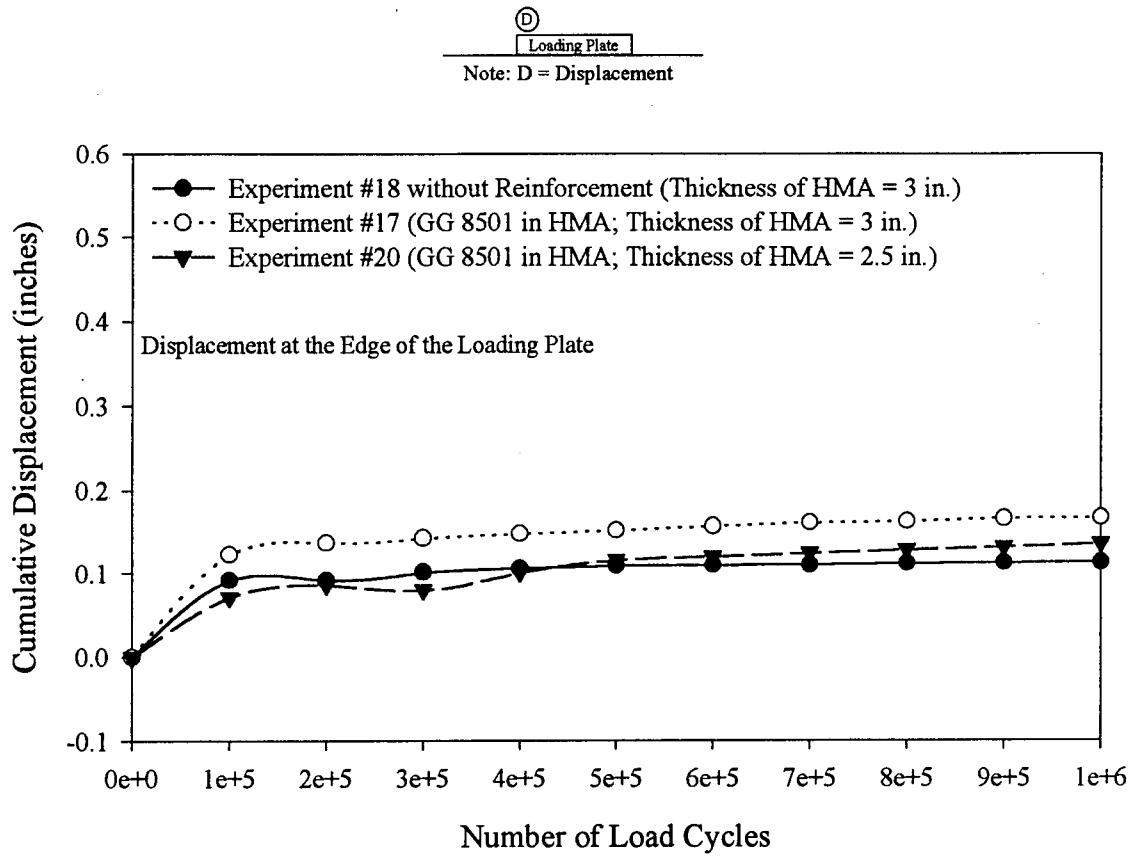


Figure 4-16: Influence of Reinforcement on Cumulative Displacement
[Thickness of HMA = 2.5 in. (63.5 mm) and 3 in. (76 mm)]

4.2.5 Comparison Of Non-Reinforced 6-Inch (152 mm) Thick Asphalt Section With Thinner Reinforced Asphalt Sections

Figure 4-17 shows a comparison of performance of a 6-inch (152 mm) thick non-reinforced pavement section (Experiment #4) with thinner reinforced pavement sections (Experiments #17 and 20). The cumulative displacement for the 6-inch (152 mm) thick non-reinforced pavement section (Experiment #4) was 0.370-inch (9.398 mm). The cumulative displacement for the 3-inch (76 mm) thick reinforced pavement section (Experiment #17) was 0.168-inch (4.267 mm), while the cumulative displacement for another reinforced pavement section (Experiment #20) with a 2.5 inches (63.5 mm) thick HMA was 0.136-inch (3.454 mm). These results indicate that a 6-inch (152 mm) thick hot mix asphalt does not improve the performance of the pavement system in comparison to 2.5-inch (63.5 mm) and 3-inch (76 mm) thick glass grid reinforced hot mix asphalt sections. In fact, reinforced thinner sections show better performance than the non-reinforced thicker section.

4.2.6 Influence Of Asphalt Thickness On Cumulative Displacement

Influence of asphalt thickness on cumulative displacement can be seen in Figures 4-18 and 4-19. Figure 4-18 shows the influence of thickness on cumulative displacements in reinforced cases (Experiments #3, #5, #11, and #17). Figure 4-19 is a similar graph for non-reinforced cases (Experiments #4, #12, and #18). Figures 4-18 and 4-19 show the cumulative displacements at locations #3 and #4 on the loading plate, respectively. The cumulative displacement data at displacement gauge #3, for Experiment #11, was not available due to a failure in the gauge [Figure 4-18 (a)]. Figures 4-18 (c) and 4-19 (c) show the average cumulative displacement beneath the loading plate. Results of the cumulative displacements at displacement gages #3 and #4 follow the same trend in both figures [Figures 4-18 (a and b) and 4-19 (a and b)]. Similar trends can also be seen

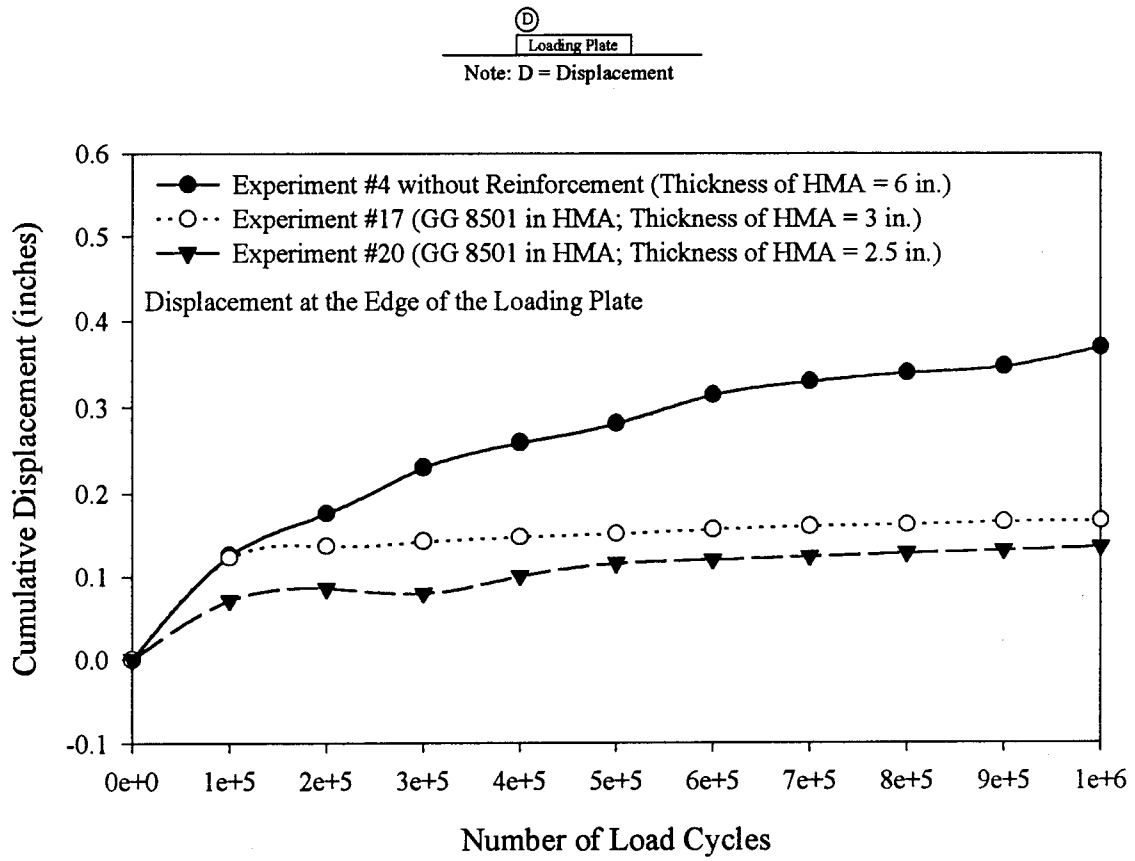
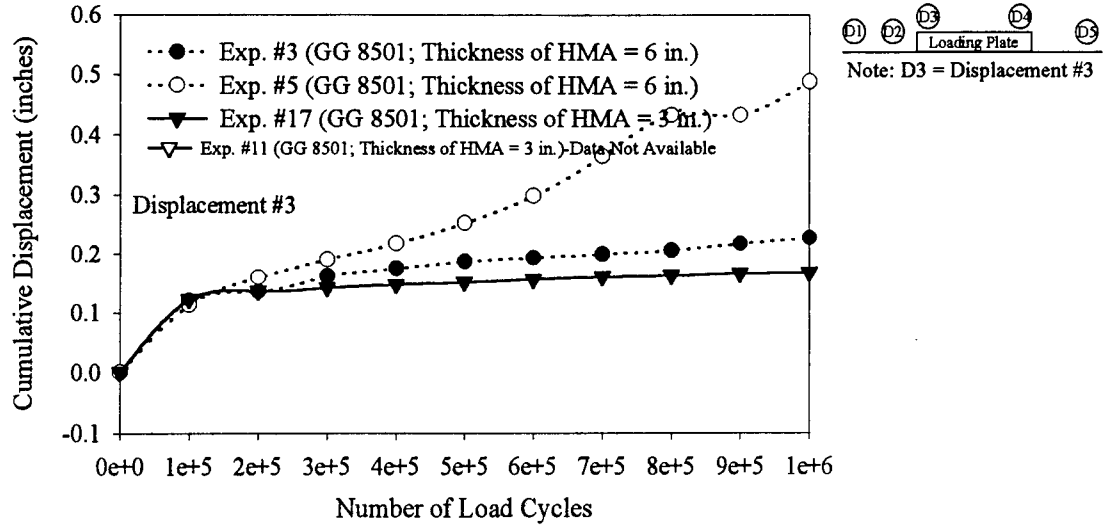
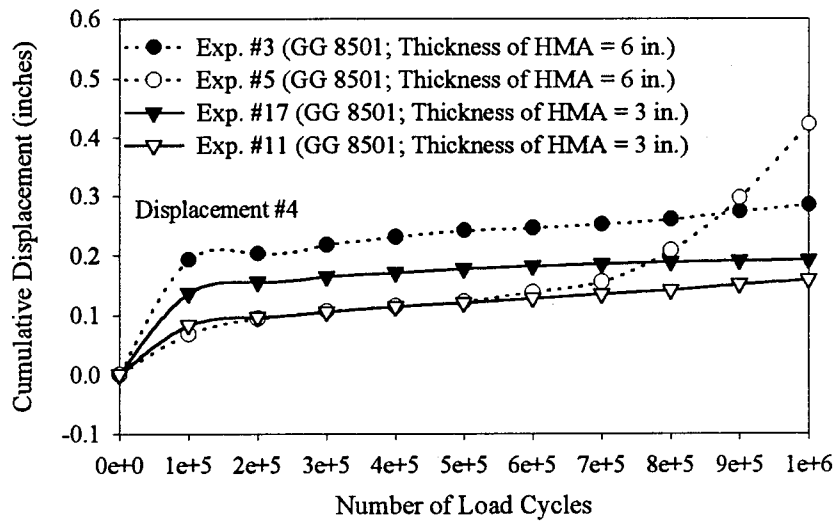


Figure 4-17: Comparison of Non-Reinforced 6-inch (152 mm) Thick Asphalt Section with Thinner Reinforced Asphalt Sections with Respect to Cumulative Displacements

a)



b)



c)

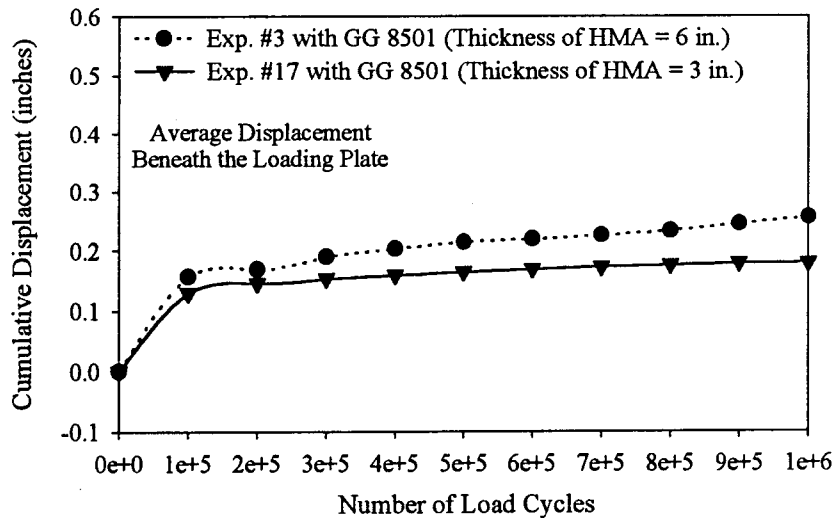


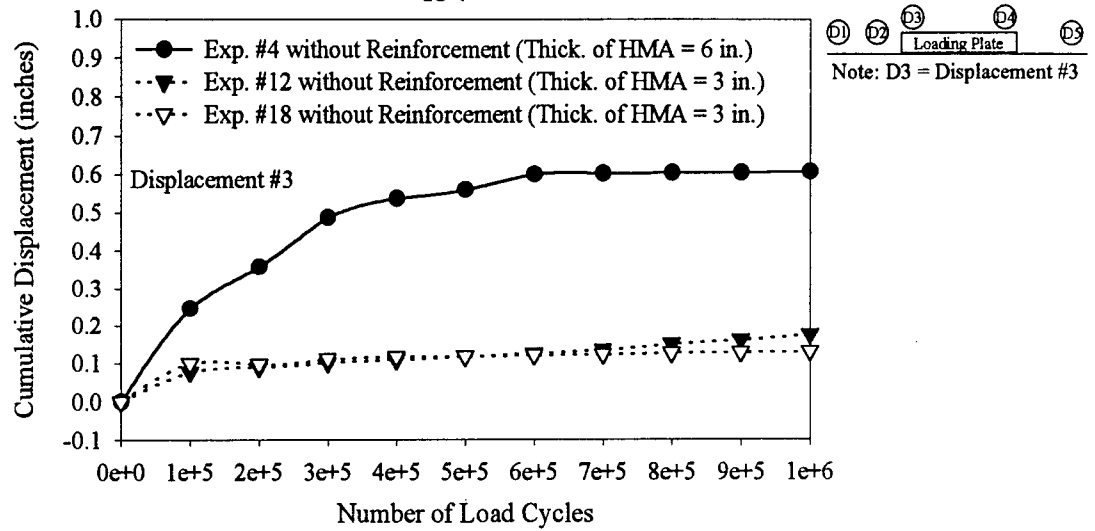
Figure 4-18: Influence of Asphalt Thickness on Cumulative Displacement in Reinforced Test Sections

a) Displacement #3

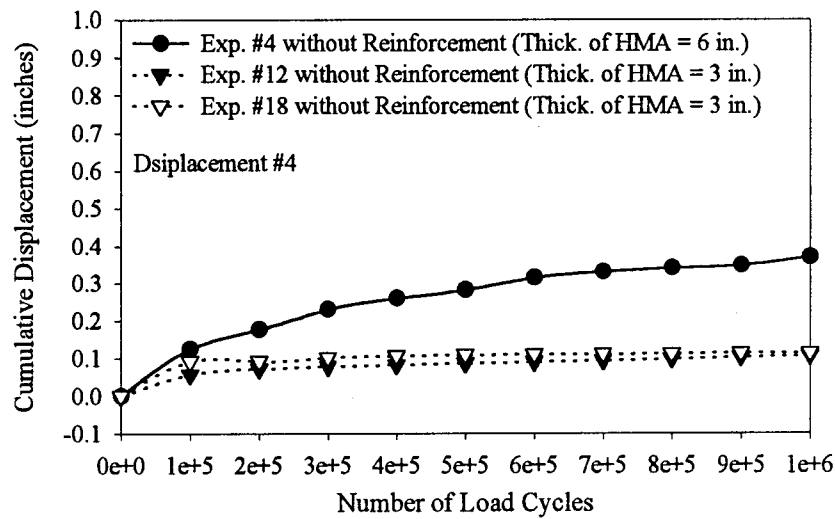
b) Displacement #4

c) Average Displacement

a)



b)



c)

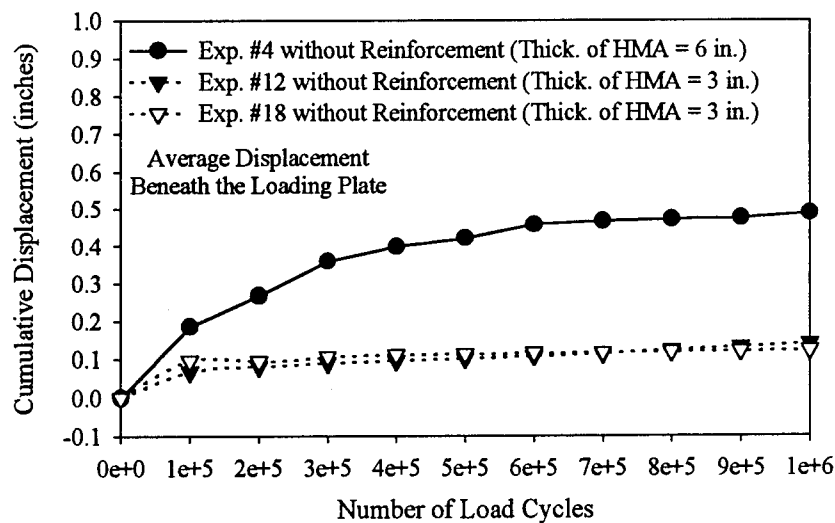


Figure 4-19: Influence of Asphalt Thickness on Cumulative Displacement in Non-Reinforced Test Sections

- a) Displacement #3
- b) Displacement #4
- c) Average Displacement

for the average cumulative displacement beneath the loading plate [Figures 4-18 (c) and 4-19 (c)]. As shown in Figure 4-18 (c), the thin reinforced pavement section (Experiment #17) showed approximately a 30% reduction in average cumulative displacement with respect to the thick reinforced pavement section (Experiment #3) at 1,000,000 load cycles. This reduction in cumulative displacement was approximately 23% at 500,000 load cycles. It should be noted that the pavement section in Experiment #5 resulted in failure due to severe rutting. Based on visual observation, the cumulative displacement at the edge of the loading plate where the dial gages were not installed was more than 1 inch (25 mm), which was considered as failure. This may have been caused by the difference in compaction effort.

As shown in Figure 4-19 (c), the thin non-reinforced pavement section (Experiment #12) showed an approximate 71% reduction in average cumulative displacement with respect to the thick pavement section (Experiment #4). This reduction was approximately 76% at 500,000 cycles. When the same comparison was made between Experiments #4 and #18, the reductions in average cumulative displacement were approximately 73% at 500,000 cycles and 75% at 1,000,000 cycles with respect to Experiment #4 [Figure 4-19 (c)].

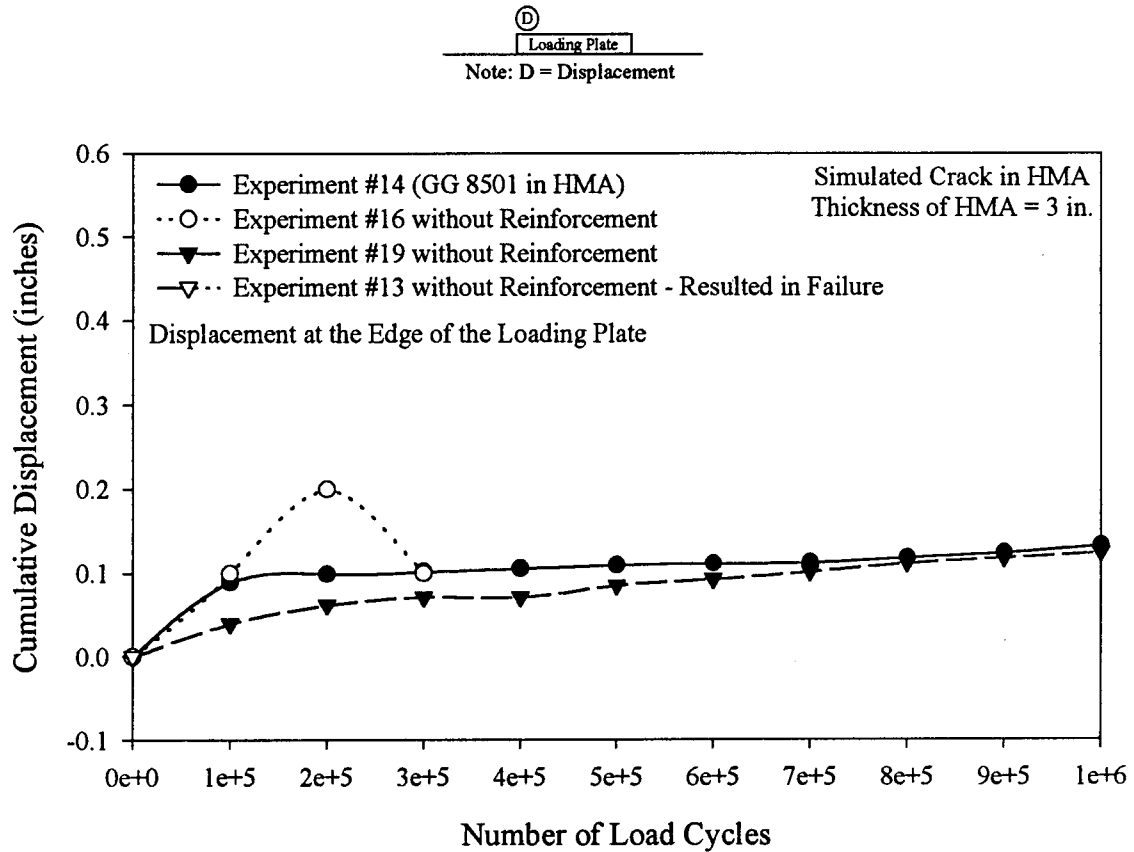
Results from both figures [Figures 4-18 and 4-19] show that the cumulative displacements for thin asphalt sections were lower than for the thick asphalt sections, for both reinforced and non-reinforced cases. These differences could be attributed to slight differences in compaction effort. The importance of slight differences in compaction effort seems more apparent since the thinner sections [3 inches (76 mm)] were compacted in two layers of 1.5 inches (38 mm) in thickness, while the thick asphalt sections were compacted in two layers of 3 inches (76 mm) in thickness.

4.2.7 Influence Of Reinforcement On Cumulative Displacement In A Pavement Section With A Simulated Crack

Figure 4-20 shows the comparison of reinforced and non-reinforced thin asphalt sections with simulated cracks with respect to cumulative displacement. The test section with reinforcement (Experiment #14) did not result in a failure even after 1,000,000 cycles. One of the cases without reinforcement (Experiment #19) did not result in a failure. This may be the cause of good compaction effort in this particular test section. The test section without reinforcement and with the simulated crack (Experiment #13) failed after 600,000 cycles, and therefore cumulative displacement data is not available for this experiment. The cumulative displacement beneath the loading plate was well over 1 inch (25 mm) around 600,000 cycles in this experiment. As shown in Figure 4-20, the test section without reinforcement and with the simulated crack (Experiment #16) failed around 300,000 cycles. In Experiment #16, it was observed that around 300,000 cycles, the simulated crack was deformed and filled with asphalt. Therefore, this section was considered to have failed. Based on these results, it can be stated that both experiments in which a simulated crack was present resulted in failure of the pavement section.

4.2.8 Comparison Of A Non-Reinforced 6-Inch (152 mm) Thick Asphalt Section With A Reinforced Thinner Asphalt Section With A Simulated Crack

The comparison of a non-reinforced 6-inch (152 mm) thick asphalt section (Experiment #4) with reinforced thin asphalt sections [thickness of HMA = 3-inch (76 mm)] with simulated cracks (Experiments #14 and #15) is shown in Figure 4-21. Consistent with Figures 4-17, 4-18, and 4-19 (Sections 4.2.5 and 4.2.6), the cumulative displacements for reinforced test sections with simulated cracks (Experiments #14 and #15) were lower than the displacements in the test section without



Note: Experiment #16 resulted in failure of the pavement section at 300,000 load cycles.
No data is available beyond this point.

Figure 4-20: Influence of Reinforcement on Cumulative Displacement in a Pavement Section with a Simulated Crack

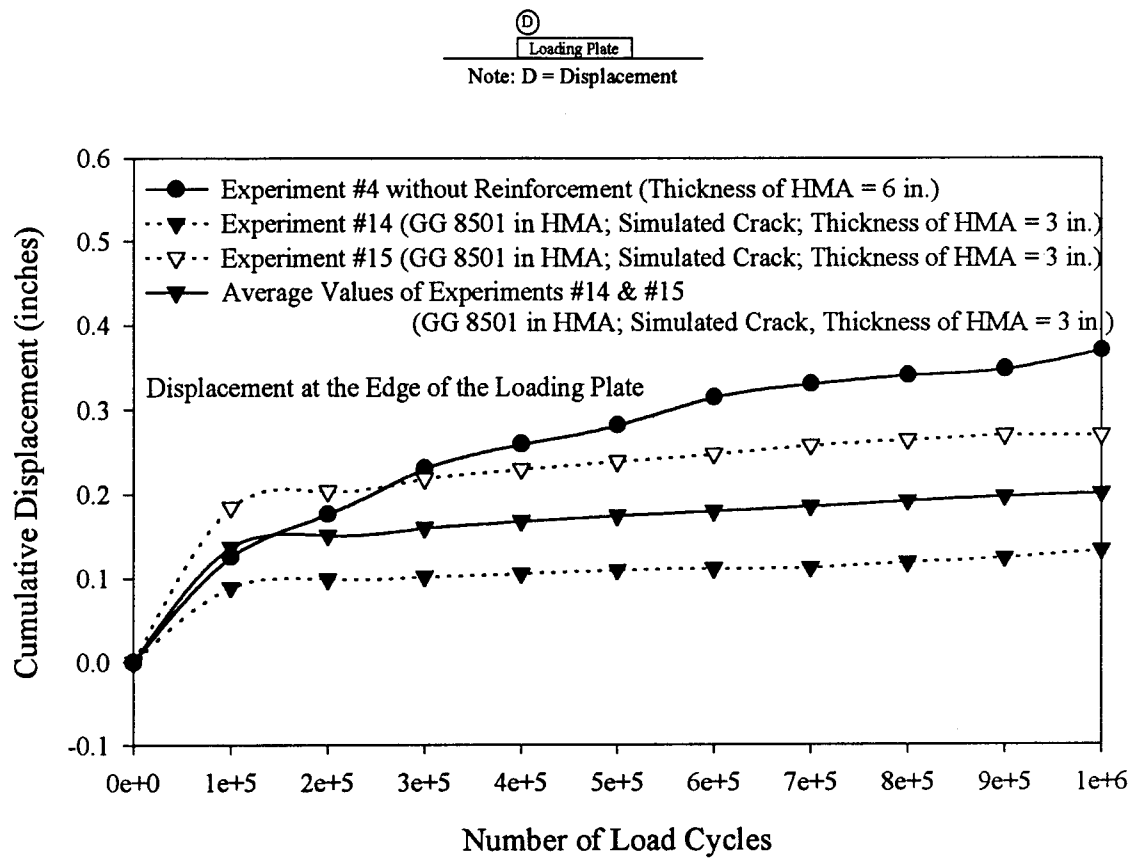


Figure 4-21: Comparison of a Non-Reinforced 6-inch (152 mm) Thick Asphalt Section with a Reinforced Thinner Asphalt Section with a Simulated Crack

reinforcement and without the simulated crack (Experiment #4). The average of the cumulative displacement for Experiments (#14 and #15) is shown in Figure 4-21. At 1,000,000 load cycles approximately 45% of improvement was achieved by reinforcing the thin asphalt section with the simulated crack in comparison to the thick asphalt section without reinforcement.

In other words, thinner reinforced asphalt layers with a simulated crack performed better than a thicker non-reinforced asphalt layers without a simulated crack. As noted earlier, failure resulted in test sections with a simulated crack when the glass grid reinforcement was not included. These results show that the reinforcement in the asphalt layer above the crack tend to arrest the crack propagation leading to failure.

4.2.9 Influence Of Simulated Crack And Reinforcement On Cumulative Displacement

Figure 4-22 shows a similar comparison except the thickness of asphalt layer in non-reinforced cases was 3 inches (76 mm). As shown in Figure 4-22 (a), two test sections (Experiments #14 and #15) with reinforcement and simulated cracks did not result in failure, and the maximum cumulative displacement was 0.270 inches (6.858 mm) for Experiment #15 after 1,000,000 load cycles, which was considered to be low. The response for one of the cases with reinforcement and the simulated crack (Experiment #14) was as good as in cases without reinforcement and without simulated cracks (Experiments #12 and #18) (Table 4-13). Based on the results from Figures 4-20 through 4-22 presented above, of five pavement sections with a simulated crack, two pavement sections were reinforced and these two reinforced pavement sections with a simulated crack did not result in failure. Of the three non-reinforced pavement sections with a simulated crack, two resulted in failure. The non-failed section may be explained by the possible differences in compaction effort put into this particular test section.

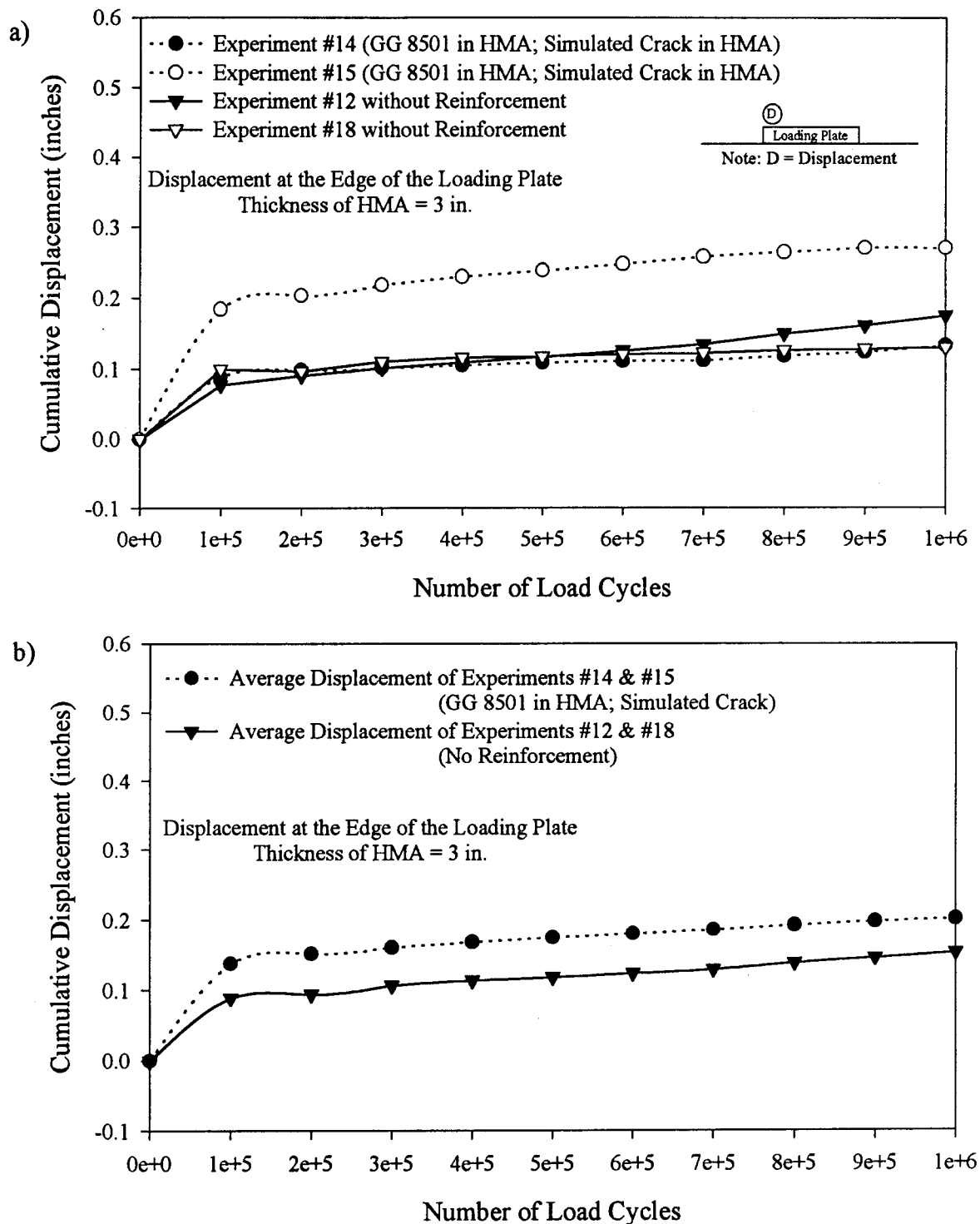


Figure 4-22: Influence of the Simulated Crack and Reinforcement on Cumulative Displacement
 a) Individual Displacements for Experiments #12, #14, #15, and #18
 b) Average Cumulative Displacement of Experiments (#14 & #15) and Experiments (#12 & #18)

Based on average displacements shown in Figure 4-22 (b), it can be stated that reinforced test sections with a simulated crack results in slightly higher displacements than non-reinforced sections without a crack. Clearly, the presence of cracks seems to increase cumulative displacements. However, the reinforcement seems to prevent pavement sections from failure.

These test results show that the negative influence of the simulated crack seems to have a slightly more impact on cumulative displacements than the positive influence of the glass grid reinforcement. Based on all these test results, it could be stated that the influence of the inclusion of glass grid in the hot mix asphalt improved the pavement performance.

4.2.10 Summary Of Laboratory Results On Cumulative Displacements

Based on the comparisons for cumulative displacement shown in Figures 4-13 through 4-22, the following conclusions are made:

- For the thick pavement sections where the thickness of asphalt was 6 inches (152 mm), a 21% to 38% improvement in cumulative displacement was possible when the weight of glass grid in the pavement section was increased. It can be stated that the cumulative displacements increased with reductions in grid weight [See Section 4.2.1].
- The results show that when the HMA thickness was 6 inches (152 mm) in a test section, the improvement in performance indicated by cumulative displacements of a doubly reinforced section (about 60%) was higher than the improvement (about 40%) observed in the singly reinforced test section in comparison to a non-reinforced test section. This substantial decrease in cumulative displacement shows that an improvement could be gained by reinforcing the structural asphalt base in a pavement section [See Section 4.2.3].
- For thinner HMA layers [2.5 inches (63.5 mm) to 3 inches (152 mm)], it appeared that the

influence of reinforcement was not significant in comparison to a non-reinforced case. This could be due to the fact that the compaction effort played a bigger role than the reinforcement [See Section 4.2.4].

- Results indicate that a 6-inch (152 mm) thick non-reinforced hot mix asphalt layer did not improve the performance of the pavement system in comparison to 2.5-inch (63.5 mm) and 3-inch (76 mm) thick glass grid reinforced hot mix asphalt sections. In fact, reinforced thinner sections showed better performance than the non-reinforced thicker section [See Section 4.2.5].
- Thinner reinforced asphalt layers with a simulated crack performed better than a thicker non-reinforced asphalt layers without a simulated crack. At 1,000,000 load cycles, approximately 45% improvement was achieved by reinforcement. As noted earlier, failure resulted in test sections with a simulated crack when the glass grid reinforcement was not included. These results show that the reinforcement in the asphalt layer above the crack tend to arrest the crack propagation leading to failure [See Section 4.2.8].
- Of the two reinforced pavement sections with a simulated crack, neither resulted in failure. Of the three non-reinforced pavement sections with a simulated crack, two resulted in failure and one did not result in failure. This non-failed section may be a result of the compaction effort put into this particular test section.
- Reinforced test sections with a simulated crack resulted in slightly higher displacements than non-reinforced sections without a crack. Clearly, the presence of a crack seems to increase cumulative displacements. However, the reinforcement seems to prevent pavement sections from failure [See Section 4.2.9].

- Test results show that the negative influence of the simulated crack seems to have a slightly more impact on cumulative displacements than the positive influence of the glass grid reinforcement.
- The influence of the inclusion of glass grid in the hot mix asphalt improved the pavement performance.

4.3 DISPLACEMENT UNDER STATIC LOADING: PAVEMENT STIFFNESS

In this research study, test sections were subjected to 1,000,000 load applications of dynamic loading, and displacements for each experiment were measured during static loading of every 100,000 cycles up to 1,000,000 load applications. Comparisons of displacements at the edge of the loading plate [Figure 3-1] under 9 kips (40 kN) of loading were studied to see the influence of glass grid reinforcement with different thicknesses of hot mix asphalt. These comparisons are presented in Figures 4-23 through 4-33. The range of displacements (under static loading) at the edge of the loading plate (Displacement #3) for each experiment is presented in Table 4-14. The results on minimum and maximum values of displacements (under static loading) corresponding to each experiment are the basis for comparisons of displacements.

4.3.1 Influence Of Different Glass Grids On Pavement Stiffness

Figure 4-23 shows the influence of different glass grids on displacement under static loading. Among test sections (Experiments #2, #3, #6, and #7) [thickness of HMA = 6 inches (152 mm)] with different grid types (GG 8501, GG 8502, and GG 8511), the highest displacement [0.033-inch (0.838 mm)] under 9 kips of loading was observed at the test section (Experiment #3) with the lightest glass grid (GG 8501). GlassGrid 8501 (GG 8501) represents the lightest glass grid while GlassGrid 8511 (GG 8511) represents the heaviest glass grid. GlassGrid 8502 (GG 8502) in Experiment #2 has a weight between those of GG 8501 and GG 8511. Displacements for the test sections (Experiments #6 and #7) with the heaviest glass grid (GG 8511) showed similar results. For both experiments the range of displacement (under static loading) varied between 0.020-inch (0.508 mm) to 0.024-inch (0.610 mm) (Table 4-14). Clearly the pavement sections (Experiments #2, #6, and #7) with the medium and heavy glass grids (GG 8502, GG 8511, and GG 8511, respectively) indicated smaller

Table 4-14: Range of Displacement Under Static Loading at the Edge of the Loading Plate (Displacement #3)

Experiment #	Range of Displacements (Under Static Loading) minimum value - maximum value (inches) [mm]
1	Not Available
2	0.015 - 0.026 [0.381 - 0.660]
3	0.025 - 0.033 [0.635 - 0.838]
4	0.029 - 0.032 [0.737 - 0.813]
5	0.021 - 0.027 [0.533 - 0.686]
6	0.022 - 0.024 [0.559 - 0.610]
7	0.020 - 0.023 [0.508 - 0.584]
8	0.021 - 0.030 [0.533 - 0.762]
9	0.024 - 0.057 [0.610 - 1.448]
10	0.025 - 0.046 [0.635 - 1.168]
11	0.025 - 0.028 [0.635 - 0.711]
12	0.019 - 0.020 [0.483 - 0.508]
13	0.015 - 0.028 [0.381 - 0.711]
14	0.025 - 0.029 [0.635 - 0.737]
15	0.029 - 0.034 [0.737 - 0.864]
16	0.018 - 0.021 [0.457 - 0.533]
17	0.026 - 0.029 [0.660 - 0.737]
18	0.017 - 0.025 [0.432 - 0.635]
19	0.019 - 0.023 [0.483 - 0.584]
20	0.030 - 0.049 [0.762 - 1.245]

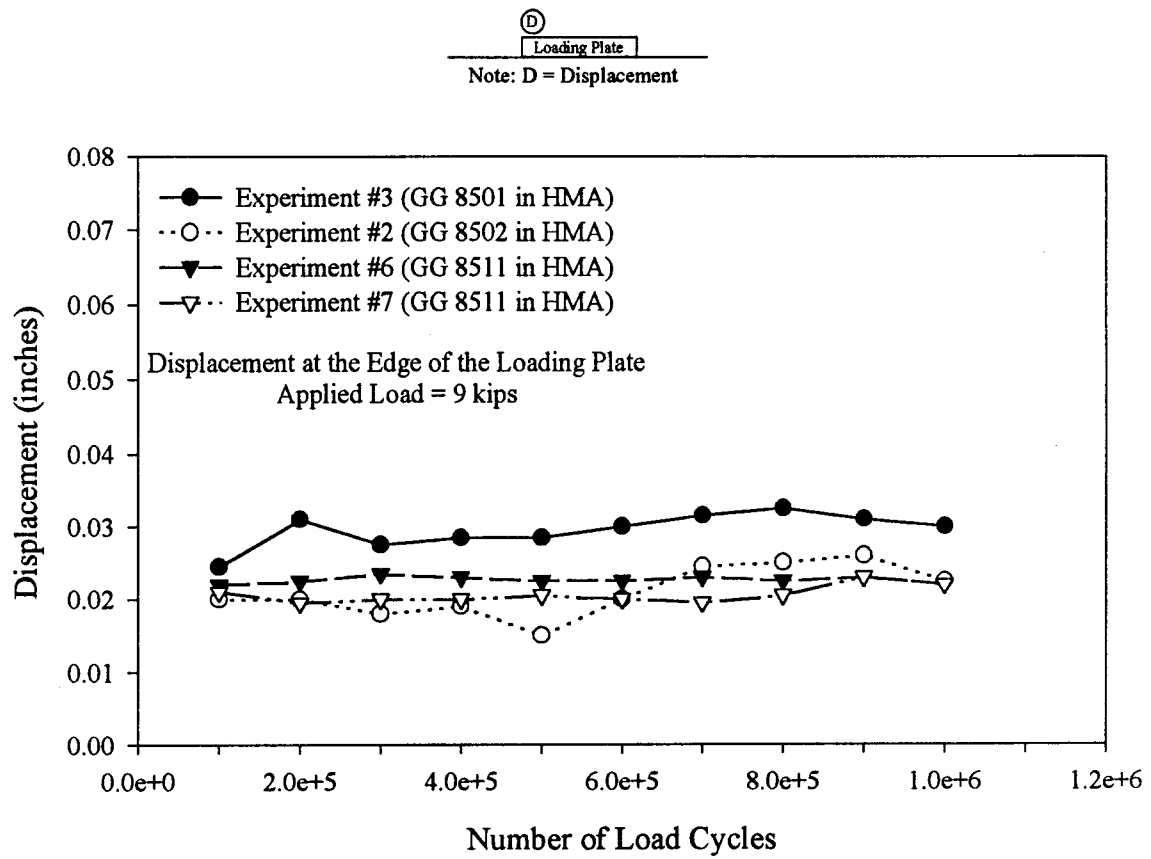


Figure 4-23: Influence of Different Glass Grids on Pavement Stiffness

displacement than the pavement section (Experiment #3) with the lightest glass grid (GG 8501). However, between 100,000 and 600,000 cycles, the displacement for the pavement section (Experiment #2) with medium weight glass grid (GG 8502) was slightly lower than the displacement for the pavement sections (Experiments #6 and #7) with heavy glass grid (GG 8511). After 600,000 cycles, the displacement for the pavement section (Experiment #2) with medium weight glass grid (GG 8502) was higher than the displacement for the pavement sections (Experiments #6 and #7) with heavy glass grid (GG 8511). Also, the difference in displacement between the minimum value of displacement for Experiment #2 and the maximum value of displacement for Experiment #3 was very small [0.018-inch (0.457 mm)]. Therefore, no clear conclusion on the influence of different glass grids on displacement (under static loading) can be made [Figure 4-23]. However, test sections with lighter glass grids seems to result in slightly larger surface deformations in comparison to test sections with heavier glass grids.

4.3.2 Influence Of Glass Grids On Pavement Stiffness Of A Doubly Reinforced Section

Figure 4-24 shows the comparison of the non-reinforced pavement section (Experiment #4) with doubly-reinforced thick asphalt sections (Experiments #8, #9, and #10) on the basis of displacements under static loading. Displacements for non-reinforced (Experiment #4) and two of the doubly-reinforced test sections (Experiments #8 and #10) followed similar patterns. For two doubly-reinforced test sections (Experiments #9 and #10), a large decrease in the displacement was observed between 100,000 and 200,000 load applications [0.033-inch (0.838 mm) for Experiment #9 and 0.021-inch (0.533 mm) for Experiment #10]. The displacement for one of the doubly-reinforced test sections (Experiment #10) remained steady and was consistent with that of other experiments (Experiments #4 and #8). With the number of load cycles, the displacement for Experiment #9

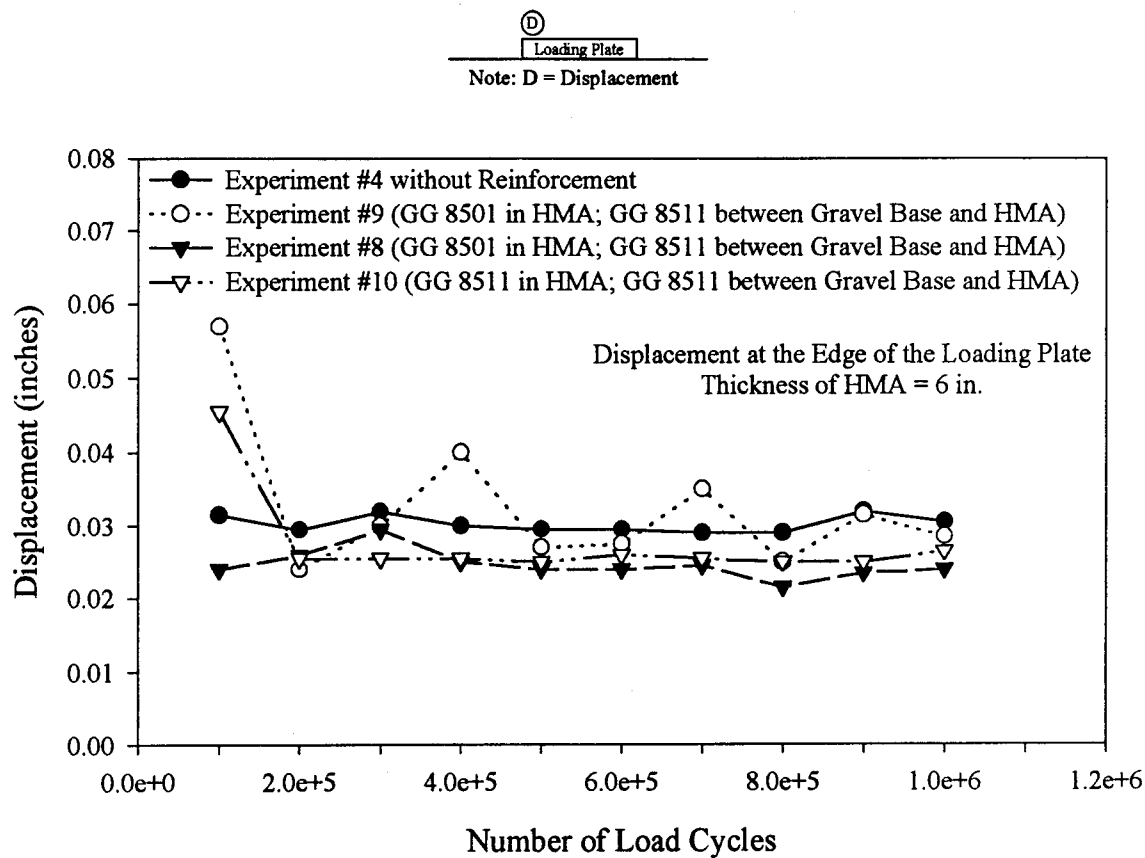


Figure 4-24: A comparison of Performance of Non-reinforced and Doubly Reinforced 6-inch (152 mm) Thick Asphalt Sections

continued to fluctuate throughout the experiment. In spite of this fluctuation, no failure was observed for this test section (Experiment #9). This figure also shows that the variation of stiffness of the hot mix asphalt layer did not seem to be affected significantly by the presence of the glass grid [Figure 4-24].

4.3.3 Influence Of Reinforcement On Pavement Stiffness [Thickness Of HMA = 6 Inches (152 mm)]

Figure 4-25 shows the comparison of the non-reinforced pavement section (Experiment #4) with reinforced pavement sections (Experiments #3 and #5) for the hot mix asphalt thickness of 6 inches (152 mm). The maximum displacement of the non-reinforced test section (Experiment #4) was 0.032-inch (0.813 mm), and the minimum displacement of the reinforced test section (Experiment #5) was 0.021-inch (0.533 mm). As shown in Figure 4-25, the displacement (under static loading) does not indicate a significant difference [0.011-inch (0.279 mm)] between the non-reinforced and reinforced pavement sections. This figure also shows that the variation in stiffness of the hot mix asphalt layer for the thick pavement sections does not seem to be affected significantly by the presence of the glass grid. For the thick asphalt sections, the insignificant differences may be caused by the difference in compaction effort.

4.3.4 Influence Of Reinforcement On Pavement Stiffness [Thickness Of HMA = 3 Inches (76 mm)]

Behavior for the thin asphalt sections [Figure 4-26] was different from behavior for the thick asphalt sections [Figure 4-25]. Figure 4-26 shows a comparison of the reinforced and non-reinforced thin pavement sections [thickness of HMA = 3 inches (76 mm)] on the basis of displacements under static loading. Displacements for reinforced pavement sections (Experiments #11 and #17) were

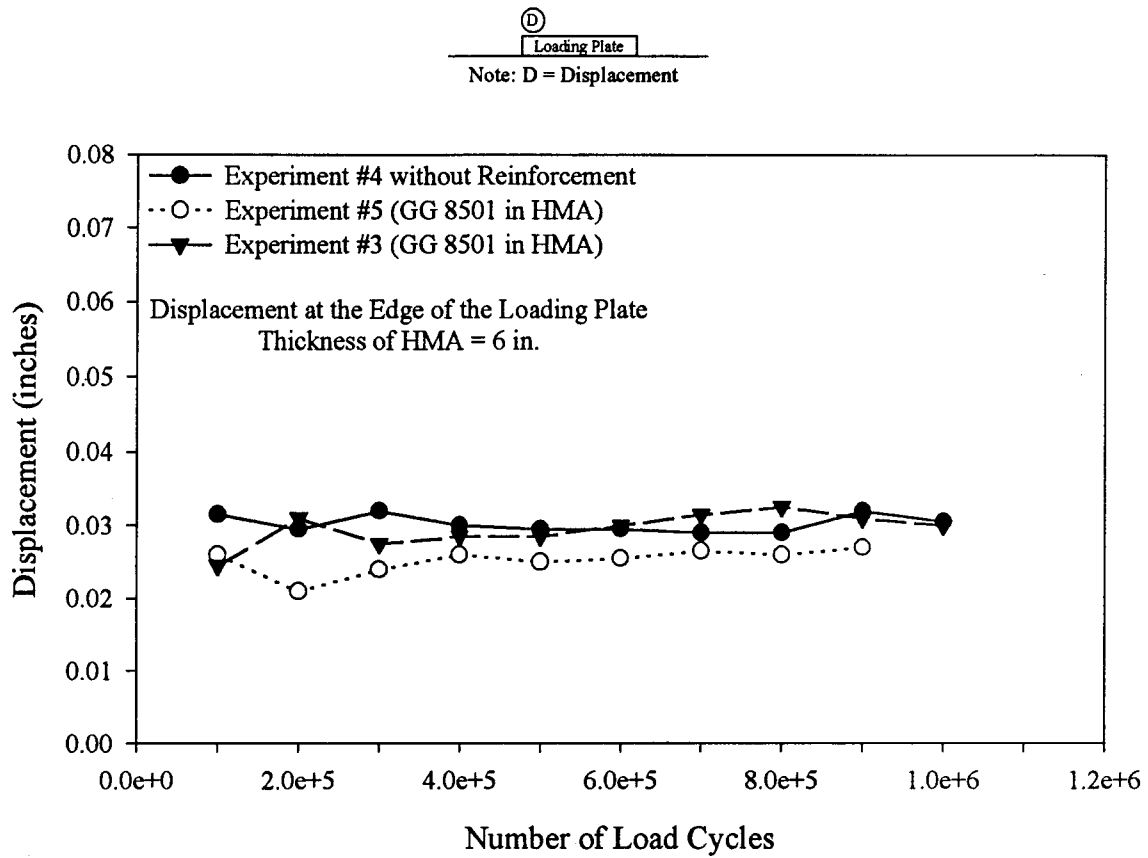


Figure 4-25: Influence of Reinforcement on Pavement Stiffness
[Thickness of HMA = 6 in. (152 mm)]

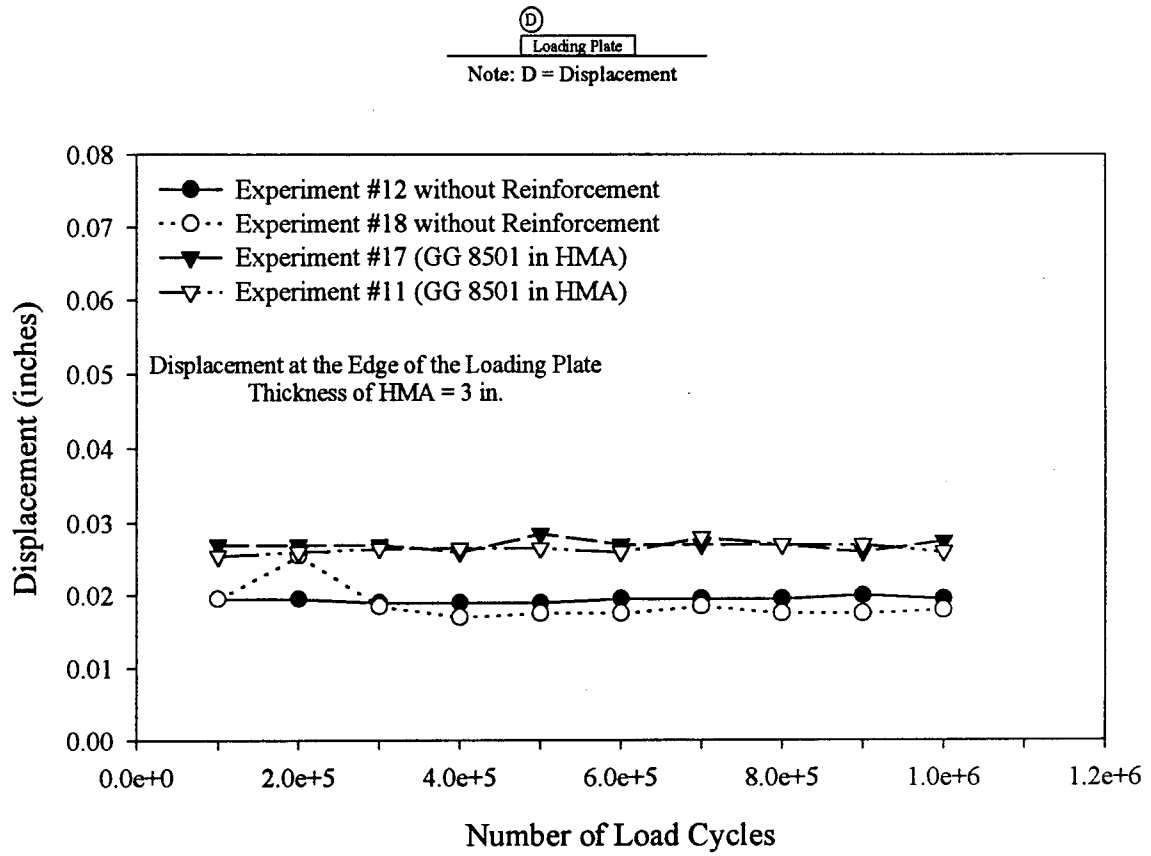


Figure 4-26: Influence of Reinforcement on Pavement Stiffness
[Thickness of HMA = 3 in. (76 mm)]

slightly higher than that of the non-reinforced pavement sections (Experiments #12 and #18). This small difference is insignificant and may be caused by the difference in compaction effort and/or by the inclusion of glass grid. Displacement for the reinforced thin pavement sections (Experiments #11 and #17) ranged between 0.025-inch (0.635 mm) and 0.029-inch (0.737 mm). The displacement for non-reinforced thin pavement sections (Experiments #12 and #18) ranged between 0.017-inch (0.432 mm) and 0.020-inch (0.508 mm), with the exception of the displacement of 0.025-inch (0.635 mm) at 200,000 load cycles for Experiment #12. This behavior shows that with the inclusion of the glass grid inside the HMA, there is a tendency for the displacement (under static loading) to increase slightly, thereby causing a decrease in stiffness of the HMA. The difference in displacement between the reinforced thin pavement section and the non-reinforced thin pavement section was insignificant.

4.3.5 Comparison Of Non-Reinforced 6-Inch (152 mm) Thick Asphalt Section With Thinner Reinforced Asphalt Sections

Figure 4-27 shows the comparison of the displacements (under static loading) of a non-reinforced pavement section (Experiment #4) with those in reinforced pavement sections (Experiments #11, #17 and #20). As shown in this figure, displacements for the non-reinforced pavement section with asphalt thickness of 6 inches (152 mm) were higher than those of the reinforced pavement sections (Experiments #11 and #17) with asphalt thickness of 3 inches (76 mm), and lower than those of the reinforced pavement section (Experiment #20) with asphalt thickness of 2.5 inches (63.5 mm). The maximum value of the displacement for the non-reinforced test section (Experiment #4) with asphalt thickness of 6 inches (152 mm) was 0.032-inch (0.813 mm), while the minimum value of the reinforced test sections (Experiments #11 and #17) with asphalt thickness of 3 inches (76 mm) was 0.025-inch (0.635 mm). The maximum difference between the non-reinforced

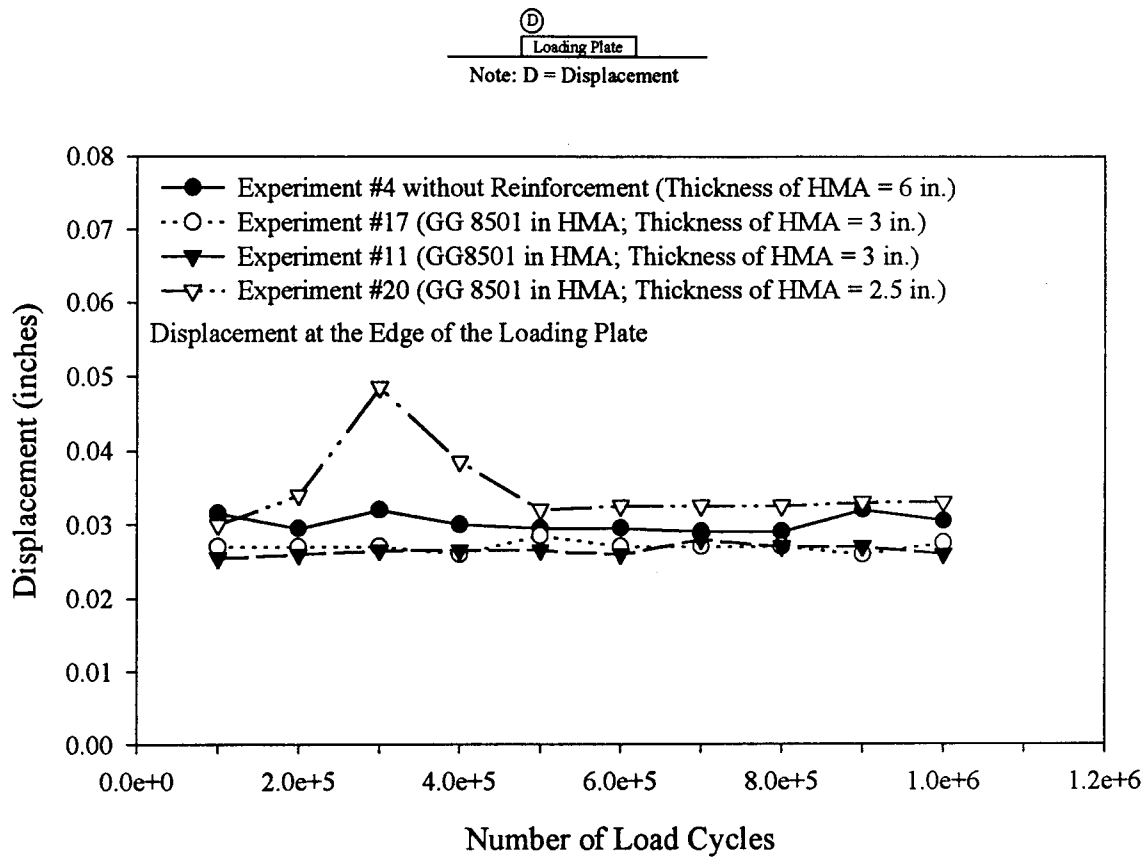


Figure 4-27: Comparison of Non-Reinforced 6-inch (152 mm) Thick Asphalt Section with Thinner Reinforced Asphalt Sections with Respect to Displacement Under Static Loading

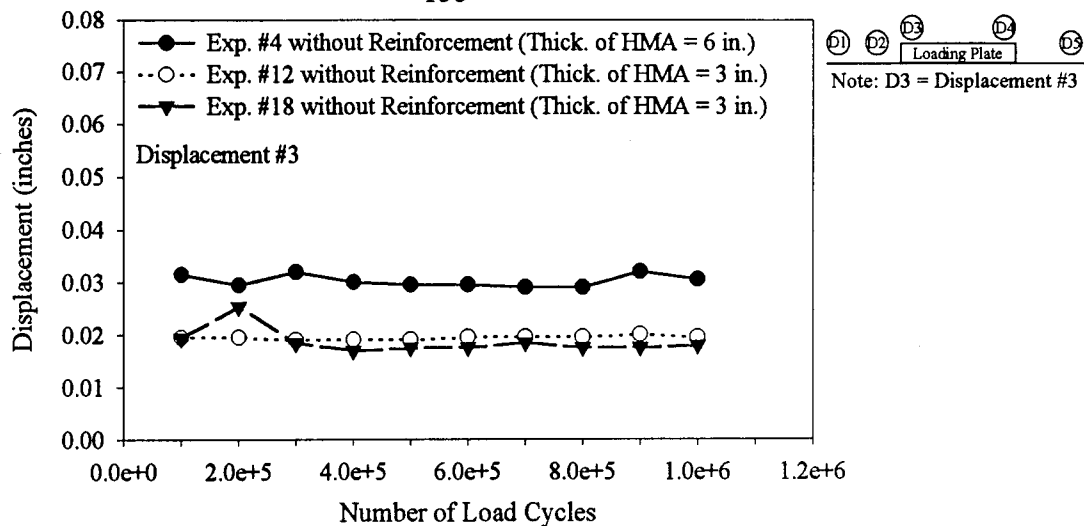
test section (Experiment #4) and reinforced test sections (Experiments #11 and #17) was only 0.007-inch (0.178 mm). This difference can be considered as insignificant. This figure shows that the stiffness of all the sections (Experiments #4, #17, #11, and #20) is very similar.

4.3.6 Influence Of Asphalt Thickness On Pavement Stiffness

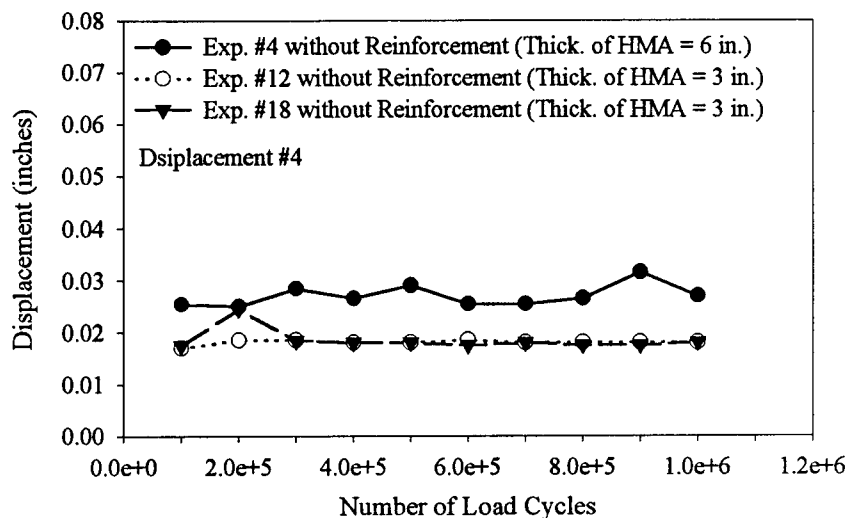
Figure 4-28 shows the influence of asphalt thickness on displacement (under static loading) for non-reinforced pavement sections. As shown in Figures 4-28 (a) and (b), displacements at gauges #3 and #4 gave consistent results, indicating that the displacements for thin non-reinforced test sections (Experiments #12 and #18) were smaller than for the thick non-reinforced test section (Experiment #4). Average displacements of Experiments #4, #12, and #18 for displacements #3 and #4 are shown in Figure 4-28 (c). The range of average displacements for the thick non-reinforced section (Experiment #4) varied between 0.027-inch (0.686 mm) and 0.032-inch (0.813 mm). The minimum value of 0.027-inch (0.686 mm) for the thick non-reinforced test section (Experiment #4) was higher than the maximum value of 0.025-inch (0.635 mm) for the thin non-reinforced sections (Experiments #12 and #18). This figure indicates that the thin pavement sections (Experiments #12 and #18) were stiffer than the thick pavement section (Experiment #4), perhaps due to the compaction effort and the thicknesses of compaction lift, which was 3 inches (76 mm) for thick and 1.5 inches (38.1 mm) for thin pavement sections. The maximum difference in average displacement was very small [0.014-inch (0.356 mm)] between the maximum value [0.032-inch (0.813 mm)] and minimum value [0.018-inch (0.457 mm)].

A similar comparison was made for the reinforced test sections for two different thicknesses of 3 inches (76 mm) and 6 inches (152 mm) [Figure 4-29]. Unlike non-reinforced test sections [Figure 4-28], only a slight distinction is apparent for the reinforced test sections for two different thicknesses

a)



b)



c)

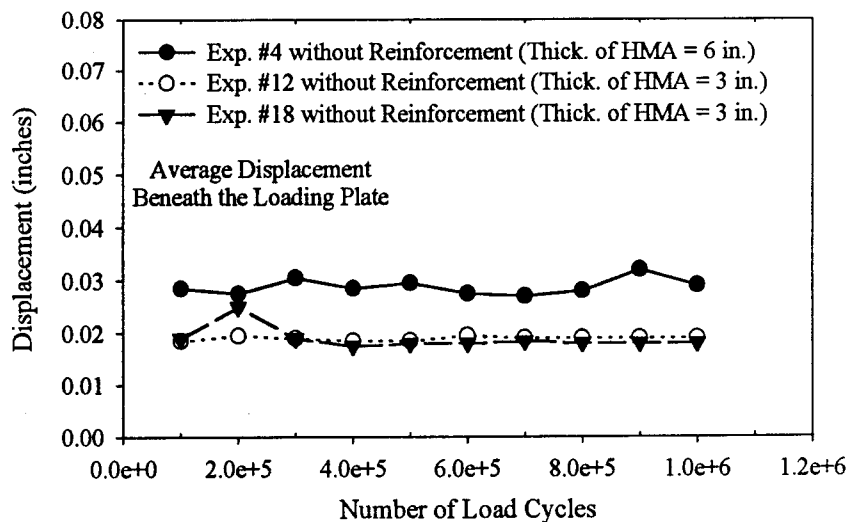


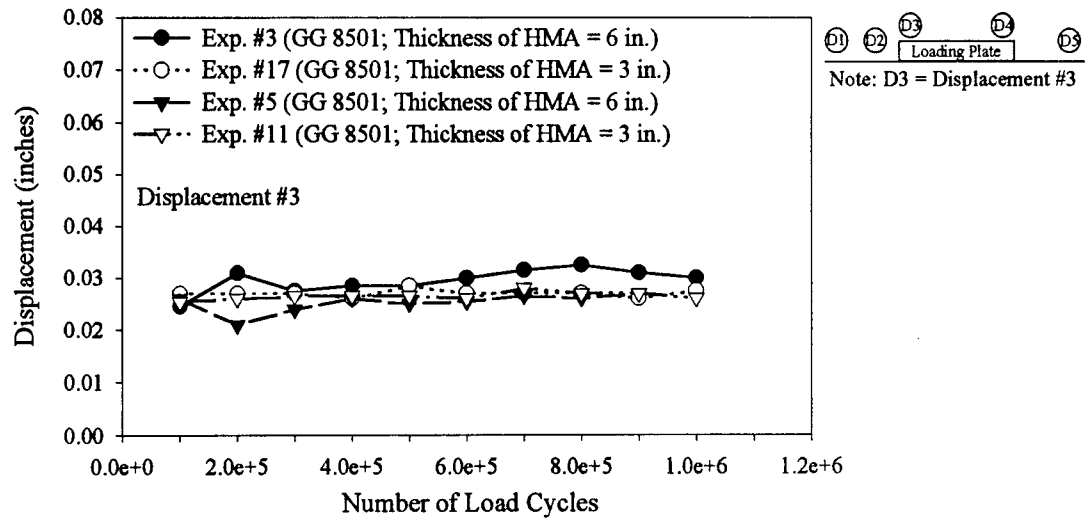
Figure 4-28: Influence of Asphalt Thickness on Pavement Stiffness of Non-Reinforced Test Sections

a) Displacement #3

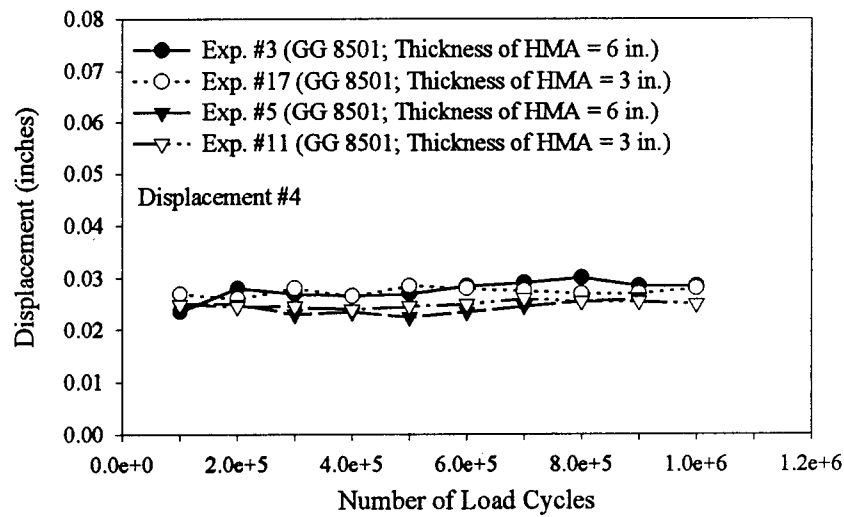
b) Displacement #4

c) Average Displacement

a)



b)



c)

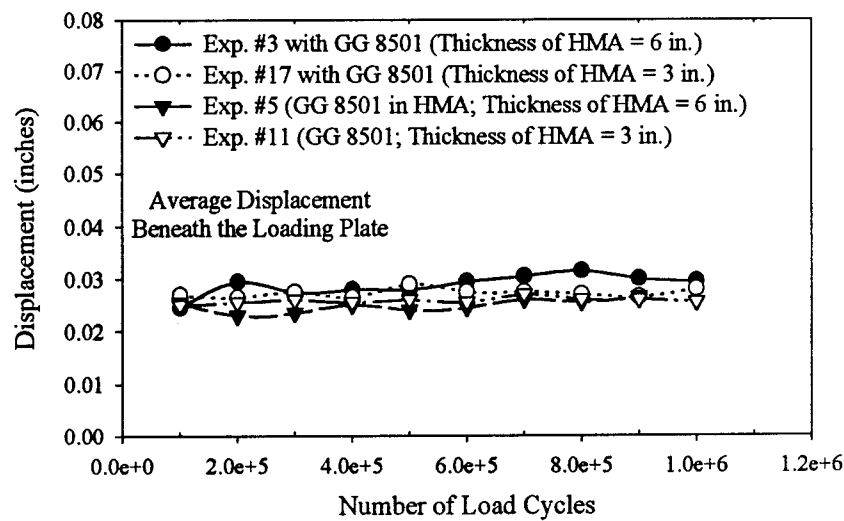


Figure 4-29: Influence of Asphalt Thickness on Pavement Stiffness of Reinforced Test Sections

a) Displacement #3

b) Displacement #4

c) Average Displacement

as shown in Figure 4-29. Displacement at gauge #3 [Figure 4-29 (a)] and displacement at gauge #4 [Figure 4-29 (b)] showed that when the pavement sections were reinforced with the glass grid, displacements (under static loading) were similar. In average displacements [Figure 4-29 (c)] for thick reinforced test sections (Experiments #3 and #5), the minimum displacement value was 0.023-inch (0.584 mm) (Experiment #5) and the maximum value was 0.032-inch (0.813 mm) (Experiment #3). For thin reinforced test sections (Experiments #11 and #17), the minimum displacement was 0.025-inch (0.635 mm) (Experiment #11) and the maximum displacement was 0.029-inch (0.737 mm) (Experiment #17). The maximum difference in average displacement between the maximum value [0.032-inch (0.813 mm)] in thick reinforced section (Experiment #3) and the minimum value [0.025-inch (0.635 mm)] in thin reinforced section (Experiment #11) was 0.007-inch (0.178 mm), which was considered insignificant [Figure 4-29 (c)]. Displacement at gauge #3 [Figure 4-29 (a)], displacement at gauge #4 [Figure 4-29 (b)], and the average displacement of displacements at gauges #3 and #4 [Figure 4-29 (c)] show that when the pavement sections were reinforced with glass grids, the displacements (under static loading) of the thick pavement sections (Experiments #3 and #5) and the thin pavement sections (Experiments #11 and #17) were approximately the same.

4.3.7 Influence Of A Simulated Crack On Stiffness Of A Non-Reinforced Pavement Section

Figure 4-30 shows the influence of a simulated crack on a non-reinforced flexible pavement section based on displacements under static loading. As shown in Figure 4-30, after 300,000 load cycles the displacement for the non-reinforced pavement section with the simulated crack (Experiment #19) was higher than that for the non-reinforced pavement section without the simulated crack (Experiment #18) and vice versa before 300,000 cycles. For the non-reinforced test section without the simulated crack (Experiment #18) the displacement ranged between 0.017-inch (0.432

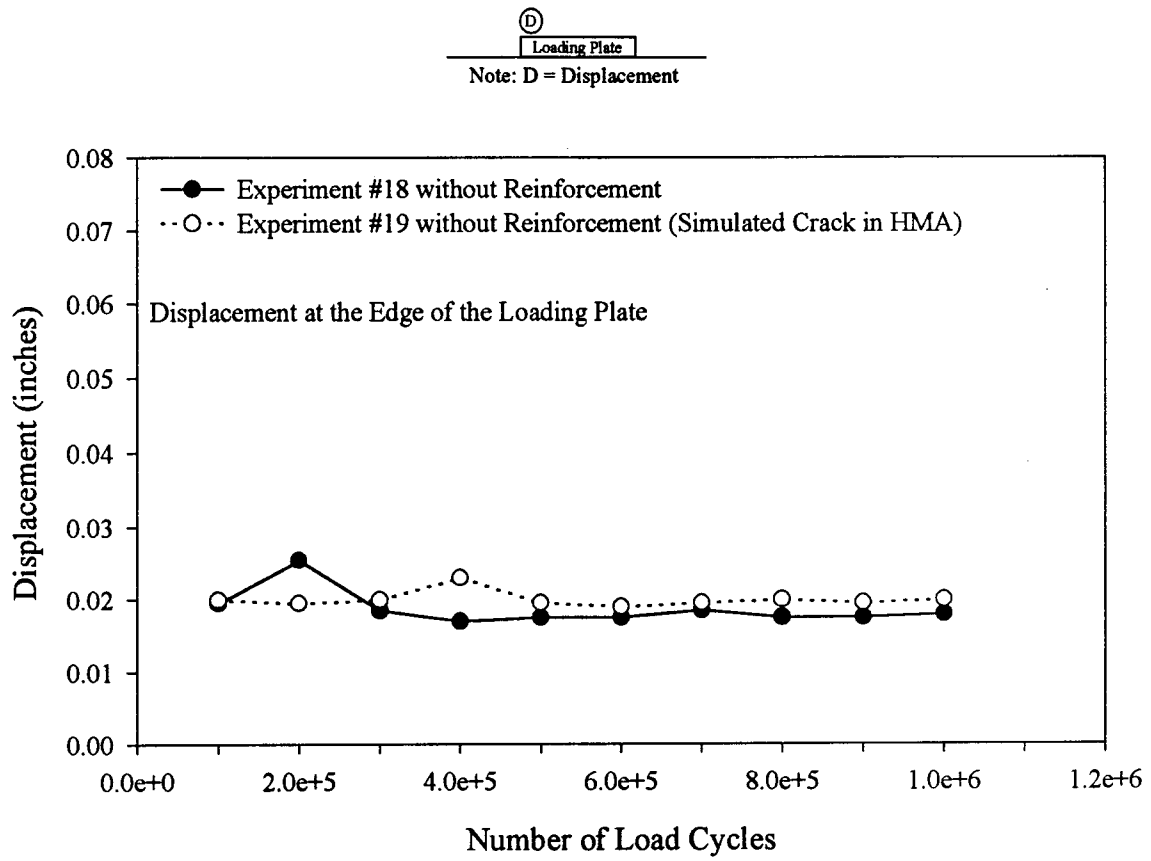


Figure 4-30: Influence of a Simulated Crack on Pavement Stiffness (Under Static Loading) in a Pavement Section without Reinforcement

mm) and 0.025-inch (0.635 mm). For the non-reinforced section with the simulated crack (Experiment #19) the displacement ranged between 0.019 (0.483 mm) and 0.023-inch (0.584 mm). Again the maximum difference in displacement (under static loading) between the pavement sections with and without simulated cracks was very insignificant. As shown in Figure 4-30, it can be stated that a non-reinforced test section with a simulated crack results in slightly higher displacements (under static loading) than that of a non-reinforced test section without a simulated crack. It appears that the presence of the crack seems to decrease the pavement stiffness slightly.

4.3.8 Influence Of Reinforcement On Stiffness Of A Pavement Section With A Simulated Crack

Observations in Figure 4-26 are similar to those noted for the thin pavement sections with a simulated crack in Figure 4-31. Figure 4-31 shows displacements (under static loading) for reinforced and non-reinforced thin pavement sections with a simulated crack. Displacements for the reinforced pavement sections (Experiments #14 and #15) were slightly higher than the non-reinforced pavement sections (Experiments #13, #16, and #19). Even though the displacement for the reinforced sections was higher than that of for non-reinforced sections, none of the reinforced sections resulted in failure. On the other hand, as shown in Figure 4-31, the non-reinforced section (Experiment #13) resulted in failure. Due to this failure, data could not be taken beyond 600,000 load cycles. Based on the displacements (under static loading) shown in Figure 4-31, it is not evident that the other non-reinforced pavement section (Experiment #16) resulted in failure; however, it was observed that the crack in this pavement section (Experiment #16) was deformed and filled with asphalt at approximately 300,000 load cycles and was considered to have failed. This figure also verifies that the stiffness of the hot mix asphalt does not seem to be affected significantly by the reinforcement of

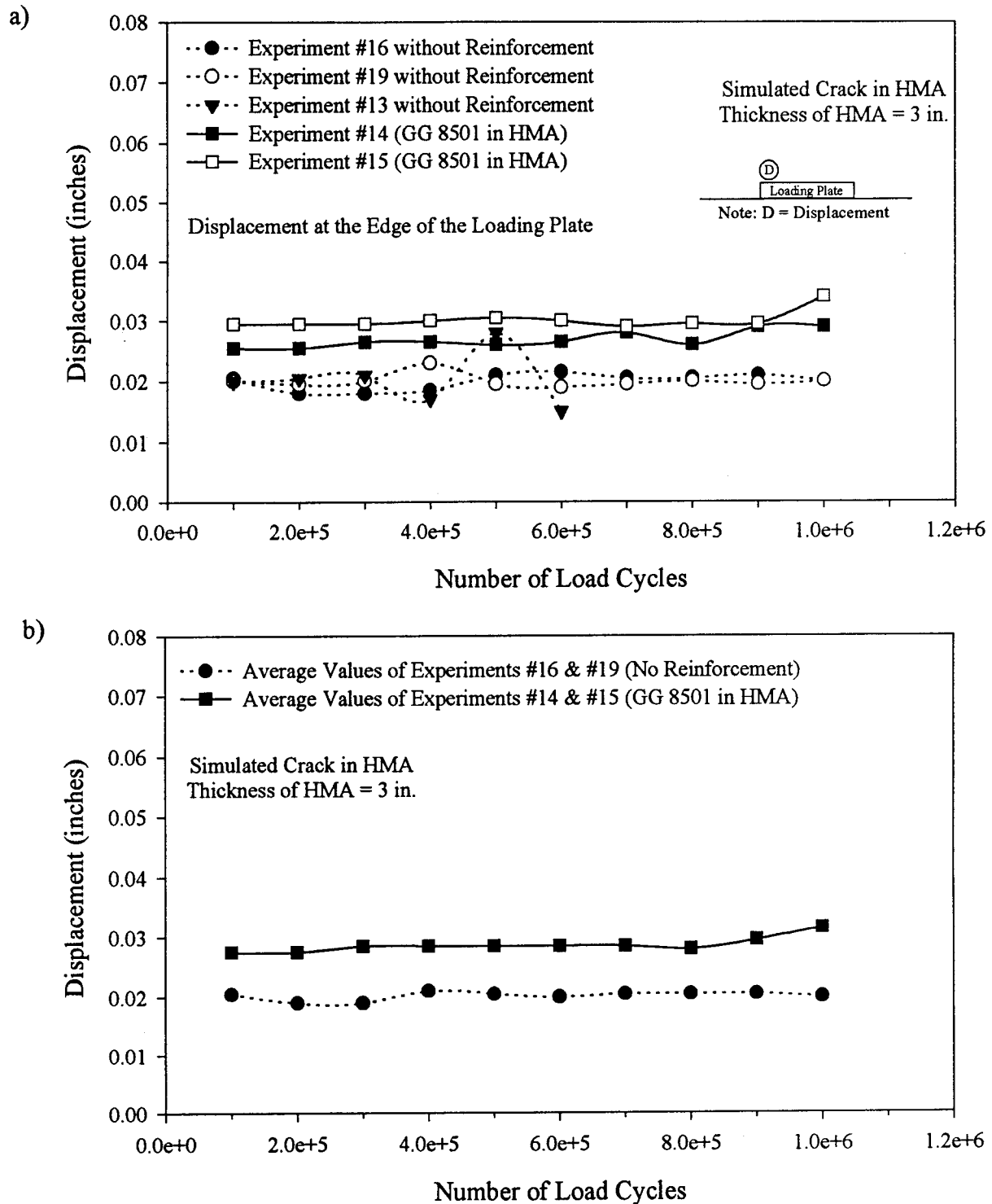


Figure 4-31: Influence of Reinforcement on Pavement Stiffness in a Pavement Section with a Simulated Crack

a) Individual Displacements for Experiments #13, #14, #15, #16, and #19

b) Average Displacement of Experiments (#14 & #15) and Experiments (#16 and #19)

the glass grid since the difference in displacement (under static loading) between the minimum value [0.015-inch (0.381 mm)] of non-reinforced and the maximum value [0.034-inch (0.864 mm)] of reinforced pavement sections is very low [0.019-inch (0.483 mm)].

4.3.9 Comparison Of A Non-Reinforced 6-Inch (152 mm) Thick Asphalt Section With A Reinforced Thinner Asphalt Section With A Simulated Crack

On the basis of displacement under static loading, the non-reinforced thick pavement section (Experiment #4) was compared with reinforced thin pavement sections with a simulated crack (Experiments #14 and #15) in Figure 4-32. Again, displacements for reinforced test sections with a simulated crack (Experiments #14 and #15) were similar to the displacement for the non-reinforced thick pavement section (Experiment #4). This behavior indicates that a similar stiffness can be obtained by reinforcing a thin asphalt section in comparison to a non-reinforced thick pavement section.

4.3.10 Influence Of A Simulated Crack And Reinforcement On Pavement Stiffness

Displacements under static loading for the reinforced thin pavement sections with simulated cracks in the HMA (Experiments #14 and #15) were compared with the non-reinforced thin pavement sections without simulated cracks (Experiments #12 and #18) [Figure 4-33]. As shown in Figure 4-33, the minimum displacement based on two reinforced test sections with simulated cracks (Experiments #14 and #15) was 0.025-inch (0.635 mm). Displacement for Experiment #14 ranged from 0.025-inch (0.635 mm) to 0.029-inch (0.737 mm), and for Experiment #15 ranged between 0.029-inch (0.737 mm) and 0.034-inch (0.864 mm). Consistent with previous results of thin pavement sections without a simulated crack [Figure 4-26], displacements were higher for the reinforced pavement sections with the simulated cracks (Experiments #14 and #15) than for non-reinforced

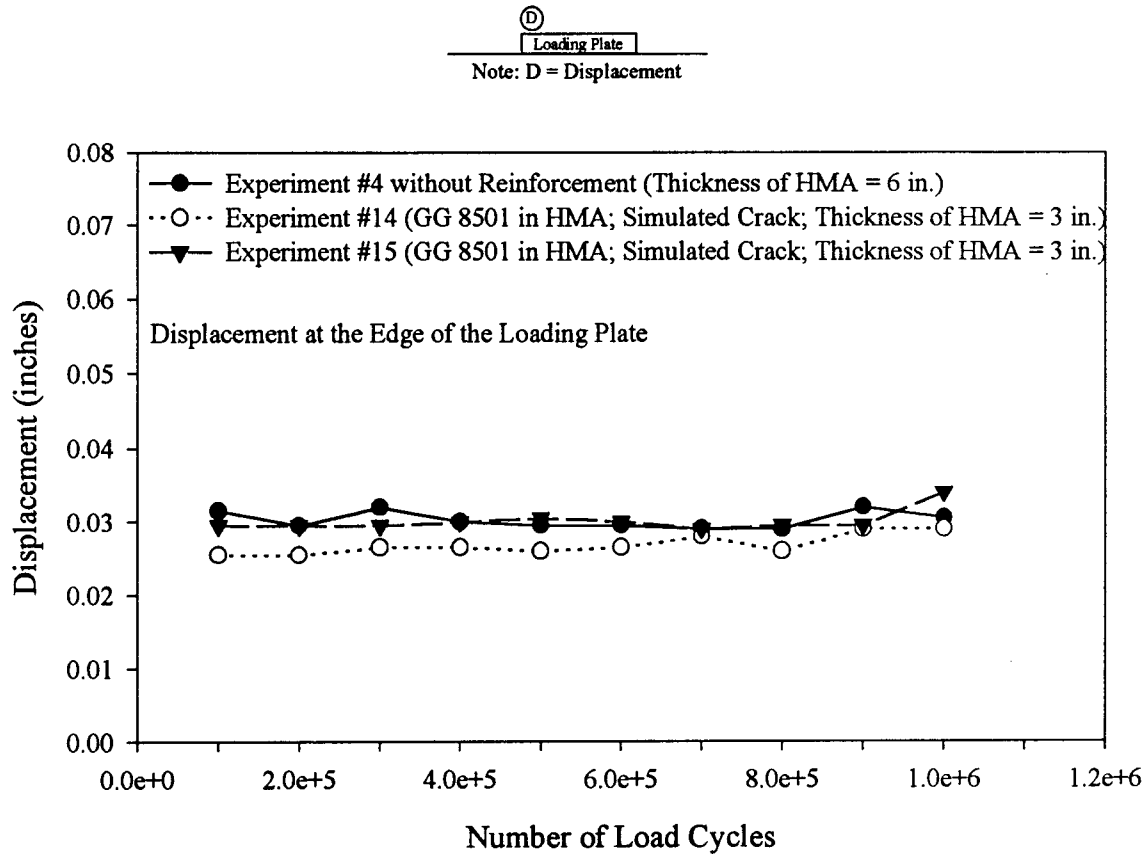


Figure 4-32: Comparison of a Non-Reinforced 6-inch (152 mm) Thick Asphalt Section with a Reinforced Thinner Asphalt Section with a Simulated Crack on the Basis of Displacement

Ⓓ

Loading Plate

Note: D = Displacement

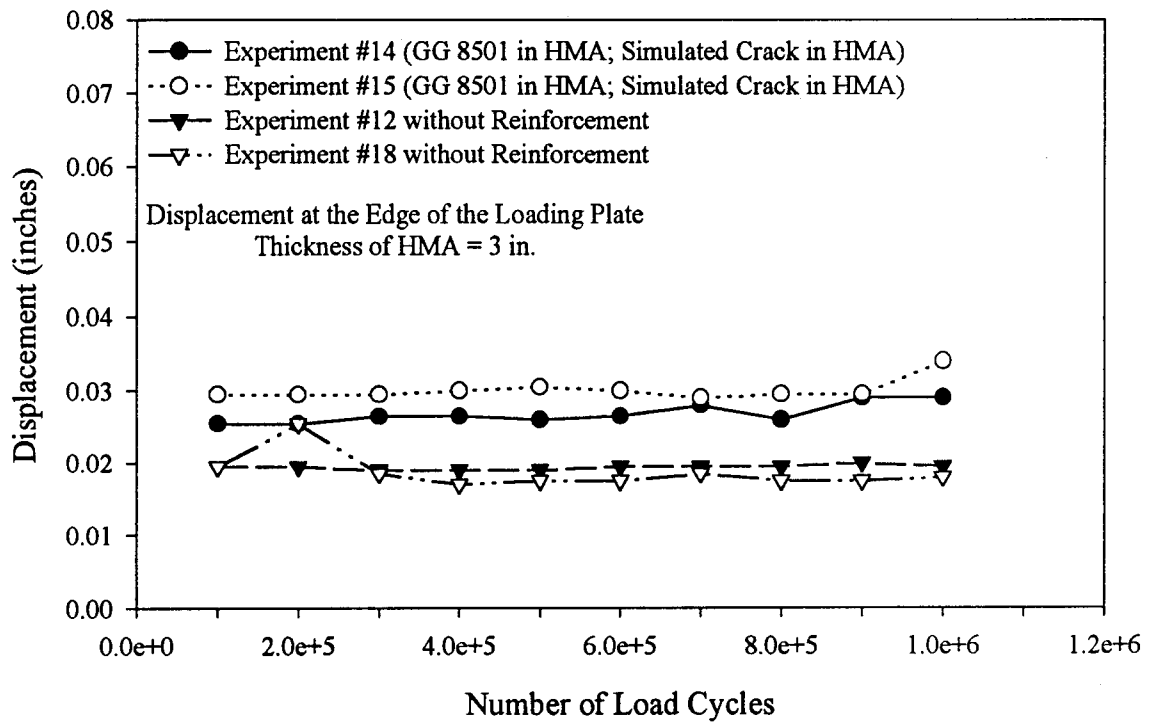


Figure 4-33: Comparison of a Non-Reinforced 3-inch (76 mm) Thick Asphalt Section with a Reinforced Asphalt Section with a Simulated Crack on the Basis of Displacement

pavement sections without simulated cracks (Experiments #12 and #18) [Figure 4-33]. Even though the difference in displacement is insignificant, this small difference could be caused by the inclusion of glass grid and/or the simulated crack.

4.3.11 Summary Of Laboratory Results On Displacements Under Static Loading

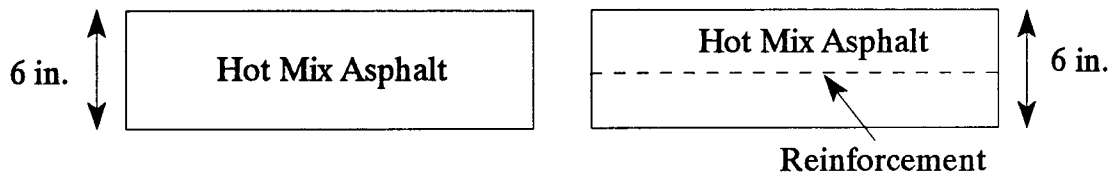
Based on the comparisons presented on displacements (under static loading) shown in Figures 4-23 through 4-33, the following conclusions are made:

- For thick pavement sections [thickness of HMA = 6 inches (152 mm)], no clear conclusion on the influence of different glass grids on displacement (under static loading) can be made. However, test sections with lighter glass grids seems to result in slightly larger surface deformations in comparison to test sections with heavier glass grids.
- The stiffness of the hot mix asphalt layer for the thick pavement sections [thickness of HMA = 6 inches (152 mm)] does not seem to be affected significantly by the presence of the glass grid. For the thick asphalt sections, the insignificant differences in displacement may be caused by the differences in compaction effort [See Section 4.3.3 and Figure 4-34 (a)].
- For the thin [thickness of HMA = 3 inches (76 mm)] pavement sections, displacements for the reinforced case were slightly higher than that of the non-reinforced case. This small difference was insignificant and may be caused by the difference in compaction effort and/or by the inclusion of glass grid [See Section 4.3.4 and Figure 4-34 (b)].
- The displacements for thin non-reinforced test sections [thickness of HMA = 3 inches (76 mm)] were smaller than for the thick non-reinforced test section [thickness of HMA = 6 inches (152 mm)]. This shows that the thin pavement sections were stiffer than the thick pavement section, perhaps due to the compaction effort and the thicknesses of compaction

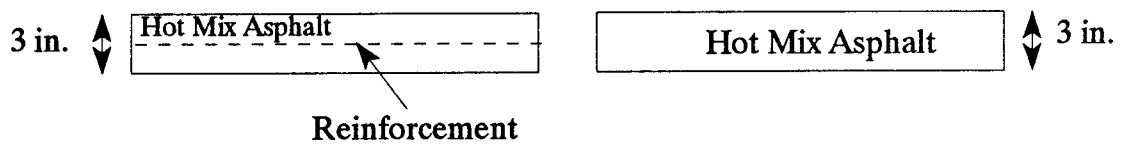
lift, which was 3 inches (76 mm) for thick and 1.5 inches (63.5 mm) for thin pavement sections [See Section 4.3.6 and Figure 4-34 (c)].

- Even though the difference in displacement (under static loading) was insignificant, it can be stated that a non-reinforced test section with a simulated crack [thickness of HMA = 3 inches (76 mm)] resulted in slightly higher displacements than that of a non-reinforced test section without a simulated crack [thickness of HMA = 3 inches (76 mm)]. The presence of the crack seems to decrease the pavement stiffness slightly [See Section 4.3.7 and Figure 4-34 (d)].
- Even though the displacement for the reinforced sections with a simulated crack [thickness of HMA = 3 inches (76 mm)] was higher than that of for non-reinforced sections with a simulated crack [thickness of HMA = 3 inches (76 mm)], the difference in displacement between the non-reinforced and the reinforced pavement sections was very low [0.019-inch (0.483 mm)]. This shows that the stiffness of the hot mix asphalt does not seem to be affected significantly by the glass grid reinforcement [Figure 4-34 (e)].
- Displacements for reinforced test sections with a simulated crack [thickness of HMA = 3 inches (76 mm)] were similar to the displacement for the non-reinforced thick pavement section [thickness of HMA = 6 inches (152 mm)]. This behavior indicates that a similar stiffness can be obtained by reinforcing a thin asphalt section in comparison to a non-reinforced thick pavement section [Figure 4-34 (f)].
- Displacements were higher for the reinforced pavement sections with the simulated cracks [thickness of HMA = 3 inches (76 mm)] than for non-reinforced pavement sections without simulated cracks [thickness of HMA = 3 inches (76 mm)]. Even though the difference in displacement was insignificant, this small difference could be caused by the inclusion of glass

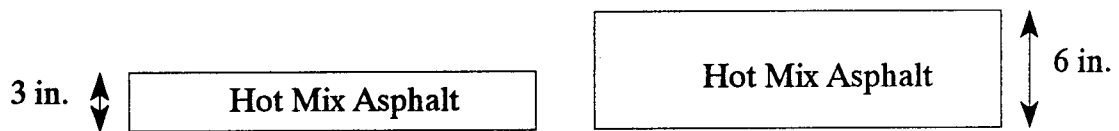
grid and/or the simulated crack [Figure 4-34 (g)].



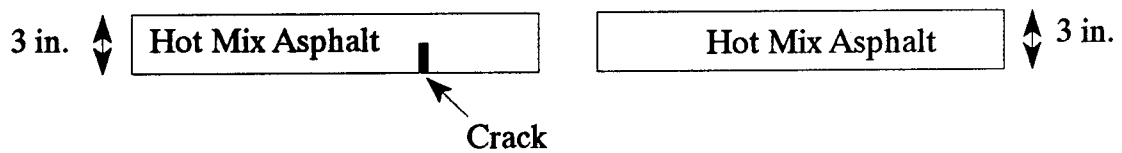
a) Non-Reinforced Thick HMA Layer versus Reinforced Thick HMA Layer



b) Reinforced Thin HMA Layer versus Non-Reinforced Thin HMA Layer

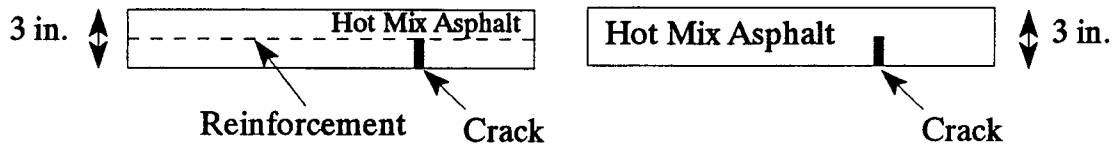


c) Non-Reinforced Thin HMA Layer versus Non-Reinforced Thick HMA Layer

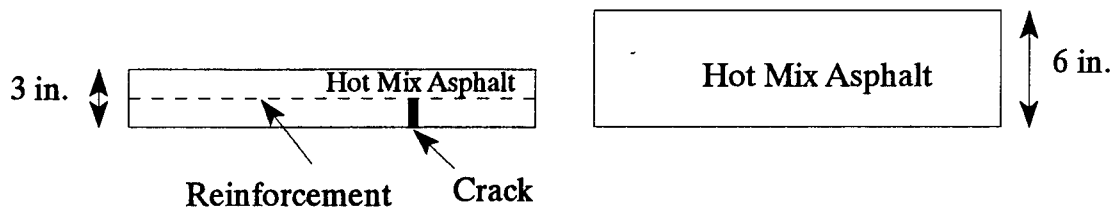


d) Non-Reinforced Thin HMA Layer with a Simulated Crack versus Non-Reinforced Thin HMA Layer

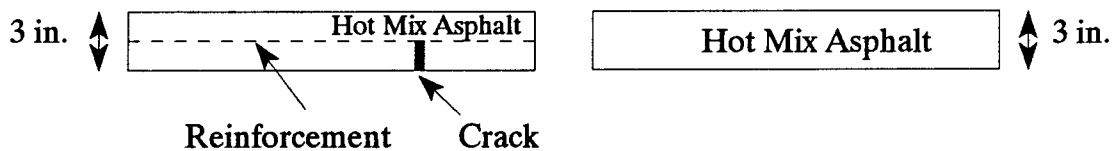
Figure 4-34: Comparison of Experimental Parameters of the HMA Layer for Displacement Under Static Loading



e) Reinforced Thin HMA Layer with a Simulated Crack versus Non-Reinforced Thin HMA Layer with a Simulated Crack



f) Reinforced Thin HMA Layer with a Simulated Crack versus Non-Reinforced Thick HMA Layer



g) Reinforced Thin HMA Layer with a Simulated Crack versus Non-Reinforced Thin HMA Layer

Figure 4-34 (continued): Comparison of Experimental Parameters of the HMA Layer for Displacement Under Static Loading

4.4 STRAIN MEASUREMENTS ON GLASS GRID REINFORCEMENT LAYER

According to the Asphalt Institute, the most critical strains are horizontal tensile strain and vertical compressive strain in the flexible pavement design procedure [Yoder and Witczak (1975)]. In this procedure, the failure criteria (damage analysis) for fatigue cracking was primarily based on horizontal tensile strain at the bottom of the asphalt layer and the failure criteria for rutting was based on vertical compressive strain on top of the subgrade layer.

In this study, measurement of strain in the reinforcement layer (glass grid) was attempted using strain gages in five experiments. Strain gage arrangement for the test sections is shown in Figure 3-1. Two of the measurements were attempted for the doubly reinforced pavement sections (Experiments #9 and #10) where the asphalt thickness was 6 inches (152 mm). The other two measurements were attempted for the pavement sections with simulated cracks (Experiments #14 and #15) where the asphalt thickness was 3 inches (76 mm). The remaining measurement was attempted for the pavement section (Experiment #20) where the asphalt thickness was 2.5 inches (63.5 mm). After the strain gages were installed, they were checked with the strain gage tester for accuracy of installation. During the installation of glass grid in the hot mix asphalt, strain gages were subjected to hostile environment conditions such as high temperature and compaction. On each glass grid six strain gages were installed. Strain Gages (SG) #4, #5, and #6 were installed as back up gages in case any one of the primary strain gages (Strain Gages #1, #2, and #3) failed. Failure of several strain gages due to compaction and dynamic loading were encountered in all five experiments. For comparison purposes, strain gages were identified by numbers 1, 2 and 3, except for the pavement sections with the simulated cracks. For example, if Strain Gage #2 failed and #4 was functional, due to symmetry it was identified as Strain Gage #2 for the pavement sections without the simulated

cracks. For Experiment #9, Strain Gages #1, #2, and #3 were successfully monitored and strains were measured. For Experiment #10, Strain Gage #1 failed during compaction and Strain Gage #2 failed after 100,000 cycles during the dynamic loading. For Experiment #14, Strain Gages #2, #4, #5, and #6 failed during compaction and Strain Gage #1 failed between 0 (zero) and 100,000 cycles. For Experiments #15 and #20, Strain Gages #1, #4, #5, and #6 failed during the compaction process. Due to the difficulties encountered during compaction and the dynamic loading process, the uncertainty and reliability of results on strain measurements should be noted.

Figures 4-35 through 4-38 present the variation of strain with number of load cycles for reinforced test sections where the strain gages were included. Figures 4-35 (a) and (b) show the variation of strain with number of load cycles for Strain Gages #1, #2, and #3. In Figure 4-35 (a), strain measurements for SG #1 fluctuated throughout the experiment (Experiment #9). Initially, the measured strains were 0.001148 for SG #1, 0.000239 for SG #2, and -0.000031 for SG #3. After the initial readings, strain at gage #1 dropped substantially to 0.00048 at 100,000 cycles. After 100,000 cycles, the strain fluctuation continued until the end of the experiment. At 1,000,000 cycles, the strain was 0.000753. Strain at gage #2 showed some fluctuations up to 200,000 load cycles. After this point the strain measurements were steady. The strain measurements at gage #3 were steady throughout the experiment.

Figure 4-35 (b) shows strain measurements for Experiment #10. The data for strain at gage #1 was not available due to a failure in gage #1. The data for strain at gage #2 were not available after 100,000 load cycles due to the same reason. Unlike in Experiment #9, the strain at gage #2 for Experiment #10 decreased from 0.000209 to 0.000076 between 0 (zero) and 100,000 load cycles. Strain at gage #3 was very low (ranged between -0.00001 at 0 (zero) load cycles and -0.00003 at

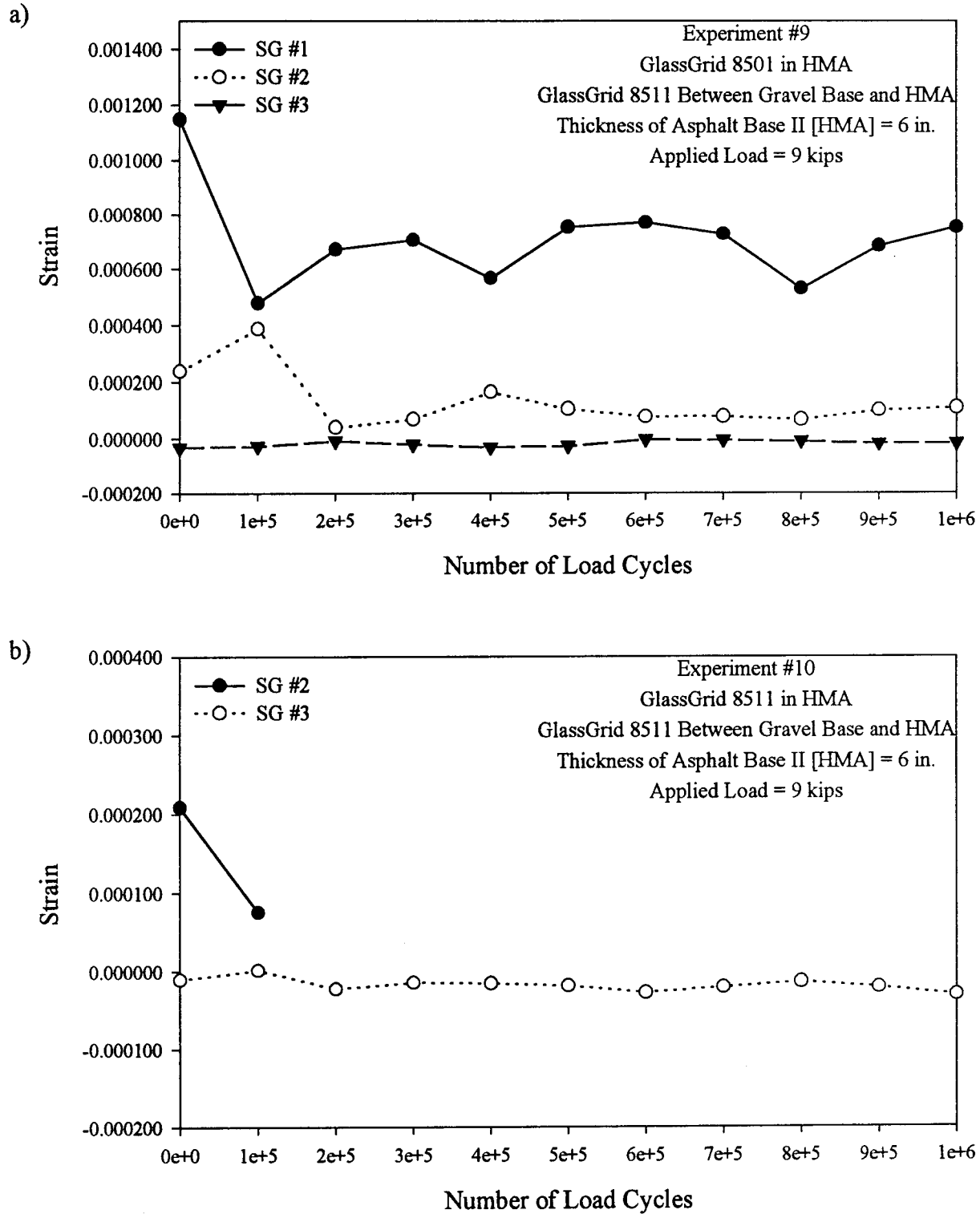


Figure 4-35: Variation of Strain with Number of Load Cycles for Doubly Reinforced Test Sections
a) Experiment #9
b) Experiment #10

1,000,000 load cycles) and steady throughout the experiment [Figure 4-35 (b)]. Strain measurements at gage #3 appear to be similar for both Experiments #9 and #10.

Strain measurements for the reinforced pavement sections with simulated cracks were also attempted and results for Experiments #14 and #15 are presented in Figures 4-36 (a) and (b). Variation of strain at gage #3 with number of load cycles for Experiment #14 can be seen in Figure 4-36 (a). Again, as consistent with other experiments, the strain at gage #3 was very low (ranged between -0.000036 at 0 (zero) load cycles and -0.000025 at 200,000 load cycles) and steady throughout the experiment. Strain at gage #1 was -0.000125 at 0 (zero) load cycles, but this gage failed after the initial reading.

Results for variation of strain for gages #2 and #3 for Experiment #15 can be seen in Figure 4-36 (b). The initial reading for strain at gage # 2 for Experiment #15 was very high (0.00125) [Figure 4-36 (b)] in comparison to the initial reading for strain at gage #2 for Experiment #9 without the simulated crack (0.000239) [Figure 4-35 (a)]. The strain at gage #2 for Experiment #15 decreased substantially to a value of 0.000509 at 100,000 load cycles. Beyond this point, strain at gage #2 continued to decrease slowly up to 600,000 load cycles (0.000317). After 600,000 load cycles, insignificant change was observed at gage #2. These strain measurements at gage #2 for Experiment #15 with the simulated crack [Figure 4-36 (b)] were much higher than the strain measurements for the same gage of Experiment #9 without the simulated crack [Figure 4-35 (a)]. It should be noted that the thicknesses of the HMA was 6 inches (152 mm) for Experiment #9 and 3 inches (76 mm) for Experiment #15. Strain measurements at gage #3 for Experiment #15 were again consistent with other experiments. After the initial reading (0.000034 at 0 (zero) load cycles), the measurements were in compression from 100,000 to 1,000,000 load cycles. Strain measurements for Experiment #15

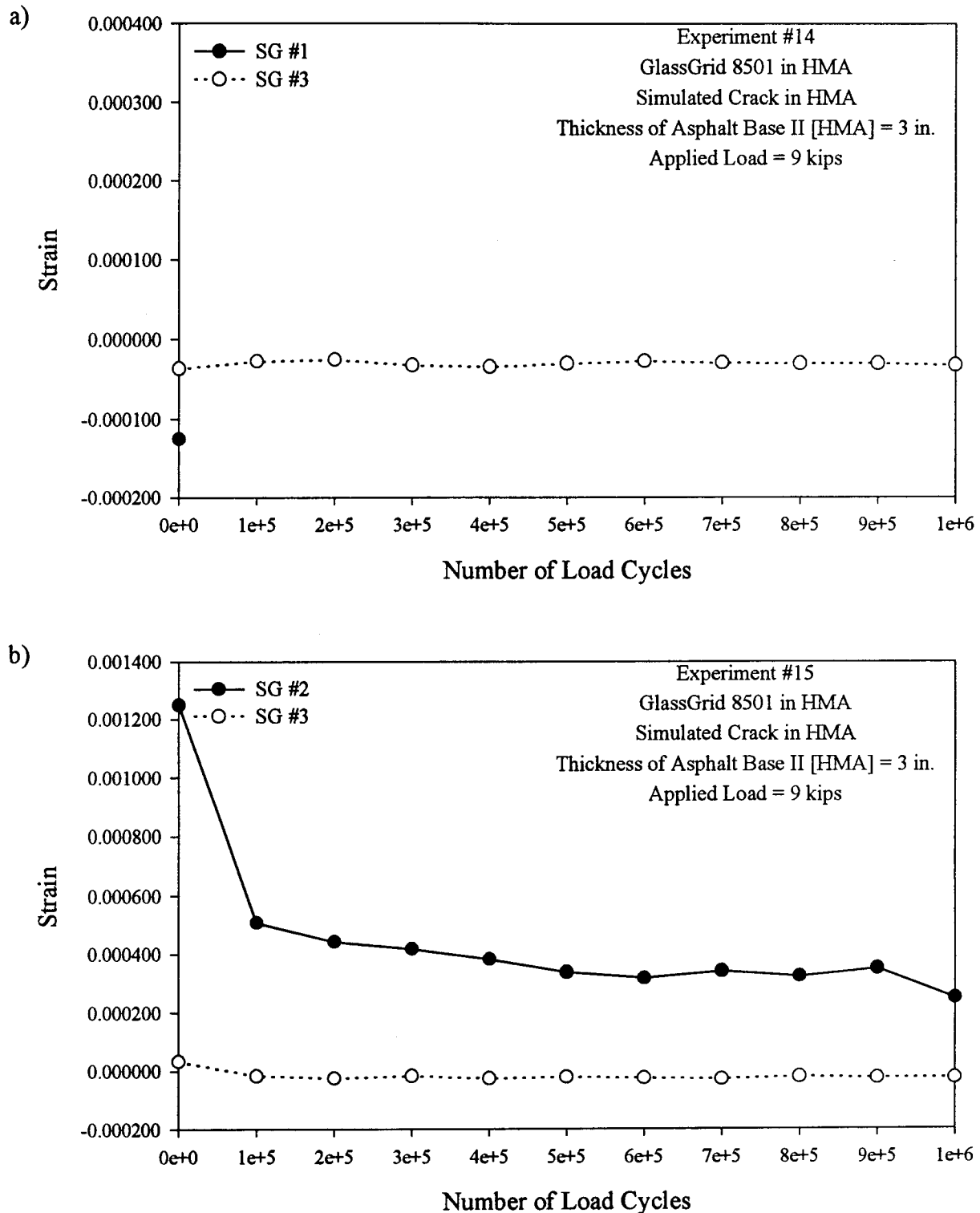


Figure 4-36: Variation of Strain with Number of Load Cycles for Singly Reinforced Test Sections with a Simulated Crack
a) Experiment #14
b) Experiment #15

were very low (ranged between 0.000034 at 0 (zero) load cycles and -0.000028 at 700,000 load cycles) and steady throughout the experiment [Figure 4-36 (b)].

Figure 4-37 shows the variation of strain at gages #2 and #3 for Experiment #20 where the thickness of the HMA was 2.5 inches (63.5 mm). Strain measurement at gage #3 was again consistent with that of other experiments and the measurements were very low (ranging between -0.000032 at 600,000 load cycles and -0.000025 at 1,000,000 load cycles). The results for gage #3 were also steady throughout the experiment. Inconsistent with Experiments #9 and #15, however, strain measurements at gage #2 were in compression and fluctuated throughout the experiment as shown in Figure 4-37.

Strain versus applied load for Experiment #9 corresponding to different static load applications is presented in Figures 4-38 (a) and (b). As can be seen from Figure 4-38 (a), the strain at gage #1 did not increase linearly during the initial static loading while the strain at the same place during the static loading after 100,000 load cycles increased in a linear manner as shown in Figure 4-38 (b). Similar behavior is observed between strain measurements at gage #2 for two different load applications [Figures 4-38 (a) and (b)]. In Figure 4-38 (a), the strain at gage #2 showed some linearity when increasing static load at 0 (zero) load cycles. However, at 100,000 load cycles the strain at gage #2 increased up to a load of 4 kips (18 kN) and then decreased as shown in Figure 4-38 (b). Again strain measurements for gage #3 were consistent throughout the load applications [Figures 4-38 (a) and (b)].

The following comments are presented for the strain gages embedded on the glass grid reinforcement:

- Despite the attempt to measure strain at gage #1, strain measurement at this location was

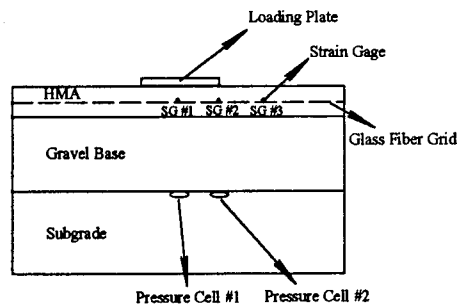
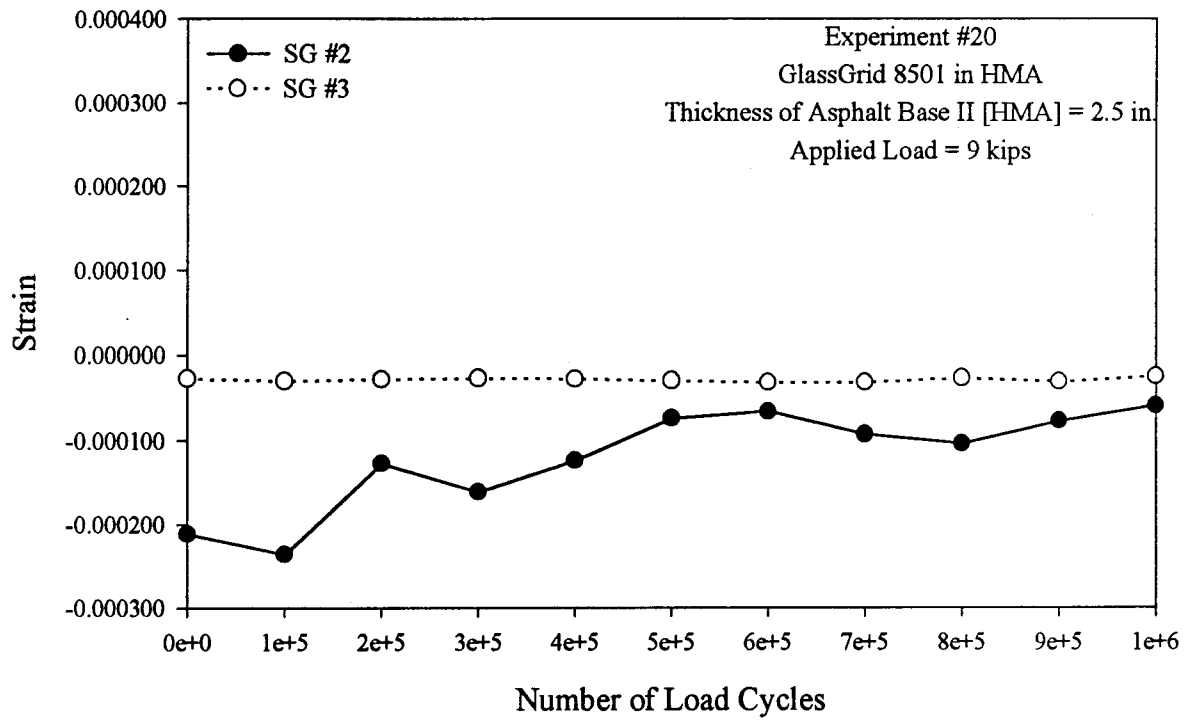


Figure 4-37: Variation of Strain with Number of Load Cycles for Experiment #20

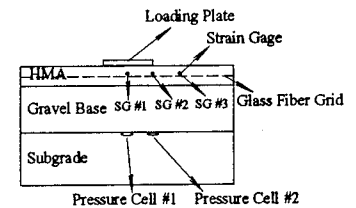
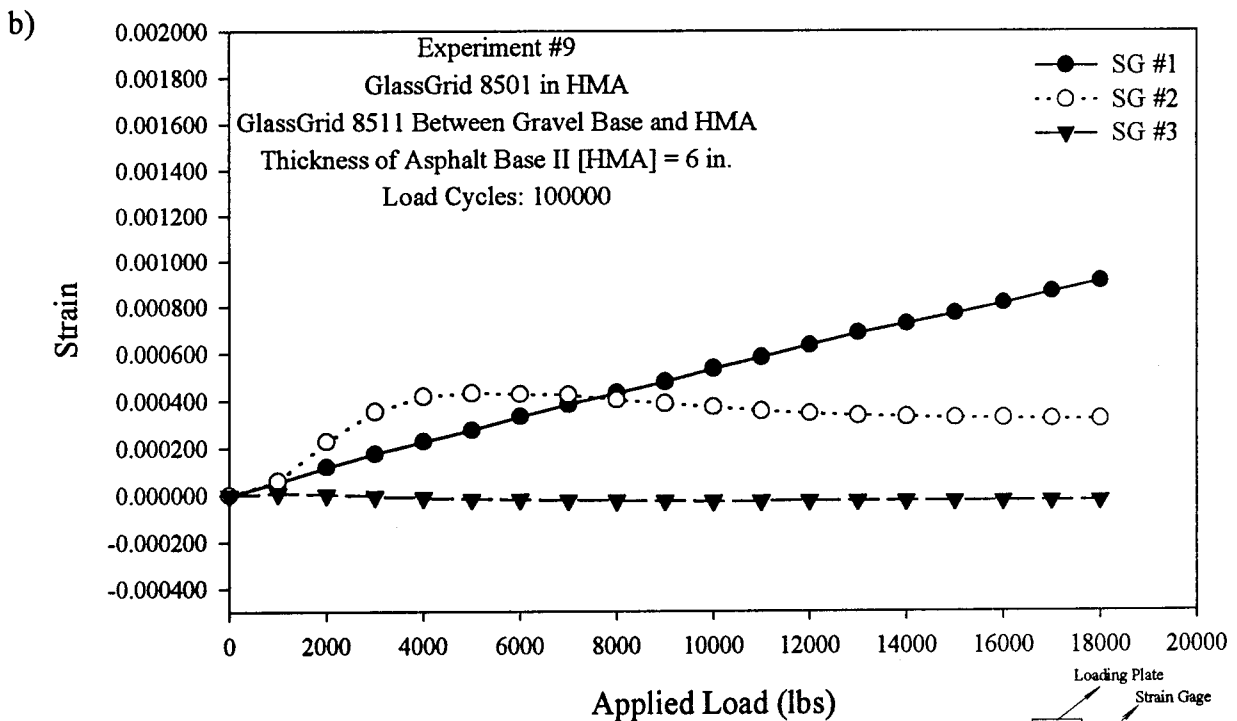
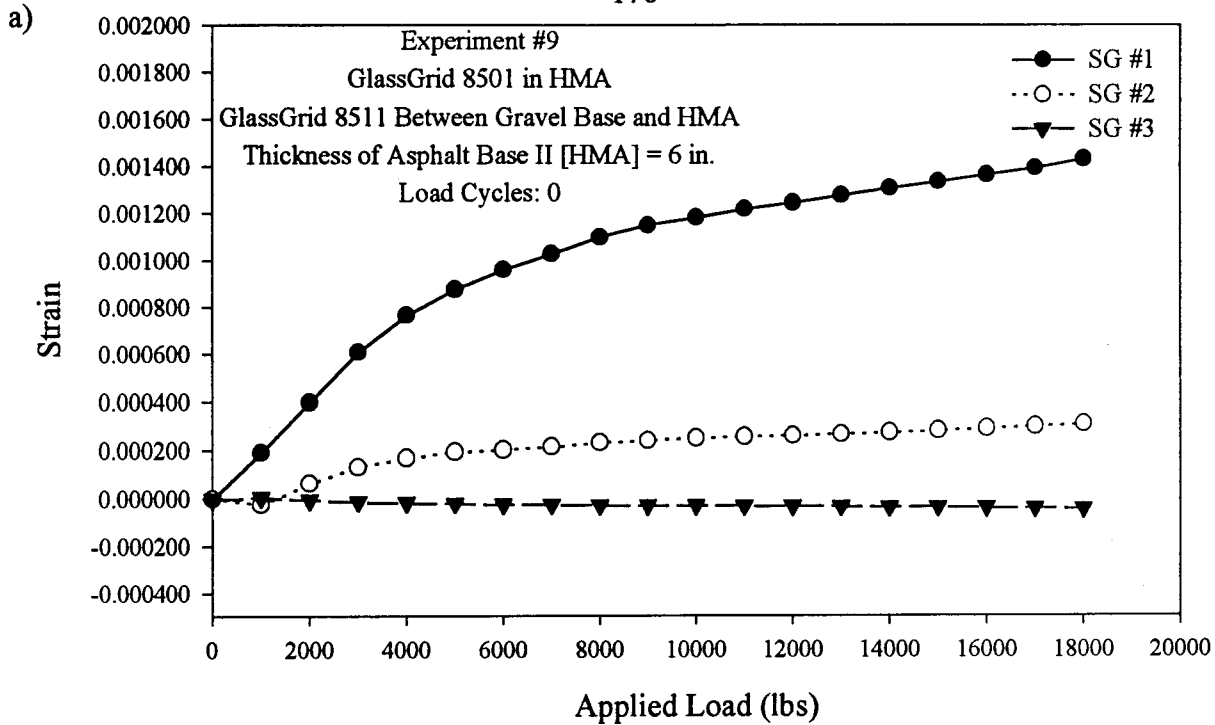


Figure 4-38: Variation of Strain with Applied Load for Experiment #9

a) Number of Load Cycles: 0

b) Number of Load Cycles: 100,000

possible only in one experiment due to failures in strain gages.

- The results showed some inconsistencies among the strain measurements at gage #2 for different experiments. Therefore, it can be stated that based on the available data, firm conclusions cannot be reached about the variation of strain on glass grid.
- Strain measurements at gage #3 gave consistent results for each experiment. Strain measurements on the glass grid, laterally 12 inches (305 mm) away from the center of the loading plate and in the middle depth of the HMA, were in compression, very low, and varied steady with the applied load.

Due to limited strain data and uncertainty of the strain measurements presented herein, no conclusions can be made on the basis of strain measurements. The computed strains and their comparisons with measurements are presented in the next chapter.

CHAPTER 5

RESULTS OF COMPUTER ANALYSES

A series of computer analyses was performed to analyze flexible pavement sections subjected to moving loads using the KENLAYER [Huang (1993)] computer program and the Finite Element Method (FEM). Throughout the KENLAYER analyses, the top asphalt layer (HMA) and the glass grid layer were considered as linear visco-elastic layers, while the remaining layers (gravel base, subgrade, and geotextile) were considered as a linear elastic layers. Also, in some cases the glass grid layer was considered as a linear elastic material since glass grid has very low (or none) creep characteristics. This study was done to investigate the effect of glass fiber grid inside the hot mix asphalt on pavement response. Linear elastic analysis was also performed by using the finite element method (FEM).

5.1 DESCRIPTION OF KENLAYER COMPUTER PROGRAM

The KENLAYER computer program was written in Fortran 77 by Huang (1993). This program can be used to analyze elastic multi-layer systems under a circular loaded area and the result can be superimposed for multiple wheels, such as single, dual-tandem, and dual-tridem. Each layer may be considered to behave differently (linear elastic, non-linear elastic, and/or visco-elastic). To evaluate the design life of a pavement system, damage analysis caused by fatigue cracking and rutting may be performed by selecting different material properties for different periods in a year. The KENLAYER program for stress analysis in a multi-layer system is based on the theory of elasticity [Huang (1993)]. In the solution of axisymmetric problems in the theory of elasticity, the conventional approach is to assume a stress function that satisfies the governing differential equations and

boundary conditions where the stresses and displacements can be determined [Huang (1993) and Timoshenko and Goodier (1987)]. The geometry of the flexible pavement system with an n-layer system in cylindrical coordinates is shown in Figure 5-1.

From the theory of elasticity, the governing equation may be written as [Huang (1993) and Timoshenko and Goodier (1987)]:

$$\nabla^4 \phi = 0 \quad (5.1)$$

where ϕ is the stress function. For an axisymmetric case, the stresses and displacements are determined as follows [Huang (1993)]:

$$\sigma_z = \frac{\partial}{\partial z} \left[(2-\nu) \nabla^2 \phi - \frac{\partial^2 \phi}{\partial z^2} \right] \quad (5.2)$$

$$\sigma_r = \frac{\partial}{\partial z} \left[\nu \nabla^2 \phi - \frac{\partial^2 \phi}{\partial r^2} \right] \quad (5.3)$$

$$\sigma_t = \frac{\partial}{\partial z} \left[\nu \nabla^2 \phi - \frac{1}{r} \frac{\partial \phi}{\partial r} \right] \quad (5.4)$$

$$\tau_{rz} = \frac{\partial}{\partial r} \left[(1-\nu) \nabla^2 \phi - \frac{\partial^2 \phi}{\partial z^2} \right] \quad (5.5)$$

$$w = \frac{1+\nu}{E} \left[(1-2\nu) \nabla^2 \phi + \frac{\partial^2 \phi}{\partial r^2} + \frac{1}{r} \frac{\partial \phi}{\partial r} \right] \quad (5.6)$$

$$u = -\frac{1+\nu}{E} \left(\frac{\partial^2 \phi}{\partial r \partial z} \right) \quad (5.7)$$

where,

r	= Radial coordinate,
z	= Vertical coordinate,
σ_z	= Vertical stress,
σ_r	= Radial stress,
σ_t	= Tangential stress,
τ_{rz}	= Shear stress,
w	= Displacement in the vertical (z) direction,
u	= Displacement in the radial (r) direction,
E	= Elastic modulus.

5.1.1 Moving Load Analysis

In the KENLAYER analysis, stresses and displacements caused by moving loads were considered. The intensity of the moving load varies with time as described by the haversine function, which is illustrated in Figure 5-2. The equation used in the KENLAYER computer program for calculating the moving load is expressed by:

$$L(t) = q \sin^2 \left(\frac{\pi}{2} + \frac{\pi t}{d} \right) \quad (5.8)$$

where,

d	= Duration of load,
q	= Applied load,
t	= Time,
$L(t)$	= Load function.

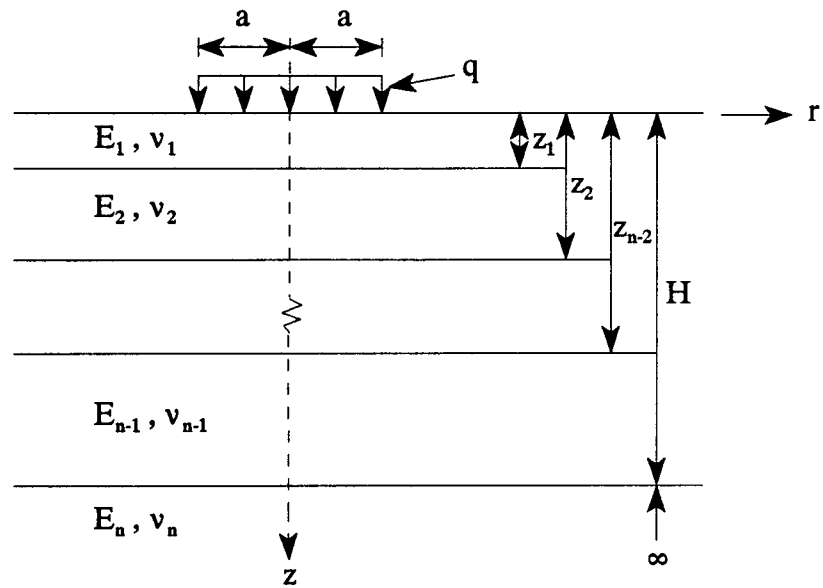


Figure 5-1: A Multilayer System in Cylindrical Coordinates [Huang (1993)]

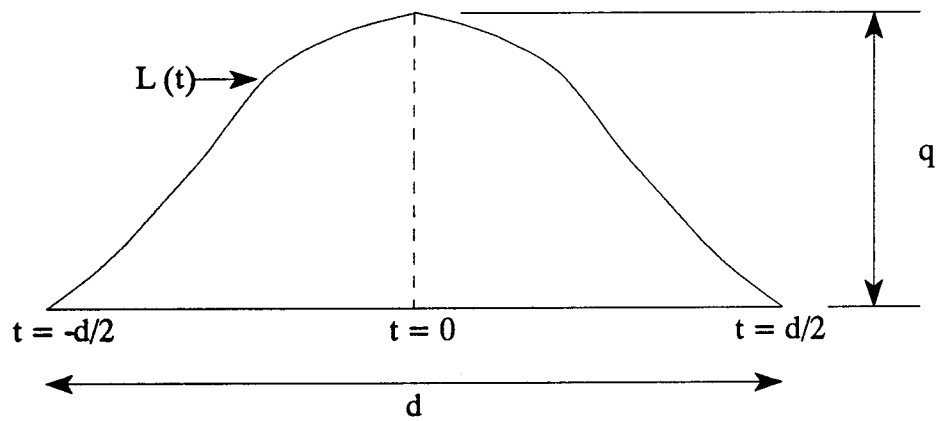


Figure 5-2: Moving Load as a Function of Time [Huang (1993)]

5.1.2 Creep Compliance Analysis

The creep compliance values are required to determine the linear visco-elastic properties of the hot mix asphalt (HMA). The creep compliance at various times is defined as [Huang (1993) and Yoder and Witczak (1975)]:

$$D(t) = \frac{\epsilon(t)}{\sigma} \quad (5.9)$$

where, $\epsilon(t)$ = time dependent strain
 σ = constant stress

The equation for creep compliance in general terms has been expressed as [Huang (1993)]

$$D(t) = \sum_{i=1}^n G_i \exp\left(-\frac{t}{T_i}\right) \quad (5.10)$$

and

$$G_i = -\frac{1}{E_i} \quad (5.11)$$

where, D = Creep compliance
 E = Elastic modulus,
 G = Unknown coefficient for creep compliance,
 T = Time duration (Retardation time),
 t = Time.

As reported in the literature [Huang (1993)], the creep compliances at a reference temperature obtained from creep tests are usually measured at 11 different time durations of 0.001, 0.003, 0.01, 0.03, 0.1, 0.3, 1, 3, 10, 30, and 100 seconds. However, any number of time durations may be used.

In KENLAYER [Huang (1993)] computer program, retardation times (T_i) of 0.01, 0.03, 0.1, 1, 10, 30, and ∞ (infinity) seconds are used for visco-elastic materials. The unknown coefficients of (G_i) and the creep compliances can be computed using Equations (5.10) and (5.11).

5.1.3 Damage Analysis

In the KENLAYER [Huang (1993)] computer program, damage analysis is based on two failure criteria: fatigue cracking and permanent deformation. The equation used to find out the allowable number of load repetition to prevent fatigue cracking is:

$$N_f = f_1 (\epsilon_t)^{-f_2} (E_1)^{-f_3} \quad (5.12)$$

where, N_f = Allowable number of load repetitions,
 ϵ_t = Horizontal tensile strain at the bottom of asphalt layer,
 E_1 = Elastic modulus of asphalt layer,
 f_1, f_2, f_3 = Constants determined from laboratory tests.

The values for these constants as recommended by the Asphalt Institute (AI) are 0.0796, 3.291 and 0.854 for f_1 , f_2 , and f_3 , respectively.

The equation used to find out the allowable number of load repetition to prevent rutting (permanent deformation) is:

$$N_d = f_4 (\epsilon_c)^{-f_5} \quad (5.13)$$

where, N_d = Allowable number of load repetitions,
 ϵ_c = Vertical compressive strain on top of subgrade,
 f_4, f_5 = Constants determined from road tests or field performance.

The values for these constants as recommended by the Asphalt Institute are 1.365×10^{-9} and 4.477 for f_4 and f_5 , respectively.

In KENLAYER, the damage ratio (D_r) is defined as the ratio between predicted and allowable number of load repetitions. The inverse of the damage ratio is defined as the design life of the pavement system. Based on an evaluation of failure criteria, fatigue cracking and rutting (permanent deformation), the design life is established as the shorter life of the two criteria.

5.2 COMPUTER ANALYSIS OF TEST SECTIONS

In this research study, the KENLAYER computer program was used with layered systems under a circular load with top asphalt layer and glass grid layer having visco-elastic characteristics and the remaining layers having linear elastic behavior. The creep compliance values of visco-elastic layers need to be specified in the computer analysis. The creep compliance values at various time durations under a reference temperature of 77 °F (25 °C) in a visco-elastic material (HMA) were obtained from the literature [Smith et al. (1995)] for the computer analysis. These values are listed in Table 5-1.

For the test sections considered in this study, the maximum applied load on the HMA surface was 9 kips (40 kN), generating a tire pressure (contact pressure) of 80 psi (551 kN/m²) through the 12 inches (305 mm) diameter loading plate. During the static loading, the maximum applied load was 18 kips (80 kN). For the computer analysis, one dual wheel of the standard 18 kips (80 kN) single axle load with a contact pressure of 80 psi (551 kN) was considered. The radius of the contact area of the tire was 6 inches (152 mm). For the test sections, since the frequency of sinusoidal dynamic load was 1.2 Hz, the duration of the load was selected as 0.83 seconds in the computer analysis.

In these analyses, damage and environmental effects were not addressed. Based on boundary conditions, the layers were assumed to be infinite in the lateral direction and finite in the vertical

direction except the last (deepest) layer. The last layer was assumed to be infinite in both the lateral and vertical directions. Throughout these analyses the elastic modulus of the HMA was kept constant while the elastic moduli of the remaining layers were varied. These elastic moduli were assumed on the basis of the values established by the Kentucky Highway Department [Yoder and Witczak (1975)]. Values for Poisson's ratio were assumed on the basis of data reported by Smith et al. (1995). The material properties used in the linear visco-elastic analyses are reported in Table 5-2. The material properties for the non-reinforced cases are the same as shown in Table 5-2.

The analyses were carried out for the reinforced and non-reinforced sections. KENLAYER [Huang (1993)] does not have the capability of including geosynthetic materials in the analyses. In this study, the glass grid reinforcement was simulated by including a very thin layer [0.039-inch (1 mm)] inside the hot mix asphalt. A similar procedure was used to model the geosynthetic layer between the gravel base and the subgrade. Results of the computer analyses corresponding to the two sections (i.e. reinforced section and non-reinforced section) are presented below.

Table 5-1: Creep Compliance Values for HMA [Smith et al. (1995)]

Loading Time (seconds)	Creep Compliance (in ² /lb)
0.001	1.632 E-06
0.003	2.209 E-06
0.01	3.078 E-06
0.03	4.166 E-06
0.1	5.803 E-06
0.3	7.854 E-06
1	1.094 E-05
3	1.481 E-05
10	2.063 E-05
30	2.792 E-05
100	3.89 E-05

Table 5-2: Assumed Material Properties Used in the Computer Analyses

Layer	Elastic Modulus (E) - psi			ν Poisson's Ratio
	Lower Bound Values (Case 1)	Mean Values (Case 2)	Upper Bound Values (Case 3)	
Hot Mix Asphalt (HMA)	270,000	270,000	270,000	0.35
Gravel Base	32,400	46,000	60,000	0.30
Subgrade	3,000	6,000	12,000	0.30
Glass Fiber Grid	4,205,000	4,205,000	4,205,000	0.35
Geotextile	100	100	100	0.30

Note: 1 lb = 4.45 N
1 inch = 25 mm

5.3 COMPUTER ANALYSES OF VERTICAL STRESS

In this section, the variation of predicted vertical stress with depth was investigated. Additionally, computed vertical subgrade stresses were compared with measured stresses corresponding to HMA layer thicknesses of 3 inches (76 mm) and 6 inches (152 mm). Results of the computed vertical stresses are shown in subsequent sections. In this analysis, the glass grid layer was considered as a visco-elastic layer, like the hot mix asphalt, and very low creep compliance values ($0.1 \text{ E-}07$) were assigned to the glass grid layer for each creep time interval. Unlike the asphalt layer, the glass grid has very low, if any, creep characteristics. The remaining layers (gravel base, subgrade, and geotextile) were considered as linear elastic.

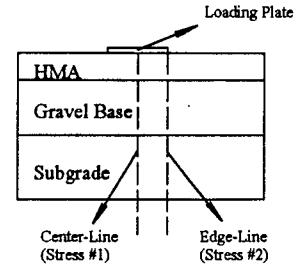
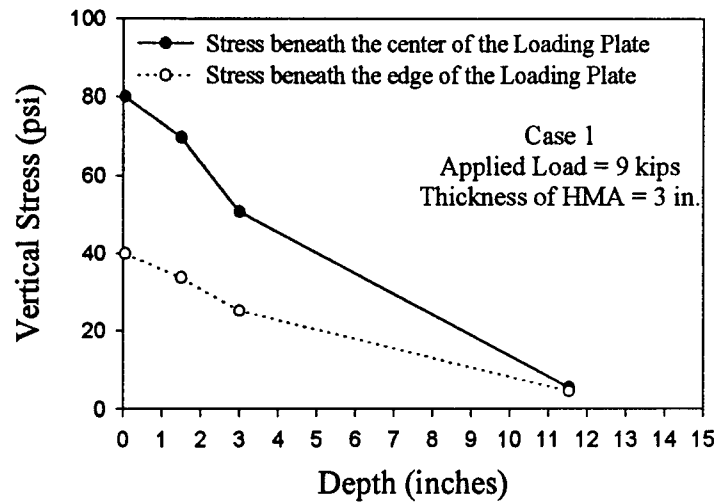
5.3.1 Predicted Vertical Stress Variation With Depth

Figures 5-3 (a), (b), and (c) show the variation of predicted vertical stress with depth for a reinforced thin asphalt section corresponding to three different cases (Case 1, Case 2, and Case 3) of material properties, which are listed in Table 5-2. Case 1 represents the chosen lower bound values, Case 3 represents the chosen upper bound values, and Case 2 represents the chosen mean values of properties used in these computer analyses. The applied load was 9 kips (40 kN) in all of these cases. In Figures 5-3 and 5-4, variation of vertical stress beneath the center of the loading plate (at the center-line) is referred as stress #1, while stress beneath the edge of the loading plate (at the edge-line) is referred as stress #2. As shown in Figures 5-3 (a), (b), and (c), the computed vertical stresses for the thin reinforced pavement section under a circular loading area decreased substantially with depth. For example, beneath the center of the loading plate (stress #1), the computed vertical stress in a thin reinforced pavement section corresponding to the Case 2 was 55.43 psi at the HMA/gravel-base interface, while the vertical stress was 6.65 psi on top of subgrade [Figure 5-3 (b)]

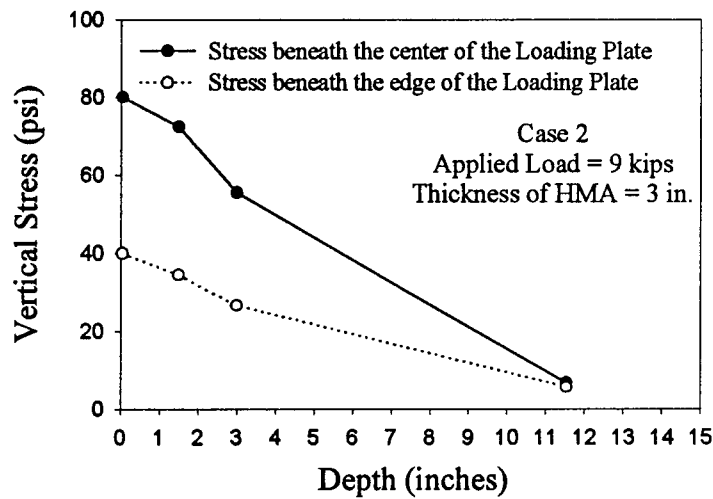
(Table 5-3). The differences between the computed stresses beneath the center of the loading plate (stress #1) and beneath the edge of the loading plate (stress #2) were significant on the HMA surface and the HMA/gravel-base interface. The stresses at both places (center-line and edge-line) on top of the subgrade were similar in each case (Case 1, Case 2, and Case 3). The variation of predicted stress at the center-line (stress #1) was almost twice as that at the edge-line (stress #2) up to the interface between the gravel base and the HMA for each case [Figures 5-3 (a), (b), and (c)] (Table 5-3).

Figures 5-4 (a), (b), and (c) show the variation of computed vertical stress (stress #1) beneath the center of the loading plate for reinforced sections. Figure 5-4 (a) corresponds to a thin pavement section where the asphalt thickness is 3 inches (76 mm) (Table 5-3). Figure 5-4 (b) shows similar results for a thicker pavement section where the asphalt thickness is 6 inches (152 mm) (Table 5-4). Comparison of the variation of vertical stresses beneath the center of the loading plate (stress #1) for the thin pavement section and the thick pavement section corresponding to Case 2 is shown in Figure 5-4 (c) and Table 5-5. This figure shows the influence of HMA layer thickness on vertical stress. As shown in Table 5-5, beneath the center of the loading plate (stress #1), the vertical stress [55.43 psi (381.91 kN/m²)] at the gravel base/HMA interface for the thin pavement section was higher than the vertical stress [27.27 psi (187.89 kN/m²)] at the same interface for the thick pavement section. The vertical stress on top of subgrade was 6.65 psi (45.82 kN/m²) for the thin pavement section, while it was 4.10 psi (28.25 kN/m²) for the thick pavement section [Figure 5-4 (c)] (Table 5-5). These computed results (Table 5-5) show that the vertical stress in the thin pavement section was almost double the stress in the thick pavement section at the HMA/gravel base interface, and the vertical stress in the thin section was almost 1.6 times the stress in the thick pavement section on top of subgrade. Based on these predicted results, increasing the HMA layer thickness from 3 inches (76

a)



b)



c)

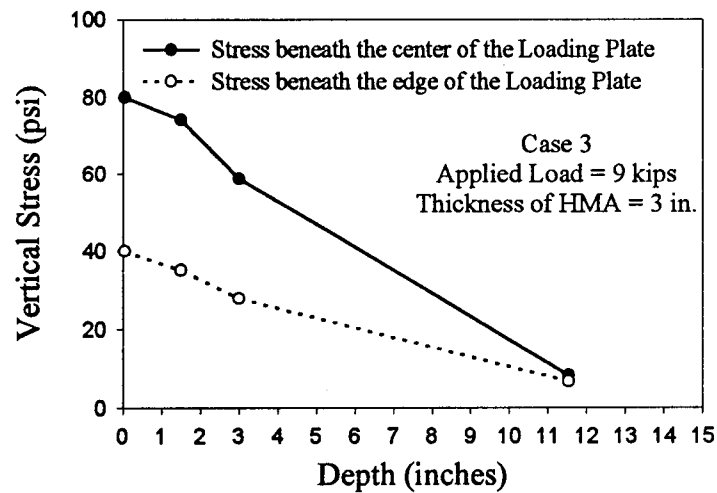


Figure 5-3: Variation of Predicted Vertical Stress with Depth for a Thin Asphalt Section with Reinforcement

- a) Case 1
- b) Case 2
- c) Case 3

Table 5-3: Computed Vertical Stresses for Thin Pavement Section [Thickness of HMA = 3 inches (76 mm)] with Reinforcement

Depth (inch) [mm]	Case 1		Case 2		Case 3	
	Vertical Subgrade Stress (Center- Line) Stress #1 (psi) [kN/m ²]	Vertical Subgrade Stress (Edge- Line) Stress #2 (psi) [kN/m ²]	Vertical Subgrade Stress (Center- Line) Stress #1 (psi) [kN/m ²]	Vertical Subgrade Stress (Edge- Line) Stress #2 (psi) [kN/m ²]	Vertical Subgrade Stress (Center- Line) Stress #1 (psi) [kN/m ²]	Vertical Subgrade Stress (Edge- Line) Stress #2 (psi) [kN/m ²]
0	80.00 [551]	39.93 [275.12]	80.00 [551]	39.93 [275.12]	80.00 [551]	39.93 [275.12]
1.5 [38.1]	69.79 [480.85]	33.68 [232.06]	72.47 [499.31]	34.48 [237.57]	74.22 [511.38]	34.99 [241.08]
3 [76]	50.69 [349.25]	25.12 [173.08]	55.43 [381.91]	26.68 [183.83]	58.72 [404.58]	27.81 [191.61]
11.5 [292.1]	5.35 [36.86]	4.50 [31.05]	6.65 [45.82]	5.50 [37.90]	8.20 [56.50]	6.71 [46.23]

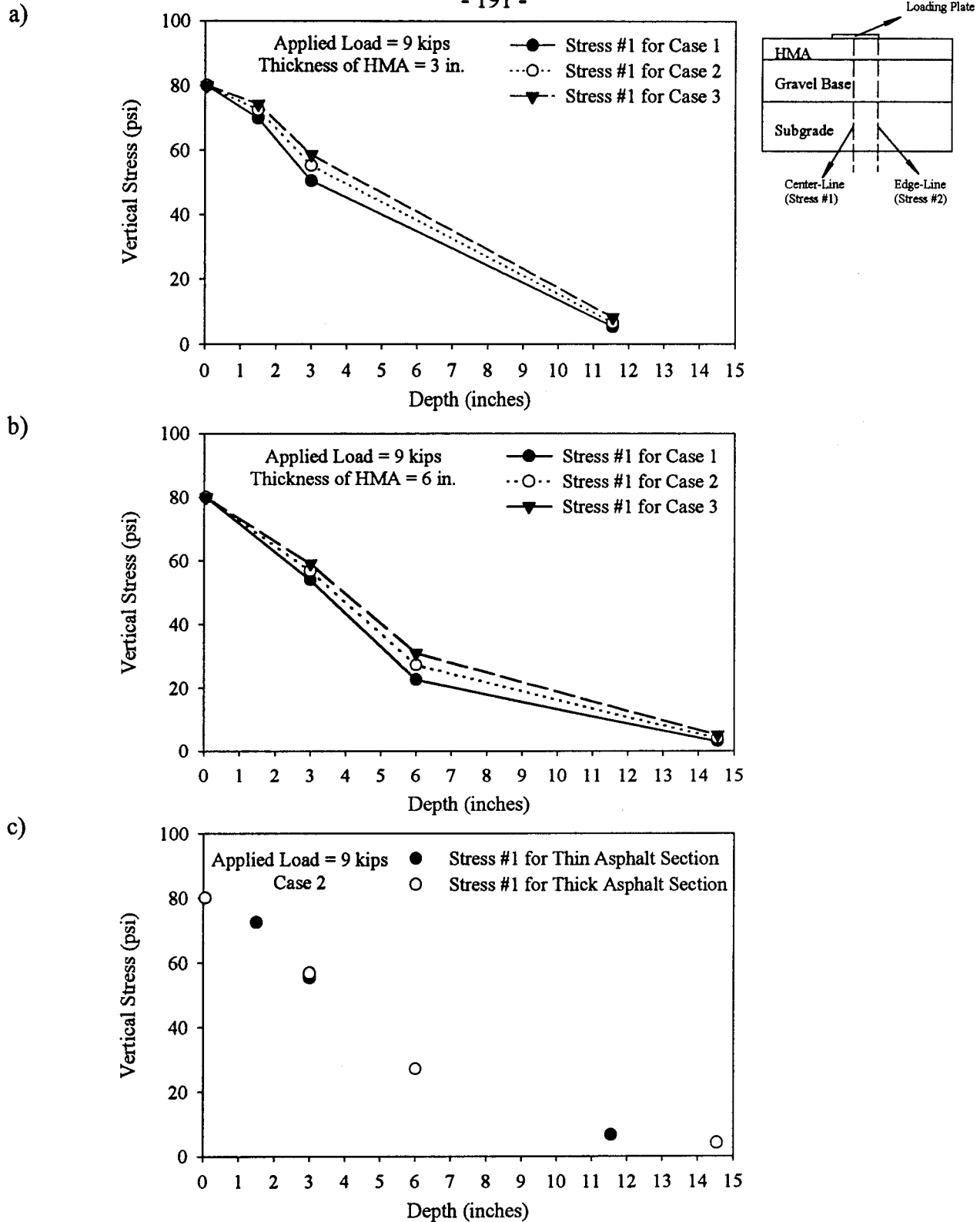


Figure 5-4: Variation of Predicted Vertical Stress Beneath the Center of the Loading Area in a Reinforced Pavement Section

- a) Comparison of Case 1, Case 2, and Case 3 (Thickness of HMA = 3-inch)
- b) Comparison of Case 1, Case 2, and Case 3 (Thickness of HMA = 6-inch)
- c) Comparison of Thin and Thick Asphalt Sections (Case 2)

Table 5-4: Computed Vertical Stresses beneath the Center of the Loading Plate for Thick Pavement Section [Thickness of HMA = 6 inches (152 mm)] with Reinforcement

Depth (inch) [mm]	Vertical Subgrade Stress at Center-Line (Stress #1) (psi) [kN/m ²]		
	Case 1	Case 2	Case 3
0	80.00 [551]	80.00 [551]	80.00 [551]
3 [76]	54.00 [372.06]	56.84 [391.63]	59.04 [406.79]
6 [152]	22.67 [156.20]	27.27 [187.89]	31.07 [214.07]
14.5 [368.3]	3.13 [21.57]	4.10 [28.25]	5.29 [36.45]

Table 5-5: Computed Vertical Stresses Beneath the Center of the Loading Plate (Stress #1) Corresponding to Case 2 for Two Different HMA Layer Thicknesses

Depth	Thick Pavement Section Case 2 Vertical Stress at Center-Line (Stress #1) (psi) [kN/m ²]	Thin Pavement Section Case 2 Vertical Stress at Center-Line (Stress #1) (psi) [kN/m ²]
On the Surface of HMA	80.00 [551]	80.00 [551]
Interface Between the HMA and the Gravel Base	27.27 [187.89]	55.43 [381.91]
Interface Between the Gravel Base and the Subgrade	4.10 [28.25]	6.65 [45.82]

mm) to 6 inches (152 mm) reduces the vertical stresses substantially at lower depths inside the pavement system. At higher depths, the vertical stresses are almost similar for different HMA layer thicknesses.

5.3.2 Comparison Of Measured And Predicted Vertical Subgrade Stresses In A 6-Inch (152 mm) Thick Asphalt Section

Figures 5-5 and 5-6 show the comparison between the experimentally measured and computed (predicted) vertical stresses in two similar thick reinforced pavement sections [thickness of HMA = 6 inches (152 mm)]. Figures 5-5 (a) and (b) show a comparison of the vertical subgrade stresses at cells #1 and #2. The computed stresses corresponding to lower and upper bound material properties (Case 1 and Case 3) are included in these figures. Vertical subgrade stress beneath the center of the loading plate (area) is shown in Figure 5-5 (a), while the vertical subgrade stress beneath the edge of the loading plate (area) is shown in Figure 5-5 (b). The measured stresses at cell #1 in the reinforced 6 inches (152 mm) thick pavement sections (Experiments #3 and #5) at 500,000 cycles were within the range of the computed stresses for lower and upper bound material properties (Case 1 and Case 3). The measured and computed stresses for Experiments #3 and #5 are shown in Table 5-6. Based on these results and as shown in Figure 5-5 (a), measured stresses at cell #1 for reinforced 6-inch (152 mm) thick pavement sections (Experiments #3 and #5) at 500,000 cycles were within the range of computed stresses corresponding to lower and upper bound values (Case 1 and Case 3) of material properties.

The measured vertical stresses at cell #2 for 6-inch (152 mm) thick pavement sections (Experiments #3 and #5) were not within the range of the computed stresses obtained by lower and upper bound material properties (Case 1 and Case 3) [Figure 5-5 (b)]. For example, under the applied

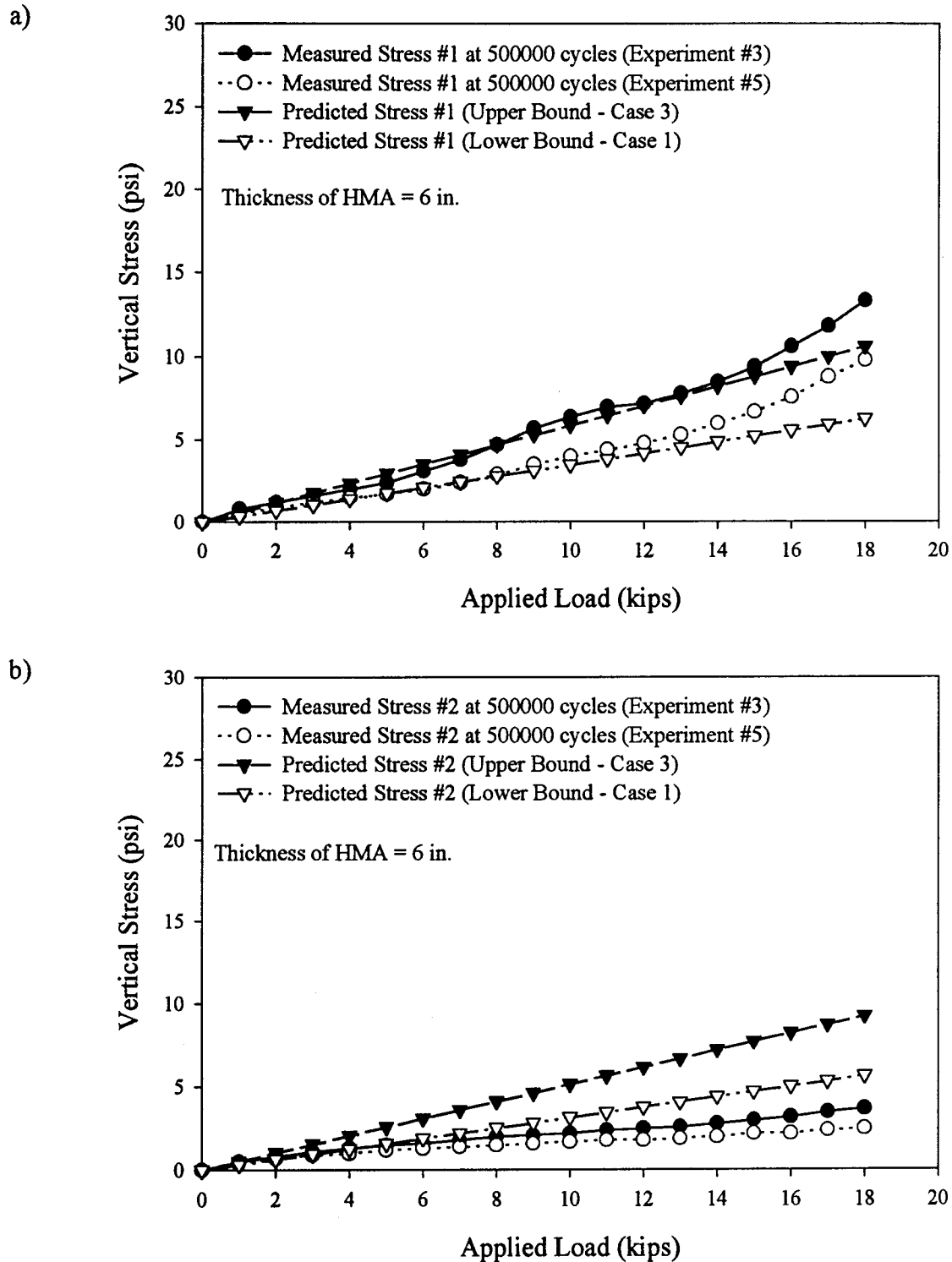


Figure 5-5: Measured and Predicted Upper and Lower Bound Vertical Stresses in a 6-inch (152 mm) Thick Asphalt Section with Reinforcement
a) Stress Beneath the Center of the Loading Area
b) Stress Beneath the Edge of the Loading Area

Table 5-6: Measured and Computed Vertical Subgrade Stresses at Cells #1 and #2 for 6-inch (152 mm) Thick Pavement Sections

	Vertical Subgrade Stress (psi) [kN/m ²] Cell #1		Vertical Subgrade Stress (psi) [kN/m ²] Cell #2	
Applied Load (kip) [kN] →	9 [40]	18 [80]	9 [40]	18 [80]
Measured Stress (Experiment #3)	5.70 [39.27]	13.30 [91.64]	2.08 [14.33]	3.66 [25.22]
Measured Stress (Experiment #5)	3.50 [24.12]	9.80 [67.52]	1.58 [10.89]	2.47 [17.02]
Computed Stress (Case 1)	3.13 [21.57]	6.27 [43.20]	2.81 [19.36]	5.62 [38.72]
Computed Stress (Case 2)	4.10 [28.25]	8.21 [56.57]	3.62 [24.94]	7.24 [49.88]
Computed Stress (Case 3)	5.28 [36.38]	10.59 [72.97]	4.61 [31.76]	9.22 [63.53]

load of 9 kips (40 kN) at 500,000 cycles, measured stress at cell #2 for the pavement section in Experiment #3 was 2.08 psi [14.33 kN/m^2] while the computed (predicted) stresses at cell #2 were 4.61 psi [31.76 kN/m^2] for the upper bound values (Case 3), and 2.81 psi [19.36 kN/m^2] for the lower bound values (Case 1) [Figure 5-5 (b)] (Table 5-6).

Figures 5-6 (a) and (b) show the comparison of measured with computed vertical subgrade stresses (under 9 kips (40 kN) of loading) corresponding to mean values of material properties (Case 2) in reinforced 6-inch (152 mm) thick pavement sections. Figure 5-6 (a) shows the measured vertical subgrade stresses at 500,000 cycles (Experiments #3 and #5) and the computed vertical subgrade stress beneath the center of the loading plate (cell #1). The measured vertical subgrade stresses at cell #1 were 5.70 psi (39.27 kN/m^2) and 3.50 psi (24.12 kN/m^2) for Experiments #3 and #5, respectively. Under 9 kips (40 kN) of loading, computed stress at cell #1 was 4.10 psi (28.25 kN/m^2). Figure 5-6 (a) shows that the computed stress values at cell #1 compare reasonably well with measurements. On the other hand, the computed stresses at cell #2, as shown in Figure 5-6 (b), did not compare well with measurements (Experiments #3 and #5). Under 9 kips (40 kN) of loading, measured values at cell #2, 2.08 psi (14.33 kN/m^2) for Experiment #3 and 1.58 psi (10.89 kN/m^2) for Experiment #5, fell well below the computed stress of 3.62 psi (24.94 kN/m^2), as shown in Figure 5-6 (b) and Table 5-6.

Similar results are shown in Figures 5-7 (a) and (b) for a non-reinforced 6-inch (152 mm) thick pavement section. Under 9 kips (40 kN) of loading, measured vertical subgrade stress at cell #1 (4.95 psi [34.11 kN/m^2]) after 500,000 cycles for non-reinforced thick pavement section (Experiment #4) compares well with the computed vertical stress at cell #1 (4.17 psi [28.73 kN/m^2]) corresponding to Case 2 [Figure 5-7 (a)]. Under the applied load of 9 kips (40 kN), the difference between the measured vertical subgrade stress at cell #1 and the computed vertical subgrade stress

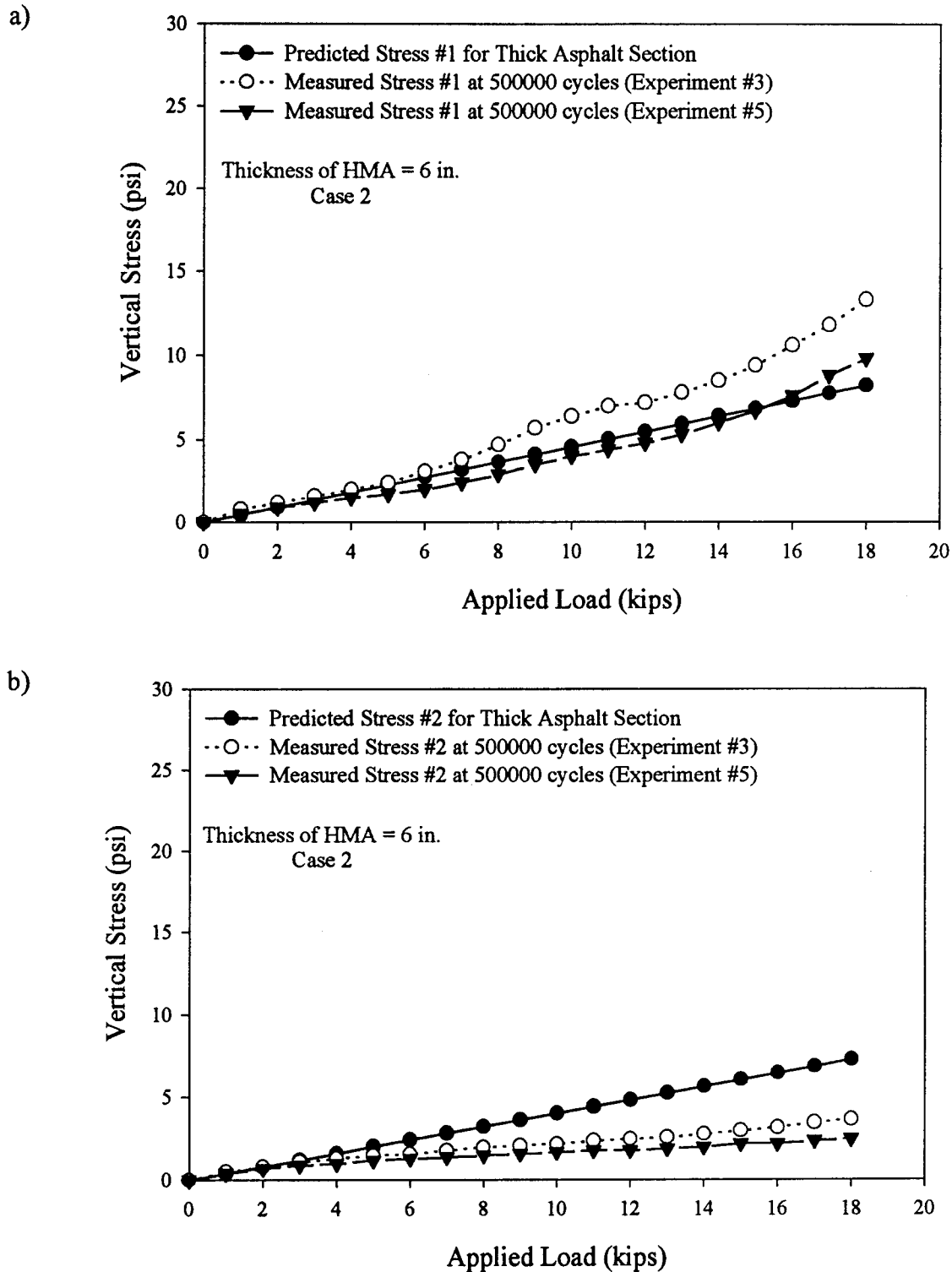
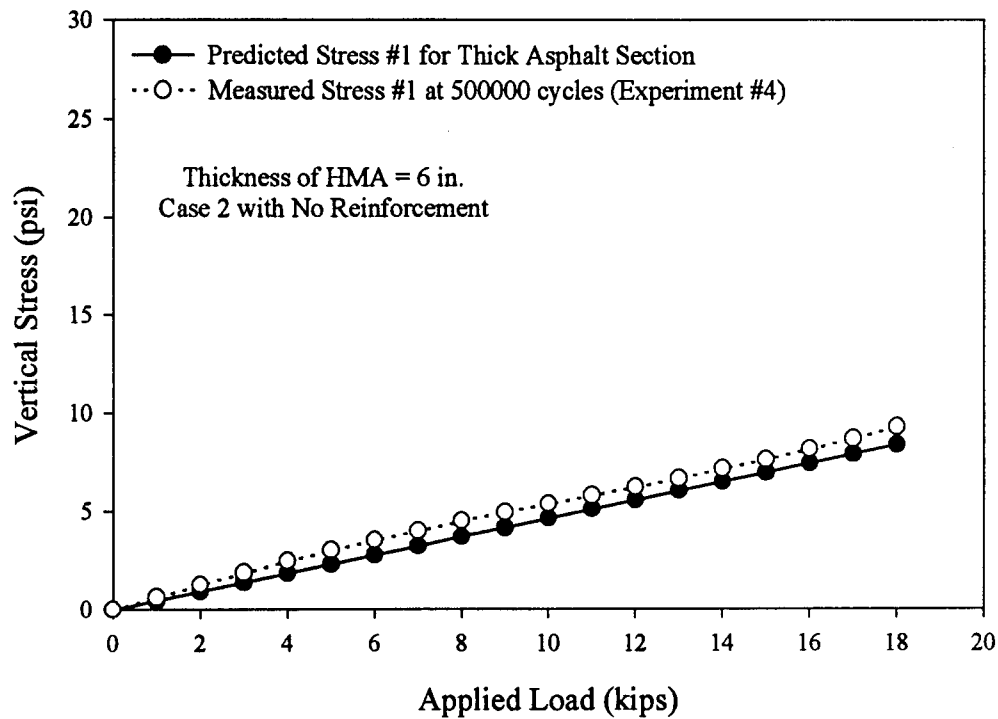


Figure 5-6: Measured and Predicted Vertical Stresses in a 6-inch (152 mm) Thick Asphalt Section with Reinforcement

a) Stress Beneath the Center of the Loading Area

b) Stress Beneath the Edge of the Loading Area

a)



b)

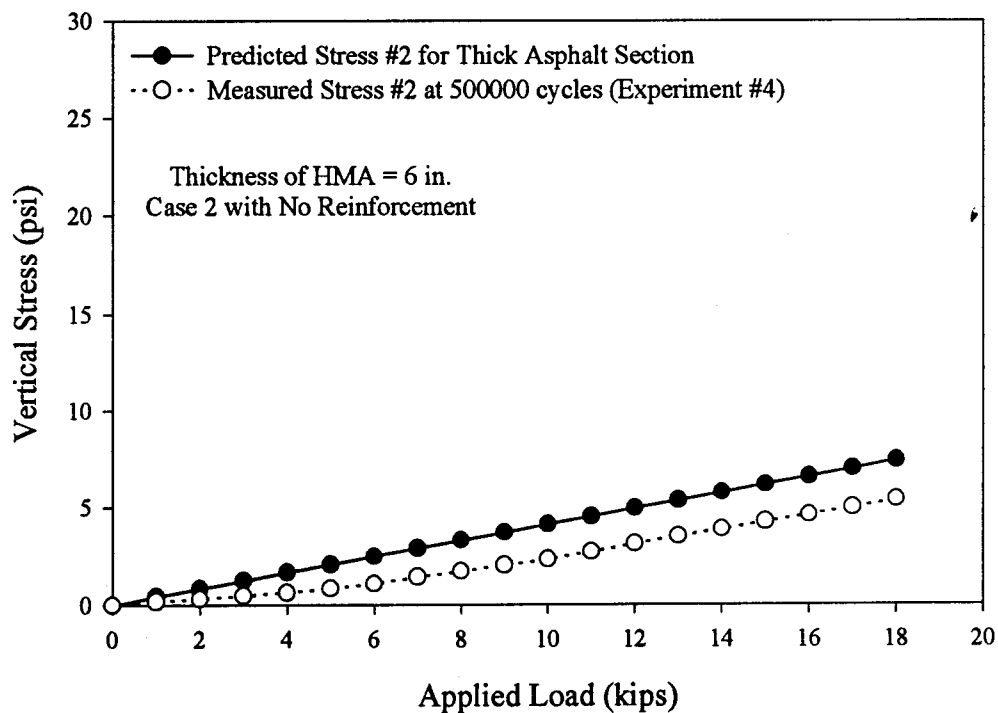


Figure 5-7: Measured and Predicted Vertical Stresses for a 6-inch (152 mm) Thick Asphalt Section with No Reinforcement
a) Stress Beneath the Center of the Loading Area
b) Stress Beneath the Edge of the Loading Area

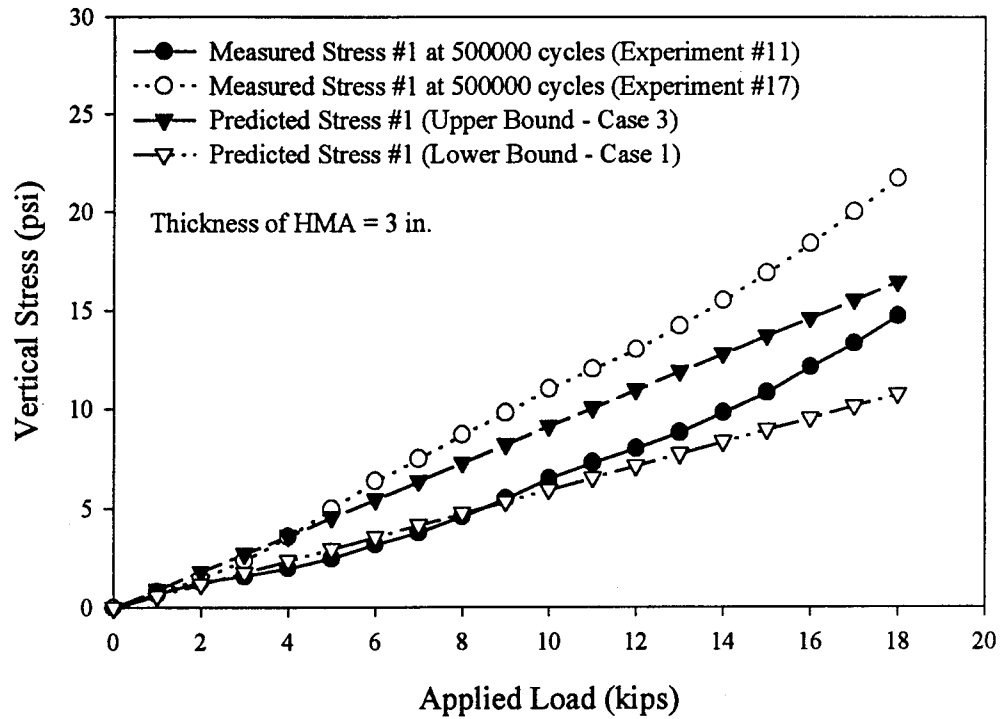
at cell #1 was 0.78 psi (5.37 kN/m²). The computed stress at cell #2 (3.70 psi [25.49 kN/m²]) did not compare well with the measurement (2.02 psi [13.92 kN/m²]) of the non-reinforced case, as shown in Figure 5-7 (b).

5.3.3 Comparison Of Measured And Predicted Vertical Subgrade Stresses In A 3-Inch (76 mm) Thick Asphalt Section

Figures 5-8 and 5-9 show the comparison between the measured vertical stresses and the computed (predicted) vertical stresses for thin reinforced pavement sections. Figures 5-8 (a) and (b) show the comparison of measured values and computed lower and upper bound values (Case 1 and Case 3) of vertical stresses. Figure 5-8 (a) shows the vertical subgrade stress beneath the center of the loading plate (stress at cell #1), and Figure 5-8 (b) shows the vertical subgrade stress at the edge of the loading plate (stress at cell #2). Under 9 kips (40 kN) of loading, computed vertical subgrade stresses at cell #1 were 5.35 psi (36.86 kN/m²) for Case 1 and 8.20 psi (56.50 kN/m²) for Case 3, respectively, while the measured values were 5.50 psi (37.90 kN/m²) and 9.80 psi (67.52 kN/m²) for Experiments #11 and #17, respectively [Figure 5-8 (a)]. Measured stress at cell #1 for one of the reinforced thin pavement sections (Experiment #11) at 500,000 cycles was within the range of the computed stresses for lower and upper bound values of material properties (Case 1 and Case 3). However, measured stress at cell #1 for the other reinforced thin pavement section (Experiment #17) was slightly higher than the computed stresses for the upper bound values of material properties (Case 3) [Figure 5-8 (a)].

The computed vertical subgrade stresses at cell #2 were higher than the measured vertical subgrade stresses as shown in Figure 5-8 (b). The measured stresses under the 9 kips (40 kN) and 18 kips (80 kN) of loading for Experiments #11 and #17, with the computed stresses corresponding

a)



b)

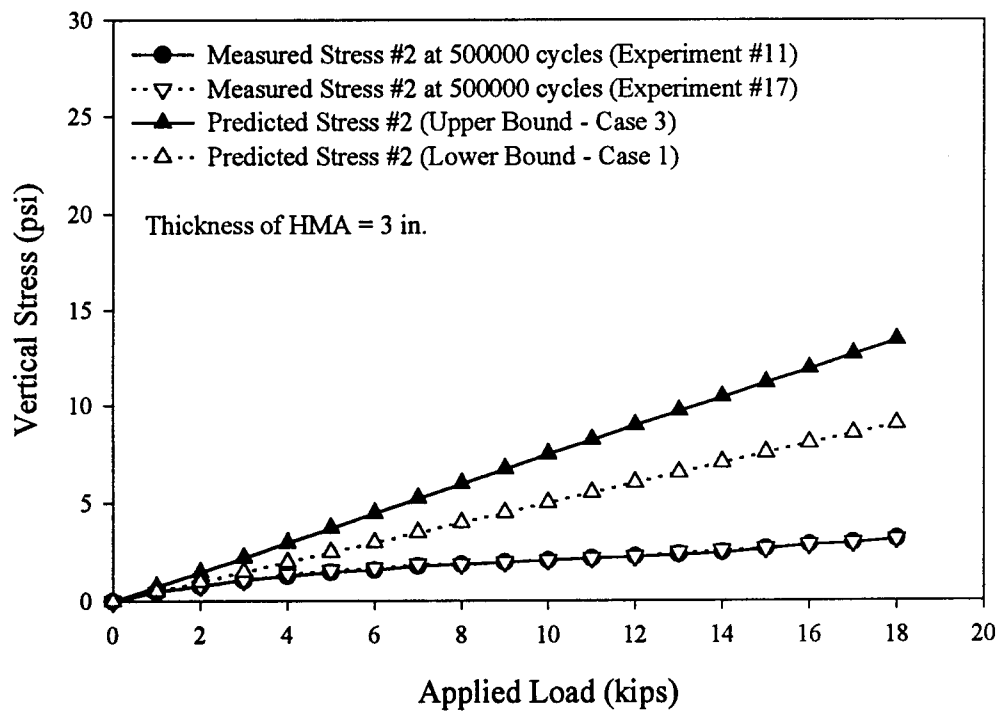


Figure 5-8: Measured and Predicted Upper and Lower Bound Vertical Stresses for Thin Asphalt Sections with Reinforcement

a) Stress Beneath the Center of the Loading Area

b) Stress Beneath the Edge of the Loading Area

to Cases 1, 2, and 3 are presented in Table 5-7. The computed stresses at cell #2 corresponding to the lower and upper bound values of material properties (Case 1 and Case 3) did not compare well with measured stresses at cell #2 for both reinforced thin pavement sections (Experiment #11 and #17) as shown in Figure 5-8 (b) and Table 5-7.

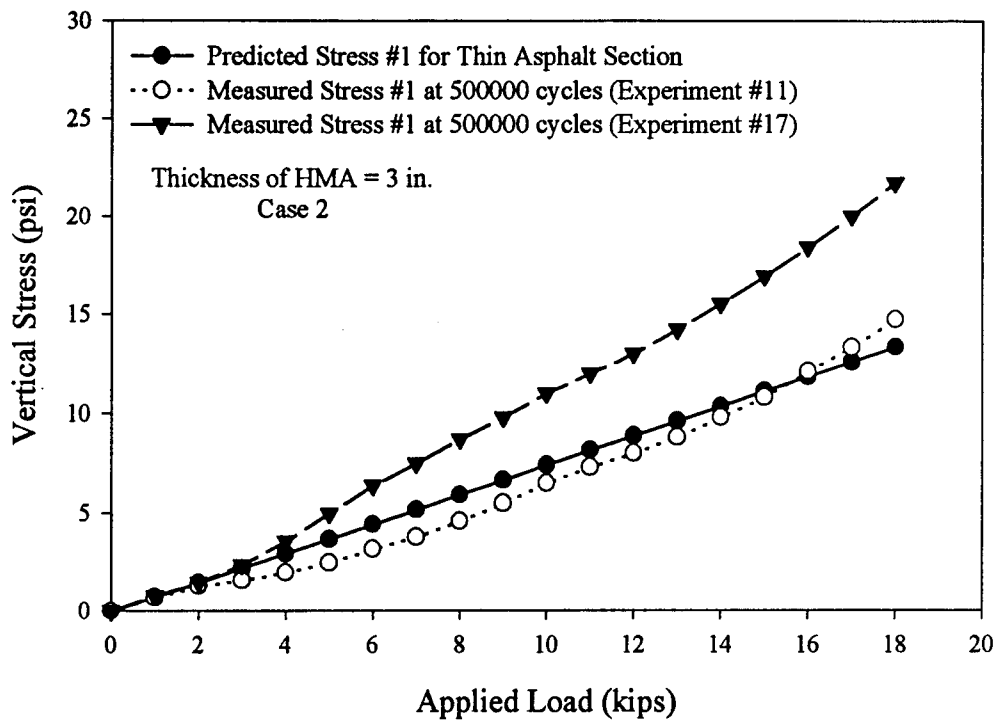
Figures 5-9 (a) and (b) show the comparison of measured vertical subgrade stresses at 500,000 cycles with computed vertical subgrade stresses corresponding to mean values of material properties (Case 2). As mentioned above, under 9 kips (40 kN) of loading, measured vertical subgrade stresses at cell #1 were 5.50 psi (37.90 kN/m²) and 9.80 psi (67.52 kN/m²) for Experiments #11 and #17, respectively. The computed vertical subgrade stress at cell #1 under 9 kips (40 kN) of loading was 6.65 psi (45.82 kN/m²). Based on the results shown in Figure 5-9 (a), it can be stated that one of the measured vertical stresses (Experiment #11) compared well with the computed vertical stresses at cell #1. The measured vertical subgrade stresses for Experiment #17 were higher than the computed results corresponding to mean values of material properties (Case 2). Figure 5-9 (b) shows the comparison of stresses at cell #2. As shown in Figure 5-9 (b), under 9 kips (40 kN) of loading, the measured value was 1.98 psi (13.64 kN/m²) in both experiments (Experiments #11 and #17), while the computed stress was 5.50 psi (37.90 kN/m²). Again the measured stresses at cell #2 did not compare well with computed vertical subgrade stresses [Figure 5-9 (b)].

Figures 5-10 (a) and (b) show the comparison of measured vertical subgrade stresses with computed vertical subgrade stresses corresponding to mean values of material properties (Case 2) for non-reinforced thin pavement sections. Under 9 kips (40 kN) of loading and at 500,000 cycles, measured vertical subgrade stresses at cell #1 were 6.92 psi (47.68 kN/m²) for Experiment #12 and 6.80 psi (46.85 kN/m²) for Experiment #18. These measured values compare well with the computed

Table 5-7: Measured and Computed Vertical Subgrade Stresses at Cells #1 and #2 for the Thin Pavement Sections [Thickness of HMA = 3 inches (76 mm)]

	Vertical Subgrade Stress (psi) [kN/m ²] Cell #1		Vertical Subgrade Stress (psi) [kN/m ²] Cell #2	
	9 [40]	18 [80]	9 [40]	18 [80]
Applied Load (kip) [kN] →				
Measured Stress (Experiment #11)	5.50 [37.90]	14.70 [101.28]	1.98 [13.64]	3.16 [21.77]
Measured Stress (Experiment #17)	9.80 [67.52]	21.70 [149.51]	1.98 [13.64]	3.16 [21.77]
Computed Stress (Case 1)	5.35 [36.86]	10.72 [73.86]	4.50 [31.01]	9.02 [62.15]
Computed Stress (Case 2)	6.65 [45.82]	13.31 [91.71]	5.50 [37.90]	11.01 [75.86]
Computed Stress (Case 3)	8.20 [56.50]	16.43 [113.20]	6.71 [46.23]	13.43 [92.53]

a)



b)

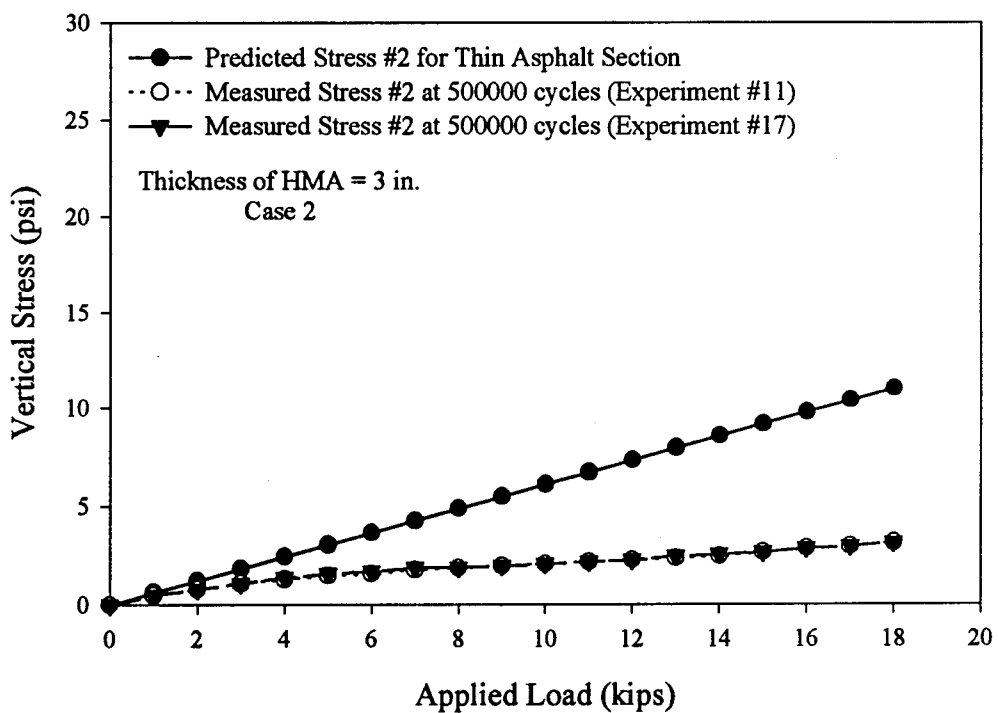
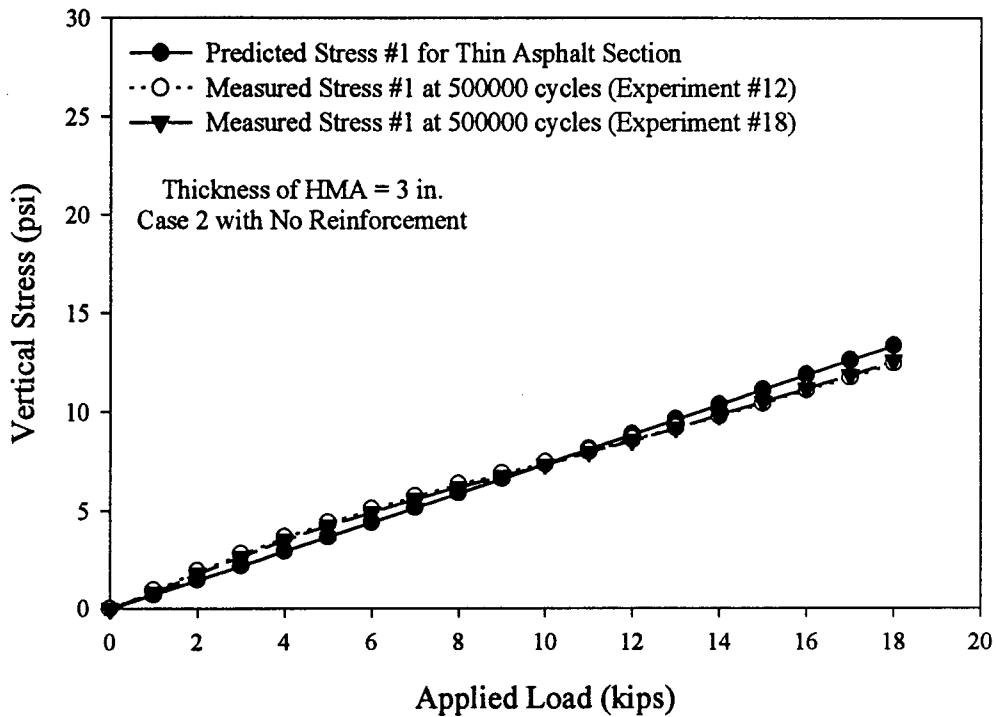


Figure 5-9: Measured and Predicted Vertical Stresses for Thin Asphalt Sections with Reinforcement
a) Stress Beneath the Center of the Loading Area
b) Stress Beneath the Edge of the Loading Area

a)



b)

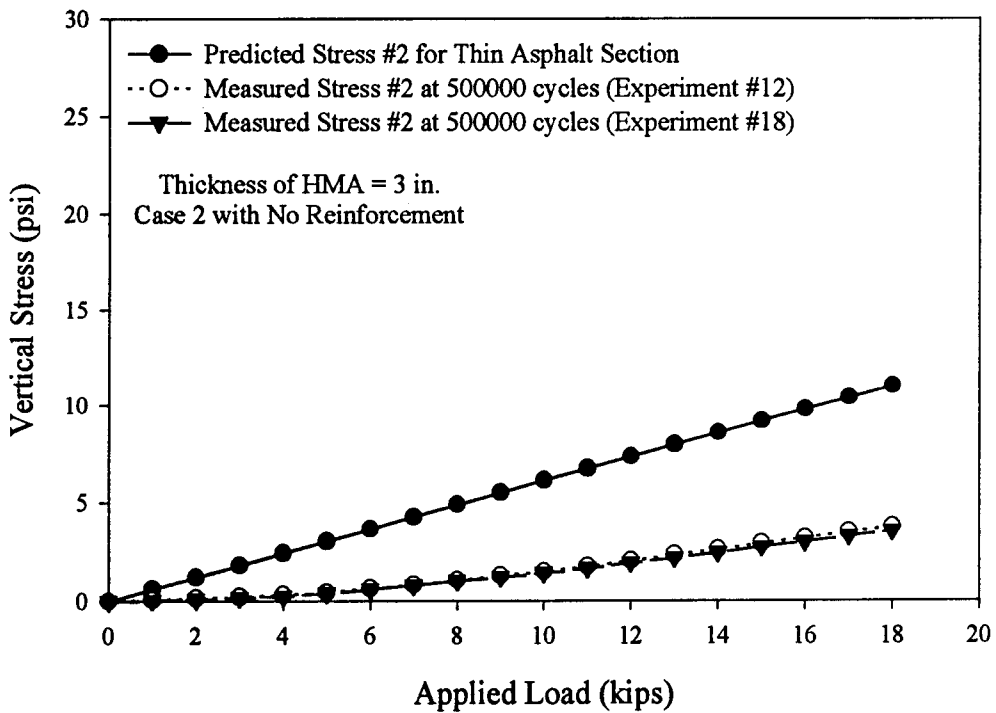


Figure 5-10: Measured and Predicted Vertical Stresses for Thin Asphalt Sections with No Reinforcement
a) Stress Beneath the Center of the Loading Area
b) Stress Beneath the Edge of the Loading Area

vertical stress at cell #1 (6.65 psi [45.82 kN/m²]) corresponding to mean values of material properties (Case 2) [Figure 5-10 (a)]. On the other hand, the computed stress at cell #2 (5.50 psi [37.90 kN/m²]) did not compare well with measurements (1.31 psi [9.03 kN/m²] for Experiment #12 and 1.22 psi [8.41 kN/m²] for Experiment #18) as shown in Figure 5-10 (b). The computed stresses (Case 2) at cell #1 compared well with measured values (Experiments #12 and #18) [Figure 5-10 (a)]. Again the computed stresses at cell #2 did not compare well with measured stresses [Figure 5-10 (b)].

5.3.4 Summary Of Results On Computed Vertical Stresses

Based on the results for thin and thick, reinforced and non-reinforced pavement sections, the following conclusions can be made:

- For thick reinforced and non-reinforced pavement sections, vertical subgrade stresses at cell #1 computed on the basis of mean values of material properties compared reasonably well with measurements. The computed stresses at cell #2 were higher than the measured values.
- For thin reinforced pavement sections, computed stresses (corresponding to mean values of material properties) and measured stresses at cell #1 for Experiment #11 compared reasonably well, while the computed vertical subgrade stresses were lower than the measured vertical subgrade stresses for Experiment #17. Again, the computed stresses at cell #2 were higher than the measured values.
- For thin non-reinforced pavement sections, computed vertical subgrade stresses at cell #1 (corresponding to mean values of material properties) compared exceptionally well with measurements. The computed stresses at cell #2 were again higher than the measured values.

5.4 INFLUENCE OF GEOSYNTHETIC ON PAVEMENT PERFORMANCE

In some cases, glass grid was assumed as a linear visco-elastic material with low creep characteristics. In some cases, the glass grid was assumed as a linear elastic material. Results from these analyses are presented below.

5.4.1 Influence Of Glass Fiber Grid On Subgrade Stress [Glass Grid Layer As A Visco-Elastic Material]

In Figures 5-11 and 5-12, the top asphalt layer (HMA) and the glass grid layer were considered as linear visco-elastic layers, while the remaining layers (gravel base, subgrade, and geotextile) were considered as linear elastic. The influence of inclusion of geosynthetic layers in the pavement section on vertical subgrade stress for a thin pavement section is shown in Figures 5-11 (a) and (b), and for a thick pavement section is shown in Figures 5-12 (a) and (b). There were calculations based on mean values of material properties (Case 2). Figures 5-11 (a) and 5-12 (a) show the influence of inclusion of a glass grid inside the HMA on subgrade stress. The glass grid was considered as a visco-elastic layer with very low creep compliance values [$D = 0.1 \text{ E-}07$ units in Equation (5.10)]. To study the influence of glass grids on subgrade stress, the elastic modulus (E) of the glass grid was hypothetically reduced from 4,205,000 psi (28,972,450 kN/m²) to 270,000 psi (1,860,300 kN/m²). The elastic modulus of HMA layer was assumed as 270,000 psi (1,860,300 kN/m²). Both computed stresses at cell #1 for two different values of elastic modulus (E) were similar to the measured stresses at cell #1 for reinforced thick and thin pavement sections at 500,000 load cycles (Experiments #5 and #11) [Figures 5-11 (a) and 5-12 (a)]. For the thin pavement section at 500,000 load cycles and under 9 kips (40 kN) of loading, measured vertical subgrade stress at cell #1 was 5.50 psi (37.90 kN/m²), while the computed vertical subgrade stresses were 6.65 psi (45.82

kN/m²) for two different values of the elastic modulus of glass grid [Figure 5-11 (a)]. Similar results were obtained for the thick pavement section. For the thick pavement section, measured vertical subgrade stress at cell #1 was 3.50 psi (24.12 kN/m²), while the computed vertical subgrade stresses were 4.10 psi (28.25 kN/m²) for two different values of the elastic modulus of glass grid [Figure 5-12 (a)]. Based on these results as shown in Figures 5-11 (a) and 5-12 (a), the stiffness of the glass grid in the middle of HMA does not influence the vertical subgrade stresses significantly.

Influence of geotextile on subgrade stress was investigated by assuming it to be a linear elastic material. Figures 5-11 (b) and 5-12 (b) show the effect of geotextile between the gravel base and the subgrade on the vertical stress distribution. Since the geotextile layer did not have a reinforcement function, hypothetically, a very low value of the elastic modulus (E) was assigned to the geotextile material. The elastic modulus of the geotextile layer was assumed as 100 psi (689 kN/m²). To determine the influence of geotextile layer on the vertical subgrade stress, the elastic modulus was increased to 6000 psi (41340 kN/m²). As shown in Figure 5-11 (b), for the thin pavement section, the measured vertical stress at cell #1 (at 500,000 cycles) under 9 kips (40 kN) of loading was 5.50 psi (37.90 kN/m²). The computed vertical subgrade stresses at cell #1 were 6.65 psi (45.82 kN/m²) for a geotextile elastic modulus of 100 psi (689 kN/m²) and 7.36 psi (50.71 kN/m²) for a geotextile elastic modulus of 6,000 psi (41340 kN/m²) [Figure 5-11 (b)]. Figure 5-11 (b) shows that the computed subgrade stress was similar for both values of elastic moduli, even though the high value of elastic modulus increased the subgrade stresses slightly in comparison to the stress corresponding to the lower value of elastic modulus. The same behavior can be seen in Figure 5-12 (b) for the reinforced thick pavement section. As shown in Figure 5-12 (b), for the thick pavement section, the measured vertical stress at cell #1 (at 500,000 cycles) under 9 kips (40 kN) of loading was 3.50 psi

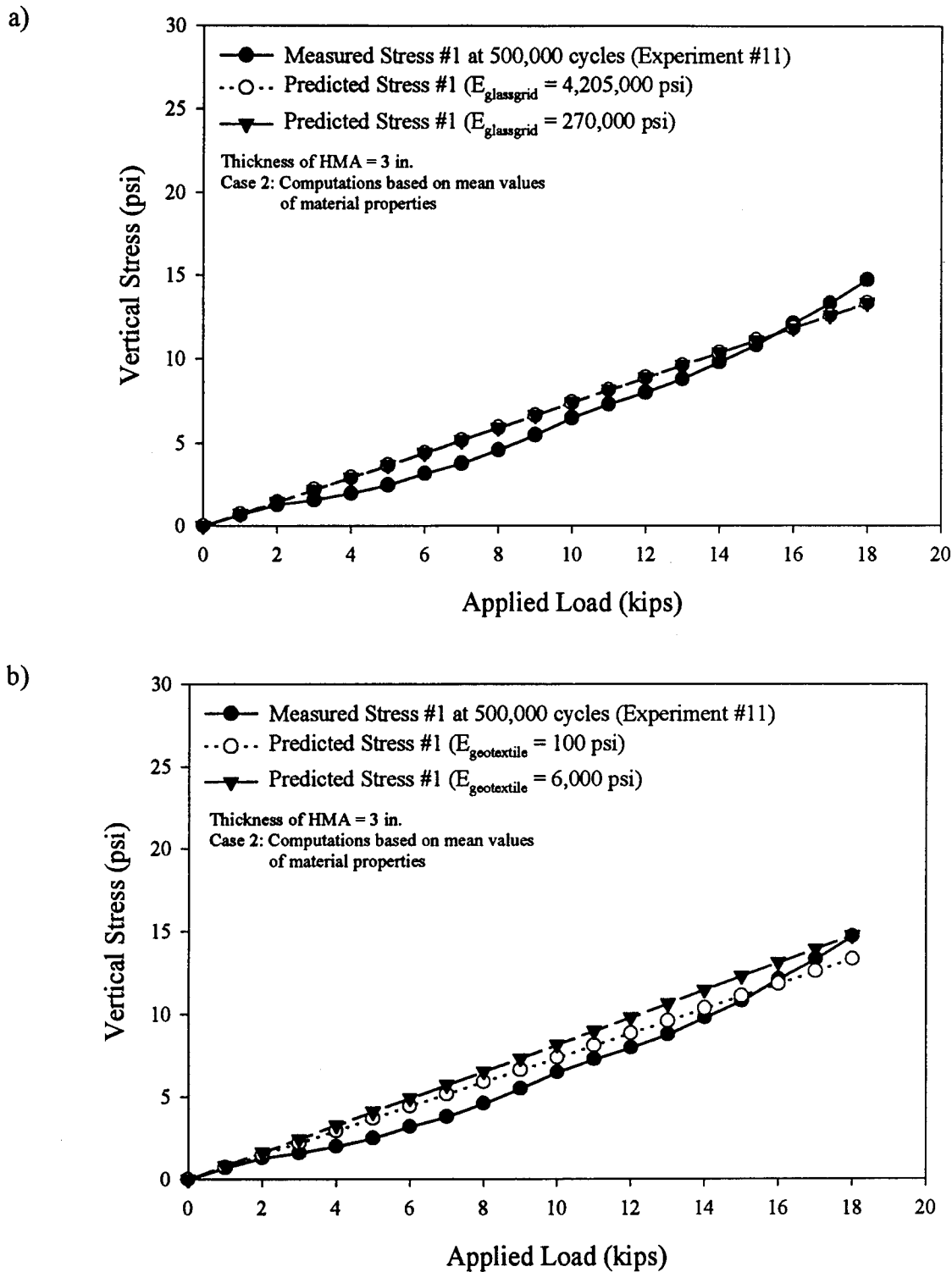


Figure 5-11: Influence of Geosynthetics on Subgrade Stress in a Thin Asphalt Section
[Glass Grid as a Visco-Elastic Material]
a) Influence of Glass Fiber Grid inside the HMA
b) Influence of Geotextile between the Gravel Base and the Subgrade

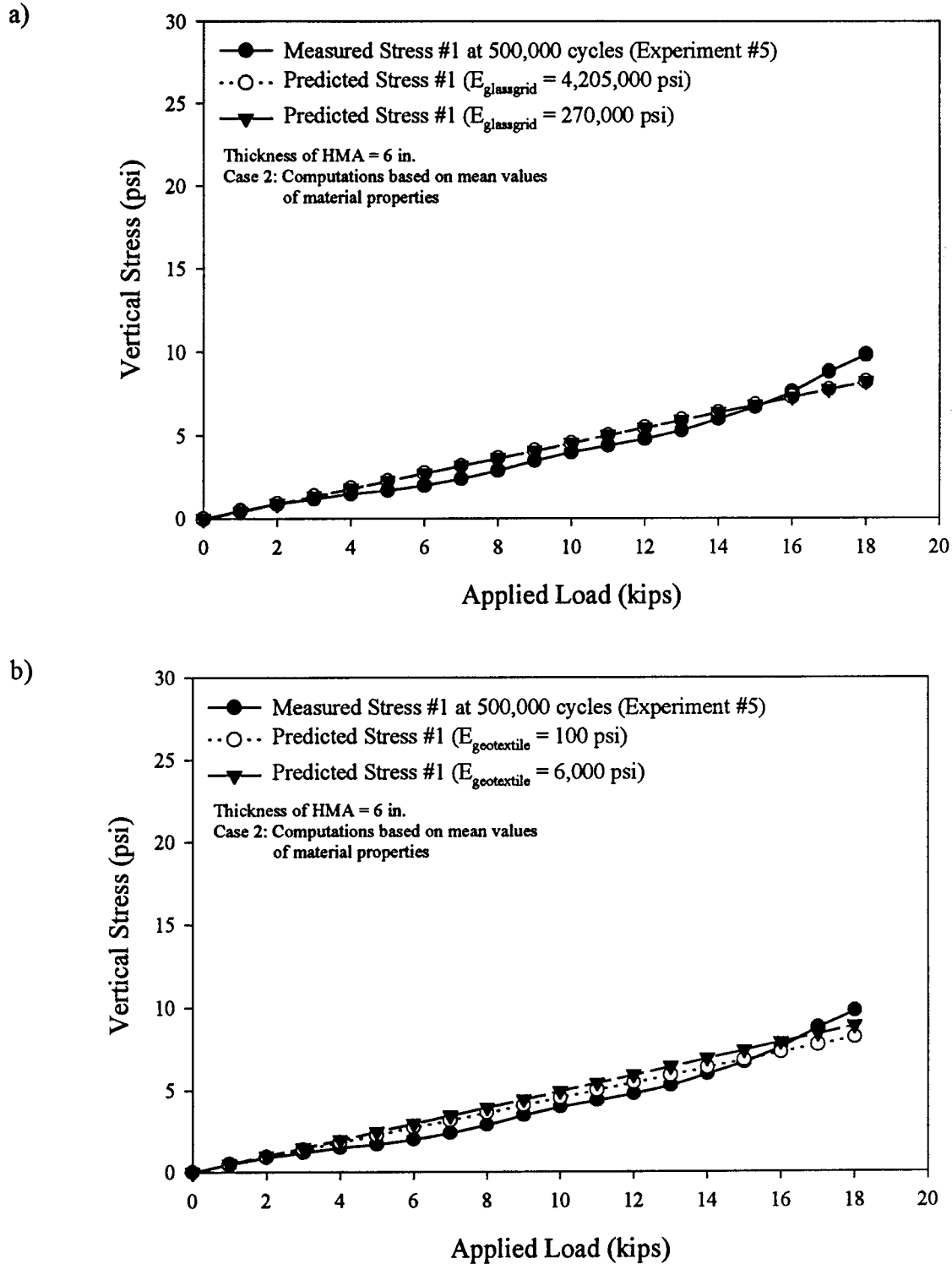


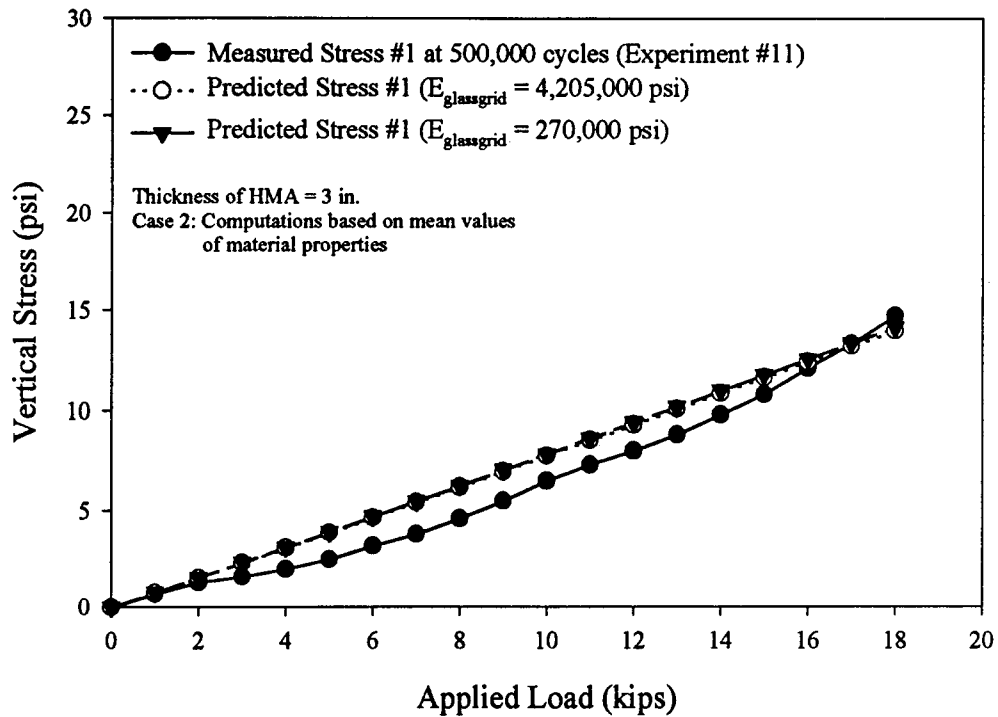
Figure 5-12: Influence of Geosynthetics on Subgrade Stress in a Thick Asphalt Section
[Glass Grid as a Visco-Elastic Material]
a) Influence of Glass Fiber Grid inside the HMA
b) Influence of Geotextile between the Gravel Base and the Subgrade

(24.12 kN/m²). The computed vertical subgrade stresses at cell #1 were 4.10 psi (28.25 kN/m²) for a geotextile elastic modulus of 100 psi (689 kN/m²) and 4.45 psi (30.66 kN/m²) for a geotextile elastic modulus of 6,000 psi (41340 kN/m²) [Figure 5-12 (b)]. The difference between the subgrade stress for high geosynthetic elastic modulus and the subgrade stress for low geosynthetic elastic modulus was even less for a thick pavement section [0.35 psi (2.41 kN/m²)] [Figure 5-12 (b)] than for a thin pavement section [0.71 psi (4.89 kN/m²)] [Figure 5-11 (b)]. This behavior shows that the stiffness of the geosynthetic fabric (between the gravel base and subgrade soil) does not influence the subgrade stress substantially. It is concluded from these analyses that the use of a very stiff geotextile material at the gravel/subgrade interface is not necessary as a reinforcement. This conclusion verifies the main purpose of using a geotextile at the interface. The main function was separation designed to prevent subgrade soil from migrating into the gravel base.

5.4.2 Influence Of Glass Fiber Grid On Subgrade Stress [Glass Grid Layer As An Elastic Material]

In Figures 5-13 (a) and (b), the glass grid layer was considered as a linearly elastic material since glass grid does not have creep characteristics. Except for the asphalt layer, the remaining layers (gravel base, subgrade, and geotextile) were considered as linearly elastic materials. The top asphalt layer (HMA) in the pavement section was assumed to have linear visco-elastic behavior. Figures 5-13 (a) and (b) show the vertical subgrade stress distribution for a thin pavement section. The vertical subgrade stresses [Figures 5-13 (a) and (b)] corresponding to the case with a linear elastic glass grid layer were almost equal to the vertical subgrade stresses [Figures 5-11 (a) and (b)] where the glass grid layer was considered as a linear visco-elastic layer with low creep values in a thin pavement section (Table 5-8).

a)



b)

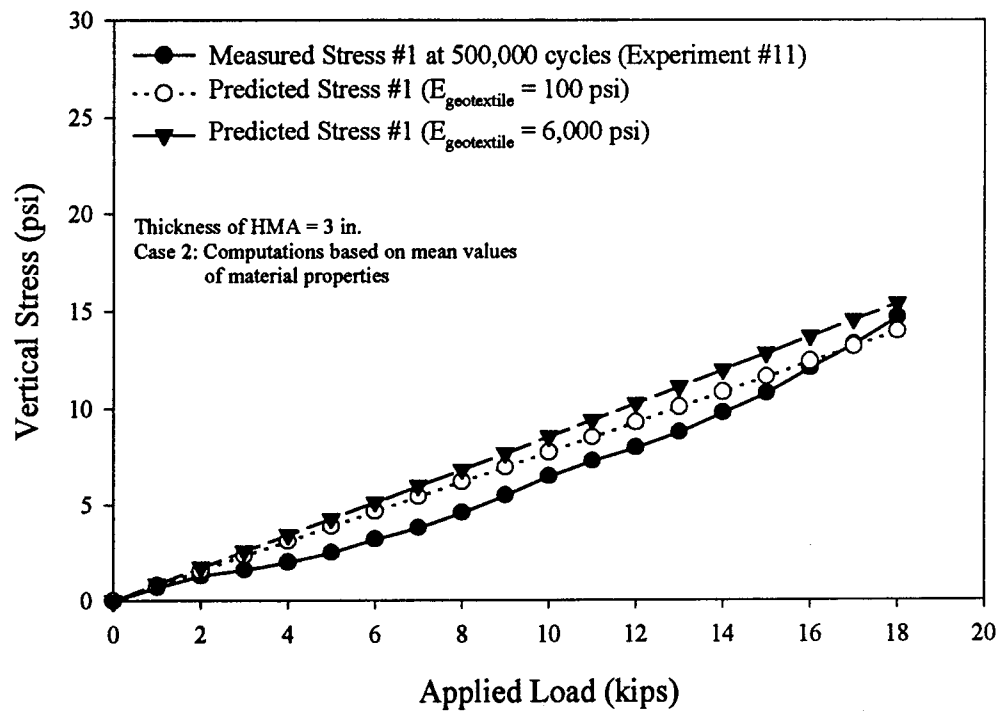


Figure 5-13: Influence of Geosynthetics on Subgrade Stress in a Thin Asphalt Section
[Glass Grid as an Elastic Material]

a) Influence of Glass Fiber Grid inside the HMA

b) Influence of Geotextile between the Gravel Base and the Subgrade

Table 5-8: Computed Vertical Stresses at Cell #1 for a Thin Pavement Section Corresponding to Different Elastic Moduli of Geosynthetic Layers for Case 2

Thickness of HMA (inch) [mm]	Applied Load (kip) [kN/m ²]	Glass Grid Layer as	Computed Vertical Subgrade Stress at Cell #1 (psi) [kN/m ²]			
			Note: E_{gg} = Elastic Modulus for Glass Grid E_{gt} = Elastic Modulus for Geotextile			
			$E_{gg} = 4,205,000$ [28,972,450] $E_{gt} = 100$ [689]	$E_{gg} = 270,000$ [1,860,300] $E_{gt} = 100$ [689]	$E_{gg} = 4,205,000$ [28,972,450] $E_{gt} = 100$ [689]	$E_{gg} = 4,205,000$ [28,972,450] $E_{gt} = 6000$ [41,340]
3 [76]	9 [40]	Linear Visco-Elastic	6.65 [45.82]	6.65 [45.82]	6.65 [45.82]	7.36 [50.71]
		Linear Elastic	6.97 [48.02]	7.05 [48.57]	6.97 [48.02]	7.69 [52.98]

As shown in Figure 5-13 (a) and Table 5-8, the computed vertical subgrade stresses were 6.97 psi [48.02 kN/m²] for a high elastic modulus of glass grid and 7.05 psi [48.57 kN/m²] for a low elastic modulus of the glass grid. These results were similar for both values of elastic moduli, which shows that the stiffness of the glass fiber grid in the middle of the HMA does not influence the vertical subgrade stresses substantially.

Influence of geotextile on subgrade stress was investigated by assuming it to be a linear elastic material. Figure 5-13 (b) shows the effect of a geotextile layer between the gravel base and the subgrade on the stress distribution. Again, a very low value of elastic modulus (E) was assigned to the geotextile fabric since the geotextile material did not have the reinforcement function. Figure 5-13 (b) and Table 5-8 show that the computed vertical subgrade stresses were 6.97 psi [48.02 kN/m²] for a low elastic modulus of geotextile and 7.69 psi [52.98 kN/m²] for a high elastic modulus of geotextile, and these results were similar for both values of elastic moduli. The computer analysis in this study verifies that the use of a very stiff geotextile material at the gravel base/subgrade interface is not necessary as a reinforcement. The use of a geotextile layer at that location was only for separation purposes to prevent subgrade soil from migrating into the gravel base.

5.4.3 Summary Of Results On Influence Of Geosynthetic On Pavement Performance

In some cases, glass grid was assumed as a linear visco-elastic material with low creep characteristics. In some cases, the glass grid was assumed as a linear elastic material. The summary of predicted results are given below:

- The stiffness of the glass grid in the middle of HMA does not influence the vertical subgrade stresses significantly.
- The stiffness of the geosynthetic fabric (between the gravel base and subgrade soil) does not

influence the subgrade stress. It can be concluded from the analyses that the use of a very stiff geotextile material at the gravel/subgrade interface is not necessary as a reinforcement. The main function of the geotextile was to prevent subgrade soil from migrating into the gravel base.

5.5 COMPUTER ANALYSES OF SURFACE DISPLACEMENTS

The computed surface displacements are compared with measured displacements for cases with a HMA layer thickness of 3 inches (76 mm) and 6 inches (152 mm). The results on computed surface displacements are shown in Figures 5-14 through 5-19. During the analysis, glass grid layer was modeled as a visco-elastic layer, similar to the hot mix asphalt; however, unlike for the asphalt layer, very low creep compliance values were assigned to the glass grid layer [$D = 0.1 \text{ E-07}$ in Equation (5.10)] corresponding to each creep time interval. The reason for this approach is that the glass grid exhibits very low to no creep characteristics. The remaining layers (gravel base, subgrade, and geotextile) were considered as linearly elastic materials.

Figures 5-14 and 5-15 show the computed elastic surface displacements for thin and thick reinforced pavement sections at different radial displacements. Figures 5-14 (a) and 5-15 (a) show the computed elastic surface displacements corresponding to lower, mean, and upper bound material property values (Case 1, Case 2, and Case 3). Figures 5-14 (b) and 5-15 (b) show the computed elastic surface displacements corresponding to different applied loads for Case 2 [1 kip (4.5 kN), 9 kips (40 kN), and 18 kips (80 kN)]. As presented in Tables 5-9 and 5-10, computed elastic surface displacements decreased when the material properties (Table 5-2) were changed from Case 1 to Case 3 [Figures 5-14 (a) and 5-15 (a)]. For example, as shown in Figure 5-14 (a), the computed elastic

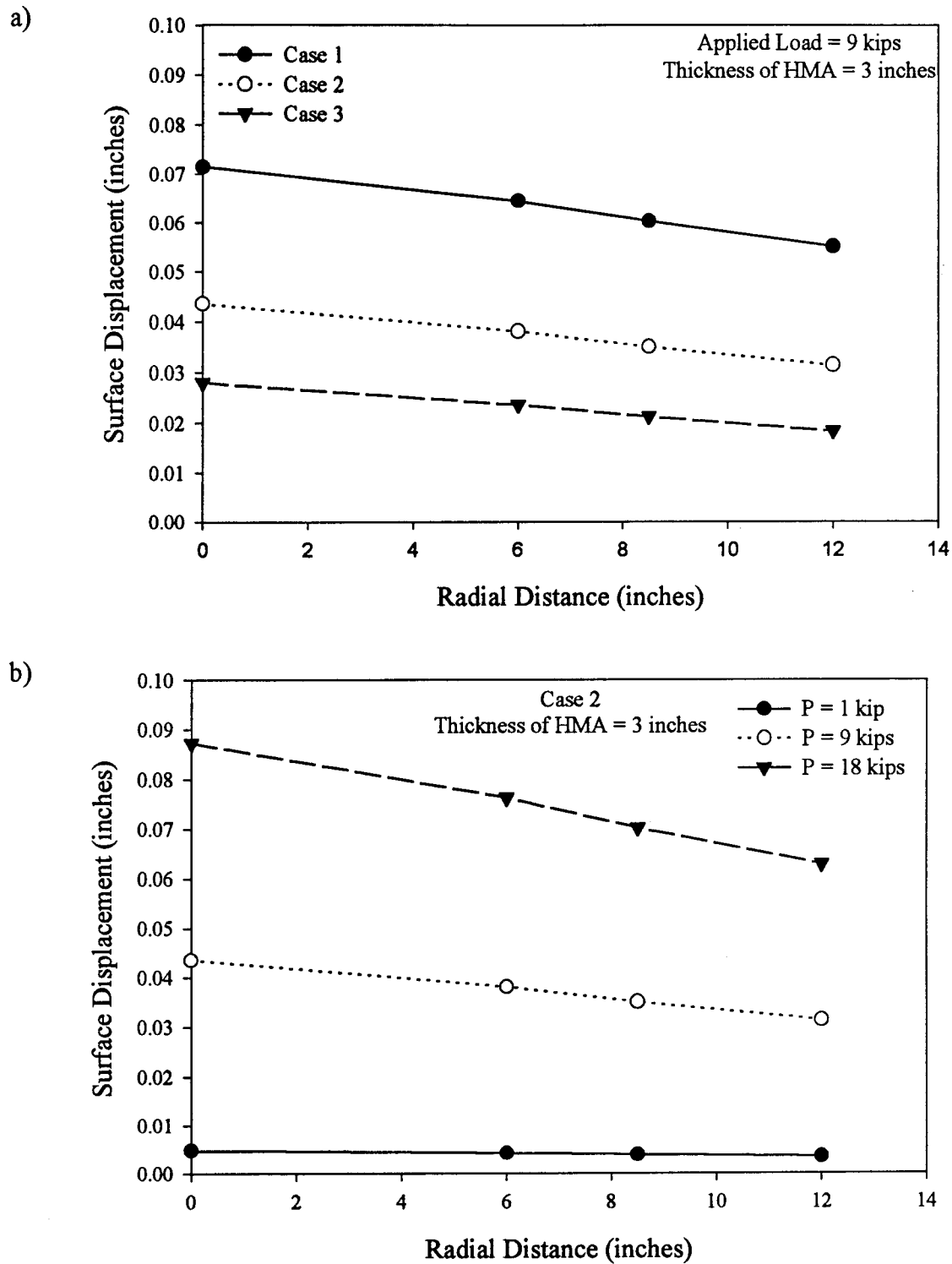


Figure 5-14: Computed Elastic Surface Displacements in a Thin HMA Section with Reinforcement
a) Corresponding to Different Cases of Material Properties
b) Corresponding to Different Applied Loads for Case 2

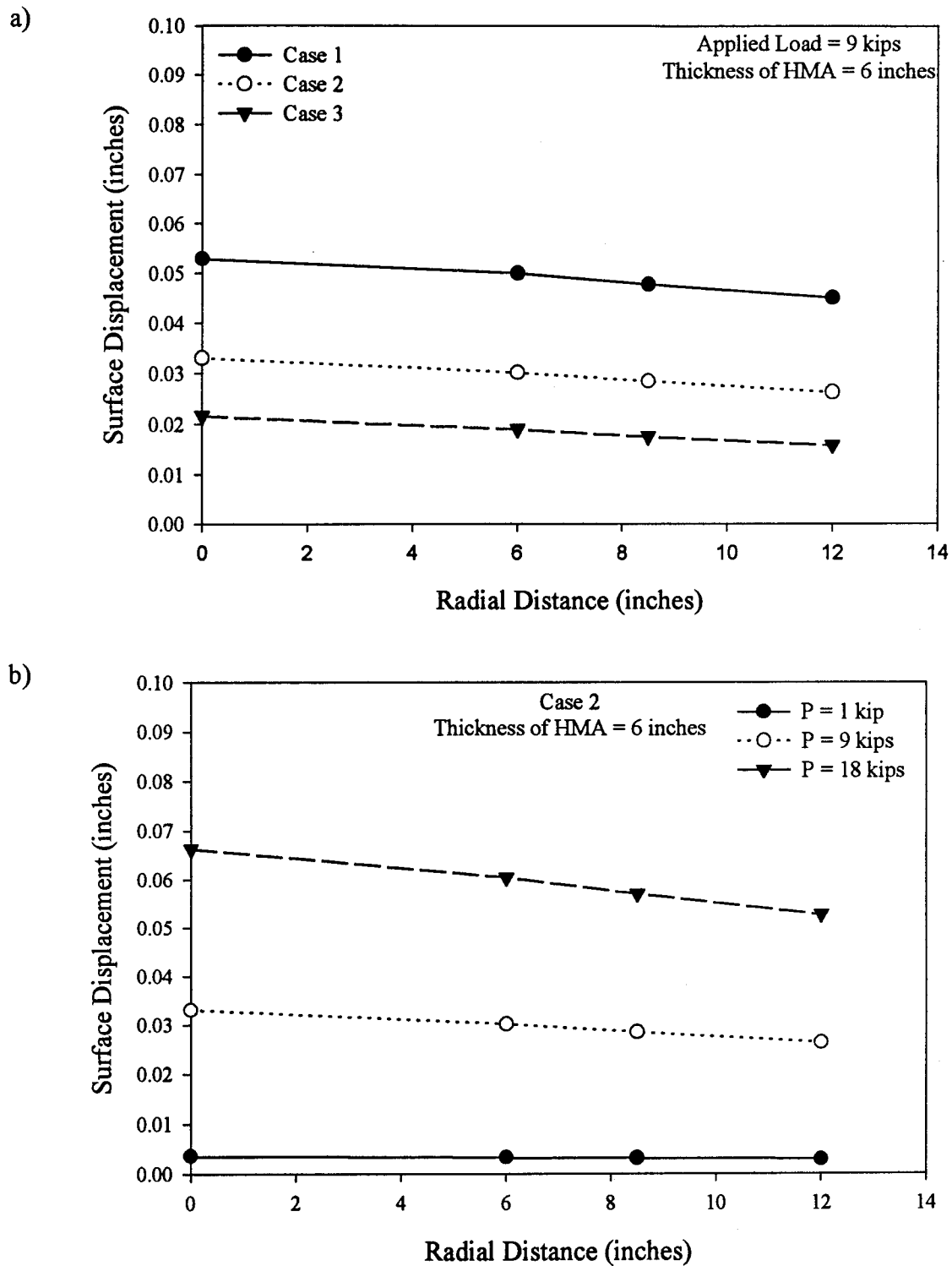


Figure 5-15: Computed Elastic Surface Displacements in a Thick HMA Section with Reinforcement
a) Corresponding to Different Cases of Material Properties
b) Corresponding to Different Applied Loads for Case 2

Table 5-9: Computed Elastic Surface Displacement for a Thin Pavement Section with Reinforcement Under 9 kips (40 kN) of Loading

Lateral Distance (inch) [mm]	Case 1	Case 2	Case 3
	Elastic Surface Displacement (inch) [mm]	Elastic Surface Displacement (inch) [mm]	Elastic Surface Displacement (inch) [mm]
0	0.072 [1.829]	0.044 [1.118]	0.028 [0.711]
6.00 [152.40]	0.065 [1.651]	0.038 [0.965]	0.024 [0.610]
8.50 [215.90]	0.060 [1.524]	0.035 [0.889]	0.021 [0.533]
12.00 [304.80]	0.055 [1.397]	0.031 [0.787]	0.018 [0.457]

Table 5-10: Computed Elastic Surface Displacement for a Thick Pavement Section with Reinforcement Under 9 kips (40 kN) of Loading

Lateral Distance (inch) [mm]	Case 1	Case 2	Case 3
	Elastic Surface Displacement (inch) [mm]	Elastic Surface Displacement (inch) [mm]	Elastic Surface Displacement (inch) [mm]
0	0.053 [1.346]	0.033 [0.838]	0.022 [0.559]
6.00 [152.40]	0.050 [1.270]	0.030 [0.762]	0.019 [0.483]
8.50 [215.90]	0.048 [1.219]	0.029 [0.737]	0.018 [0.457]
12.00 [304.80]	0.045 [1.143]	0.026 [0.660]	0.016 [0.406]

displacement at the edge of the loading plate corresponding to the lower bound material properties (Case 1) was 0.065-inch (1.651 mm). The displacement at the same period corresponding to the mean values of material properties (Case 2) was 0.038-inch (0.965 mm). It was 0.024-inch (0.610 mm) for the upper bound material properties (Case 3) (Table 5-9). As expected, the lowest elastic displacements correspond to upper bound values of material properties for both thin and thick reinforced pavement sections (Tables 5-9 and 5-10).

Figures 5-14 (b) and 5-15 (b) show that with increasing load the elastic displacements increase as expected (Tables 5-11 and 5-12). Also, under 9 kips (40 kN) of loading, the cumulative displacement at the edge of the loading plate was 0.038-inch (0.965 mm) for the thin pavement section (Table 5-11) while the elastic displacement at the same place was 0.030-inch (0.762 mm) for the thick pavement section (Table 5-12). Based on these results, it can be stated that the computed elastic displacements at the surface decrease when the thickness of hot mix asphalt layer increases.

5.5.1 Comparison Of Computed Displacements With Measurements Corresponding To A 3-Inch (76 mm) Thick HMA Layer

Computed values with measured surface displacements for thin and thick pavement sections with and without reinforcement are presented in Tables 5-13 through 5-16, and Figures 5-16 through 5-19. Displacements at radial distances of 6 inches (152 mm) [edge of the loading plate], 8.5 inches (215.9 mm), and 12 inches (305 mm) away from the center of the load plate were obtained from computer analysis and experimental measurements. Figure 5-16 shows the comparison of measured surface displacements (under static loading) with computed values for the thin reinforced HMA section. As presented in Table 5-13, surface displacements (under static loading) for both reinforced thin pavement sections (Experiments #11 and #17) at 500,000 load cycles were very close to the

Table 5-11: Computed Elastic Displacement in a Thin Pavement Section with Reinforcement for Case 2 of Material Properties

Lateral Distance (inch) [mm]	Elastic Surface Displacement for Case 2 [Thickness of HMA = 3 inches (76 mm)] (inch) [mm]		
	P = 1 kip (4.5 kN)	P = 9 kips (40 kN)	P = 18 kips (80 kN)
0	4.849 E-3 [0.123]	0.044 [1.118]	0.087 [2.210]
6.00 [152.40]	4.242 E-3 [0.108]	0.038 [0.965]	0.076 [1.930]
8.50 [215.90]	3.902 E-3 [0.099]	0.035 [0.889]	0.070 [1.778]
12.00 [304.80]	3.495 E-3 [0.089]	0.031 [0.787]	0.063 [1.600]

Table 5-12: Computed Elastic Displacement in a Thick Pavement Section with Reinforcement for Case 2 of Material Properties

Lateral Distance (inch) [mm]	Elastic Surface Displacement for Case 2 [Thickness of HMA = 6 inches (152 mm)] (inch) [mm]		
	P = 1 kip (4.5 kN)	P = 9 kips (40 kN)	P = 18 kips (80 kN)
0	3.685 E-3 [0.094]	0.033 [0.838]	0.066 [1.676]
6.00 [152.40]	3.358 E-3 [0.085]	0.030 [0.762]	0.060 [1.524]
8.50 [215.90]	3.174 E-3 [0.081]	0.029 [0.737]	0.057 [1.448]
12.00 [304.80]	2.931 E-3 [0.074]	0.026 [0.660]	0.053 [1.346]

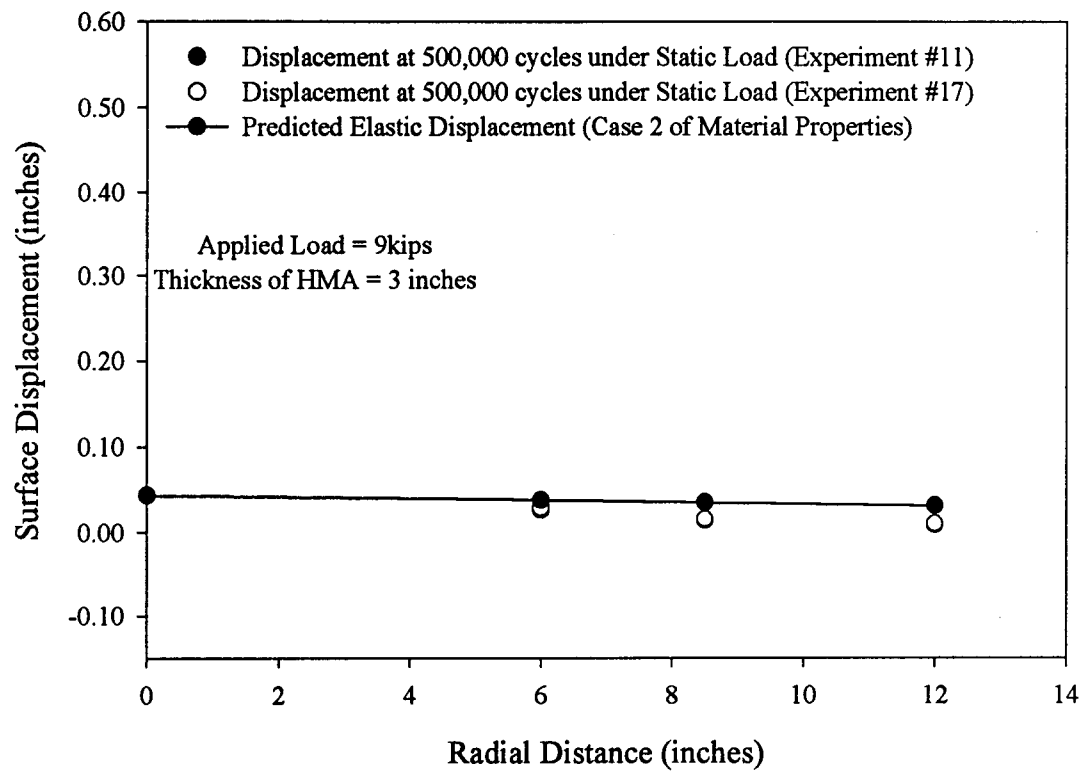


Figure 5-16: Measured Displacement versus Predicted Elastic Surface Displacement for a Thin HMA Section with Reinforcement

Table 5-13: Computed Elastic Surface Displacement versus Measured Displacement in a Thin HMA Section with Reinforcement

		Surface Displacement (inch) [mm]		
Lateral Distance (inch) [mm] →		6 [152]	8.5 [215.9]	12 [152]
Computed Values (Case 2)		0.038 [0.965]	0.035 [0.889]	0.031 [0.787]
Measured Values	Exp. #11	0.027 [0.686]	0.014 [0.356]	0.009 [0.229]
	Exp. #17	0.029 [0.737]	0.016 [0.406]	0.010 [0.254]

computed values corresponding to Case 2 of material properties [Figure 5-16]. Surface displacements (under static loading) at the edge of the loading plate [at 6 inches (152 mm)] for Experiments #11 [0.027-inch (0.686 mm)] and #17 [0.029-inch (0.737 mm)] matched better with the computed result [0.038-inch (0.965 mm)] than the displacements which were away from the center of the loading plate [at 8.5 inches (215.9 mm) and 12 inches (305 mm)] (Table 5-13).

A similar comparison was performed for the thin non-reinforced pavement section in Figure 5-17 and Table 5-14. Figure 5-17 shows the comparison of computed elastic surface displacement, corresponding to Case 2, with measured surface displacements (under static loading) of thin pavement sections with no reinforcement (Experiments #12 and #18). Results for the surface displacements (under static loading) of the both non-reinforced sections (Experiments #12 and #18) at 500,000 load cycles were very close to the computed values corresponding to Case 2 [Figure 5-17] (Table 5-14). As presented in Table 5-14, the surface displacements for Experiments #12 and #18 were 0.019-inch (0.483 mm) and 0.018-inch (0.457 mm), respectively, at the edge of the loading plate. Again, the measured displacements for both non-reinforced pavement sections (Experiments #12 and #18) were closer to computed values at the edge of the loading plate than the displacements away from the center of the loading plate [at 8.5 inches (215.9 mm) and 12 inches (305 mm)] [Figure 5-17] (Table 5-14).

5.5.2 Comparison Of Computed Displacements With Measurements Corresponding To A 6-Inch (152 mm) Thick HMA Layer

Figure 5-18 shows the comparison of measured (under static loading) with computed surface displacements (elastic) for a reinforced thick pavement section. Similar to the reinforced thin pavement section, surface displacements (under static loading) in both reinforced thick pavement

sections (Experiments #3 and #7) at 500,000 load cycles compared very well with the computed displacement corresponding to Case 2 of material properties [Figure 5-18]. As shown in Table 5-15 and Figure 5-18, the measured surface displacements (under static loading) for Experiments #3 and #7 were 0.029-inch (0.737 mm) and 0.021-inch (0.533 mm), respectively, at the edge of the loading plate, while the computed elastic displacement at the same place was 0.030-inch (0.762 mm). Again similar to the results for the reinforced thin pavement section, the measured surface displacements (Experiments #3 and #7) were very similar to the computed elastic surface displacements. Measured surface displacements (under static loading) were closer to the computed (elastic) displacements at the edge of the loading plate than those at distances of 8.5 inches (215.9 mm) and 12 inches (305 mm) [Figure 5-18] (Table 5-15).

Measured (under static loading) versus computed (elastic) surface displacements for the non-reinforced thick pavement section were compared in Figure 5-19 and Table 5-16. As shown in Figure 5-19, measured and computed displacements matched very well at distances of 6 inches (152 mm), 8.5 inches (215.9 mm) and 12 inches (305 mm). Surface displacements (under static loading) at 500,000 load cycles for the non-reinforced thick pavement section (Experiment #4) were almost the same as the computed displacements corresponding to Case 2 of material properties [Figure 5-19]. The measured surface displacement (under static loading) was 0.029-inch (0.737 mm), which is almost identical to the computed result [0.031-inch (0.787 mm)] at the edge of the loading plate (Table 5-16). The difference between the measured surface displacements (under static loading) and the computed (elastic displacement) results increased with increasing radial distance [Figure 5-19].

In summary, all these results showed that computed elastic surface displacements corresponding to Case 2 of material properties compare well with the measured values (under static

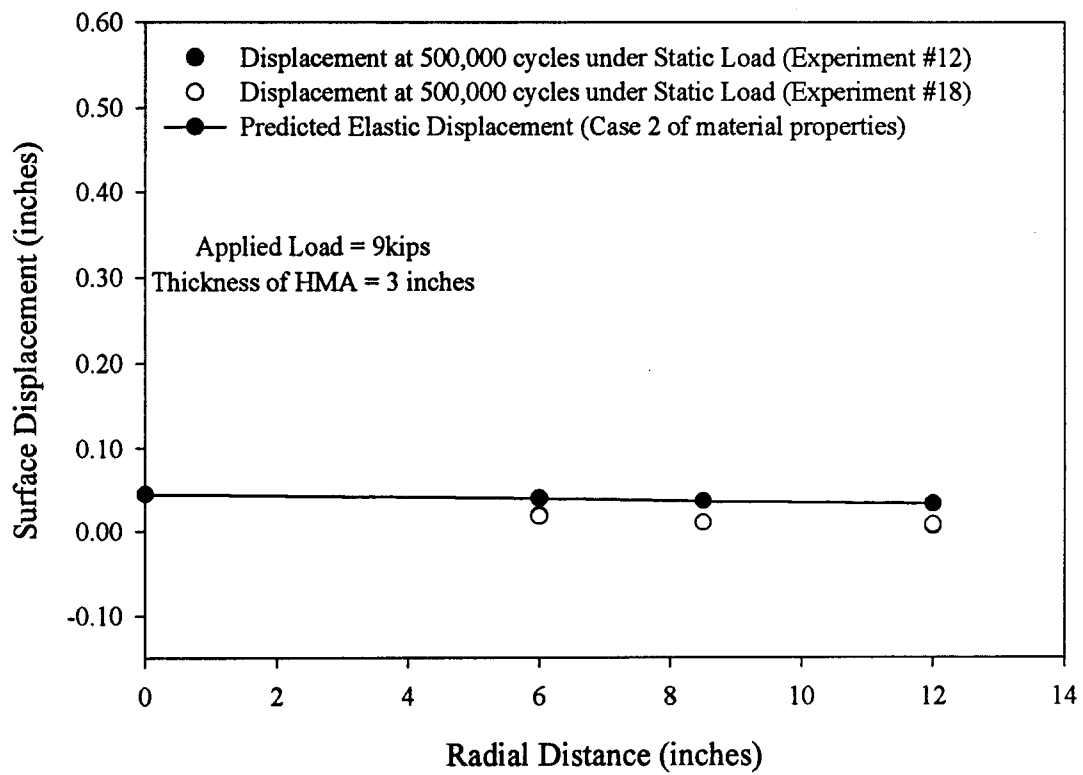


Figure 5-17: Measured Displacement versus Predicted Elastic Surface Displacement for a Thin HMA Section with No Reinforcement

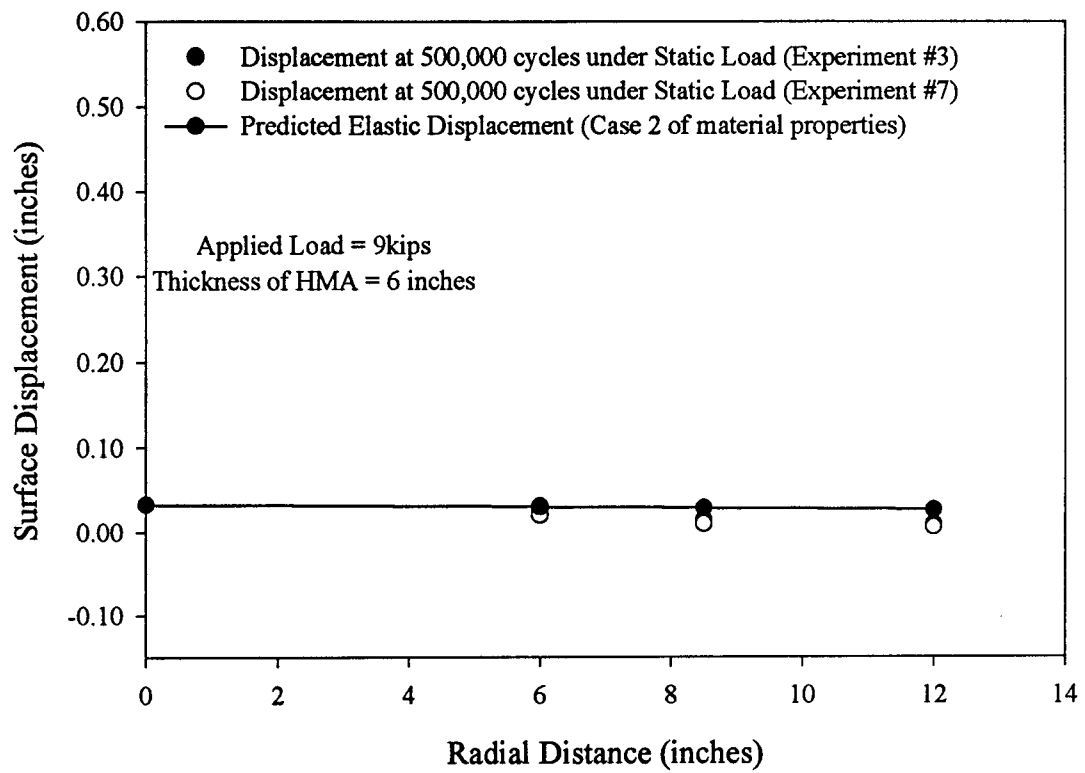


Figure 5-18: Measured Displacement versus Predicted Elastic Surface Displacement for a Thick HMA Section with Reinforcement

Table 5-14: Computed Elastic Surface Displacement versus Measured Displacement in a Thin HMA Section with No Reinforcement

		Elastic Surface Displacement (inch) [mm]		
Lateral Distance (inch) [mm] →		6 [152]	8.5 [215.9]	12 [152]
Computed Values (Case 2)		0.039 [0.991]	0.036 [0.914]	0.032 [0.813]
Measured Values	Exp. #12	0.019 [0.483]	0.010 [0.254]	0.006 [0.152]
	Exp. #18	0.018 [0.457]	0.010 [0.254]	0.007 [0.178]

Table 5-15: Computed Elastic Surface Displacement versus Measured Displacement in a Thick HMA Section with Reinforcement

		Elastic Surface Displacement (inch) [mm]		
Lateral Distance (inch) [mm] →		6 [152]	8.5 [215.9]	12 [152]
Computed Values (Case 2)		0.030 [0.762]	0.029 [0.737]	0.026 [0.660]
Measured Values	Exp. #3	0.029 [0.737]	0.015 [0.381]	0.009 [0.229]
	Exp. #7	0.021 [0.533]	0.010 [0.254]	0.006 [0.152]

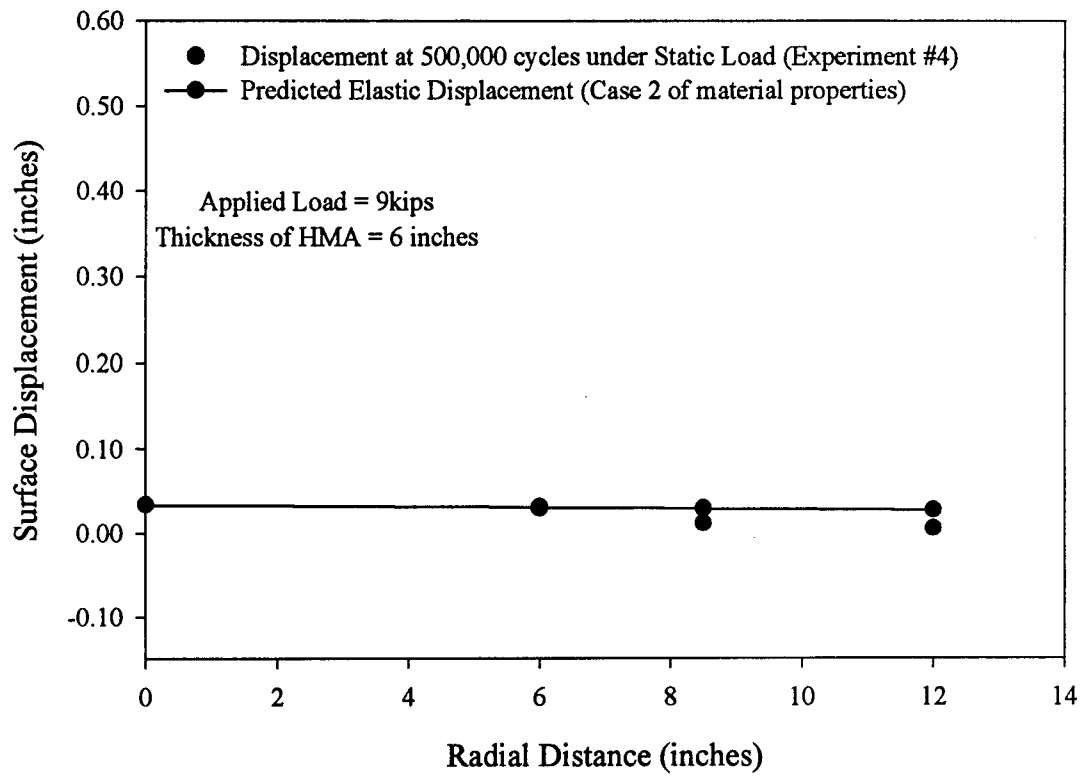


Figure 5-19: Measured Displacement versus Predicted Elastic Surface Displacement for a Thick HMA Section with No Reinforcement

Table 5-16: Computed Elastic Surface Displacement versus Measured Displacement in a Thick HMA Section with No Reinforcement

		Elastic Surface Displacement (inch) [mm]		
Lateral Distance (inch) [mm] →		6 [152]	8.5 [215.9]	12 [152]
Computed Values (Case 2)		0.031 [0.787]	0.029 [0.737]	0.027 [0.686]
Measured Values	Exp. #4	0.029 [0.737]	0.012 [0.305]	0.006 [0.152]

loading) for different thicknesses of reinforced and non-reinforced pavement sections. Especially at the edge of the loading plate, surface displacements at 500,000 load cycles matched very well with the computed elastic displacements. Even though the difference between the computed elastic displacement and measured displacement increased with the radial distance, this difference was considered as acceptable in view of the small values of displacements. These comparisons indicate that the computed results have the same trends as measurements.

5.6 COMPUTER ANALYSES OF STRAINS

As a result of difficulties encountered during compaction, coupled with the dynamic loading effects, failure of several strain gages occurred in the laboratory testing program. The modeling of the influence of glass grid reinforcement was performed using the KENLAYER computer program [Huang (1993)]. This modeling was undertaken in order to better understand the mechanics of glass grid reinforcements. In the strain analyses presented in this section, the top asphalt layer (HMA) and the glass grid layer were considered as linearly visco-elastic materials, while the remaining layers (gravel base, subgrade, and geotextile) were considered as linearly elastic materials. As previously described in Section 5.2, glass grid reinforcement in the computer analysis was simulated by including a very thin layer [0.039-inch (1 mm)] inside the HMA. Computed strains are based on the mean values of material properties (Case 2) as shown in Table 4-13.

Since the most critical strains are horizontal tensile strain at the bottom of HMA and vertical compressive strain on top of the subgrade (according to the Asphalt Institute) [Yoder and Witczak (1975)], variation of computed radial and vertical strains with depth for two different thicknesses [3 inches (76 mm) and 6 inches (152 mm)] were studied and the results are presented in Sections 5.6.1

and 5.6.2. Also as a supplement, the variation of computed tangential strain with depth is presented in these sections. As shown in Figure 5-20 (a), the variation of computed strain (with depth) beneath the center of the loading plate (line A-A) is referred to as strain along the line A-A. The variation of computed strain (with depth) beneath the edge of the loading plate (line B-B) is referred to as strain along the line B-B. The strain along the line C-C is shown in Figure 5-20 (a).

Strain gages #1, #2, and #3 in Figure 5-20 (b) were located on the glass grid beneath the center of the loading plate, beneath the edge of the loading plate, and at a radial distance of 12 inches (305 mm), respectively. Strains were also computed at the same locations. The computed strains at these locations are referred to as Strain #1 (at SG #1), Strain #2 (at SG #2), and Strain #3 (at SG #3). Also, it is important to know the orientation of the strain gage placement on the glass grid in order to compare computed strains with measurements. For this purpose, the computed radial and tangential strains in the glass grid (reinforcement) layer were studied. As shown in Figure 5-21 (a), the radial strain is defined as the strain along the radius of the loading area, while the tangential strain is defined as the strain which is perpendicular to the radial direction. Locations of radial and tangential strains in the experimental setup are shown in Figure 5-21 (b). The variations of computed strains (radial and tangential) with applied load in the glass grid layer are presented in Sections 5.6.3 and 5.6.4. A comparison of computed strain in the thick and thin pavement sections under different applied loads is presented in Section 5.6.5. Measured and computed strains (in the reinforcement layer) for thick and thin pavement sections are presented in Section 5.6.6.

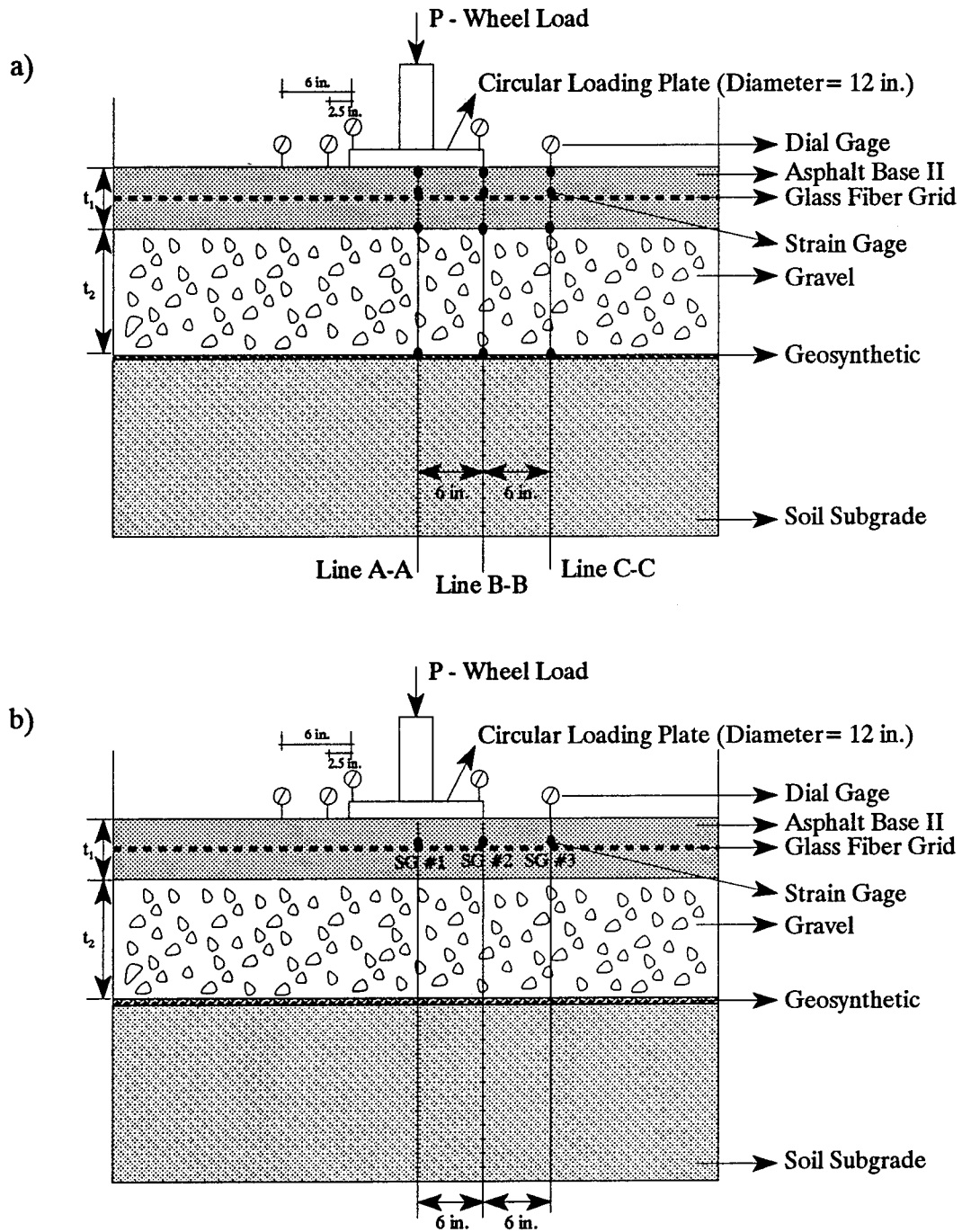
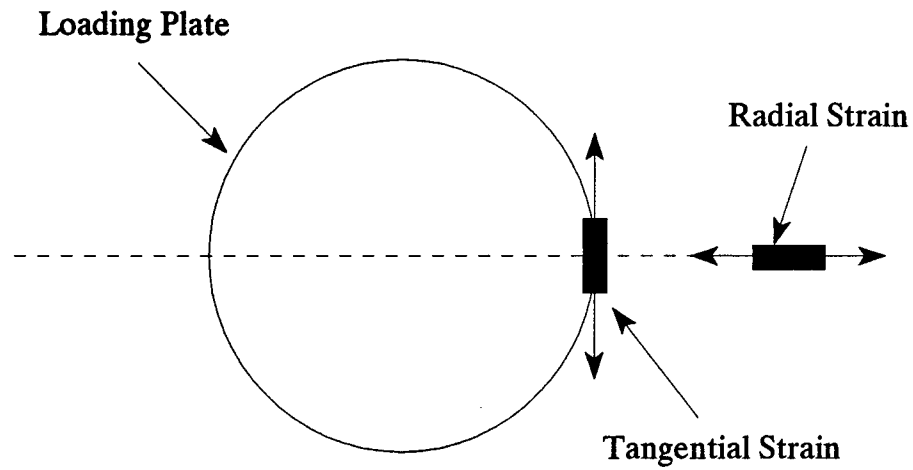


Figure 5-20: Locations of Computed Strains

- a) Reference Lines for Strain in the Pavement Section
b) Reference Points for Strain on Glass Grid

a)



b)

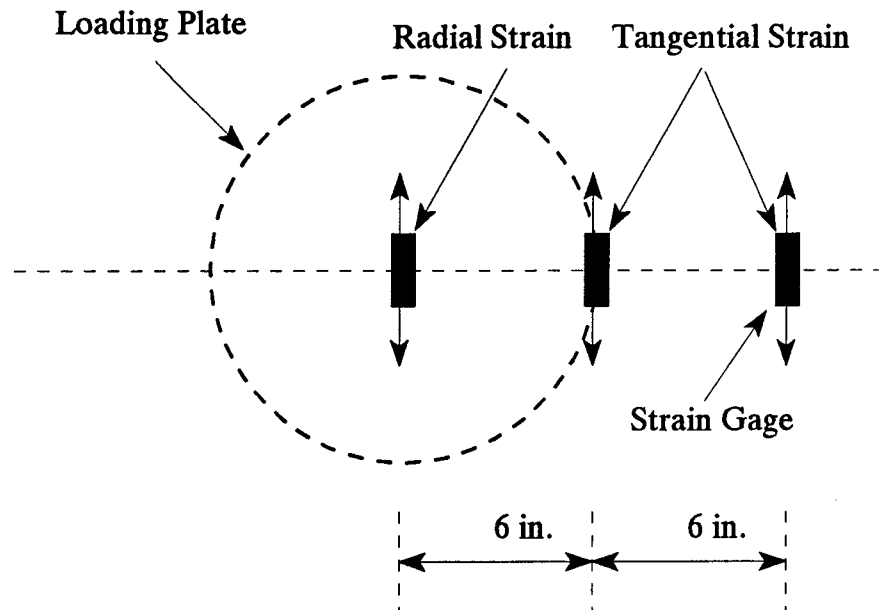


Figure 5-21: Location and Direction of Strains in Computer Analysis
a) Illustration of Tangential and Radial Strains
b) Locations of Strain Gages in the Experimental Setup

5.6.1 Variation Of Computed Strain With Depth In A Thick Pavement Section

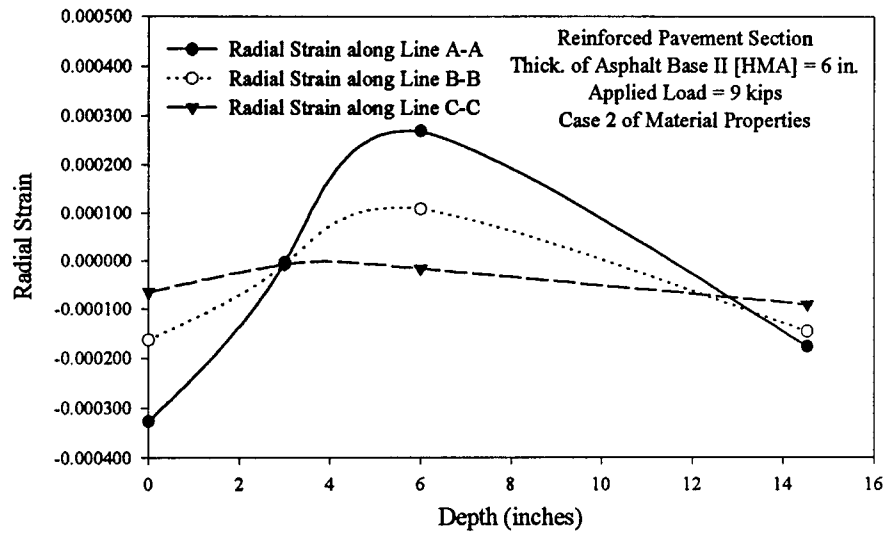
Variation of computed strain with depth for a thick reinforced pavement section [thickness of HMA = 6 inches (152 mm)] is shown in Figures 5-22 (a), (b), and (c). The effect of depth on radial strain is presented in Figure 5-22 (a) and Table 5-17. From this, the following comments are made:

- At the bottom of the HMA, the highest radial strain was 2.687 E-4 (in tension). At this depth, the radial strain along the line A-A was approximately 60% higher than the radial strain along the line B-B. Radial strain along the line C-C was in compression [Figure 5-22 (a)].
- In the middle of HMA layer, radial strains (along the lines A-A, B-B, and C-C) were in compression and were very small [Figure 5-22 (a)].
- As expected, the largest horizontal (radial) strain occurred at the bottom of HMA. At this depth, the horizontal tensile strain is an important factor for evaluating reflection cracking [Yoder and Witczak (1975)].

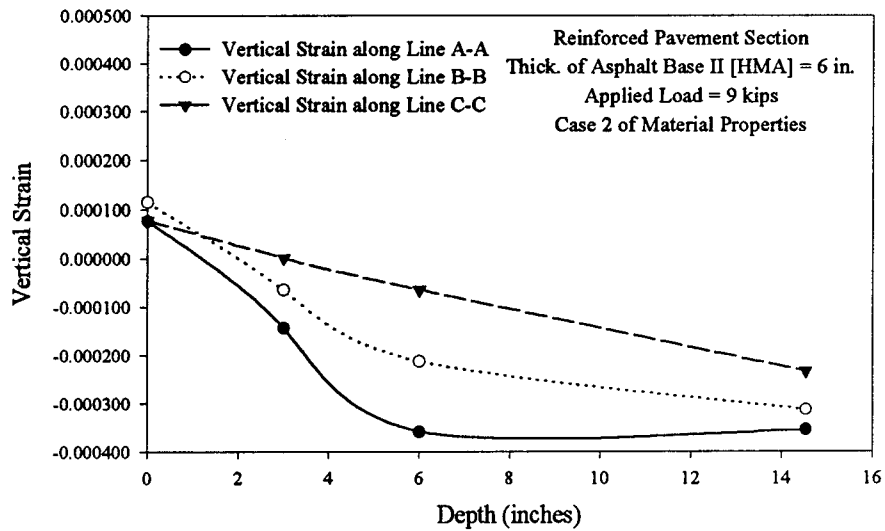
The effect of depth on vertical strain is presented in Figure 5-22 (b) and Table 5-17, and the following comments are made:

- Vertical strains along the lines A-A, B-B, and C-C were in compression. Even though the highest vertical strain was observed at the bottom of HMA along the line A-A, the vertical strain on top of subgrade was very close to the value at the bottom of HMA. The vertical strain along the line A-A was -3.588 E-4 at the bottom of HMA and -3.552 E-4 on top of the subgrade. This decrease was approximately 1% [Figure 5-22 (b)].
- Along the lines B-B and C-C, the highest vertical strains were observed on top of the

a)



b)



c)

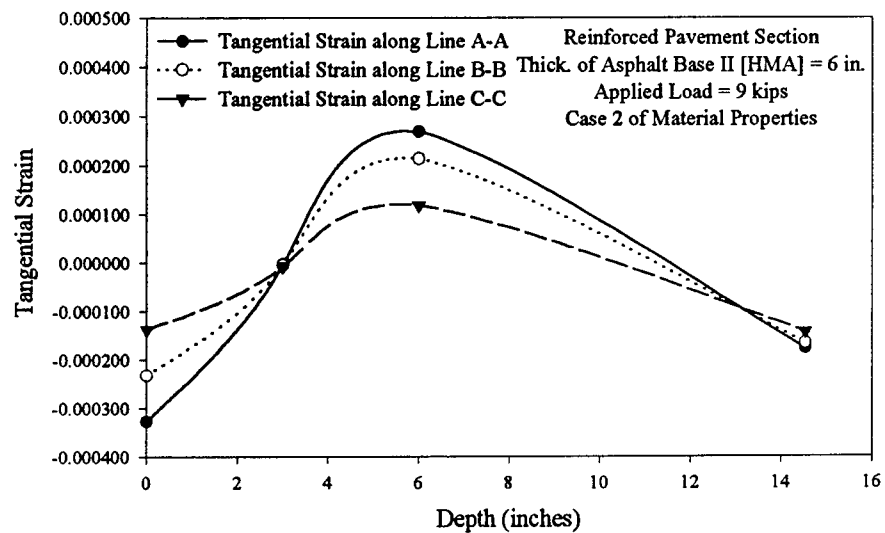


Figure 5-22: Variation of Computed Strain with Depth in a Thick Pavement Section

a) Radial Strain

b) Vertical Strain

c) Tangential Strain

Table 5-17: Effect of Depth on Computed Radial and Vertical Strains in Thick and Thin Pavement Sections

Thickness of Asphalt (in.) [mm]	Material Type	Depth of Computed Strain	Radial Strain along Line A-A	Radial Strain along Line B-B	Radial Strain along Line C-C	Vertical Strain along Line A-A	Vertical Strain along Line B-B	Vertical Strain along Line C-C
6 [152]	HMA	0	-3.271 E-4	-1.645 E-4	-6.584 E-5	7.752 E-5	1.152 E-4	7.856 E-5
		3 [76]	-3.491 E-6	-8.377 E-6	-7.701 E-6	-1.435 E-4	-6.480 E-5	2.036 E-6
	Gravel Base	6 [152]	2.687 E-4	1.082 E-4	-1.692 E-5	-3.588 E-4	-2.131 E-4	-6.408 E-5
	Subgrade	14.54 [369.32]	-1.775 E-4	-1.467 E-4	-9.107 E-5	-3.552 E-4	-3.135 E-4	-2.338 E-4
3 [76]	HMA	0	-5.307 E-5	-1.662 E-5	-5.429 E-6	2.213 E-4	1.383 E-4	6.433 E-5
		1.5 [38.1]	-2.237 E-6	-1.671 E-6	-6.485 E-7	-1.669 E-4	-7.185 E-5	8.733 E-6
	Gravel Base	3 [76]	3.722 E-5	6.593 E-6	-7.933 E-6	-5.040 E-4	-2.406 E-4	-1.882 E-5
	Subgrade	11.54 [293.12]	-3.202 E-5	-2.387 E-5	-1.121 E-5	-5.760 E-4	-4.765 E-4	-3.091 E-4

subgrade.

- On top of the subgrade soil, vertical compressive strain along the line A-A was approximately 12% higher than the vertical compressive strain along the line B-B and approximately 34% higher than the vertical compressive strain along the line C-C.
- The vertical compressive strain on top of subgrade is shown in Figure 5-22 (b). At this depth, the vertical strain is an important factor for evaluating rutting effects [Yoder and Witczak (1975)].

Variation of tangential strain with depth is shown in Figure 5-22 (c) and Table 5-18, and the following comments are made:

- The highest tangential strain was observed at the HMA/gravel-base interface along the line A-A, where it was in tension [Figure 5-22 (c)].
- At the HMA/gravel-base interface, the tangential strain along the line A-A was 2.687 E-4 (in tension). This was approximately 20% higher than tangential strain along the line B-B and approximately 56% higher than tangential strain along the line C-C.
- At the gravel-base/subgrade interface, the tangential strains were in compression.

5.6.2 Variation Of Computed Strain With Depth In A Thin Pavement Section

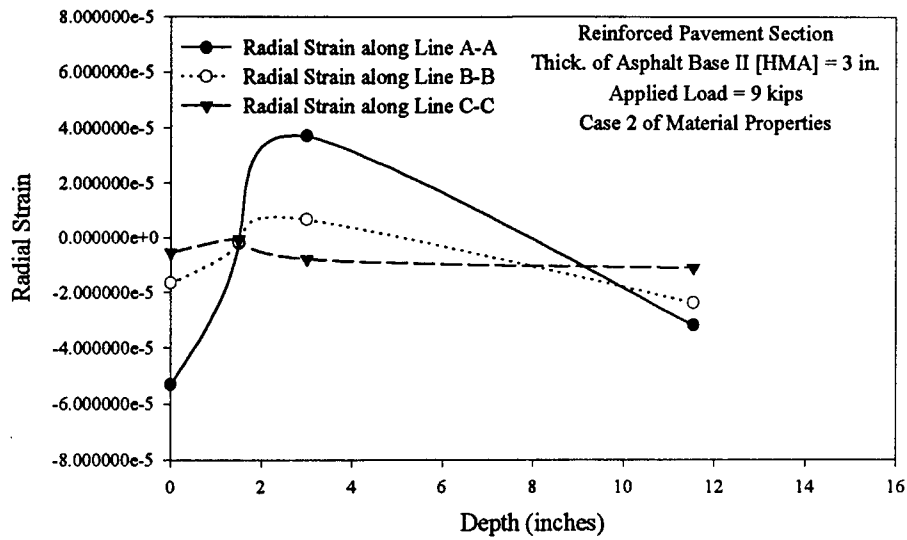
Similar comparisons were made for a thin reinforced pavement section. The thickness of HMA was 3 inches (76 mm) at this section. Variation of computed strain with depth for the thin reinforced pavement section is shown in Figures 5-23 (a), (b), and (c). Figure 5-23 (a) shows the effect of depth on radial strain and the comments are presented below:

- Similar to the thick reinforced pavement section, the highest radial strain was observed beneath the center of the loading area (radial strain along the line A-A) at

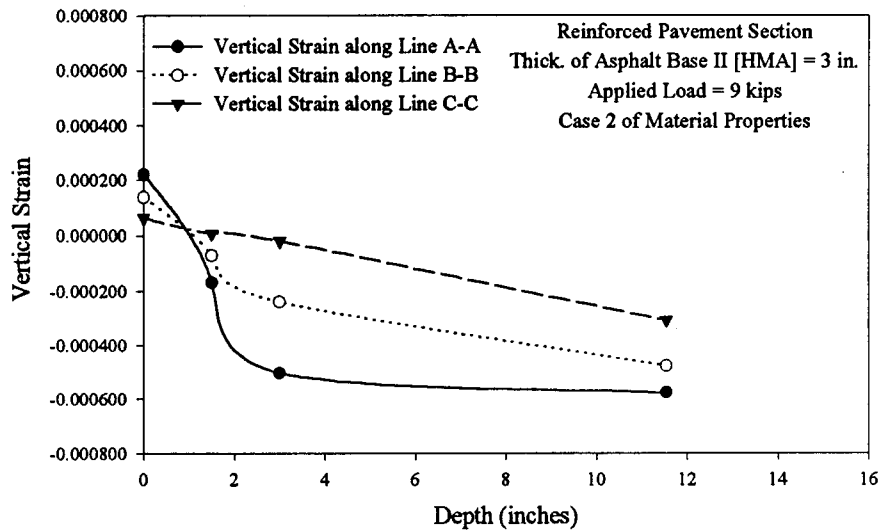
Table 5-18: Effect of Depth on Computed Tangential Strains in Thick and Thin Pavement Sections

Thickness of Asphalt (in.) [mm]	Material Type	Depth of Computed Strain	Tangential Strain along Line A-A	Tangential Strain along Line B-B	Tangential Strain along Line C-C
6 [152]	HMA	0	-3.271 E-4	-2.322 E-4	-1.372 E-4
		3 [76]	-3.491 E-6	-4.914 E-6	-7.150 E-6
	Gravel Base	6 [152]	2.687 E-4	2.140 E-4	1.187 E-4
	Subgrade	14.54 [369.32]	-1.775 E-4	-1.666 E-4	-1.426 E-4
3 [76]	HMA	0	-5.307 E-5	-3.350 E-5	-1.422 E-5
		1.5 [38.1]	-2.237 E-6	-2.034 E-6	-1.595 E-6
	Gravel Base	3 [76]	3.722 E-5	2.879 E-5	1.088 E-5
	Subgrade	11.54 [293.12]	-3.202 E-5	-2.911 E-5	-2.316 E-5

a)



b)



c)

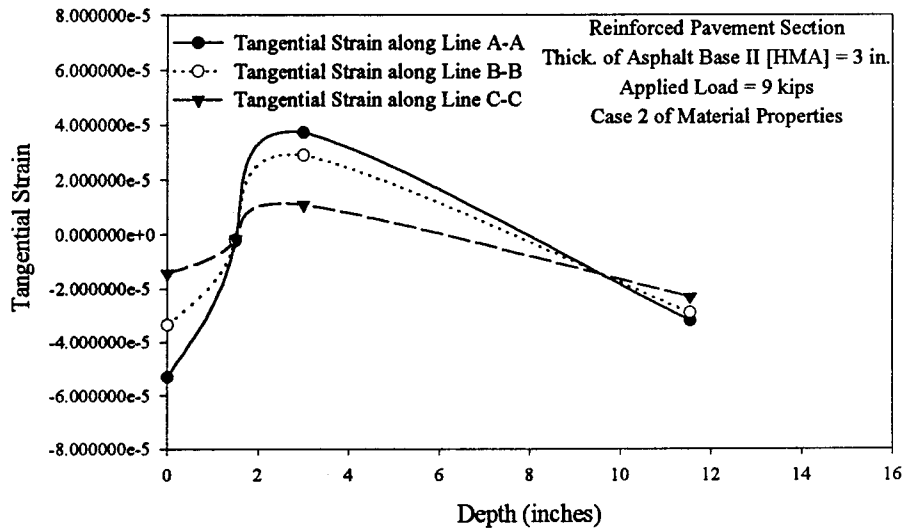


Figure 5-23: Variation of Computed Strain with Depth in a Thin Pavement Section

- a) Radial Strain
- b) Vertical Strain
- c) Tangential Strain

the HMA/gravel-base interface. Radial strain along the line A-A was 3.722 E-5 (in tension) and was approximately 82% higher than the radial strain along the line B-B at the HMA/gravel base interface. Radial strain along the line C-C was in compression [Figure 5-23 (a)].

- In the middle of the HMA, radial strains (along the lines A-A, B-B, and C-C) were in compression and were very small.
- Similar to the results for the thick pavement section, the highest horizontal tensile (radial) strain occurred at the bottom of the HMA for the thin reinforced pavement section.

The effect of depth on vertical strain is presented in Figure 5-23 (b) and Table 5-17. The following comments are made:

- As expected, the vertical strains on top of the subgrade were in compression.
- The highest vertical compressive strains along the lines A-A, B-B, and C-C were observed on top of the subgrade [Figure 5-23 (b)].
- On top of the subgrade, vertical strain along the line A-A was approximately 17% higher than vertical strain along the line B-B and approximately 46% higher than vertical strain along the line C-C (Table 5-17).
- As shown in Table 5-17, from the HMA/gravel-base interface to the gravel-base/subgrade interface, vertical strains increased. This increase was approximately 13% for vertical strain along the line A-A, 50% for vertical strain along the line B-B, and 94% for vertical strain along the line C-C.
- The vertical compressive strain on top of subgrade is shown in Figure 5-23 (b).

Similar to the reinforced thick pavement section, the vertical strain is an important factor for evaluating rutting effects at this depth [Yoder and Witczak (1975)].

Variation of tangential strains with depth is shown in Figure 5-23 (c) and Table 5-18. The following comments are made:

- At the HMA/gravel-base interface, similar to the results for thick reinforced pavement section, the highest tangential strain was observed along the line A-A. At the bottom of the HMA, tangential strains were in tension.
- As shown in Table 5-18, at the HMA/gravel-base interface (at the bottom of the HMA), tangential strain along the line A-A was approximately 23% larger than tangential strain along the line B-B and approximately 71% larger than tangential strain along the line C-C.
- Tangential strains were in compression on top of the subgrade.

5.6.3 Computed Strain In The Reinforcement Layer In A 6-Inch (152 mm) Thick HMA Layer

The variation of computed strains (radial and tangential) in the reinforcement layer with the applied load for the thick pavement section is shown in Figure 5-24. Computed radial strains on the reinforcement layer located in the middle of the HMA for this section are shown in Figure 5-24 (a), while the computed tangential strains are shown in Figure 5-24 (b). The following items highlight the results of the radial strain analysis [Figure 5-24 (a)] and are presented in Table 5-19:

- Highest radial strains occurred at the edge of the loading area (radial strain #2), while the lowest radial strains occurred at the center of the loading area (radial strain #1).
- Under the 9 kips (40 kN) of applied load, the radial strain #2 was approximately 8%

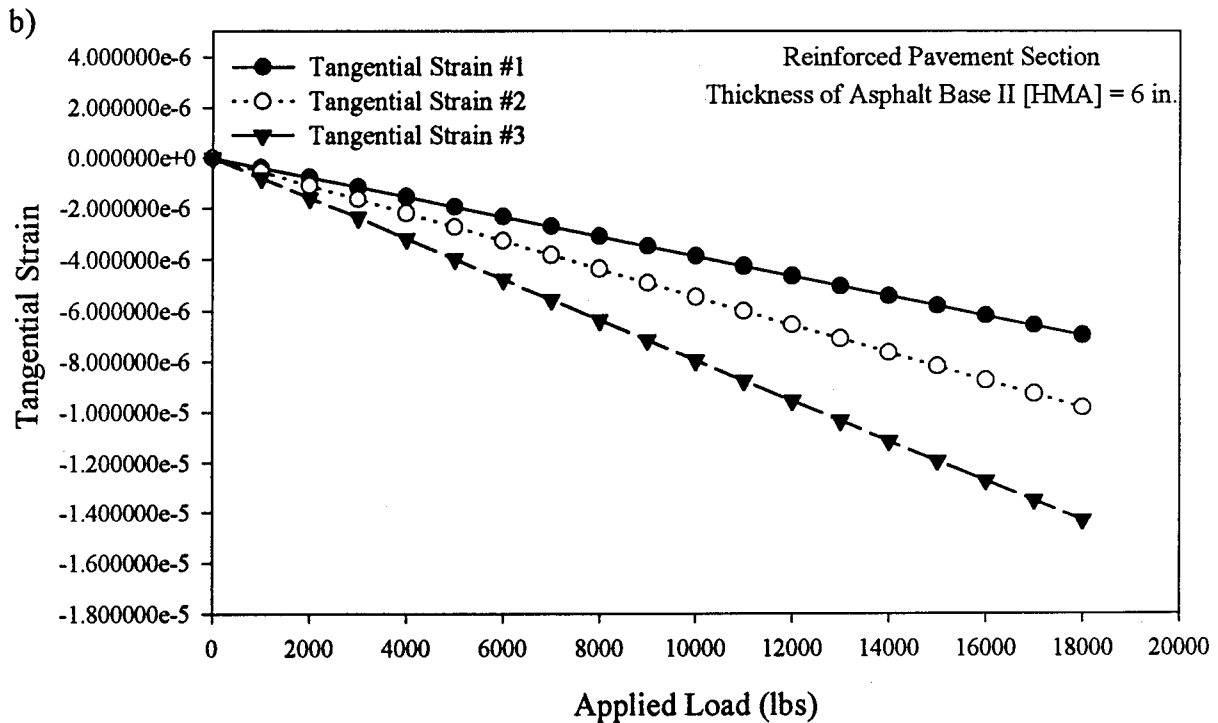
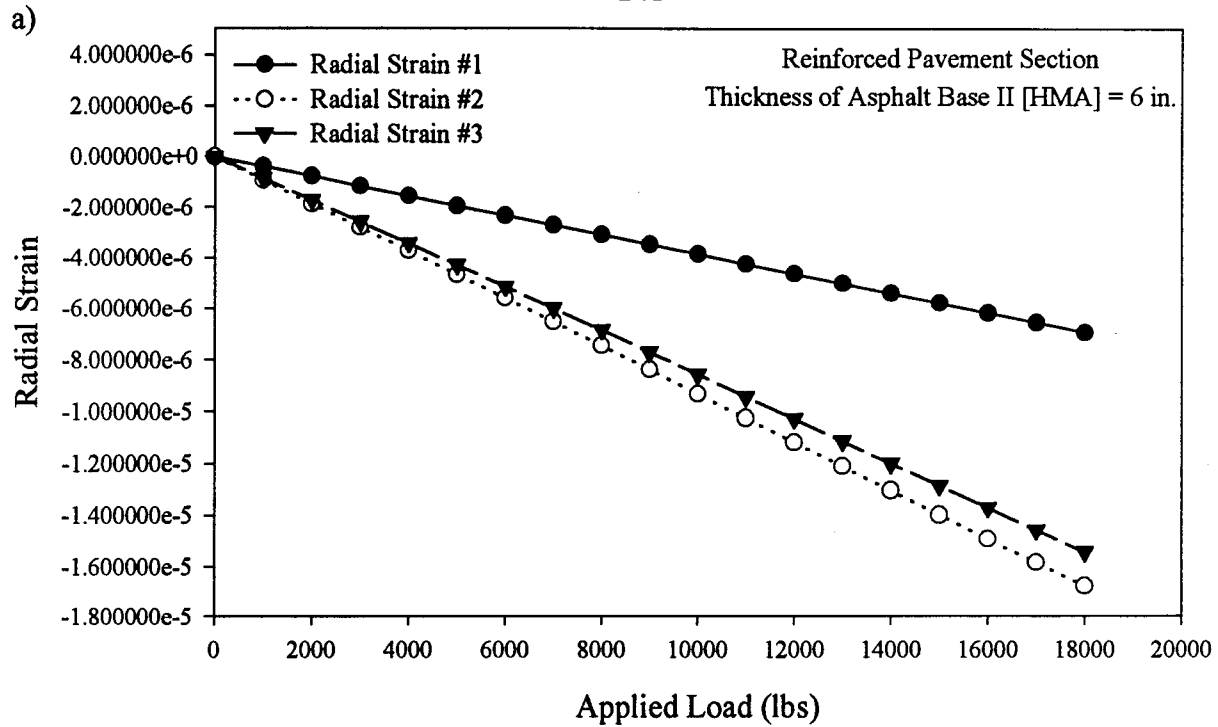


Figure 5-24: Computed Strain in the Reinforcement Layer in a Thick Pavement Section
a) Radial Strain
b) Tangential Strain

Table 5-19: Computed Radial and Tangential Strains on the Reinforcement Layer in Thick and Thin Pavement Sections

Thickness of Asphalt (in.) [mm]	Depth of Computed Strain	Applied Load (kip)[kN]	Radial Strain #1	Radial Strain #2	Radial Strain #3	Tangential Strain #1	Tangential Strain #2	Tangential Strain #3
6 [152]	3 [76]	9 [40]	-3.474 E-6	-8.374 E-6	-7.703 E-6	-3.474 E-6	-4.901 E-6	-7.145 E-6
		18 [80]	-6.957 E-6	-1.677 E-5	-1.543 E-5	-6.957 E-6	-9.816 E-6	-1.431 E-5
3 [76]	1.5 [38.1]	9 [40]	3.346 E-4	5.925 E-5	-7.131 E-5	3.346 E-4	2.588 E-4	9.777 E-5
		18 [80]	6.701 E-4	1.187 E-4	-1.428 E-4	6.701 E-4	5.184 E-4	1.958 E-4

higher than the radial strain #3, and approximately 59% higher than the radial strain #1 in the reinforcement layer (Table 5-19).

- Radial strains #1, #2, and #3 were in compression.

Figure 5-24 (b) shows the variation of tangential strain in the reinforcement layer, which is located in the middle of HMA. The following comments can be made on the basis of Figure 5-24 (b) and Table 5-19:

- Highest tangential strains occurred at the strain gage (tangential strain #3) which was the furthest away from the applied load. Tangential strain increased with increasing radial distance measured from the center of load.
- Under the 9 kips (40 kN) of loading, tangential strain #3 was approximately 31% higher than tangential strain #2 and approximately 51% higher than tangential strain #1 (Table 5-19).
- Tangential strains were in compression.

5.6.4 Computed Strain In The Reinforcement Layer In A 3-Inch (76 mm) Thick HMA Layer

A similar comparison was performed for a thin pavement section. Figure 5-25 (a) shows the radial strain in the reinforced layer, which is located in the middle of HMA. Based on the Figure 5-25 (a) and Table 5-19, the following comments can be made:

- Unlike the results for the thick pavement section, the radial strains #1 and #2 were in tension. Radial strain #3 was in compression. The variation of computed strains (radial strains #1, #2, and #3) with load was linear, which is similar to that in a thick pavement section.
- Under the 9 kips (40 kN) of applied load, radial strain #1 was approximately 82%

higher than radial strain #2 (Table 5-19).

Figure 5-25 (b) shows the variation of tangential strain in the reinforcement layer. Based on Figure 5-25 (b) and Table 5-19, the following comments can be made:

- Unlike the results for the thick pavement section, the tangential strains (tangential strains #1, #2, and #3) for the thin pavement section were all in tension.
- The highest tangential strains occurred at the strain gage (tangential strain #1) beneath the center of the applied load.
- Unlike with the thick pavement section, the tangential strain decreased with the increasing radial distance.
- Under the 9 kips (40 kN) of loading, tangential strain #1 was approximately 23% higher than tangential strain #2 and approximately 71% higher than tangential strain #3.

5.6.5 Influence Of HMA Thickness On Computed Strains in the Reinforcement Layer

Computed strains in thick and thin pavement sections are shown in Figures 5-26 (a) and (b) for different values of applied loads. Based on these results, the following comments can be made:

- In the reinforcement layer, radial strains #1 and #3 for the thick pavement section were in compression while only radial strain #3 was in compression for the thin pavement section [Figure 5-26 (a)].
- Tangential strains were in compression for the thick pavement section and in tension for the thin pavement section [Figure 5-26 (b)].
- The highest tangential strain (in tension) was observed beneath the center of the loading plate for the thin pavement section. For the thick pavement section, the

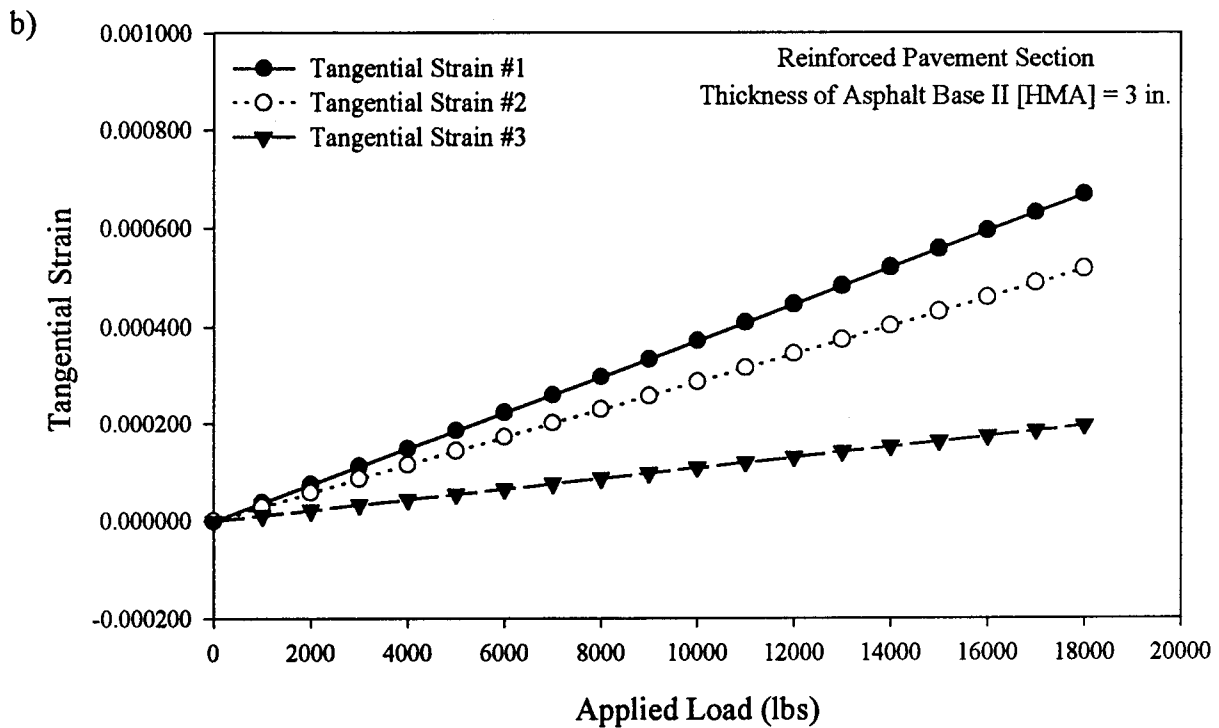
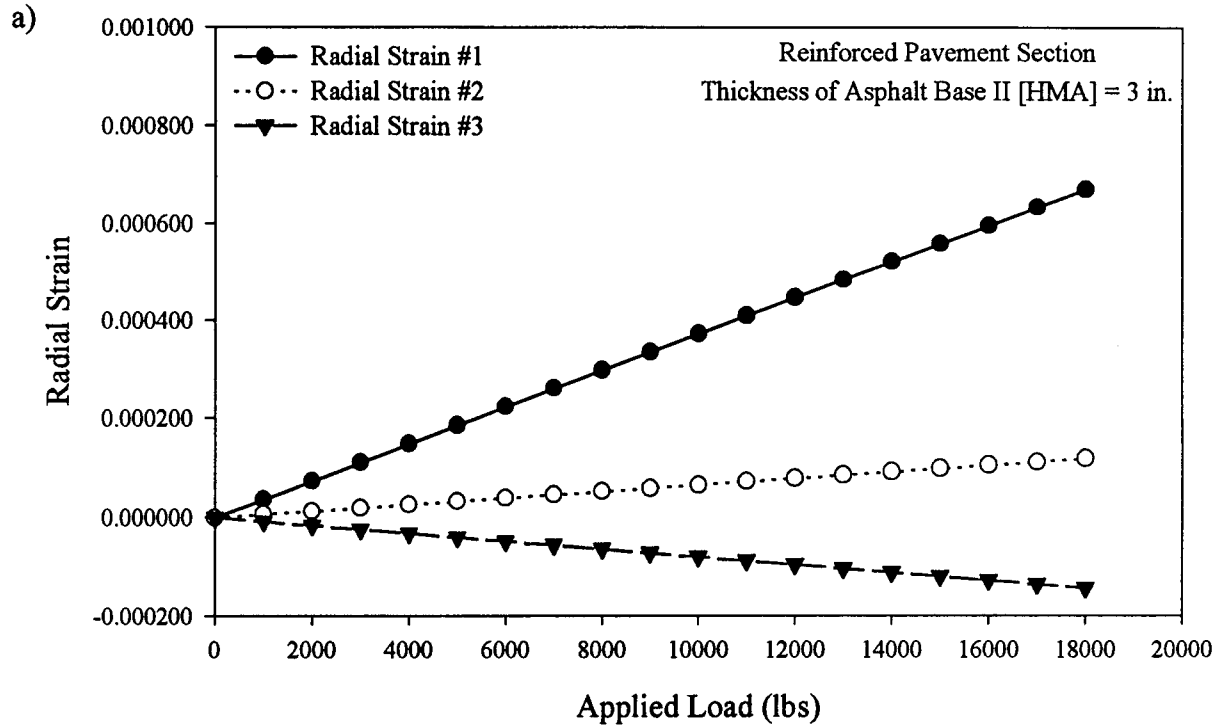


Figure 5-25: Computed Strain in the Reinforcement Layer in a Thin Pavement Section
a) Radial Strain
b) Tangential Strain

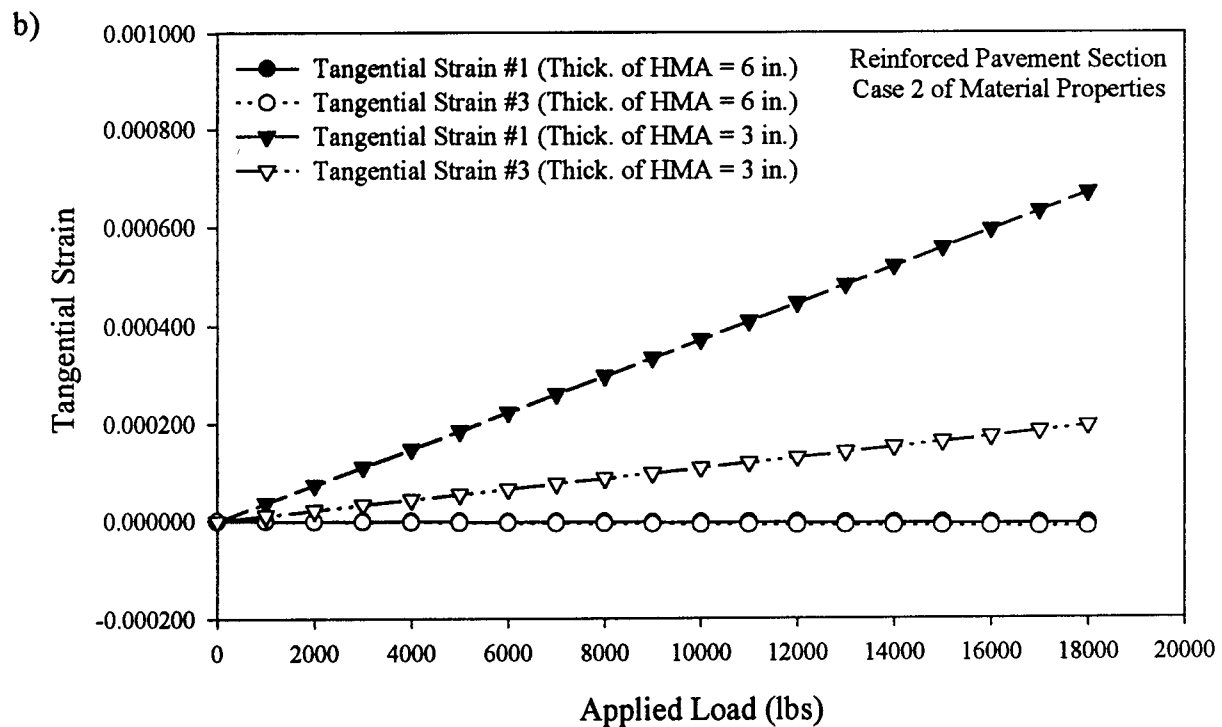
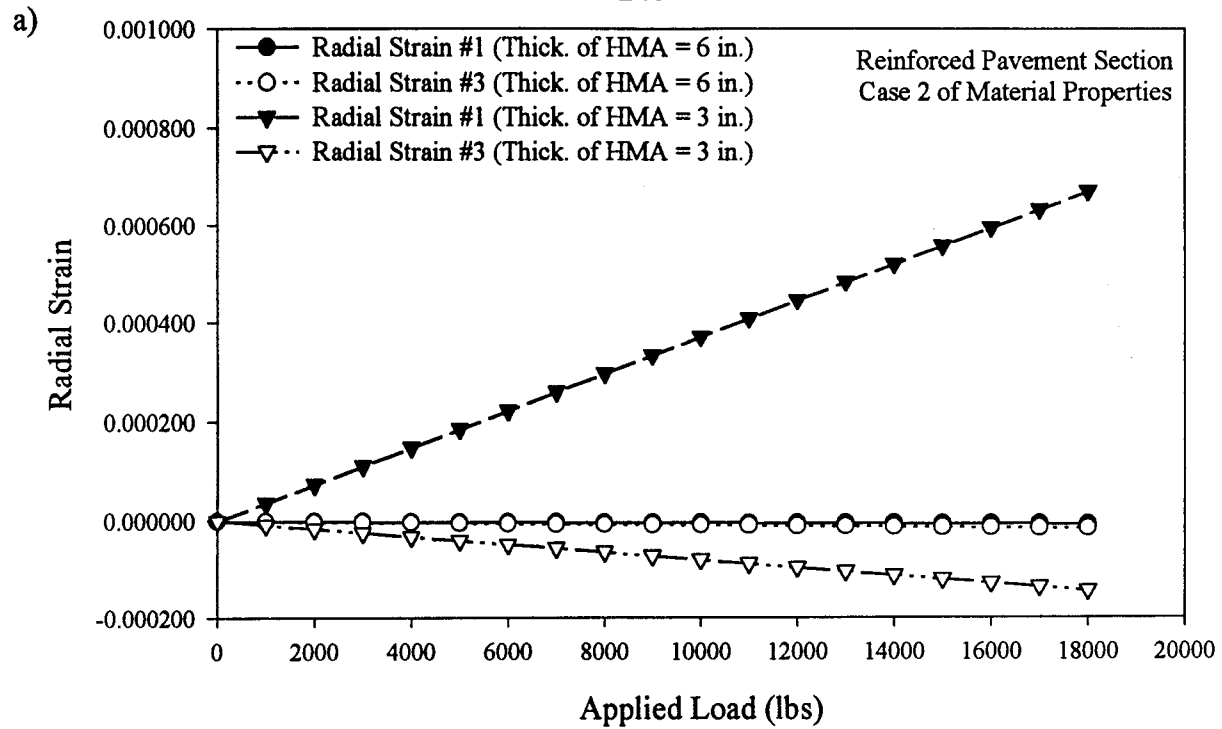


Figure 5-26: Influence of HMA Thickness on Computed Strains
a) Radial Strain
b) Tangential Strain

highest tangential strain (in compression) occurred at the strain gage (strain #3), which was the furthest away from the applied load.

- Radial and tangential strains for the thick pavement section were smaller than those for the thin pavement section [Figures 5-26 (a) and (b)] (Table 5-19).
- Radial and tangential strains for the thick pavement section were very small; under the 18 kips (80 kN) of loading, the maximum radial strain was -1.677 E-5 (in compression) and the maximum tangential strain was -1.431 E-5 (in compression) for the thick pavement section (Table 5-19).
- Under the 18 kips (80 kN) of loading, the maximum radial strain was 6.701 E-4 (in tension) and the maximum tangential strain was 6.701 E-4 (in tension) for the thin pavement section (Table 5-19).

5.6.6 Comparison Of Computed Strains With Measurements

A comparison between the computed strain and the measured strain for the thick [thickness of HMA = 6-inch (152 mm)] and thin [thickness of HMA = 3-inch (76 mm)] pavement sections with reinforcement is shown in Figures 5-27 (a) and (b). As mentioned in Section 4.4, the strain gages were placed on the glass grid. The measured strains for the glass grid and the computed strains in the HMA obtained by the KENLAYER [Huang (1993)] computer analysis are fundamentally different since KENLAYER does not have the capability of calculating the strains on the glass grid. However, the locations (depth) of these strains are the same.

Figure 5-27 (a) shows the comparison between the measured and the computed tangential strains at radial distances of 6 inches (152 mm) and 12 inches (305 mm) for the thick reinforced pavement sections and the following comments are made:

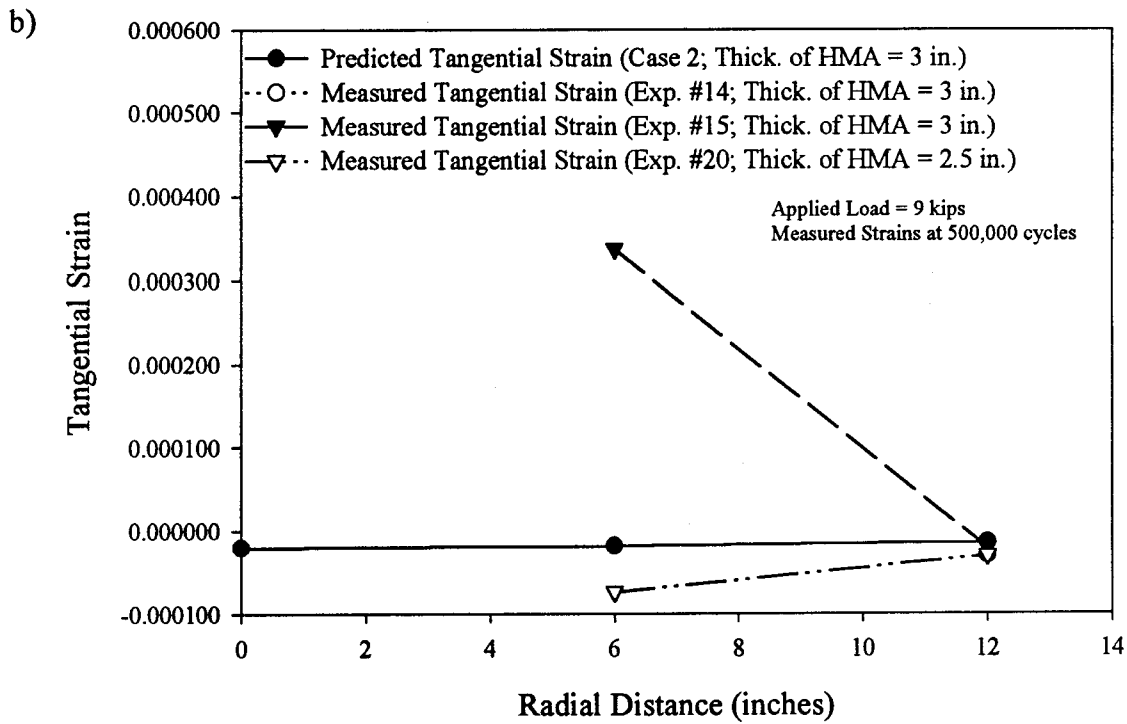
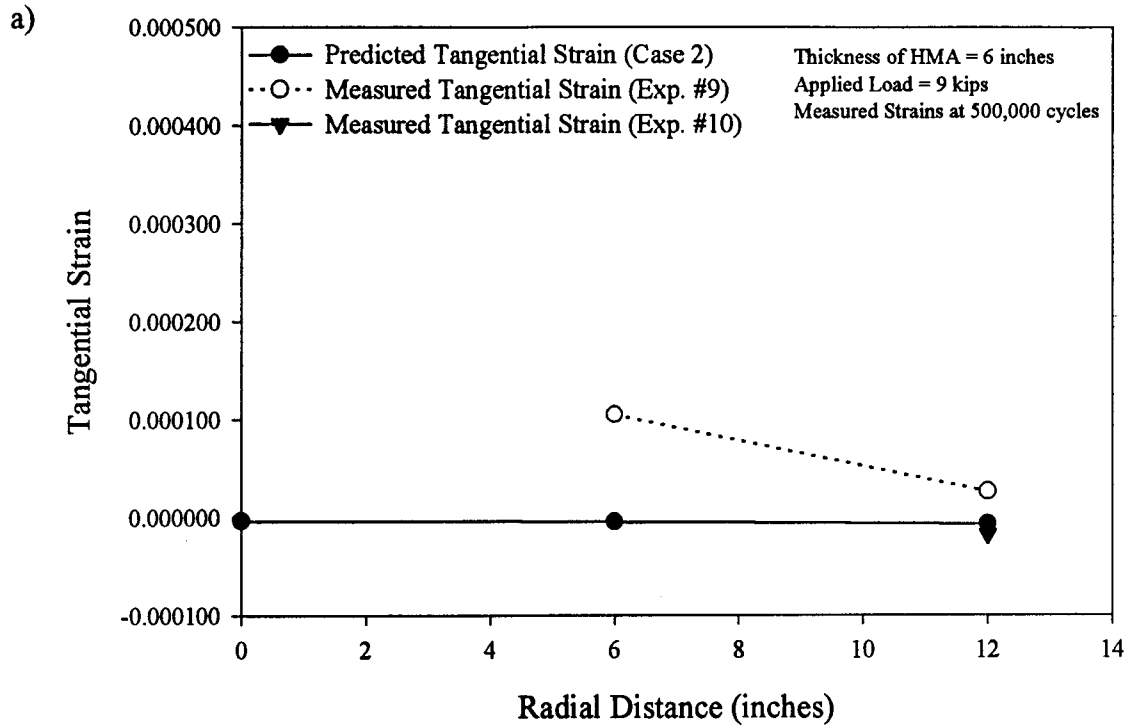


Figure 5-27: Comparison of Measured and Computed Tangential Strains
a) Thick HMA Section
b) Thin HMA Section

- The computed tangential strains were in compression and increased with the increasing radial distance.
- Measured tangential strain for Experiment #9 at the edge of the loading area [at a radial distance of 6 inches (152 mm)] was in tension and did not match very well with the computed tangential strain. Measured tangential strain for Experiment #10 at this location was not available [Figure 5-27 (a)].
- At a radial distance of 12 inches (305 mm), the measured tangential strains (in the reinforcement layer) for Experiments #9 and #10 matched closely with the computed tangential strains.

Figure 5-27 (b) shows a similar comparison for the thin reinforced pavement sections [thickness of HMA = 2.5-inch (63.5 mm) and (3-inch (76 mm))]. The following comments are presented:

- Computed tangential strains were in compression and decreased with increasing radial distance.
- Measured tangential strain at the edge of the loading area [at a radial distance of 6 inches (152 mm)] for Experiment #15 [thickness of HMA = 3 inches (76 mm)] did not match well with the computed tangential strain. Measured tangential strain for Experiment #20 [thickness of HMA = 2.5 inches (63.5 mm)] was closer than the strain for Experiment #15 to the computed tangential strain. Measured tangential strain for Experiment #14 [thickness of HMA = 3 inches (76 mm)] at this location was not available. While the measured strain for Experiment #15 was in tension at this location, the measured strain for Experiment #20 was in compression [Figure 5-27

(b)].

- At a radial distance of 12 inches (305 mm), the measured tangential strains (in the reinforcement layer) for Experiments #14, #15, and #20 were in compression. These measurements compared well with the computed strains [Figure 5-27 (b)].

5.6.7 Summary Of Results On Computed Strain Analyses

Based on the results presented above, the following conclusions can be made for the computed strains inside the pavement section:

Variation of Computed Strain with Depth in a Thick and a Thin Pavement Sections

- The highest radial and tangential strains were observed beneath the center line of the loading plate (along the line A-A) at the HMA/gravel-base interface. At this depth, the radial strains (along the lines A-A and B-B) and the tangential strains (along the lines A-A, B-B, and C-C) were in tension [See Sections 5.6.1 and 5.6.2 and Figure 5-20 (a)].
- In the middle of the HMA, radial strains along the lines A-A, B-B, and C-C [Figure 5-20 (a)] were in compression.
- The highest vertical compressive strains were observed on top of the subgrade.
- Tangential strains were in compression on top of the subgrade.

Influence of HMA Thickness on Computed Strains in the Reinforcement Layer

- In the reinforcement layer, radial strains #1 and #3 [Figure 5-20 (b)] for the thick pavement section were in compression while only radial strain #3 was in compression for the thin pavement section.
- Tangential strains were in compression for the thick pavement section and in tension for the thin pavement section [See Section 5.6.5].

- The highest tangential strain (in tension) was observed beneath the center of the loading plate for the thin pavement section. For the thick pavement section, the highest tangential strain (in compression) occurred at the strain gage (strain #3), which was the furthest away from the applied load [See Section 5.6.5].
- Radial and tangential strains for the thick pavement section were smaller than those for the thin pavement section.

Comparison of Computed Strains with Measurements

- At a radial distance of 12 inches (305 mm), the measured tangential strains (in the reinforcement layer) for the thick and the thin pavement sections matched closely with the computed tangential strains [See Section 5.6.6].
- At a radial distance of 6 inches (152 mm) (at the edge of the loading area), the measured tangential strains in the reinforcement layer for the thin and the thick pavement sections did not match well with the computed tangential strains.

5.7 FINITE ELEMENT ANALYSIS (FEA)

There have been a few applications of the finite element method (FEM) to study problems associated with flexible pavement systems [Duncan et al. (1968), Jayawickrama and Lytton (1987), Raad and Figueroa (1980), Wathugala et al. (1996), Zaghoul and White (1993) and Jenq et al. (1993)]. Finite element method is a powerful tool for solving complex problems like flexible pavements. The computer program used for finite element analysis in this research study was developed by Siriwardane (1983). Four noded isoparametric quadrilateral elements were used in the FEM analysis. The equilibrium equations for an element can be written as [Desai (1979) and Zienkiewicz (1977)] :

$$[k] \{q\} = \{Q\} \quad (5.14)$$

where

$[k]$ = the element stiffness matrix,
 $\{q\}$ = the element displacement vector, and
 $\{Q\}$ = the element load vector.

These terms can be expressed as:

$$[k] = \int \int \int_V [B]^T [C] [B] dV \quad (5.15)$$

$$\{Q\} = \int \int \int_V [N]^T \{\bar{X}\} dV + \int \int_{SI} [N]^T \{\bar{T}\} ds - \int \int \int_V [B]^T \{\sigma_o\} dV \quad (5.16)$$

where

- $[B]$ = the strain displacement relationship
- $[C]$ = the constitutive relationship
- $\{\sigma_o\}$ = the vector of initial stresses such as insitu stresses
- $\{X\}$ = the body force vector
- $\{T\}$ = the surface traction vector
- $[N]$ = the matrix of interpolation functions
- S_i = the surface on which the surface traction is applied
- V = the volume of the element

Different constitutive models of geological materials can be found in the literature [Desai and Siriwardane (1983)]. Both axisymmetric and plane strain idealization were considered in the FEM analyses in this research study. The laboratory experiments were analyzed using the axis-symmetric idealization. In the axisymmetric idealization, the loading plate was considered symmetrical about its centerline axis as shown in Figure 5-28. Figure 5-29 shows the plane strain approximation for a strip load. In plane strain idealization, the load is considered to be applied in the plane of the structure (the x-y plane). It is assumed that the displacement component in the $\{z\}$ direction is zero, and other displacement components in the $\{x, y\}$ directions are independent of the displacement component in the $\{z\}$ direction. Detailed information for both cases can be found in the literature [Desai (1979) and Zienkiewicz (1977)].

5.7.1 Results Of The Finite Element Analyses Of Laboratory Test Section

In addition to the KENLAYER [Huang (1993)] computer analyses, the Finite Element Method (FEM) was used to analyze a flexible pavement system reinforced with glass grid in this research study. Linear elastic constitutive relationship was used for modeling the idealized flexible pavement section. Linear elastic finite element analyses were based on both the axisymmetric and the

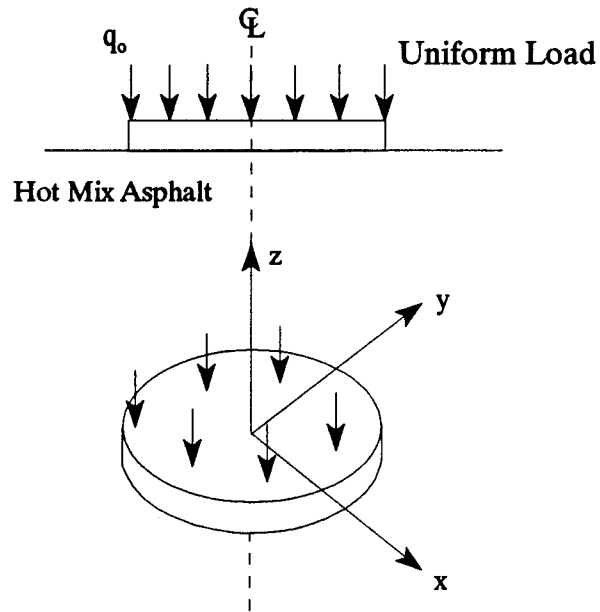


Figure 5-28: Axisymmetric Approximation

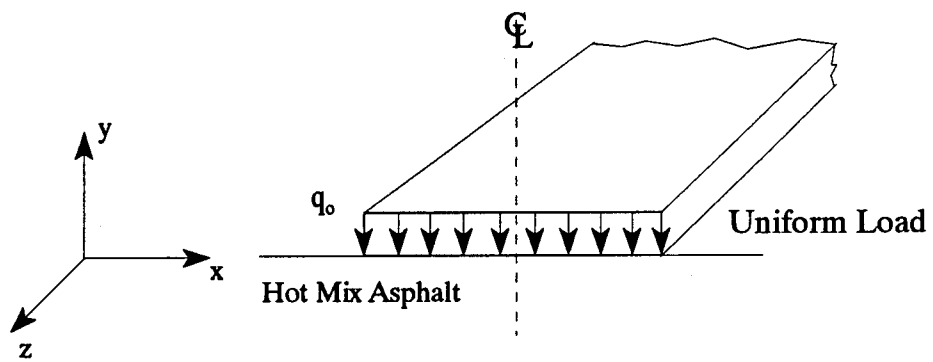


Figure 5-29: Plane Strain Approximation

plane strain idealizations. For these analyses, the hot mix asphalt (HMA) thickness for a reinforced flexible pavement section was 3 inches (76 mm). The dimensions for the axisymmetric case were obtained from the laboratory experiments. The finite element mesh of the flexible pavement section is shown in Figure 5-30. This mesh was used in both axis-symmetric and plane strain analysis. Material properties used in the finite element analysis are shown in Table 5-20. These properties were obtained on the basis of information reported in the literature [Agarwal and Broutman (1990), Desai and Siriwardane (1983), Smith et al. (1995), Thompson and Elliot (1985) and Yoder and Witczak (1975)].

The plane strain analysis was also performed for an actual field case with a 12-foot (0.3 m) traffic lane by applying the dual wheel load on one half of the 12-foot (3.7 m) lane. The spacing between the center of tires in a set of dual wheel was chosen as 13.5 inches (34.3 cm). The dimensions for the traffic lanes were adopted from the American Association of State Highway and Transportation Officials (AASHTO) Standard Specifications for Highway Bridges (1992). A tire width of 6.22 inches (15.80 cm) was chosen for the finite element analysis [Huang (1993)]. The thickness of the section was taken as 1 unit in the plane strain analysis. A tire pressure of 80 psi (551 kN/m²) was used for both the axisymmetric and the plane strain cases. Geometric details of this pavement section are shown in Figure 5-31. The finite element mesh dimensions for this particular pavement section are shown in Figure 5-32. The results of the FEM analyses are presented below.

Axisymmetric Idealization Of The Laboratory Test Section

Figures 5-33 through 5-39 show the results of the finite element (FE) analyses corresponding to the modeling of the laboratory test section where the thickness of the HMA is 3 inches (76 mm). Figure 5-33 shows the vertical stress computed by using the finite element analysis (axisymmetric

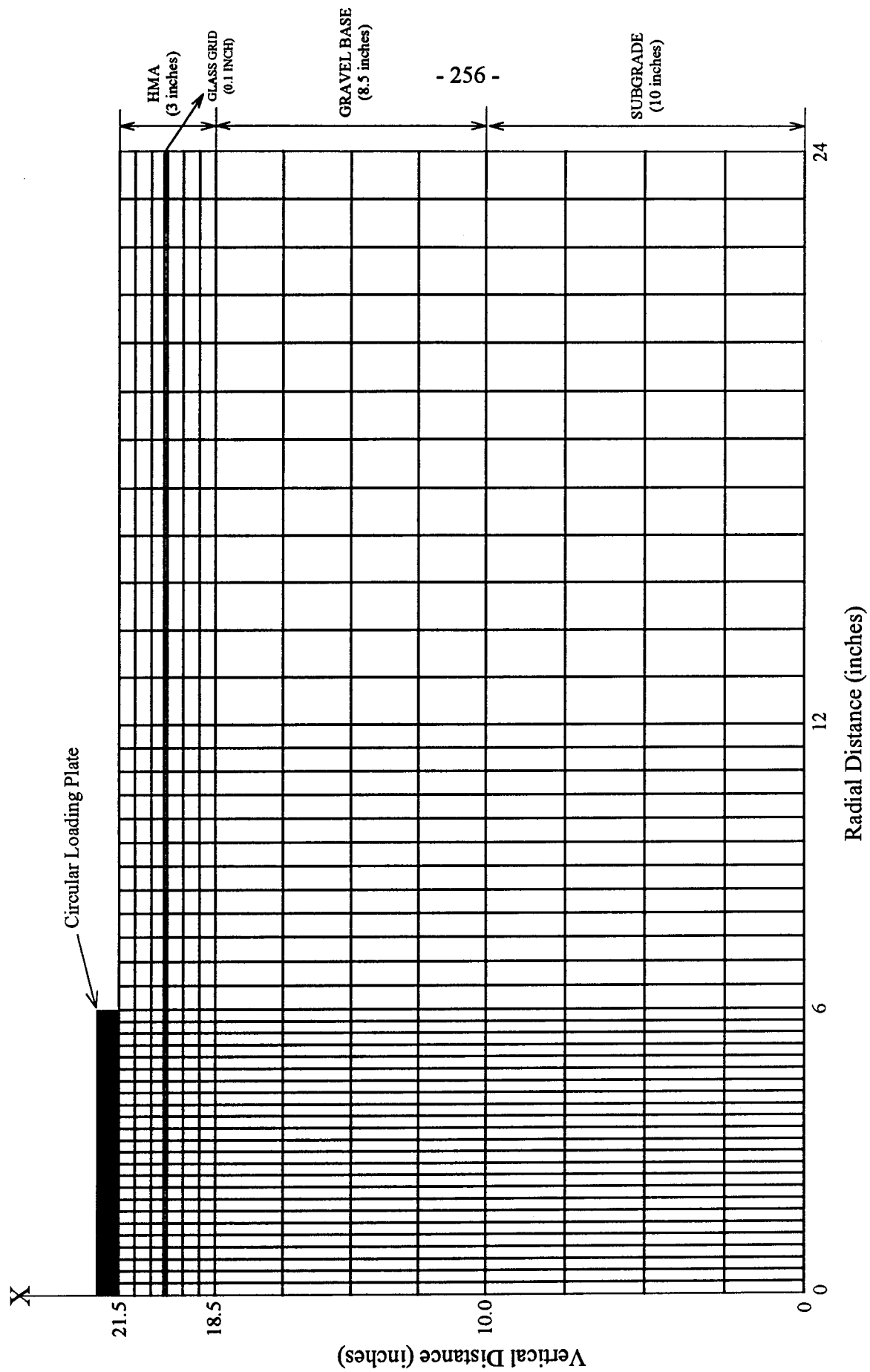


Figure 5-30: Finite Element Mesh Used for Thin Pavement Section (Axisymmetric Case)

Table 5-20: Assumed Material Properties Used in the Finite Element Analysis

Layer	Elastic Modulus (E) - psi [kN/m ²]	Poisson's Ratio (v)
Hot Mix Asphalt (HMA)	270,000 [1,860,300]	0.35
Gravel Base	46,000 [316,940]	0.30
Subgrade	6,000 [41,340]	0.30
Glass Fiber Grid	4,205,000 [28,972,450]	0.30

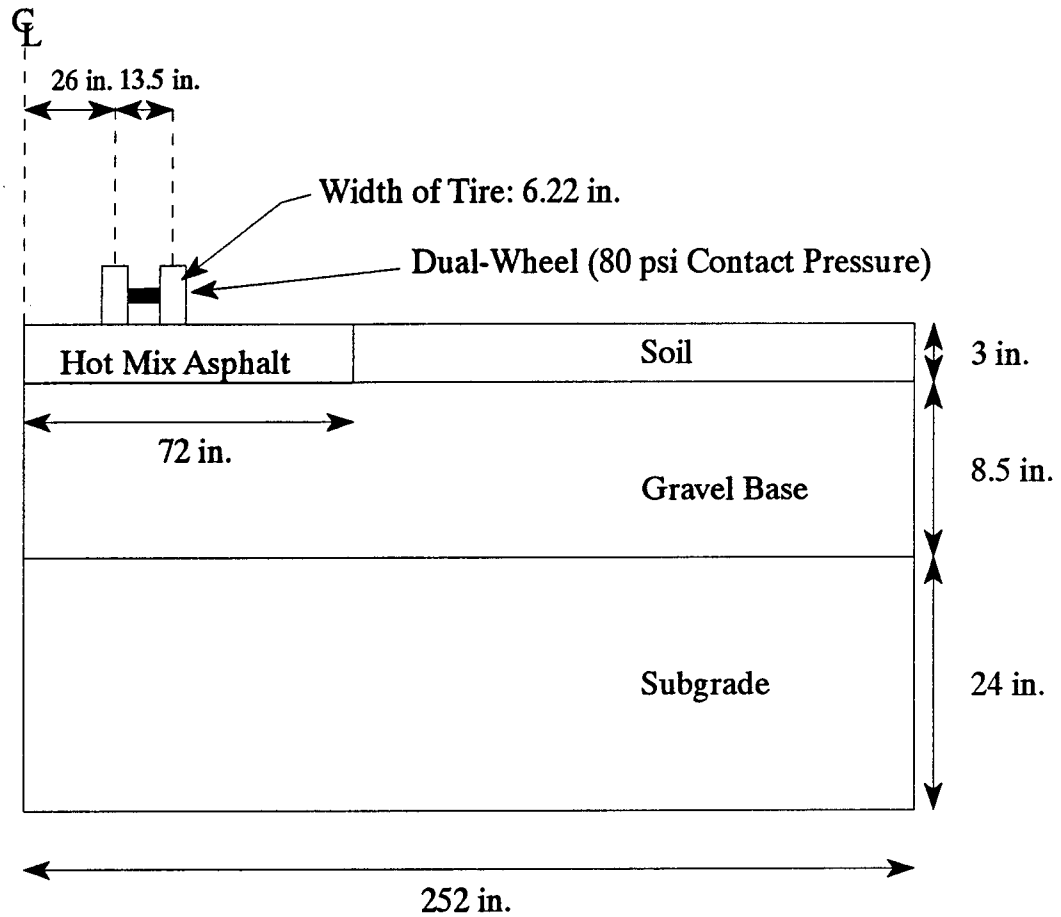


Figure 5-31: Schematic Details of a 12-foot (365 mm) Wide Pavement Section

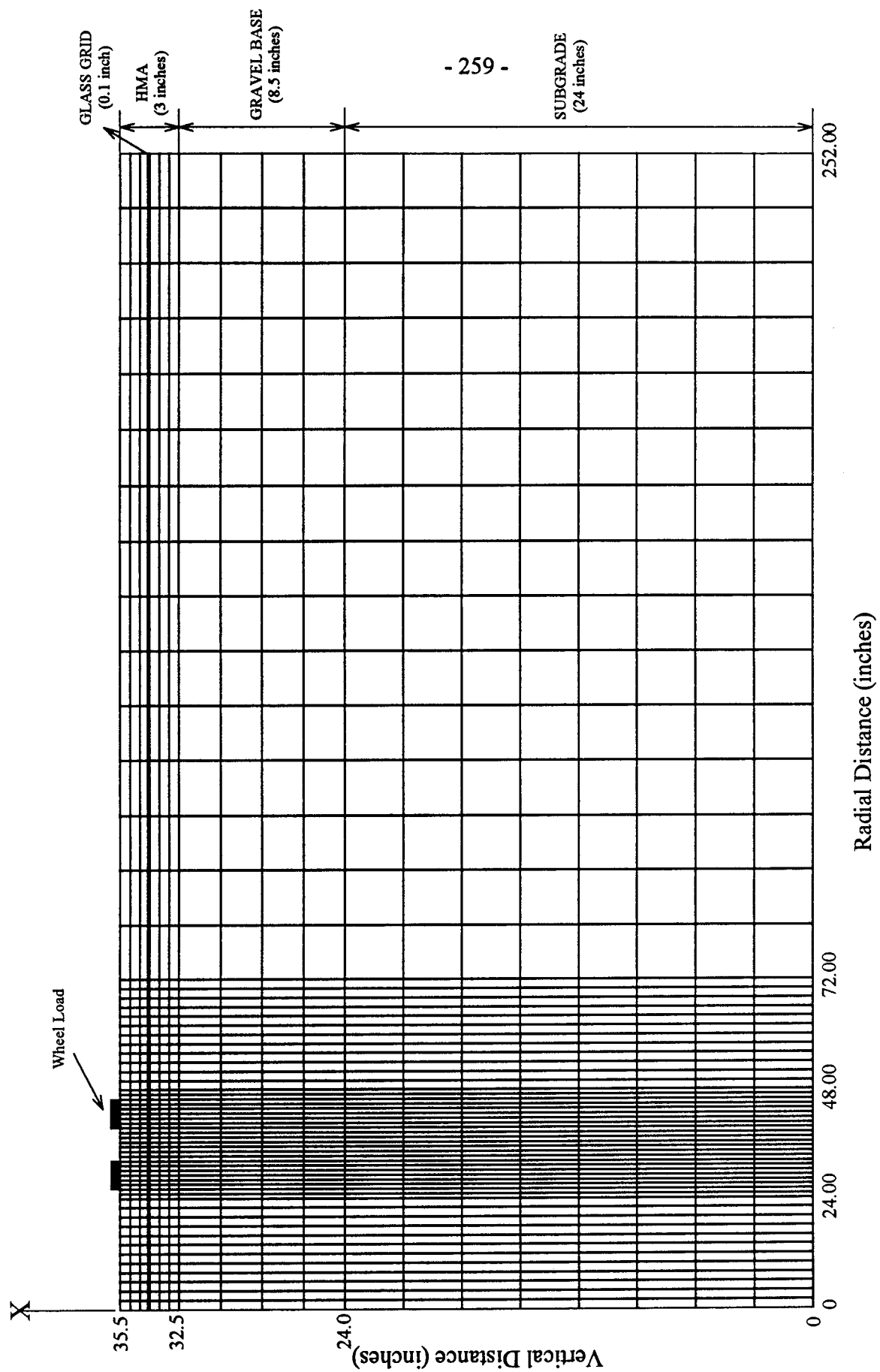


Figure 5-32: Finite Element Mesh Used for Thin Pavement Section (Plane Strain Case)

Assumed Material Properties for Finite Element Method (FEM) and KENLAYER Analyses

$E_{\text{subgrade}} = 6,000 \text{ psi}$
 $E_{\text{gravel base}} = 46,000 \text{ psi}$
 $E_{\text{asphalt}} = 270,000 \text{ psi}$
 $E_{\text{glass grid}} = 4,205,000 \text{ psi}$

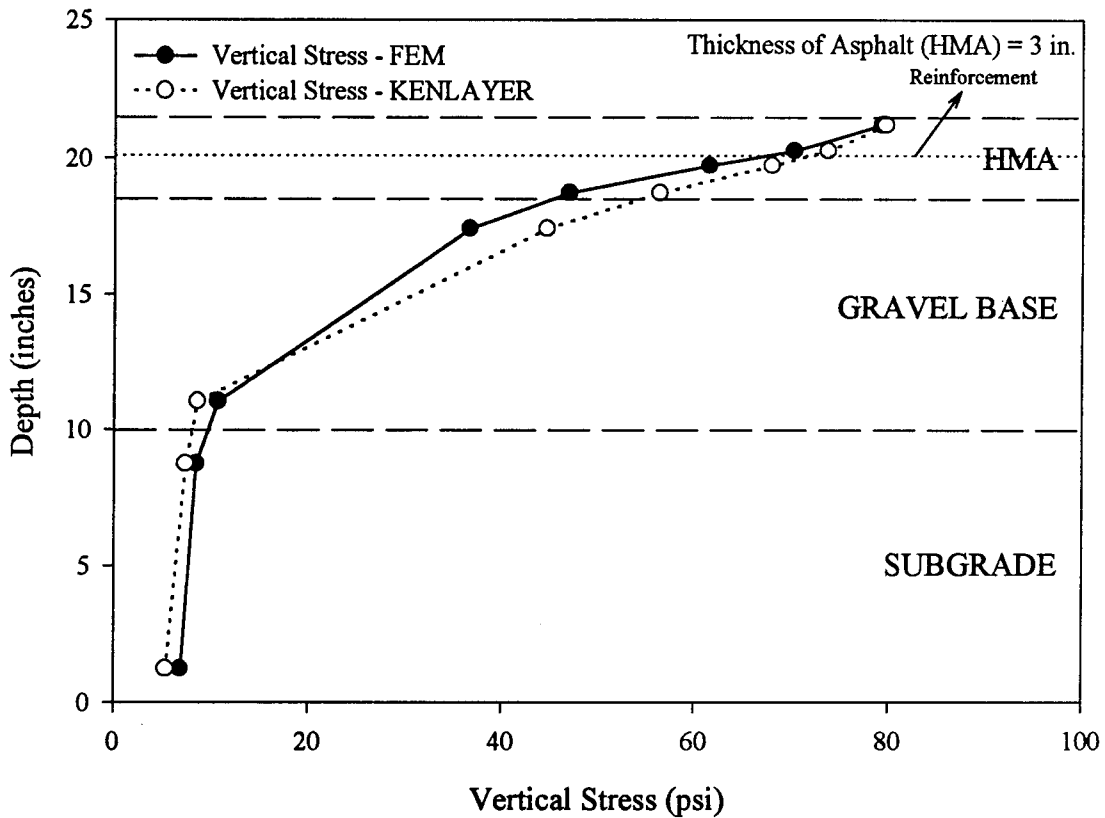


Figure 5-33: Comparison of Vertical Stress Variation Based on Finite Element Analysis (Axisymmetric Case) and KENLAYER Analysis

case) and the KENLAYER [Huang (1993)] analysis. As shown in this figure, the stresses from both computer analyses are comparable. At the upper layers, the stresses from KENLAYER seem to be slightly larger than the stresses from the finite element (FE) analysis, while the opposite is true for stresses at the subgrade level. The comparison in this figure verifies the accuracy of the results from these two different analyses (KENLAYER and FEA).

Similar to the KENLAYER analyses (Section 5.4), influence of glass grid reinforcement was studied by using the finite element method. Figure 5-34 shows the vertical stress variation with depth based on the axisymmetric finite element analysis. The influence of reinforcement was studied by decreasing the elastic modulus (E) value of the reinforcement material (glass grid) from 4,205,000 psi (28,972,450 kN/m²) to 270,000 psi (1,860,300 kN/m²). As shown in this figure, the results for the two extreme cases are very similar, suggesting that the stiffness of the reinforcement material does not have a significant effect on the performance of a pavement system.

The influence of subgrade stiffness on vertical stress variation is shown in Figure 5-35. The increase in subgrade stiffness, from 6,000 psi (41340 kN/m²) to 12,000 psi (82680 kN/m²) caused vertical subgrade stresses to increase by approximately 20% as shown in this figure.

Comparison of measured vertical subgrade stresses with the computed values (FEM) for axisymmetric case is shown in Figure 5-36. As shown in this figure, measured vertical subgrade stresses beneath the center of the loading area (Pressure Cell #1) compares well with the computed values more closely than at the edge of the loading area (Pressure Cell #2). Beneath the center of the loading area (Pressure Cell #1), the measured vertical subgrade stress at 500,000 load cycles fell between the computed values corresponding to different subgrade stiffnesses, as shown in Figure 5-36. On the other hand, the measured vertical subgrade stress at 1,000,000 load cycles was below

Assumed Material Properties (Case a)

$E_{\text{subgrade}} = 6,000 \text{ psi}$
 $E_{\text{gravel base}} = 46,000 \text{ psi}$
 $E_{\text{asphalt}} = 270,000 \text{ psi}$
 $E_{\text{glass grid}} = 4,205,000 \text{ psi}$

Assumed Material Properties (Case b)

$E_{\text{subgrade}} = 6,000 \text{ psi}$
 $E_{\text{gravel base}} = 46,000 \text{ psi}$
 $E_{\text{asphalt}} = 270,000 \text{ psi}$
 $E_{\text{glass grid}} = 270,000 \text{ psi}$

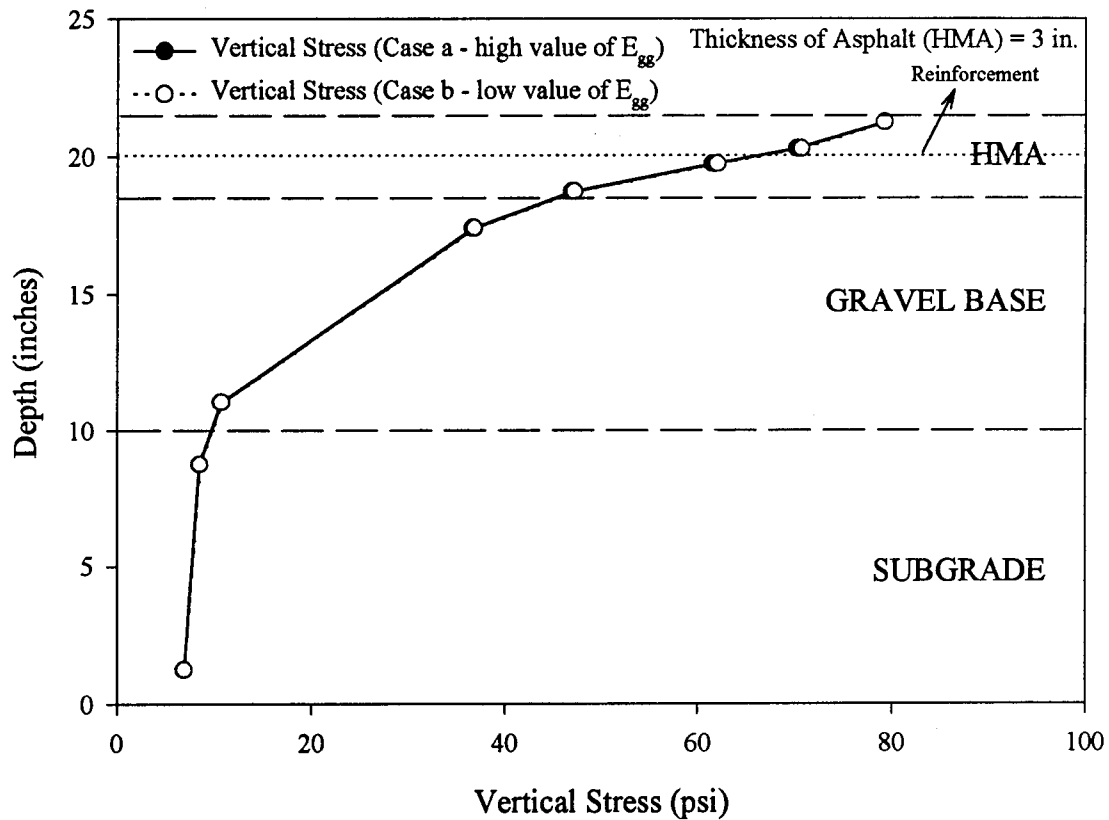


Figure 5-34: Influence of Glass Grid Reinforcement on Vertical Stress Variation with Depth Based on Finite Element Analysis (Axisymmetric Case)

Assumed Material Properties (Case a)

$E_{\text{subgrade}} = 12,000 \text{ psi}$
 $E_{\text{gravel base}} = 46,000 \text{ psi}$
 $E_{\text{asphalt}} = 270,000 \text{ psi}$
 $E_{\text{glass grid}} = 4,205,000 \text{ psi}$

Assumed Material Properties (Case b)

$E_{\text{subgrade}} = 6,000 \text{ psi}$
 $E_{\text{gravel base}} = 46,000 \text{ psi}$
 $E_{\text{asphalt}} = 270,000 \text{ psi}$
 $E_{\text{glass grid}} = 4,205,000 \text{ psi}$

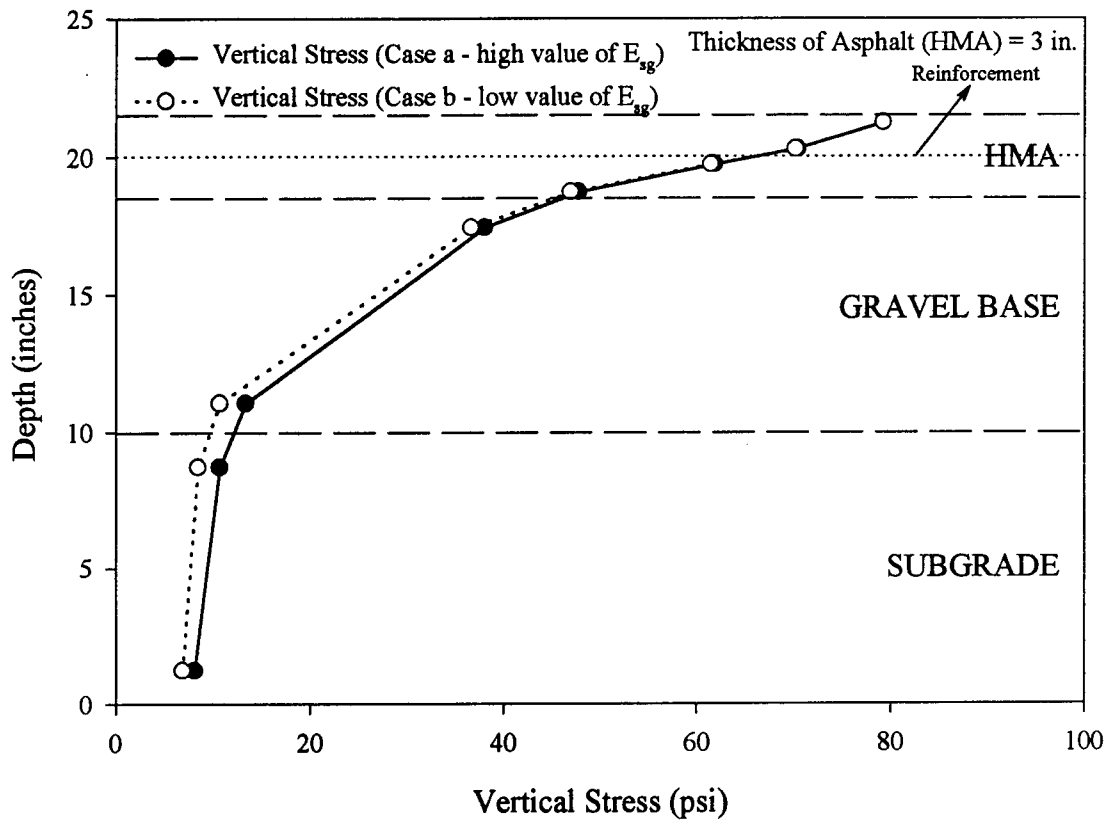


Figure 5-35: Influence of Subgrade Stiffness on Vertical Stress Variation with Depth Based on Finite Element Analysis (Axisymmetric Case)

Assumed Material Properties (Case a)

$E_{\text{subgrade}} = 12,000 \text{ psi}$
 $E_{\text{gravel base}} = 46,000 \text{ psi}$
 $E_{\text{asphalt}} = 270,000 \text{ psi}$
 $E_{\text{glass grid}} = 4,205,000 \text{ psi}$

Assumed Material Properties (Case b)

$E_{\text{subgrade}} = 6,000 \text{ psi}$
 $E_{\text{gravel base}} = 46,000 \text{ psi}$
 $E_{\text{asphalt}} = 270,000 \text{ psi}$
 $E_{\text{glass grid}} = 4,205,000 \text{ psi}$

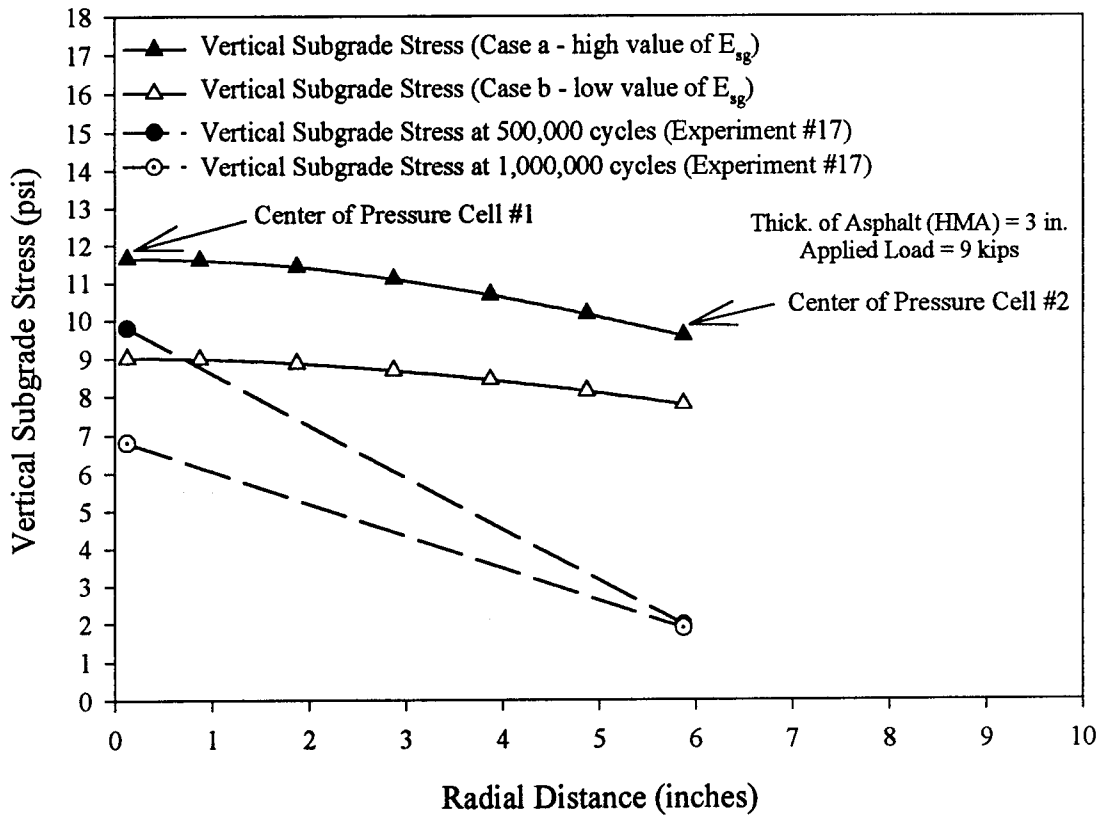


Figure 5-36: Comparison of Measured Vertical Subgrade Stresses with the Computed Values Based on Finite Element Analysis (Axisymmetric Case)

the computed values corresponding to different subgrade stiffnesses [Figure 5-36].

As shown previously in Figure 5-34, the stiffness of the reinforcement material did not have a significant influence on vertical stress distribution. When the stiffness of the glass grid was decreased from 4,205,000 psi (28,972,450 kN/m²) to 270,000 psi (1,860,300 kN/m²), the increase in vertical stress beneath the reinforcement layer (inside the HMA) was negligible. However, it was believed that the thickness of the reinforcement material with high stiffness had some influence on the vertical stress distribution. Therefore, the influence of reinforcement (glass grid) thickness was investigated [Figure 5-37]. Thickness of the reinforcement material was increased from 0.1 inch (2.5 mm) to 0.5 inch (12.7 mm). With this increase, as shown in Figure 5-37, the vertical stress dropped noticeably (approximately 13%), from 61.45 psi (423.39 kN/m²) to 53.68 psi (369.86 kN/m²) immediately below the reinforcement. Above the level of reinforcement, the vertical stresses were similar.

To further verify the effect of reinforcement thickness on vertical stress, hypothetically the thickness was increased from 0.1 inch (2.5 mm) to 1 inch (25.4 mm) [Figure 5-38]. This increase in thickness clearly caused a substantial decrease in vertical stress. Immediately below the reinforcement material, the vertical stress decreased from 61.45 psi (423.39 kN/m²) to 42.03 psi (289.59 kN/m²) (approximately 32%) [Figure 5-38]. This substantial decrease in vertical stress suggests that the high stiffness of the reinforcement material alone is not enough, if the thickness of the reinforcement is very small. This hypothetical increase in thickness suggests that the reinforcement material needs to be at a certain thickness. For reinforcement to take place efficiently, the required thickness, attained with the help of high stiffness of reinforcement needs to be evaluated in order to develop some design guidelines.

Assumed Material Properties for Finite Element Method (FEM) Analysis

$$\begin{aligned} E_{\text{subgrade}} &= 6,000 \text{ psi} \\ E_{\text{gravel base}} &= 46,000 \text{ psi} \\ E_{\text{asphalt}} &= 270,000 \text{ psi} \\ E_{\text{glass grid}} &= 4,205,000 \text{ psi} \end{aligned}$$

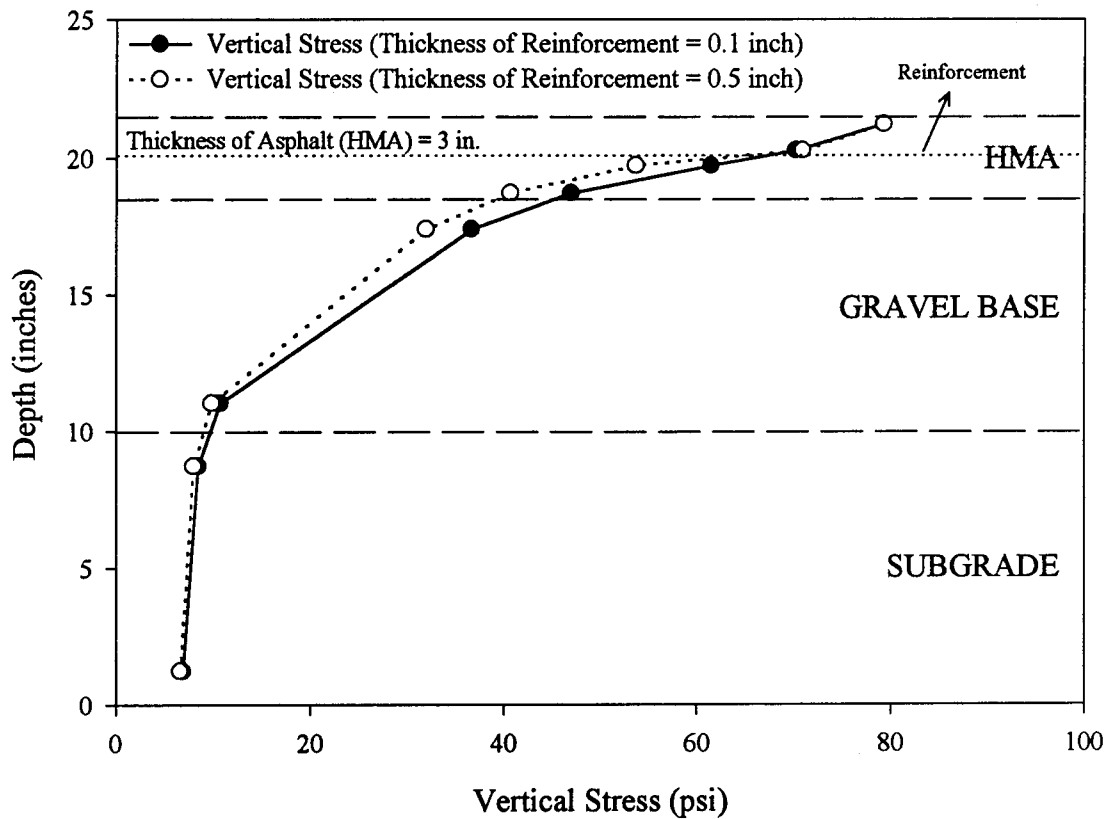


Figure 5-37: Influence of Reinforcement Thickness on Vertical Stress Variation Based on Finite Element Analysis (Axisymmetric Case)
[Thickness of Reinforcement = 0.5 in. (12.7 mm)]

Assumed Material Properties for Finite Element Method (FEM) Analysis

$E_{\text{subgrade}} = 6,000 \text{ psi}$
 $E_{\text{gravel base}} = 46,000 \text{ psi}$
 $E_{\text{asphalt}} = 270,000 \text{ psi}$
 $E_{\text{glass grid}} = 4,205,000 \text{ psi}$

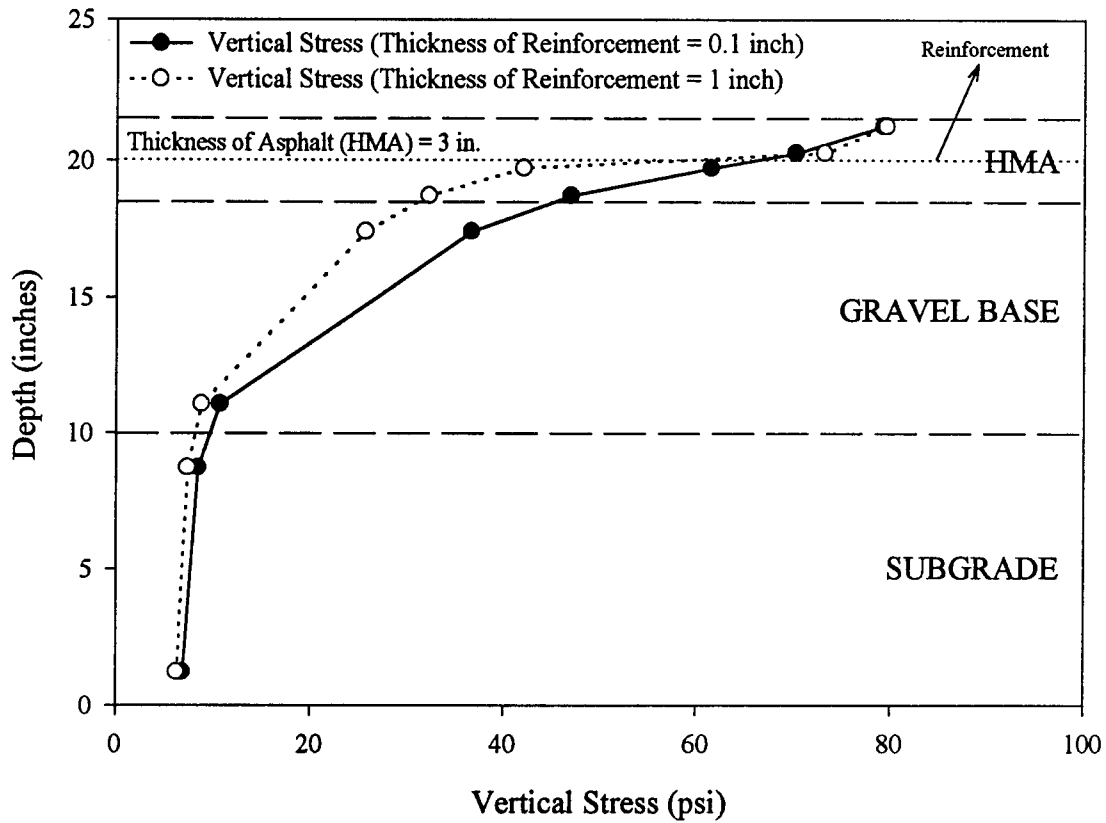


Figure 5-38: Influence of Reinforcement Thickness on Vertical Stress Variation Based on Finite Element Analysis (Axisymmetric Case)
[Thickness of Reinforcement = 1 in. (25 mm)]

Plane Strain Idealization Of The Laboratory Test Section

It was suspected that the influence of reinforcement could be observed better in the plane strain case than in the axisymmetric case. Another analysis was performed by assuming plane strain idealization for the laboratory test section. A comparison between the axisymmetric case and the plane strain case with respect to vertical stress variation for the laboratory test section is shown in Figure 5-39. This figure shows that the vertical stresses are much larger at greater depths for the plane strain case than for the axisymmetric case. The vertical stress on top of subgrade was 8.44 psi (58.15 kN/m²) for the axisymmetric case, while it was 26.44 psi (182.17 kN/m²) for the plane strain case. Additionally, the dual wheel effect on one half of a 12-foot (3.7 m) wide traffic lane was analyzed by using the plane strain idealization.

5.7.2 Results Of The Finite Element Analyses Of A Hypothetical Field Section

In this section, plane strain idealization of a 12-foot (365 mm) traffic lane was studied [Figure 5-31]. Figure 5-40 shows the influence of reinforcement for the plane strain case which is shown in Figure 5-31. The finite element mesh used in this study is shown in Figure 5-32. To study the influence of the reinforcement, the stiffness of the reinforcing material (glass grid) was reduced from 4,205,000 psi (28,972,450 kN/m²) to 270,000 psi (1,860,300 kN/m²). As shown in Figure 5-40, results are similar for two different values of elastic moduli (E). This shows that the stiffness of the reinforcement alone does not have a significant influence on the vertical stresses.

As previously described in Section 5.2 (Chapter 4), KENLAYER [Huang (1993)] computer analyses did not have the capability of modeling the reinforcement material as an interface. This problem was overcome by using the finite element method (FEM). Figure 5-41 shows the vertical stress variation with depth for the plane strain case, where the reinforcement layer was modeled as

Assumed Material Properties

$E_{\text{subgrade}} = 6,000 \text{ psi}$

$E_{\text{gravel base}} = 46,000 \text{ psi}$

$E_{\text{asphalt}} = 270,000 \text{ psi}$

$E_{\text{glass grid}} = 4,205,000 \text{ psi}$

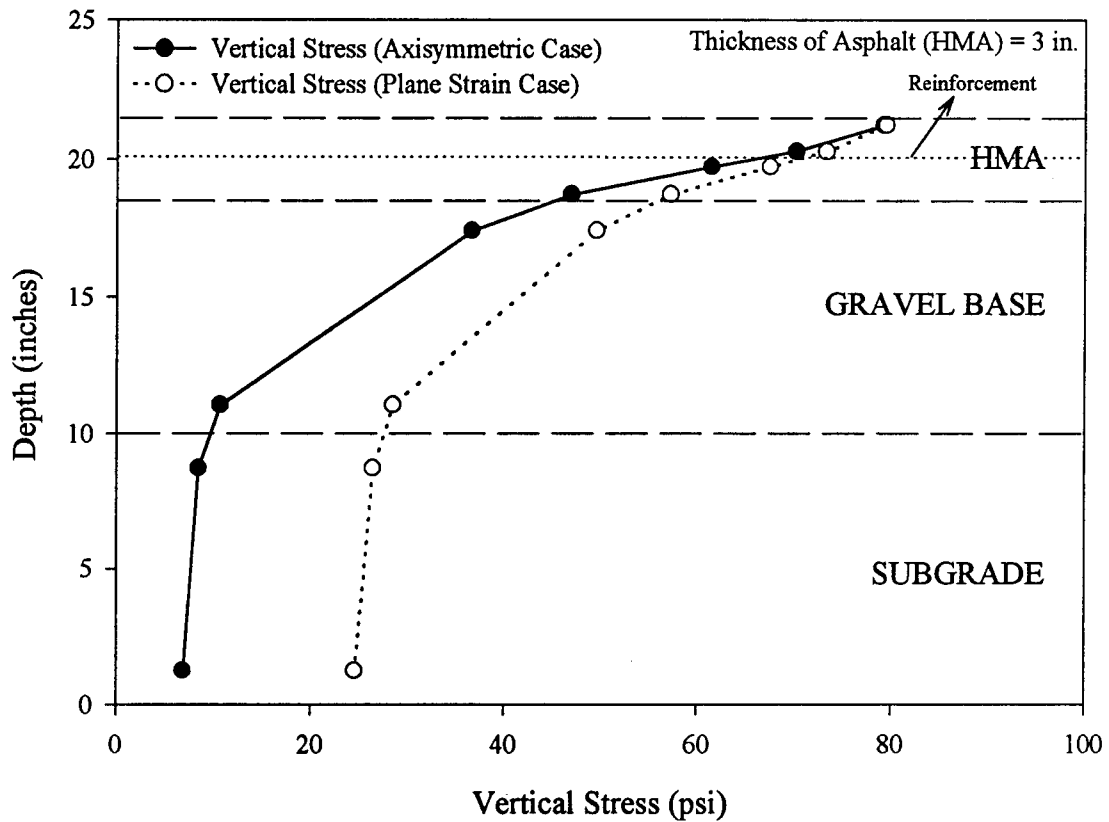


Figure 5-39: Vertical Stress Variation with Depth Based on Finite Element Analysis

Assumed Material Properties (Case a)

$E_{\text{subgrade}} = 6,000 \text{ psi}$
 $E_{\text{gravel base}} = 46,000 \text{ psi}$
 $E_{\text{asphalt}} = 270,000 \text{ psi}$
 $E_{\text{glass grid}} = 4,205,000 \text{ psi}$

Assumed Material Properties (Case b)

$E_{\text{subgrade}} = 6,000 \text{ psi}$
 $E_{\text{gravel base}} = 46,000 \text{ psi}$
 $E_{\text{asphalt}} = 270,000 \text{ psi}$
 $E_{\text{glass grid}} = 270,000 \text{ psi}$

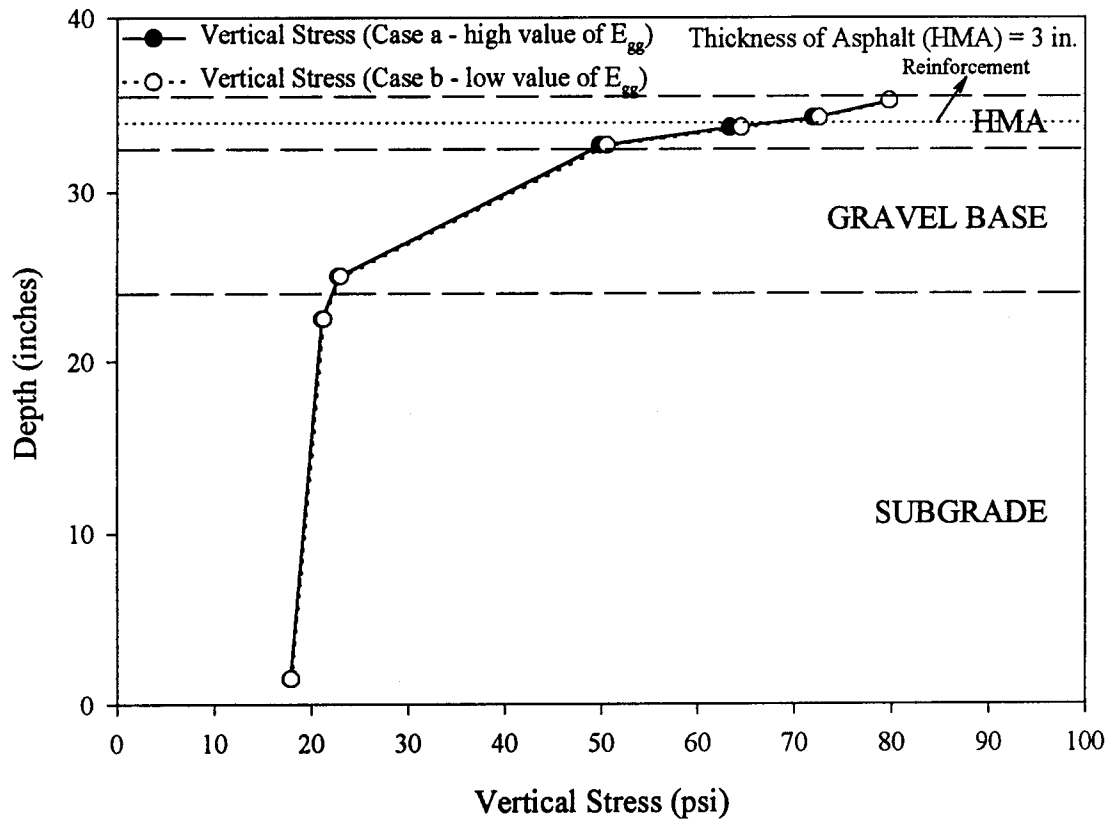


Figure 5-40: Influence of Glass Grid Reinforcement on Vertical Stress Variation with Depth Based on Finite Element Analysis (Plane Strain Case)

Assumed Material Properties (Case a)

$E_{\text{subgrade}} = 6,000 \text{ psi}$
 $E_{\text{gravel base}} = 46,000 \text{ psi}$
 $E_{\text{asphalt}} = 270,000 \text{ psi}$
 $E_{\text{glass grid}} = 1,000 \text{ psi}$
 $G_{\text{interface}} = 4,200,000 \text{ psi}$

Assumed Material Properties (Case b)

$E_{\text{subgrade}} = 6,000 \text{ psi}$
 $E_{\text{gravel base}} = 46,000 \text{ psi}$
 $E_{\text{asphalt}} = 270,000 \text{ psi}$
 $E_{\text{glass grid}} = 1,000 \text{ psi}$
 $G_{\text{interface}} = 10 \text{ psi}$

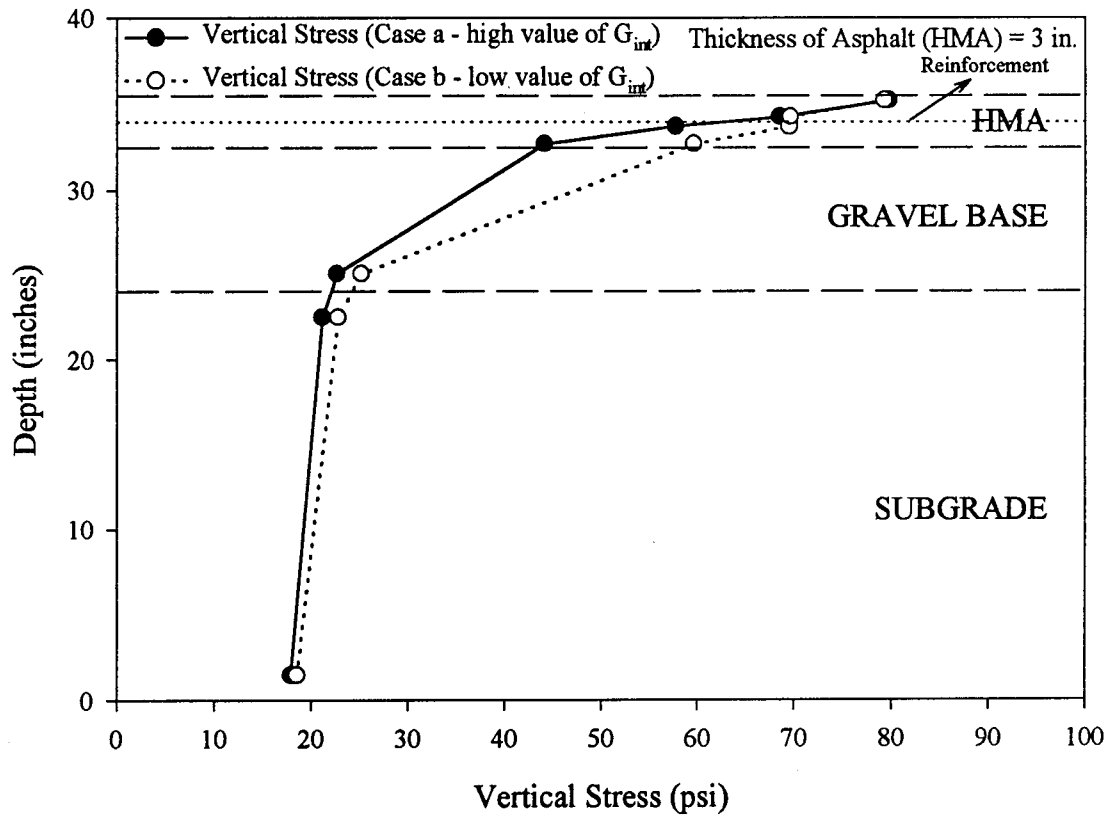


Figure 5-41: Influence of Shear Stiffness (G_{int}) for Interface Layer on Vertical Stress Variation with Depth Based on Finite Element Analysis (Plane Strain Case)

an interface layer [Desai (1979), Desai and Siriwardane (1983) and Zienkiewicz (1977)]. In the plane strain case, modeling the reinforcement layer as an interface would bring the shear stiffness (G_{int}) of the reinforcement layer into consideration. In this figure, influence of shear stiffness for the interface layer is shown. Two values of G_{int} were assigned for the shear stiffness of the reinforcement layer. The first assigned value was high [4,200,000 psi (28,938,000 kN/m²)], suggesting a good bonding between the HMA and the interface layer. This high value of G_{int} simulates a condition where the reinforcement layer does not slip inside the HMA providing good bonding between the reinforcement layer and the HMA. Additionally, low shear stiffness value [10 psi (68.9 kN/m²)] was assigned to the reinforcement layer to simulate little bonding. As shown in Figure 5-41, the influence of shear stiffness on vertical stress is clearly apparent beneath the reinforcement layer. When the shear stiffness was increased, the vertical stress directly beneath the reinforcement layer decreased by approximately 17% [from 69.48 psi (478.72 kN/m²) to 57.72 psi (397.69 kN/m²)]. The vertical stress directly above the reinforcement layer was almost the same for both values of shear stiffness. When the shear stiffness was 10 psi (68.9 kN/m²), the vertical stress was 69.58 psi (479.41 kN/m²). When the shear stiffness was 4,200,000 psi (28,938,000 kN/m²), the vertical stress was 68.47 psi (471.76 kN/m²).

To prevent detrimental pavement deformations, one of the functions of the pavement system is to reduce the vertical stresses on top of subgrade [Huang (1993) and Yoder and Witczak (1975)]. Since vertical stress on top of subgrade is an important factor, vertical compressive stress on top of subgrade soil was predicted by using the finite element method using the mesh shown in Figure 5-32. Influence of the reinforcement layer on subgrade stress is shown in Figure 5-42. When the stiffness of the reinforcement layer was increased from 270,000 psi (1,860,300 kN/m²) to 4,205,000 psi (28,972,450 kN/m²), the vertical stress on top of subgrade decreased approximately by 1.1% at the

Assumed Material Properties (Case a)

$E_{\text{subgrade}} = 6,000 \text{ psi}$
 $E_{\text{gravel base}} = 46,000 \text{ psi}$
 $E_{\text{asphalt}} = 270,000 \text{ psi}$
 $E_{\text{glass grid}} = 4,205,000 \text{ psi}$

Assumed Material Properties (Case b)

$E_{\text{subgrade}} = 6,000 \text{ psi}$
 $E_{\text{gravel base}} = 46,000 \text{ psi}$
 $E_{\text{asphalt}} = 270,000 \text{ psi}$
 $E_{\text{glass grid}} = 270,000 \text{ psi}$

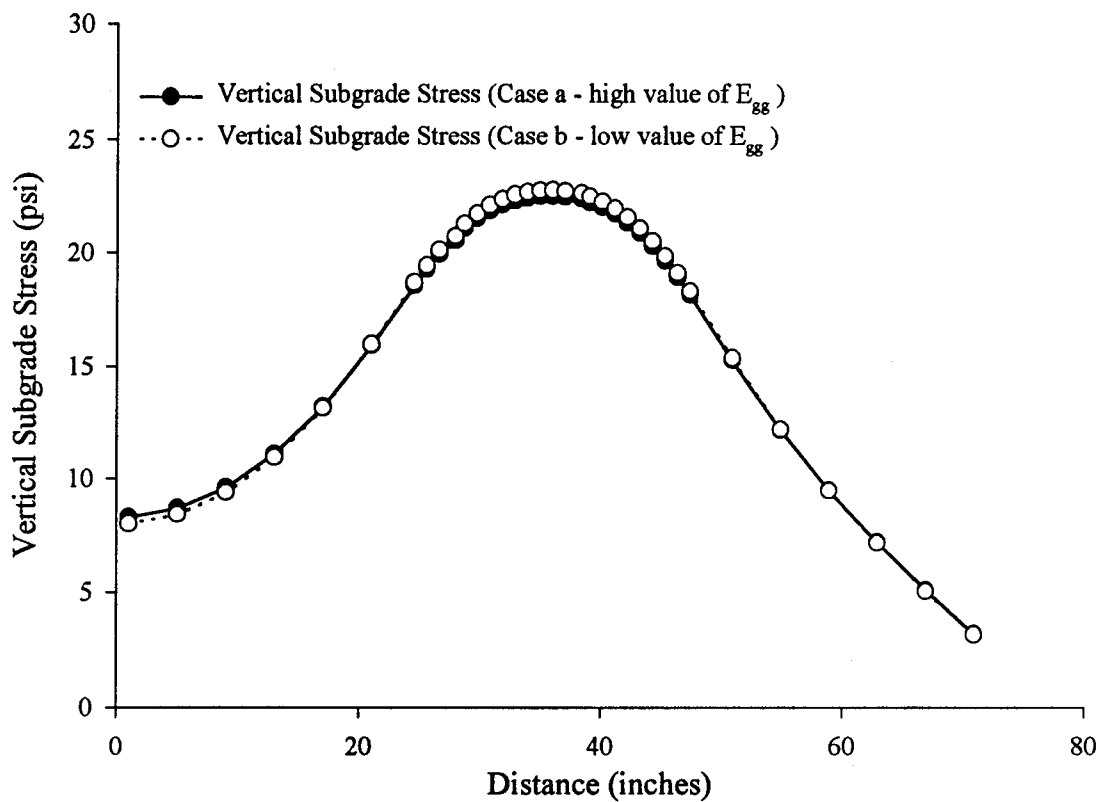


Figure 5-42: Influence of Reinforcement (Glass Grid) on Vertical Subgrade Stress on Top of Subgrade Based on Finite Element Analysis (Plane Strain Case)

maximum point of the subgrade stress. Additionally, the influence of the reinforcement layer on subgrade strain is shown in Figure 5-43. By increasing the stiffness of the reinforcement layer, vertical compressive strain on top of subgrade decreased approximately by 1.1% at the maximum point of the vertical compressive strain. The maximum point of the vertical compressive strain and vertical stress on subgrade occurred in the middle of the dual-wheel [Figures 5-31, 5-32, 5-42, and 5-43].

Other important function of the pavement system is to reduce the horizontal tensile strain at the bottom of asphalt layer to prevent reflection and/or fatigue cracking. Therefore, influence of reinforcement on the horizontal tensile strain at the bottom of HMA was also investigated [Figure 5-44]. At the bottom of HMA, the maximum tensile strains occurred in the middle of each individual tire [3.455 E-3 and 3.293 E-3]. In the middle of dual-wheel, maximum horizontal strain at the bottom of HMA was in compression as shown in Figure 5-44 [-5.216 E-3 and -1.090 E-4]. Horizontal tensile strains were approximately similar for different elastic modulus values of the reinforcement material ($E_{\text{glassgrid}}$). It is important to notice that the increase in stiffness of the reinforcement material has a tendency to slightly increase the maximum horizontal tensile strain at the bottom of HMA (Figure 5-44). Therefore, it is apparent that the stiffness of the reinforcement alone does not influence the vertical compressive strain on top of subgrade and the horizontal tensile strain at the bottom of the HMA substantially.

Influence of shear stiffness of the interface layer on vertical compressive strain on top of subgrade was investigated for a plane strain case. As shown in Figure 5-45, when the value of shear stiffness ($G_{\text{interface}}$) is decreased, the maximum vertical compressive strain increases approximately by 6.8%. Maximum vertical compressive strain on top of subgrade occurred in the middle of the dual wheel [Figures 5-31 and 5-32].

Assumed Material Properties (Case a)

$E_{\text{subgrade}} = 6,000 \text{ psi}$
 $E_{\text{gravel base}} = 46,000 \text{ psi}$
 $E_{\text{asphalt}} = 270,000 \text{ psi}$
 $E_{\text{glass grid}} = 4,205,000 \text{ psi}$

Assumed Material Properties (Case b)

$E_{\text{subgrade}} = 6,000 \text{ psi}$
 $E_{\text{gravel base}} = 46,000 \text{ psi}$
 $E_{\text{asphalt}} = 270,000 \text{ psi}$
 $E_{\text{glass grid}} = 270,000 \text{ psi}$

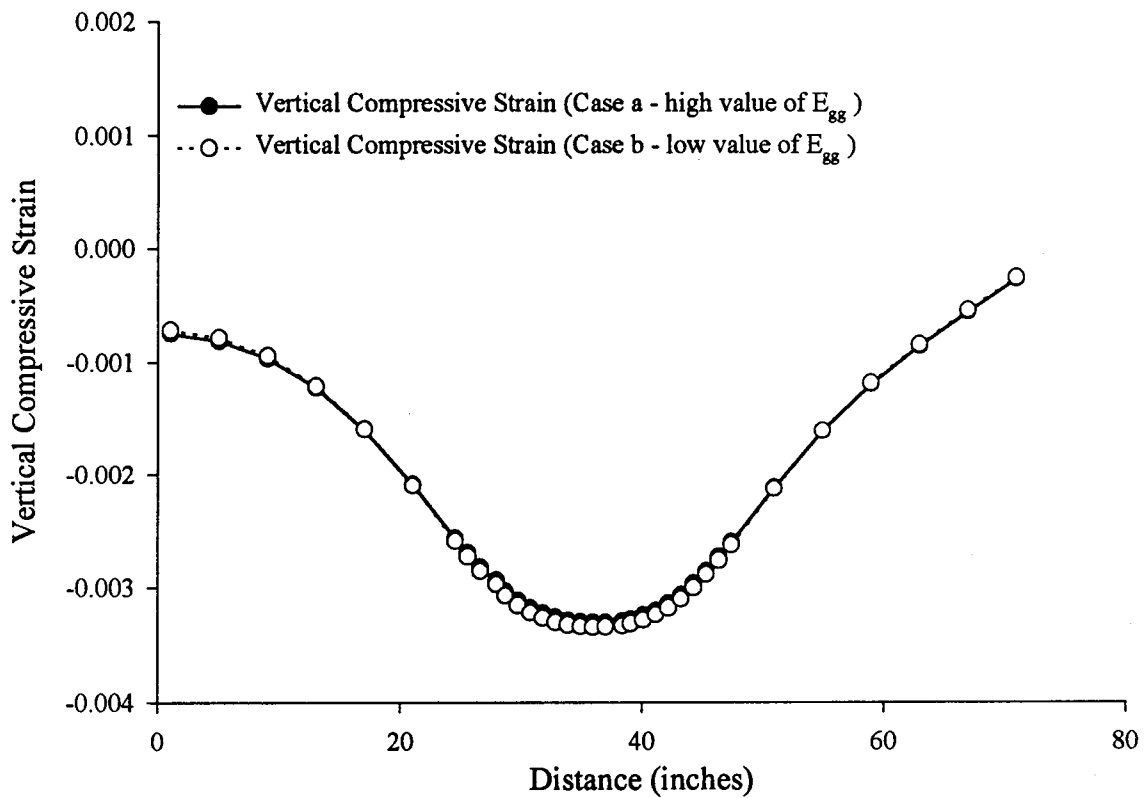


Figure 5-43: Influence of Reinforcement (Glass Grid) on Vertical Compressive Strain on Top of Subgrade Based on Finite Element Analysis (Plane Strain Case)

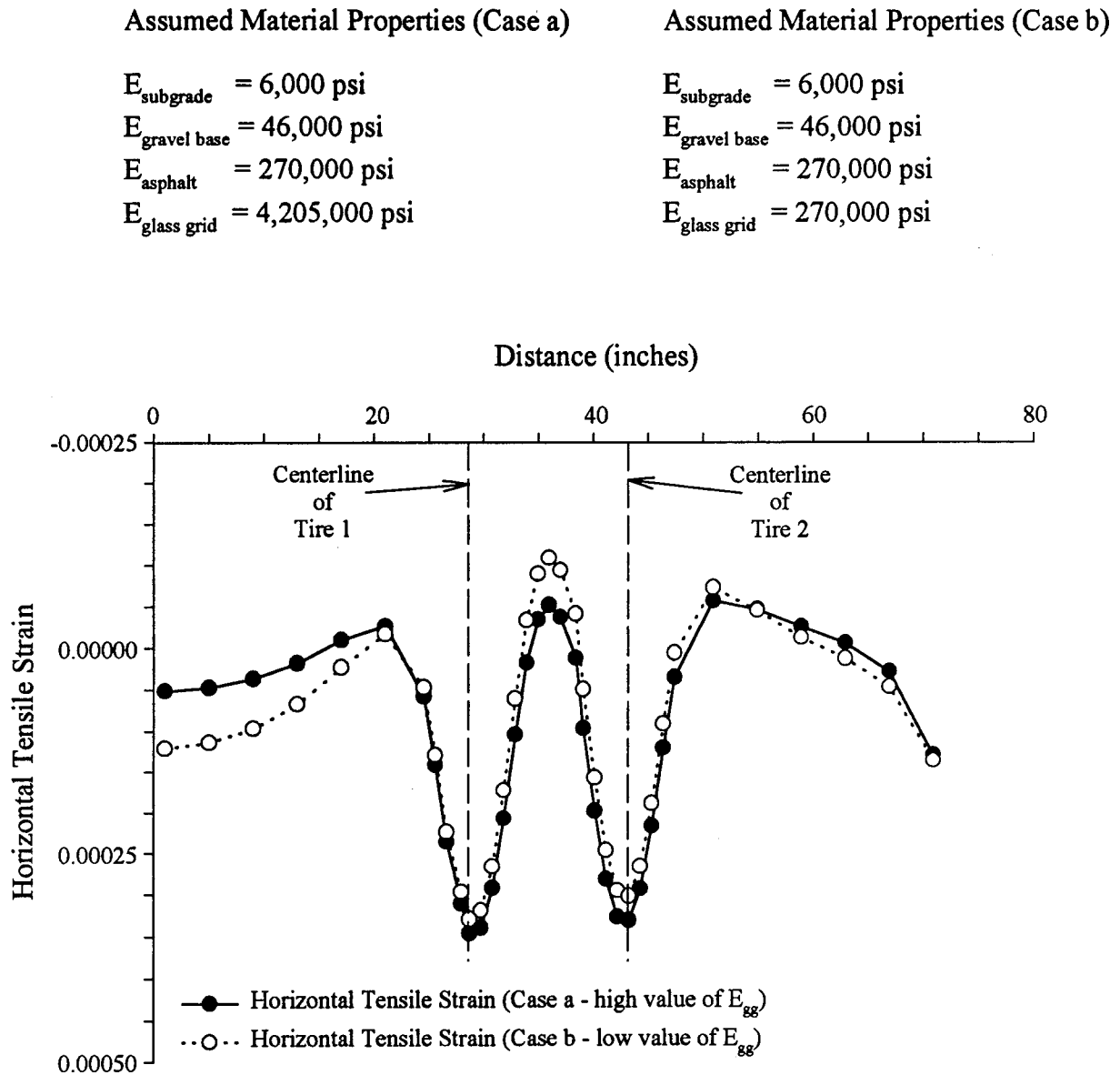


Figure 5-44: Influence of Reinforcement on Predicted Horizontal Tensile Strain at the Bottom of HMA Based on Finite Element Analysis (Plane Strain Case)

Assumed Material Properties (a)

$E_{\text{subgrade}} = 6,000 \text{ psi}$
 $E_{\text{gravel base}} = 46,000 \text{ psi}$
 $E_{\text{asphalt}} = 270,000 \text{ psi}$
 $E_{\text{glass grid}} = 1,000 \text{ psi}$
 $G_{\text{interface}} = 4,200,000 \text{ psi}$

Assumed Material Properties (b)

$E_{\text{subgrade}} = 6,000 \text{ psi}$
 $E_{\text{gravel base}} = 46,000 \text{ psi}$
 $E_{\text{asphalt}} = 270,000 \text{ psi}$
 $E_{\text{glass grid}} = 1,000 \text{ psi}$
 $G_{\text{interface}} = 10 \text{ psi}$

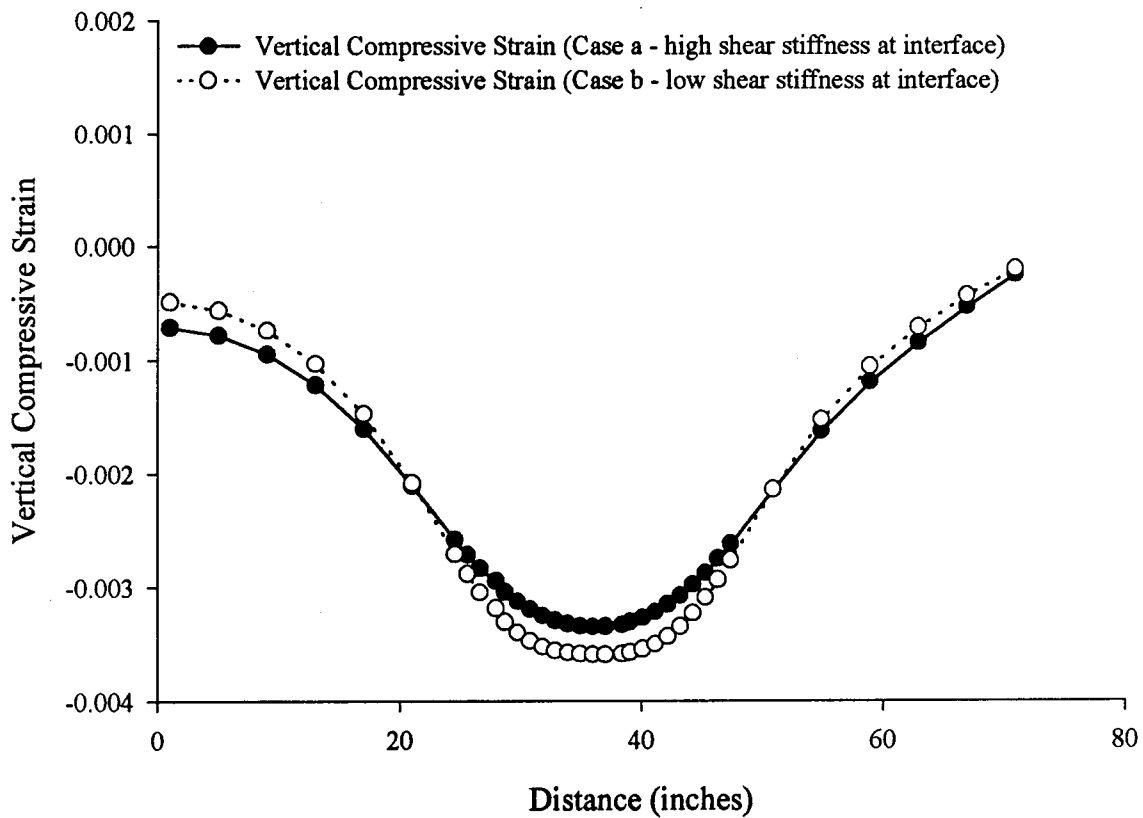


Figure 5-45: Influence of Shear Stiffness (G_{int}) for Interface Layer on Predicted Vertical Compressive Strain on Top of Subgrade Based on Finite Element Analysis (Plane Strain Case)

Figure 5-46 shows the predicted horizontal tensile strain at the bottom of HMA. Influence of shear stiffness of the reinforcement material was evaluated by using interface elements for the reinforcement layer for a plane strain case. As shown in this figure, the influence of shear stiffness is noticeable. The low value of shear stiffness [$G_{\text{interface}} = 10 \text{ psi (68.9 kN/m}^2\text{)}$] causes the horizontal tensile strain at the bottom of HMA (beneath the center of the one wheel) to be 83% lower than the horizontal tensile strain with the high value of shear stiffness [$G_{\text{interface}} = 4,200,000 \text{ psi (28,938,000 kN/m}^2\text{)}$]. This low value of shear stiffness simulate the case where the reinforcement (interface) material is poorly bonded with the HMA, causing shearing of the HMA at the interface.

Influence of reinforcement on surface displacements was investigated for a plane strain case [Figure 5-32]. Figure 5-47 shows the surface displacements under a dual wheel load. As previously described in Figure 5-40, the influence of reinforcement was studied by reducing the stiffness of the reinforcing material (glass grid) from a hypothetical value of 4,205,000 psi (28,972,450 kN/m²) to 270,000 psi (1,860,300 kN/m²). Figure 5-47 shows that the stiffness of the glass grid in the middle of the HMA does not influence the surface displacement (elastic) as evident from the negligible difference between the surface displacements for different values of elastic moduli (Table 5-21). As shown in the enlarged area in Figure 5-47, the maximum surface displacements under each wheel (of the dual-wheel) took place at the inner edge of the wheels. Table 5-21 presents these maximum surface displacements under each wheel for two different glass grid stiffness ($E_{\text{glassgrid}}$) values.

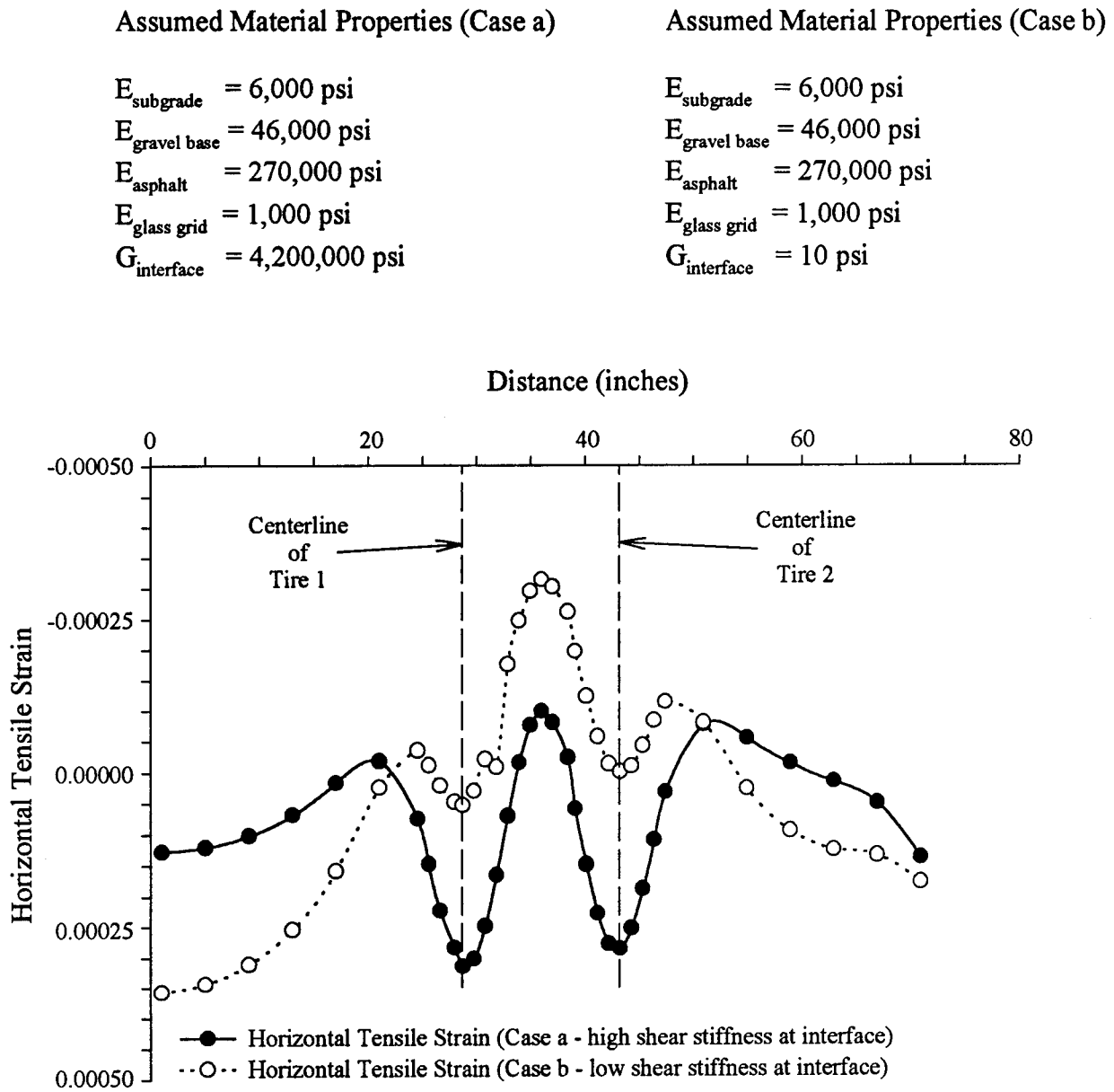


Figure 5-46: Influence of Shear Stiffness (G_{int}) for Interface Layer on Predicted Horizontal Tensile Strain at the Bottom of HMA Based on Finite Element Analysis (Plane Strain Case)

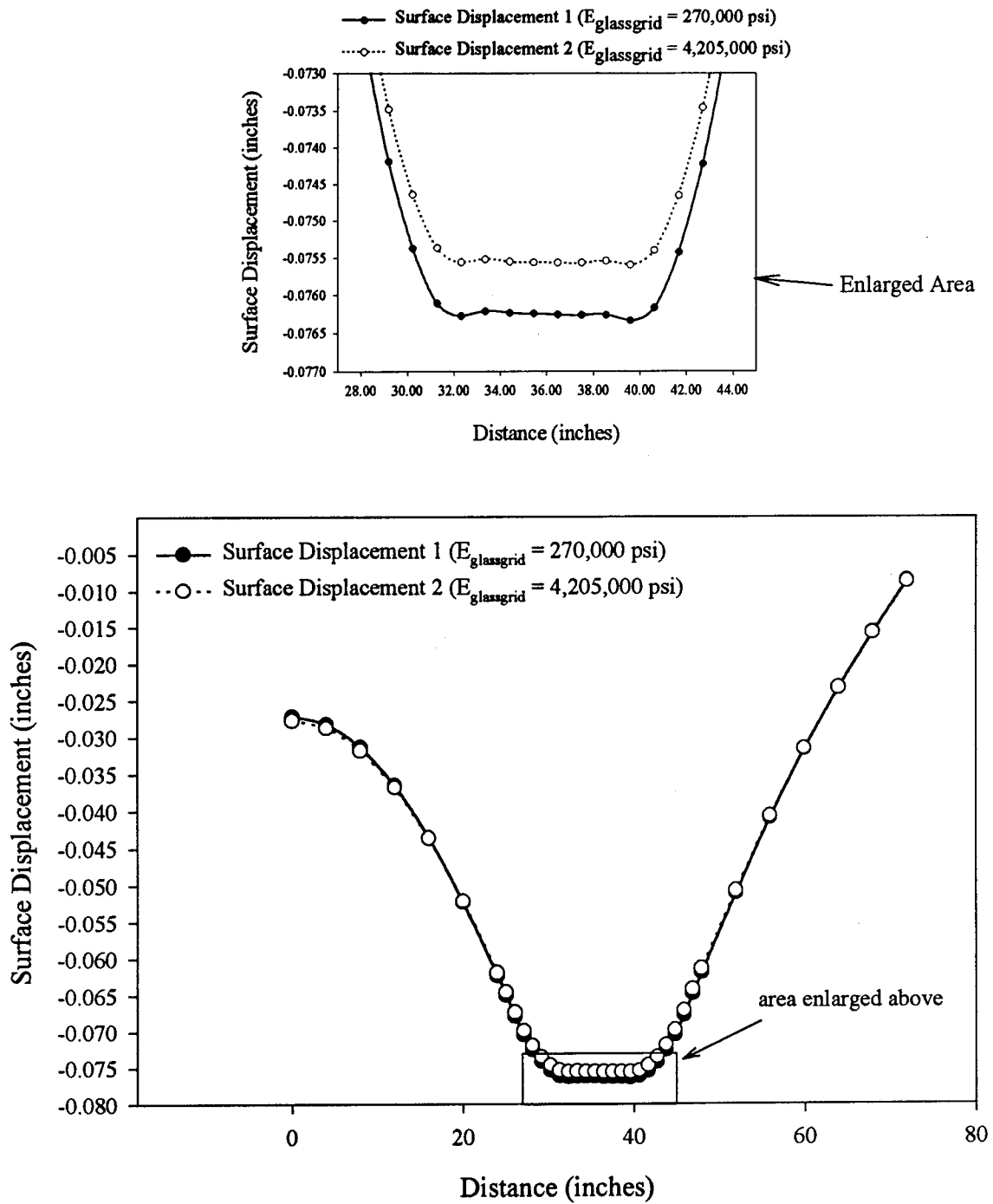


Figure 5-47: Influence of Reinforcement on Surface Displacement Based on Finite Element Analysis (Plane Strain Case)

Table 5-21: Maximum Surface Displacements Under the Inner Edge of Each Wheel

Wheel	$E_{\text{glassgrid}} = 270,000 \text{ psi}$ [1,860,300 kN/m ²]	$E_{\text{glassgrid}} = 4,205,000 \text{ psi}$ [28,972,450 kN/m ²]
	Surface Displacement (inches) [mm]	Surface Displacement (inches) [mm]
1	0.07628 [1.93741]	0.07556 [1.91923]
2	0.07634 [1.93903]	0.07559 [1.92011]

5.7.3 Summary Of Results On Finite Element Analyses

Summary of results from the finite element method (FEM) of analyses is summarized below:

Axisymmetric Idealization Of The Laboratory Test Section

- The vertical stress variation obtained from the finite element analysis (axisymmetric idealization) is comparable with the stress variation predicted by the KENLAYER [Huang (1993)] analysis. At the upper layers, the stresses from KENLAYER seem to be slightly larger than the stresses from the finite element (FE) analysis, while the opposite is true for stresses at the subgrade level [See Section 5.7.1].
- The influence of reinforcement was studied by decreasing the elastic modulus (E) value of the reinforcement material (glass grid) from 4,205,000 psi (28,972,450 kN/m²) to 270,000 psi (1,860,300 kN/m²). The results for the two extreme cases are very similar, suggesting that the stiffness of the reinforcement material does not have a significant effect on the performance of a pavement system [See Section 5.7.1].
- The increase in subgrade stiffness, from 6,000 psi (41340 kN/m²) to 12,000 psi (82680 kN/m²) caused vertical subgrade stresses to increase by approximately 20%.
- Measured vertical subgrade stresses beneath the center of the loading area (Pressure Cell #1) compared well with the computed values more closely than at the edge of the loading area (at Pressure Cell #2).
- A substantial decrease in vertical stress caused by the increase in thickness of the reinforcement layer suggests that the high stiffness of the reinforcement material alone is not enough, if the thickness of the reinforcement is very small. For reinforcement to take place efficiently, the required thickness, attained with the help of high stiffness of reinforcement

needs to be evaluated in order to develop some design guidelines.

Plane Strain Idealization Of A Hypothetical Field Section

- In plane strain idealization of a 12-foot (365 mm) traffic lane, the stiffness of the reinforcement alone did not have a significant influence on the vertical stresses.
- When the shear stiffness of the reinforcement layer was increased from 10 psi (68.9 kN/m²) to 4,200,000 psi (28,938,000 kN/m²), the vertical stress directly beneath the reinforcement layer decreased by approximately 17%. The vertical stress directly above the reinforcement layer was almost the same for both values of shear stiffness [See Section 5.7.2].
- It is apparent that the stiffness of the reinforcement alone did not influence the vertical compressive strain on top of subgrade and the horizontal tensile strain at the bottom of the HMA substantially.
- When the value of shear stiffness ($G_{\text{interface}}$) was decreased, the maximum vertical compressive strain on top of subgrade increased approximately by 6.8%.
- When the value of shear stiffness ($G_{\text{interface}}$) was decreased, the horizontal tensile strain at the bottom of HMA (beneath the center of the one wheel) decreased approximately by 83%.
- The stiffness of the glass grid in the middle of the HMA did not influence the surface displacement (elastic) as evident from the negligible difference between the surface displacements for different values of elastic moduli.

CHAPTER 6

SUMMARY, CONCLUSIONS, AND RECOMMENDATIONS

6.1 SUMMARY

As a result of economic constraints and the need to extend pavement service life, a significant portion of the pavement construction and rehabilitation efforts in many states have focused on improving pavement performance and design life. In support of this long-term objective, development of pavement reinforcement materials has become one research area receiving increased attention. The major objective of the research project presented herein was to determine the influence of glass fiber grids used within the asphalt base course on the performance of pavement sections. To achieve this objective, experimental and theoretical investigations were performed to determine whether the flexible pavement sections could be effectively reinforced by the use of glass fiber grid. Factors such as permanent (cumulative) displacement of the asphalt surface, change in pavement stiffness with number of load cycles, resistance to cracking, strain in the glass fiber grid, and variation of subgrade stress in reinforced pavement sections were evaluated and compared with results from non-reinforced pavement sections. For the experimental study, twenty flexible pavement sections, with and without glass fiber grids, were constructed and tested in the laboratory. The experimental pavement sections were built in a rectangular container with dimensions of 4 feet x 6 feet x 2.5 feet (1.2 m x 1.8 m x 0.8 m). Two containers were constructed of steel for testing flexible pavement sections. Five analog dial gages [1-inch (25 mm)] were placed on the top of the asphalt surface to measure permanent vertical displacements. Two earth pressure cells were used in each soil container (test box) and were located at the top of the subgrade soil. The depth of the buried pressure cells was 8.5-inch (215.9 mm) below the asphalt gravel base interface. Six strain gages were bonded to top of the glass fiber grid to

evaluate the behavior of the reinforcement layer. For the test sections, the maximum applied load on the HMA surface was 9 kips (40 kN), simulating a tire pressure of 80 psi (551 kN/m²) through a 12-inch (305 mm) diameter loading plate. The frequency of sinusoidal dynamic load was 1.2 Hz. Additionally, a series of computer analyses (KENLAYER and Finite Element Method) was performed. The experimental results from this study were compared with the results from the computer analysis of the pavement sections. In Chapters 4 and 5 of this report, results for experimental and theoretical studies were presented in detail. Important findings are summarized in the following sections.

6.2 CONCLUSIONS

The following sections present a summary of conclusions based on laboratory and computed test results.

6.2.1 Laboratory Test Results

In the following sections, a summary of experimental results are presented.

Summary Of Results On Vertical Subgrade Stress

1. The influence of different glass grids reinforcement on vertical subgrade stress was not significant when the thickness of asphalt base was 6 inches (152 mm) [See Section 4.1.1].
2. Observations on doubly reinforced cases indicated that the vertical stress in the subgrade was lower in pavement sections with stronger glass grids [See Section 4.1.2].
3. Observations on 6-inch (152 mm) thick asphalt sections indicated that the glass grid reinforcement seems to spread the load over a larger area in the lower layers causing lower subgrade stresses [See Section 4.1.3].

4. Observations on thin asphalt sections [thickness of HMA = 2.5 in. (63.5 mm) and 3 in. (76 mm)] indicated that the vertical stress for the reinforced cases without the simulated crack (Experiments #11 and #20) was lower than the vertical stress for the reinforced case with the simulated crack (Experiment #14). This behavior indicates that the vertical stress was influenced by the presence of a simulated crack [See Section 4.1.4].
5. Observations indicated that a reinforced thinner section [thickness of HMA = 3 inches (76 mm)] behaved similar to that of a non-reinforced thicker pavement section [thickness of HMA = 6 inches (152 mm)].
6. When the thickness of the HMA was increased from 3 inches (76 mm) to 6 inches (152 mm), the influence of HMA thickness on vertical subgrade stress was clear: the higher the thickness of the asphalt layer, the lower the vertical subgrade stress [See Section 4.1.6].
7. It was shown that a reinforced thinner section behaves similar to that of a non-reinforced thicker section [Figure 4-12 (a)]. It is also clear that the average vertical subgrade stress for the case [thickness of HMA = 3 inches (76 mm)] with a simulated crack in a thin reinforced section is higher than the stress in a 6-inch (152 mm) thick non-reinforced pavement [Figure 4-12 (b)]. Therefore, the difference in the behavior can be attributed to the simulated crack.
8. Observations on thinner pavement sections indicated that the increase in vertical subgrade stress caused by a simulated crack is offset by the decrease in vertical subgrade stress due to the reinforcement of the pavement section.

Summary Of Results On Cumulative Displacements

1. The cumulative displacements increased for reductions in grid weight in thick pavement sections where the thickness of asphalt was 6 inches (152 mm) [See Section 4.2.1].
2. The results show that when the HMA thickness was 6 inches (152 mm) in a test section, the improvement in performance indicated by cumulative displacements of a doubly reinforced section (about 60%) was higher than the improvement (about 40%) observed in the singly reinforced test section in comparison to a non-reinforced test section. This substantial decrease in cumulative displacement shows that an improvement could be gained by reinforcing the structural asphalt base in a pavement section [See Section 4.2.3].
3. For thinner HMA layers [2.5 inches (63.5 mm) to 3 inches (152 mm)], it appeared that the influence of reinforcement was not significant in comparison to a non-reinforced case. This could be due to the fact that the compaction effort played a bigger role than the reinforcement [See Section 4.2.4].
4. Results indicate that a 6-inch (152 mm) thick non-reinforced hot mix asphalt layer did not improve the performance of the pavement system in comparison to 2.5-inch (63.5 mm) and 3-inch (76 mm) thick glass grid reinforced hot mix asphalt sections. In fact, reinforced thinner sections showed better performance than the non-reinforced thicker section [See Section 4.2.5].
5. Thinner reinforced asphalt layers with a simulated crack performed better than a thicker non-reinforced asphalt layers without a simulated crack. As noted earlier, failure resulted in test sections with a simulated crack when the glass grid reinforcement was not included. These results show that the reinforcement in the asphalt layer above the crack tend to arrest the

crack propagation leading to failure [See Section 4.2.8].

6. Of the two reinforced pavement sections with a simulated crack, neither resulted in failure. Of the three non-reinforced pavement sections with a simulated crack, two resulted in failure and one did not result in failure. This non-failed section may be a result of the compaction effort put into this particular test section.
7. Reinforced test sections with a simulated crack resulted in slightly higher displacements than non-reinforced sections without a crack. The presence of a crack seems to increase cumulative displacements. However, the reinforcement seems to prevent pavement sections from failure [See Section 4.2.9].
8. Test results show that the negative influence of the simulated crack seems to have a slightly more impact on cumulative displacements than the positive influence of the glass grid reinforcement.
9. The influence of the inclusion of glass grid in the hot mix asphalt improved the pavement performance.

Summary Of Laboratory Results On Displacement Under Static Loading

1. For thick pavement sections [thickness of HMA = 6 inches (152 mm)], no clear conclusion on the influence of different glass grids on displacement (under static loading) can be made. However, test sections with lighter glass grids seems to result in slightly larger surface deformations in comparison to test sections with heavier glass grids.
2. The stiffness of the hot mix asphalt layer for the thick pavement sections [thickness of HMA = 6 inches (152 mm)] does not seem to be affected significantly by the presence of the glass grid. For the thick asphalt sections, the insignificant differences in displacement may be

caused by the differences in compaction effort [See Section 4.3.3 and Figure 4-34 (a)].

3. For the thin [thickness of HMA = 3 inches (76 mm)] pavement sections, displacements for the reinforced case were slightly higher than that of the non-reinforced case. This small difference was insignificant and may be caused by the difference in compaction effort and/or by the inclusion of glass grid [See Section 4.3.4 and Figure 4-34 (b)].
4. Thin pavement sections were stiffer than the thick pavement section, perhaps due to the difference in compaction lift thickness. The lift thickness was 3 inches (76 mm) for thick and 1.5 inches (63.5 mm) for thin pavement sections, respectively [See Section 4.3.6 and Figure 4-34 (c)].
5. Even though the difference in displacement (under static loading) was insignificant, it can be stated that a non-reinforced test section with a simulated crack [thickness of HMA = 3 inches (76 mm)] resulted in slightly higher displacements than that of a non-reinforced test section without a simulated crack [thickness of HMA = 3 inches (76 mm)]. The presence of the crack seems to decrease the pavement stiffness slightly [See Section 4.3.7 and Figure 4-34 (d)].
6. Even though the displacement for the reinforced sections with a simulated crack [thickness of HMA = 3 inches (76 mm)] was higher than that of for non-reinforced sections with a simulated crack [thickness of HMA = 3 inches (76 mm)], the difference in displacement between the non-reinforced and the reinforced pavement sections was very low [0.019-inch (0.483 mm)]. This shows that the stiffness of the hot mix asphalt does not seem to be affected significantly by the glass grid reinforcement [Figure 4-34 (e)].
7. Displacements for reinforced test sections with a simulated crack [thickness of HMA = 3 inches (76 mm)] were similar to the displacement for the non-reinforced thick pavement

section [thickness of HMA = 6 inches (152 mm)]. This behavior indicates that a similar stiffness can be obtained by reinforcing a thin asphalt section in comparison to a non-reinforced thick pavement section.

Strain Measurements On Glass Grid Reinforcement Layer

1. Despite the attempt to measure strain at gage #1, strain measurement at this location was possible only in one experiment due to failures in strain gages.
2. The results showed some inconsistencies among the strain measurements at gage #2 for different experiments. Therefore, it can be stated that based on the available data, firm conclusions cannot be reached about the variation of strain on glass grid.
3. Strain measurements at gage #3 gave consistent results for each experiment. Strain measurements on the glass grid, laterally 12 inches (305 mm) away from the center of the loading plate and in the middle depth of the HMA, were in compression, very low, and varied steady with the applied load.
4. Due to limited strain data and uncertainty of the strain measurements presented herein, no conclusions can be made on the basis of strain measurements.

6.2.2 Results Of Computer Analyses

In the following sections, a summary of computed results are presented.

Predicted Results On Vertical Stress

Based on the results for thin and thick, reinforced and non-reinforced pavement sections, the following conclusions can be made:

1. For thick reinforced and non-reinforced pavement sections, computed vertical subgrade stresses at cell #1 computed on the basis of mean values of material properties compared

reasonably well with measurements. The computed stresses at cell #2 were higher than the measured values.

2. For thin reinforced pavement sections, computed stresses (corresponding to mean values of material properties) and measured stresses at cell #1 for Experiment #11 compared reasonably well, while the computed vertical subgrade stresses were lower than the measured vertical subgrade stresses for Experiment #17. Again, the computed stresses at cell #2 were higher than the measured values.
3. For thin non-reinforced pavement sections, computed vertical subgrade stresses at cell #1 (corresponding to mean values of material properties) compared exceptionally well with measurements. The computed stresses at cell #2 were again higher than the measured values.

Influence Of Geosynthetic On Pavement Performance

In some cases, glass grid was assumed as a linear visco-elastic material with low creep characteristics. In some cases, the glass grid was assumed as a linear elastic material. A summary of predicted results are given below [See Sections 5.4.1 and 5.4.2]:

1. The stiffness of the glass grid in the middle of HMA does not influence the vertical subgrade stresses significantly.
2. The stiffness of the geosynthetic fabric (between the gravel base and subgrade soil) does not influence the subgrade stress substantially. It can be concluded from the analyses that the use of a very stiff geotextile material at the gravel/subgrade interface is not necessary as a reinforcement. The main function of the geotextile was to prevent subgrade soil from migrating into the gravel base.

Computer Analyses Of Surface Displacements

1. The computed elastic displacements at the top surface decreased when the thickness of hot mix asphalt layer was increased.
2. The computed elastic surface displacements corresponding to mean values of material properties (Case 2) compared well with the measured values (under static loading) for different thicknesses of reinforced and non-reinforced pavement sections.

Variation of Computed Strain with Depth in a Thick and a Thin Pavement Sections

1. The highest radial and tangential strains were observed beneath the center line of the loading plate (along the line A-A) at the HMA/gravel-base interface. At this depth, the radial strains (along the lines A-A and B-B) and the tangential strains (along the lines A-A, B-B, and C-C) were in tension [See Sections 5.6.1 and 5.6.2 and Figure 5-20 (a)].
2. In the middle of the HMA, radial strains along the lines A-A, B-B, and C-C [Figure 5-20 (a)] were in compression.
3. The highest vertical compressive strains were observed on top of the subgrade.

Influence of HMA Thickness on Computed Strains in the Reinforcement Layer

1. In the reinforcement layer, radial strains #1 and #3 [Figure 5-20 (b)] for the thick pavement section were in compression while only radial strain #3 was in compression for the thin pavement section.
2. Tangential strains in the reinforcement layer were in compression for the thick pavement section and in tension for the thin pavement section [See Section 5.6.5].
3. The highest tangential strain (in tension) was observed beneath the center of the loading plate for the thin pavement section. For the thick pavement section, the highest tangential strain (in

compression) occurred at the strain gage (strain #3), which was the furthest away from the applied load [See Section 5.6.5].

4. Radial and tangential strains for the thick pavement section were smaller than those for the thin pavement section.

Comparison of Computed Strains with Measurements

1. At a radial distance of 12 inches (305 mm), the measured tangential strains (in the reinforcement layer) for the thick and the thin pavement sections matched closely with the computed tangential strains [See Section 5.6.6].
2. At a radial distance of 6 inches (152 mm) (at the edge of the loading area), the measured tangential strains in the reinforcement layer for the thin and the thick pavement sections did not match well with the computed tangential strains.

Summary Of Results On Finite Element Analyses

Summary of the results from the finite element method (FEM) of analyses are summarized below:

Axisymmetric Idealization Of The Laboratory Test Section

1. The vertical stress variation obtained from the finite element analysis (axisymmetric idealization) is comparable with the stress variation predicted by the KENLAYER [Huang (1993)] analysis. At the upper layers, the stresses from KENLAYER seem to be slightly larger than the stresses from the finite element (FE) analysis, while the opposite is true for stresses at the subgrade level [See Section 5.7.1].
2. The influence of reinforcement was studied by decreasing the elastic modulus (E) value of the reinforcement material (glass grid) from 4,205,000 psi (28,972,450 kN/m²) to 270,000 psi

(1,860,300 kN/m²). The results for the two extreme cases are very similar, suggesting that the stiffness of the reinforcement material does not have a significant effect on the performance of a pavement system [See Section 5.7.1].

3. Measured vertical subgrade stresses beneath the center of the loading area (Pressure Cell #1) compared well with the computed values more closely than at the edge of the loading area (at Pressure Cell #2).

Plane Strain Idealization Of A Hypothetical Field Section

1. When the shear stiffness of the reinforcement layer was increased from 10 psi (68.9 kN/m²) to 4,200,000 psi (28,938,000 kN/m²), the vertical stress directly beneath the reinforcement layer decreased by approximately 17%. The vertical stress directly above the reinforcement layer was almost the same for both values of shear stiffness [See Section 5.7.2].
2. It is apparent that the stiffness of the reinforcement alone does not influence the vertical compressive strain on top of subgrade and the horizontal tensile strain at the bottom of the HMA substantially.
3. The stiffness of the glass grid in the middle of the HMA did not influence the surface displacement (elastic) as evident from the negligible difference between the surface displacements for different values of elastic moduli.

6.3 RECOMMENDATIONS FOR FUTURE RESEARCH

1. Since the horizontal tensile strain at the bottom of HMA is an important factor for evaluating reflection cracking [Yoder and Witczak (1975)], it would be useful to experimentally investigate the influence of glass fiber grid by placing it beneath an asphalt overlay (blacktop).

The findings should be verified with the help of a powerful numerical method such as the Finite Element Method (FEM).

2. Investigate the delamination (slippage) of glass grid inside the HMA in laboratory conditions.
3. Investigate the influence of glass fiber grids on multiple fractures inside the HMA. Powerful numerical methods such as the FEM can be used in such an investigation.
4. For laboratory analyses, environmental effects were not considered. Changes in material properties in terms of temperature and moisture variances should be considered. Laboratory conditions under controlled environment should simulate thermal cycling to improve the reliability of the performance analysis. The effects of freeze-thaw cycling should be established for a better understanding of reinforced flexible pavement performance.
5. Based on laboratory test results, field test sections under controlled conditions should be constructed and monitored for performance evaluation.

REFERENCES

- Abdelhalim, A. O.** 1983. *Geogrid Reinforcement of Asphalt Pavements*. Ph. D. Thesis, University of Waterloo, Ontario.
- Abdelhalim, A. O., R. Haas, J. Walls, R. Bathurst & W. A. Phang** 1982. *A New Method for Effective Reinforcement of Asphalt Pavements*. Proceedings of the Roads and Transportation Association of Canada, Halifax.
- Agarwal, B. D. & L. J. Broutman** 1990. *Analysis and Performance of Fiber Composites*. Second Edition, John Wiley & Sons Inc., USA.
- American Association of State Highway and Transportation Officials (AASHTO)** 1992. *Standard Specifications for Highway Bridges, Fifteenth Edition*, AASHTO. Washington, D.C.
- American Association of State Highway and Transportation Officials (AASHTO)** 1993. *AASHTO Guide for Design of Pavement Structures*, AASHTO. Washington, D.C.
- Amoco Manufacturer's Literature** 1994. Atlanta, Georgia
- Asphalt Institute** 1981. *Thickness Design-Asphalt Pavements for Highways and Streets*. Asphalt Institute Manual Series No: 1 (MS-1).
- Asphalt Institute** 1983. *Principles of Construction of Hot-Mix Asphalt Pavements*. Asphalt Institute Manual Series No: 22 (MS-22).
- Asphalt Institute** 1989. *The Asphalt Handbook*. Asphalt Institute Manual Series No: 4 (MS-4).
- Barksdale, R. D.** 1991. *Fabrics in Asphalt Overlays and Pavement Maintenance*. Report NCHRP 171, Transportation Research Board, Washington, D.C.
- Brown, S. F., B. V. Brodrick & D. A. B. Hughes** 1984. *Tensar Reinforcement of Asphalt: Laboratory Studies*. Proceedings of the Symposium on Polymer Grid Reinforcement in Civil Engineering, Institution of Civil Engineers, London.
- Brown, S. F., J. M. Brunton, D. A. B. Hughes & B. V. Brodrick** 1985. *Polymer Grid Reinforcement of Asphalt*. Proceedings of the Association of Asphalt Paving Technologies, Vol. 54, pp. 18-45.
- Brownridge, F. C.** 1964. *An Evaluation of Continuous Wire Mesh Reinforcement in Bituminous Resurfacing*. Proceedings of the Association of Asphalt Technologies, Vol. 33, pp. 459-501.

Button J. W. & R. L. Lytton 1987. *Evaluation of Fabrics, Fibers and Grids in Overlays*. Proceedings, 6th International Conference on Structural Design of Asphalt Pavements, Vol. 1, pp. 925-934.

Carroll, R. G. Jr., J. C. Walls & R. Haas 1987. *Granular Base Reinforcement of Flexible Pavement Using Geogrids*. Geosynthetic Conference, New Orleans, LA.

Coetzee, N. F. & C. L. Monismith 1979. *Analytical Study of Minimization of Reflection Cracking in Asphalt Concrete Overlays by Use of a Rubber-Asphalt Interlayer*. Transportation Research Record 700: Pavement Evaluation and Overlay Design, Transportation Research Board, National Research Council, Washington, D.C.

Desai, C. S. 1979. *Elementary Finite Element Method*. Prentice Hall, Inc., Englewood Cliffs, NJ.

Desai, C. S. & H. J. Siriwardane 1984. *Constitutive Laws for Engineering Materials with Special Emphasis on Geologic Media*. Prentice Hall, Inc., Englewood Cliffs, NJ.

Duncan, J. M., C. L. Monismith & E. L. Wilson 1968. *Finite Element Analyses of Pavements*. Highway Research Record 228, Highway Research Board, Washington, D.C., pp. 18-33.

Geotechnical Association Fabrics International 1995. *Geotechnical Fabrics Report 1996 Specifier's Guide*.

Giroud, J. P., C. Ah-Line & R. Bonaparte 1984. *Design of Unpaved Roads and Trafficked Areas with Geogrids*. Proceedings of the Symposium on Polymer Grid Reinforcement in Civil Engineering, Institution of Civil Engineers, London.

Giroud, J. P. & L. Noiray 1981. *Geotextile Reinforced Unpaved Road Design*. Journal of the Geotechnical Division, ASCE, Vol. 107, No. GT9, pp. 1233-1254.

Glass Grid Manufacturer's Literature 1995. *Pavement Reinforcement*. Ontario, Canada.

Haas, R. 1984. *Structural Behavior of Tensar Reinforced Pavements and Some Field Applications*. Proceedings of the Symposium on Polymer Grid Reinforcement in Civil Engineering, Institution of Civil Engineers, London.

Holtz, R. D. & W. D. Kovacs 1981. *An Introduction to Geotechnical Engineering*. Prentice Hall, Englewood Cliffs, NJ.

Hozayen, H., M. Gervais, A. O. Abdelhalim & R. Haas 1993. *Analytical and Experimental Investigations of Operating Mechanisms in Reinforced Asphalt Pavements*. Pavement Design, Management, and Performance-Rigid and Flexible Pavement Design and Rehabilitation, Transportation Research Record 1388, Transportation Research Board, National Research

Council, Washington, D.C., pp. 80-87.

Huang, Y. H. 1993. *Pavement Analysis and Design*. Prentice Hall, Englewood, NJ.

Jackson, R. D. 1980. *Use of Fabrics and Other Measures for Reflective Cracking of Asphaltic Concrete Overlays*. Final Report, Report No: WES/MP/GL-80-2, FAA/RD-80/8, Waterways Experiment Station, Corps of Engineers, Vicksburg, MS.

Jewel, R. A., G. W. E. Milligan, R. W. Sarsby & D. Dubois 1984. *Interaction Between Soil and Geogrids*. Proceedings of the Symposium on Polymer Grid Reinforcement in Civil Engineering, Institution of Civil Engineers, London.

Jayawickrama, P. W. & R. L. Lytton 1987. *Methodology for Predicting Asphalt Concrete Overlay Life Against Reflection Cracking*. Proceedings of the Sixth International Conference on Structural Design of Pavements, Ann Arbor, Michigan, pp. 912-924.

Jenq, Y.-S., C.-J. Liaw & P. Liu 1993. *Analysis of Crack Resistance of Asphalt Concrete Overlays - A Fracture Mechanics Approach*. Pavement Design, Management, and Performance-Rigid and Flexible Pavement Design and Rehabilitation, Transportation Research Record 1388, Transportation Research Board, National Research Council, Washington, D.C., pp. 160-166.

Kennepohl, G. & N. I. Kamel 1984. *Construction of Tensar Reinforced Asphalt Pavements*. Proceedings of the Symposium on Polymer Grid Reinforcement in Civil Engineers, London.

Kennepohl, G., N. Kamel, J. Walls & R. C. G. Haas 1985. *Geogrid Reinforcement of Flexible Pavements Design Basis and Field Trials*. Proceedings of the Association of Asphalt Paving Technologies, Vol. 54, pp. 45-76.

Koerner, R. M. 1994. *Designing with Geosynthetics*. Third Edition, Prentice Hall, Upper Saddle River, NJ.

Lytton, R. L. 1989. *Use of Geotextiles for Reinforcement and Strain Relief in Asphalt Concrete*. Geotextiles and Geomembranes. Vol. 8, pp. 217-237.

Merritt, F. S. 1983. *Standard Handbook for Civil Engineers*. Third Edition, McGraw-Hill Book Company.

Paris P. C. & F. A. Erdogan 1963. *Critical Analysis of Crack Propagation Laws*. Transactions of the ASME, Journal of Basic Engineering, Series D, 85. No. 3, pp. 528-534.

Raad, L. & J. L. Figueroa 1980. *Load Response of Transportation Support Systems*. Transportation Engineering Journal, ASCE, Vol. 106, No. TE1, pp. 111-128.

Siriwardane, H. J. 1983. *Users Manual and Background for a Computer Code for Non-Linear Two Dimensional Finite Element Analysis of Some Geotechnical Problems*. Report, Department of Civil Engineering, West Virginia University, Morgantown.

Siriwardane H. J. & B. Kutuk 1997. *Evaluation of Flexible Pavements Reinforced with Glass Fiber Grids*. Proceedings of the Ninth International Conference on Computer Methods and Advances in Geomechanics, A. A. Balkema Publishers, The Netherlands.

Smith, L. L. & W. Gartner 1959. *Welded Wire Fabric Reinforcement for Asphaltic Concrete*. Highway Research Board, Bulletin 322, pp. 1-20.

Smith R. D. 1983. *Laboratory Testing of Fabric Interlayers for Asphalt Concrete Paving - Interim Report*. Transportation Research Record 916: Engineering Fabrics in Transportation Construction, Transportation Research Board, National Research Council, Washington, D.C.

Smith, T. E., T. L. Brandon, I. L. Al-Qadi, B. A. Lacina, S. A. Bhutta & S. E. Hoffman 1995. *Laboratory Behavior of Geogrid and Geotextile Reinforced Flexible Pavements*. Final Report, Virginia Polytechnic Institute and State University, Blacksburg, VA.

Thompson, M. R. & R. P. Elliott 1985. *ILLI-PAVE-Based Response Algorithms for Design of Conventional Flexible Pavements*. Transportation Research Record 1043, Transportation Research Board, National Research Council, Washington, D.C., pp. 50-57.

Timoshenko, S. P. & J. N. Goodier 1987. *Theory of Elasticity*. Third Edition, McGraw Hill, Inc., USA.

Tons, E. and E. M. Korokosky 1960. *A Study of Welded Wire Fabric Strip Reinforcement In Bituminous Concrete Resurfacing*. Proceedings of the Association of Asphalt Paving Technologies, Vol. 29, pp. 43-76.

Wathugala, G. W., B. Huang & S. Pal 1996. *Numerical Simulation of Geosynthetic-Reinforced Flexible Pavements*. Transportation Research Record 1534, Transportation Research Board, National Research Council, Washington, D.C., pp. 58-65.

Webster, S. L. 1992. *Geogrid Reinforced Base Courses for Flexible Pavements for Light Aircraft: Test Section Construction, Behavior Under Traffic, Laboratory Tests, and Design Criteria*. Final Report, Geotechnical Laboratory, Department of the Army, Waterways Experiment Station, Vicksburg, MS.

West Virginia Department of Highways 1986. *Standard Specifications, Roads and Bridges*. Charleston, WV.

Yoder, E. J. & M. W. Witczak 1975. *Principles of Pavement Design*. Second Edition, John Wiley & Sons Inc., NY.

Zaghloul, S. & T. White 1993. *Use of a Three-Dimensional, Dynamic Finite Element Program for Analysis of Flexible Pavement*. Pavement Design, Management, and Performance-Rigid and Flexible Pavement Design and Rehabilitation, Transportation Research Record 1388, Transportation Research Board, National Research Council, Washington, DC., pp. 60-69.

Zienkiewicz, O. C. 1977. *The Finite Element Method in Engineering Science*. Third Edition, McGraw-Hill, London.